Development and Testing of Tailored Tool Surfaces for Sheet Metal Forming

PhD Thesis
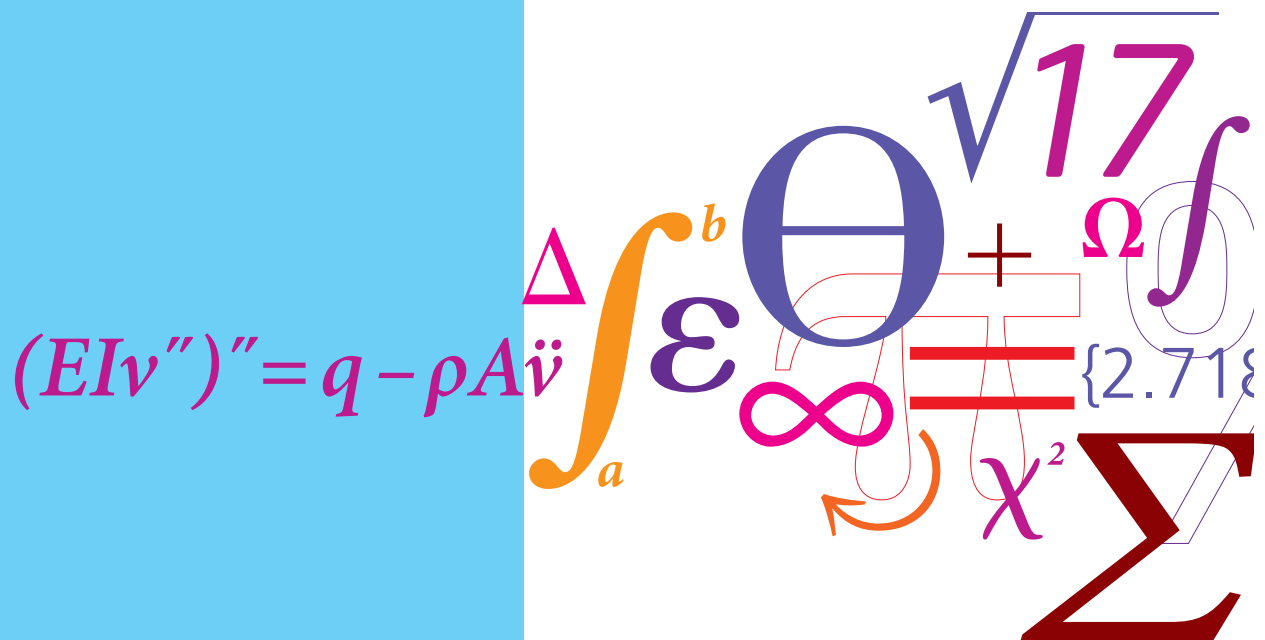
$$(EIv'')'' = q - \rho A\ddot{v}$$

Mohd Hafis Bin Sulaiman
September 2017

Development and Testing of Tailored Tool Surfaces for Sheet Metal Forming

PhD Thesis

Mohd Hafis Bin Sulaiman

Department of Mechanical Engineering

Technical University of Denmark

September 2017

Segala puji bagi Allah Robbil 'Aalamiin

Untuk Nur Farahana, Affan Hafiy dan Afeef Fikri yang dicintai

Untuk Sulaiman, Hindun, Husny, Rushilawaty, Norsuhaida dan Abu Hanifah yang disayangi

Untuk Ramli, Ruziah dan Adib Firas yang dikasihi

PhD student

Mohd Hafis Bin Sulaiman, MEng
Department of Mechanical Engineering
Technical University of Denmark

Supervisors

Professor Emeritus Niels Bay, PhD, DSc, Dr. h.c.
Department of Mechanical Engineering
Technical University of Denmark

Associate Professor Chris Valentin Nielsen, PhD
Department of Mechanical Engineering
Technical University of Denmark

Peter Christiansen, PhD
Department of Mechanical Engineering
Technical University of Denmark

Examining Committee

Professor Leonardo De Chiffre, PhD, DSc, Dr. h.c.
Department of Mechanical Engineering
Technical University of Denmark

Professor Laurent Dubar, PhD
Directeur TEMPO EA 4542
Institute Carnot ARTS
Université de Valenciennes et du Hainaut Cambrésis, France

Ermano Ceron, PhD
Senior Engineer
Grundfos A/S, Denmark

PREFACE

This thesis is submitted in partial fulfillment of the requirements for obtaining the degree of PhD at the Technical University of Denmark (DTU). This PhD project was carried out in the period from 1st October 2014 to 30th September 2017 within the new environmentally benign sheet metal forming tribology systems (SHETRIB) project framework under supervision of Professor Emeritus Dr. Tech. Niels Bay, Associate Professor Dr. Chris Valentin Nielsen and Dr. Peter Christiansen. This PhD project was funded by the Ministry of Education, Malaysia and Universiti Malaysia Perlis.

My sincere gratitude goes to my supervisors for their guidance and continual support throughout the course of this project. I equally appreciated their wisdom, tolerance, patience and challenging criticism. I am very grateful to all staffs at the DTU-MEK workshop who helped with the fabrication work, development of the test rig, and for dealing with all of my last minute requests with great humour and professionalism. Special thanks to my officemates for their companionship, helpful insights and friendly working environment.

Many thanks to SHETRIB project partner Dr. Ermano Ceron from Grundfos A/S, Allan de Neergaard and Casper Fjordbak Larsen from CemeCon Scandinavia A/S, Karsten Sørensen from Carbo Tech Nordic ApS, Professor Tatsuhiko Aizawa from Shibaura Institute of Technology Japan and Morita Hiroshi from Nano Film and Coat Laboratory LLC Japan for consultations and materials. Many thanks also to Professor Habil. Paulo AF Martins from University of Lisbon, Portugal for fruitful discussions and guidance in the first year of my PhD project.

And most importantly, the unconditional love, support and care from my family, my parents and parents in law, my beloved wife and kids, my siblings and siblings in law, have been unsurpassed at all times, and for this, I am eternally indebted.

Whenever I think of the past 3-year PhD journey, it brings back so many memories. I learnt Danish work-life balance environments and cultures, I enjoyed my first-time skiing and I am delighted with those opportunities to meet up with prominent professors, researchers, experts and PhD students in the field of metal forming during seminars, industrial visits, conferences and summer holiday events in several places like Copenhagen, Jutland, Nuremberg, Munich, Hirschegg, Phuket and Cambridge.

Mohd Hafis Bin Sulaiman
September 30th, 2017

Abstract

This thesis describes measures taken to minimize or substitute environmentally hazardous lubricants applied in sheet metal forming processes by less harmful lubricants or not applying lubricant at all. The breakdown of lubricant film often leads to galling, and therefore application of the hazardous lubricants has spurred industrial interest. In order to face a serious challenge in trying to stimulate less consumptions of such hazardous lubricants, the PhD project was intended to lead to improvements in resistivity towards galling in sheet metal forming by studying three different subjects; compressibility of lubricants, application of structured tool surfaces and application of anti-seizure tool coatings.

In order to analyze the mechanisms of lubricant entrapment and escape, knowledge of the lubricant bulk modulus characterizing the compressibility of lubricant is required. Two methods were studied to achieve this purpose. A simple laboratory test consisting of upsetting a specially designed metal cylinder with a lubricant reservoir together with elasto-plastic, numerical modelling of the metal cylinder is carried out in order to determine the bulk modulus at low pressure regimes of approximately 100 MPa. The above mentioned simple experimental procedure for determining lubricant bulk modulus gives a first rough estimate, and it is supplemented by a more advanced laboratory test based on a newly designed equipment. The lubricant compressibility experiment with a direct pressure measurement inside the high-pressure container allows for the direct determination of the bulk modulus at various pressure levels with no influence from friction in the sealing between punch and container. Using water as a reference, a good agreement between the experimental bulk modulus and values suggested in literature was found. Testing of liquid lubricants has revealed a nonlinear relationship between the bulk modulus and the pressure.

While texturing of workpiece surfaces to promote lubrication in sheet metal forming has been applied for several decades, tool surface texturing is rather new. A detailed background investigation and fundamental analysis of different textured tool surface arrangements have been carried out by Strip Reduction Test (SRT). Low as well as high viscosity oils were tested at varying sliding speeds. Micro-textured surfaces on the tool were made using an in-house micro-milling machine for the manufacturing. The SRT tools were manufactured with longitudinal, shallow pocket geometries oriented perpendicular to the sliding direction. The pockets have small angles to the workpiece surface and varying distance. The experiments show an optimum distance between the pockets to exist that creates a table mountain topography with flat plateaus and narrow pockets in between. If the flat plateaus are too narrow, an increase in drawing load and pick-up on the tool plateaus is observed. The same occurs for too wide plateaus. The tool textures were advantageous at larger sliding speeds when using higher viscosity oils, which facilitates the escape of trapped lubricant by micro-plasto-hydrodynamic lubrication. Large lubricant viscosity results in higher sheet plateau roughness and prevents pick-up and galling.

A theoretical friction model for a soft workpiece deforming against a textured tool surface was proposed. The friction model takes into account the plastic wave motion appearing, when the workpiece material flows into and out of local pockets between the flat plateaus of a table mountain tool surface topography. The friction model supports the experimental findings of an optimum distance between the pockets, where the contribution to friction by mechanical interlocking of the strip in the pockets is limited and lubrication of the plateaus is enhanced by micro-plasto-hydrodynamic lubrication. It was found that an optimum amount of tool texture exists which reduces friction and thus drawing load for the table-mountain tool surface topography.

Stamping of sheet metal components without lubrication or using minimum amount of hazard free lubricant is a possible solution to diminish health hazards to personnel and environmental impact and to reduce production costs. Adopting SRT, which emulates industrial ironing production of deep drawn, stainless steel cans, Diamond-Like Carbon (DLC) coating were deposited on SRT tools. The DLC coated tools with multi-, double- and single-layer coating structures were tested under severe tribological conditions, i.e, high normal pressure and temperature. A screening test campaign on a manually operated sheet tribo-tester is carried out to identify promising candidates. The screening tests revealed that the double layer coating worked successfully, i.e. with no sign of galling using no lubrication even at elevated tool temperature, while the other coatings peeled off and resulted in severe galling unless lubrication was applied. The next test campaign on an automatic sheet tribo-tester examines the durability of the promising candidate as regards persistence towards pick-up. It is shown that the double-layer coating, DLC/Hyperlox®, can function effectively if a minimum quantity of hazard free lubricant is applied and hence, avoid peeling off of the coating leading to galling. Numerical simulation using a thermo-mechanical analysis supports the experimental findings, where lubrication lowers the temperature at the tool/workpiece interface by reducing the friction.

Resumé (in Danish)

Denne afhandling beskriver forskellige metoder til at minimere eller eliminere brugen af miljøskadelige smøremidler i pladeformgivningsprocesser. Nedbrud af smørefilm fører ofte til rivninger, og derfor har det endnu ikke været muligt at udfase disse smøremidler i industrien. Det har været dette phd-projekts mål at forsøge at udvikle metoder til at udfase miljøskadelige smøremidler ved at studere tre forskellige emner: kompressibilitetsmodul af smøremidler, strukturerede værktøjsoverflader samt værktøjsbelægninger.

For at kunne analysere indfangning og undslippelse af smøremidler fra overfladeteksturer er det nødvendigt at have kendskab til smøremidlets kompressibilitetsmodul. To forskellige metoder er anvendt til dette formål. En simpel laboratorietest bestående af stukning af et aluminiumemne med et smøremiddelresevoir og en invers FEM-beregning af stukningen, hvorved smøremidlets kompressibilitetsmodul kan bestemmes for hydrostatiske tryk op til cirka 100MPa. Denne simplificerede test er komplementeret med en mere avanceret laboratorietest baseret på et nyudviklet forøgsudstyr. Ved at måle trykopbygningen direkte i et lukket kammer kan smøremidlets kompressibilitetsmodul bestemmes. Herved undgås friktionstab i pakningerne mellem stempel og trykkammervæg. Udstyret er afprøvet med vand, hvor der er tilgængelige data i litteraturen for kompressibilitetsmodulet som funktion af det hydrostatiske tryk. Der er konstateret god overensstemmelse mellem litteratur og forsøg. Når der udføres kompressibilitetstest af smøremidler, er der fundet en ulineær sammenhæng mellem tryk og kompressibilitetsmodul.

Mens teksturering af emneoverflader for at forbedre smøringen i pladeformgivningsprocesser har været kendt i flere årtier, er det relativt nyt at teksturere værktøjets overflader for at forbedre smøringen. En detaljeret undersøgelse og analyse af forskellige værktøjstexturinger er blevet udført ved hjælp af stripreduktionstest (SRT). Der er både anvendt lav- og højviskose smøremidler samt forskellige glidehastigheder. Mikroteksturerede værktøjsoverflader blev fremstillet med en fræsemaskine. SRT-værktøjerne blev udstyret med aflange, lavbundede smørelommer orienteret vinkelret i forhold til glideretningen og med flade plateauer imellem. Smørelommernes kanter havde en lille vinkel i forhold til værktøjsoverfladen. Afstanden mellem smørelommerne blev også varieret. Forsøgene viser, at der er en optimal afstand mellem smørelommerne, hvor friktionen mellem emne og værktøj minimeres. Hvis de flade plateauer mellem smørelommerne er for lille, øges den nødvendige trækkraft, og der fås også pickup på værktøjet. Det samme sker hvis plateauafstanden er for lille. Teksturingen var især virkningsfuld ved høje glidehastigheder og anvendelse af højviskose smøremidler. Dette tilskrives mikrohydrodynamisk smøring. Når der anvendes et højviskost smøremiddel, fås en større overfladeruhed af emnet samt minimering af pickup og rivninger.

Der er udviklet en teoretisk friktionsmodel for et stift værktøj med en tekstureret overflade, der udfører relativ glidning i forhold til et plant, deformerbart emne. Friktionsmodellen tager højde for den plastiske bølgebevægelse, der opstår når

iv

emnematerialet glider ind og ud af værktøjets smørelommer mellem de flade plateauer. Friktionsmodellen understøttes af eksperimenter, hvor det vises, at der eksisterer en optimal teksturering af værktøjsoverfladen med hensyn til at minimere den nødvendige trækkraft. Optimummet skyldes en balance mellem den nødvendige trækkraft til at overvinde den mekaniske deformation af emnet når det glider ind og ud af tekstureringens fordybninger, samt at sikre en tilstrækkelig smøring af de flade plateauer mellem smørelommerne som følge af mikrohydrodynamisk smøring.

Presformgivning af pladeemner med et minimum af miljøvenligt smøremiddel, eller helt uden, er en måde at reducere helbredsfare og produktionsomkostninger. Stripreduktionstesten, der imiterer strækningsreduktion af dybtrukne emner, anvendes til forsøg med forskellige værktøjsbelægninger. Diamond-Like Carbon (DLC) belægning blev lagt på værktøjerne. DLC-belagte værktøjer med mono-, dobbelt- og flerlagsbelægninger blev anvendt til forsøgene, der har tribologisk vanskelige forhold såsom store fladetryk og forøget temperatur. En præliminær forsøgsserie blev udført på en manuel tribotester for at identificere de bedste belægningstyper. Den præliminære forsøgsserie viste at dobbeltlagsbelægningen virkede, dvs. den gav ikke anledning til pickup eller rivninger. Heller ikke selvom der anvendes forøget værktøjstemperatur og intet smøremiddel. De andre belægningstyper blev skrællet af og der opstod kraftige rivninger, medmindre der anvendtes et smøremiddel. Dernæst blev der udført en længerevarende, repetitiv test på en automatisk tribotester med dobbeltlagsbelægningen på værktøjerne. Formålet var at undersøge belægningens modstandsdygtighed mod pickup og rivninger ved gentagen påvirkning. Det blev fundet, at den undersøgte belægning, DLC/Hyperlox®, kunne fungere tilfredsstillende, dvs. uden pickup og rivninger, hvis en mindre mængde miljøvenligt smøremiddel blev påført emnet. En numerisk simulering af processen underbyggede de eksperimentelle resultater ved at vise, at varmeudviklingen reduceres som følge af en reduktion af friktionen ved at anvende en mindre mængde smøremiddel i forhold til ikke at anvende noget smøremiddel.

List of Publications

Part I: Compressibility of Lubricants
1. M.H. Sulaiman, P. Christiansen, P.A.F. Martins, N. Bay, "*Determination of lubricant bulk modulus in metal forming by means of a simple laboratory test and inverse FEM analysis*". Proceedings of the 7th International Conference on Tribology in Manufacturing Processes. 28 Feb – 2 Mac 2016. p. 316-323.
2. M.H. Sulaiman, P. Christiansen, N. Bay, "*Direct measurement of lubricant bulk modulus at high pressures*". Submitted to Lubrication Science, *review in progress*.

Part II: Structured Tool Surfaces
1. M.H. Sulaiman, P. Christiansen, N. Bay, "*The influence of tool texture on friction and lubrication in strip reduction testing*". Special issue – Tribology in Manufacturing Process, Journal "*Lubricants*", 2017, 5 (3), p. 1-11.
2. M.H. Sulaiman, P. Christiansen, N. Bay, "*The influence of tool texture on friction and lubrication in strip reduction*". 12th Int. Conf. on Technology of Plasticity (ICTP), Cambridge, United Kingdom, 17-22 Sept. 2017.

Part III: Anti-Seizure Tool Coatings
1. M.H. Sulaiman, P. Christiansen, N. Bay, "*A study of DLC coatings in ironing of stainless steel*". 36th Int. Deep Drawing Research Group (IDDRG) conference, Munich, Germany, 2-6 July 2017.
2. M.H. Sulaiman, P. Christiansen, N. Bay, "*A study of anti-seizure tool coatings for ironing of stainless steel*". Submitted to Jurnal Tribologi – Special issue: WTC2017, *Accepted for publication*.

Contents

Nomenclature

A	Contact area	[mm^2]
A_o	Nominal contact area	[mm^2]
A_{met}	Metal-to-metal contact area	[mm^2]
B	Strength coefficient	[MPa]
C	Strength coefficient	[MPa]
D_o	Diameter (Chapter 4)	[mm]
d	Pocket depth	[mm]
d_o	Top diameter for surface pocket (Chapter 4)	[mm]
d_i	Base diameter for surface pocket (Chapter 4)	[mm]
DR	Drawing ratio	[-]
E	Elastic modulus	[GPa]
F	Force	[N]
F_{avg}	Average drawing force	[N]
F_b	Back tension force	[N]
F_f	Front tension force	[N]
F_N	Normal force	[N]
F_D	Drawing force	[N]
H_o	Height (Chapter 4)	[mm]
HTC	Heat transfer coefficient	[W/m^2K]
HV	Vickers hardness	kp/mm^2
ΔH	Height change	[mm]
h	Thickness	[mm]
h_{avg}	Average thickness	[mm]
h_o	Initial thickness (Chapter 2)	[mm]
h_o	Height for surface pocket (Chapter 4)	[mm]
h_1	Final thickness	[mm]
K	Bulk modulus	[GPa]
L	Sliding length	[mm]
l	Length	[mm]
m	Friction factor	[-]
m_{met}	Local friction factor between strip and flat plateau	[-]
m_{low}	Friction factor on lower tool surface	[-]
m_{lub}	Friction factor due to viscous drag forces	[-]

x

m_{pock}	Local pocket friction factor	[-]
m_{tex}	Friction factor of textured tool surface	[-]
m_{up}	Friction factor on upper tool surface	[-]
m_{wave}	Apparent friction factor	[-]
n	Strain hardening exponent	[-]
p	Normal pressure	[MPa]
p	Hydrostatic pressure (Chapter 5)	[MPa]
p_f	Forward normal pressure	[MPa]
p_i	Instantaneous hydrostatic pressure (Chapter 5)	[MPa]
p_r	Backward normal pressure	[MPa]
q_o	Hydrostatic pressure of trapped lubricant within pocket	[MPa]
R	Radius of curvature	[mm]
Ra	Average surface roughness	[μm]
r	Radial direction (Chapter 5)	[-]
r	Thickness reduction	[-]
Δr	Radial expansion change (Chapter 5)	[mm]
s	Sliding length	[mm]
T	Temperature	[°C]
T_i	Initial temperature	[°C]
ΔT	Temperature change	[°C]
t	Time	[s]
u	Speed	[mm/s]
V	Volume	[mm^3]
V_o	Initial volume	[mm^3]
ΔV	Volume change (Chapter 5)	[mm^3]
w	Width	[mm]
W	Total width	[mm]
x	Distance between pockets	[mm]
X	Total length	[mm]
y	Length	[mm]
Y	Total length	[mm]
z	Vertical direction (Chapter 5)	[-]
Δz	Vertical loading length change	[mm]
α	Contact angle (Chapter 6)	[°]
α	Contact area ratio (Chapter 7)	[-]

γ	Slope of inclined ceiling surface	[°]
ε	Strain	[-]
ε_{eff}	Effective strain	[-]
ε_o	Effective strain	[-]
$\bar{\varepsilon}$	Initial effective strain or pre-straining	[-]
$\bar{\varepsilon}_1$	Effective strain of material after drawing	[-]
η	Viscosity, referring to kinematic viscosity	[cSt]
η_o	Dynamic viscosity	[Pa.s]
η_v	Kinematic viscosity	[cSt]
θ	Angle	[°]
θ	Slope of inclined pocket wall (Chapter 4)	[°]
κ	Thermal conductivity	W/(m.°C)
μ	Friction coefficient	[-]
ν	Poisson ratio	[-]
ρ	Density	[g/cm^3]
σ	Stress	[MPa]
σ_d	Drawing stress	[MPa]
σ_f	Flow stress	[MPa]
σ_o	Initial yield stress	[MPa]
σ_r	Radial stress	[MPa]
$\bar{\sigma}_f$	Average flow stress	[MPa]
σ_∞	Maximum flow stress	[MPa]
τ	Torque	[Nm]
τ_s	Shear stress	[MPa]
υ	Speed	[mm/s]

Chapter 1: Introduction

1.1   Background

Galling is undesirable and it occurs in situations where lubricant film breaks down, pick-up of workpiece material on the tool surface occurs, Figure 1.1a, and thereby subsequent scoring of the workpiece due to pick-up on the tool surface, Figure 1.1b. Galling is usually a gradual process, but can also occur abruptly and spread rapidly as the pick-up and cold-welding of the workpiece material to the tool surface induce more galling. Galling will generally disrupt the manufacturing line and production schedule. These situations often leads to the need for maintenance, i.e, dismounting, repolishing and surface treatment of the tool surface.

(a)   (b)
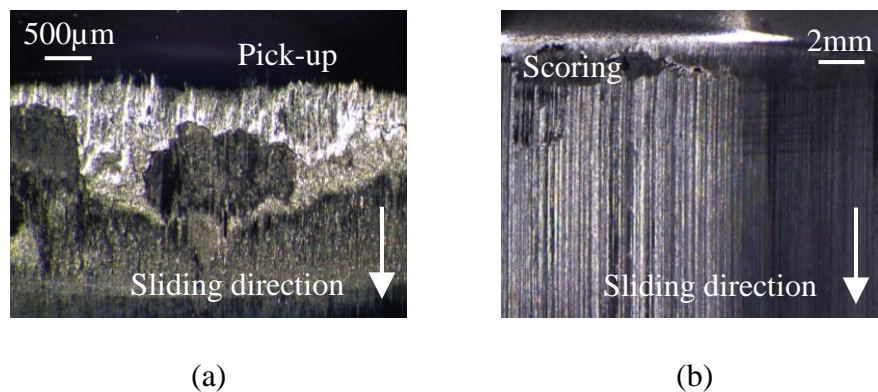
Figure 1.1: a) Pick-up of workpiece material on the tool surface, and b) scoring on the workpiece surface.

Lubrication is usually applied in sheet metal forming to prevent the galling problem especially under extreme tribological conditions. The lubrication serves two purposes: First, to separate the tool and the workpiece surfaces, where shearing of the lubricant film due to the sliding motion will generate a lower friction stress and a smaller load needed to deform the workpiece. Secondly, to cool down the heat generated either by plastic deformation of the workpiece or by frictional work at the tool/workpiece interface.

Efficient tribological systems are necessary to prevent the occurrence of galling. To achieve this, proper selection of lubricants is important. Chlorinated paraffin mineral oil is known to be the best selection in sheet metal forming because it has good boundary lubrication properties. At present, the chlorinated paraffin oil is often being applied in sheet stamping production of tribologically difficult materials, i.e. stainless steel, high strength steel, aluminium alloys and titanium alloys. The advantage of such efficient but hazardous lubricants is due to the chlorine in the oil that can provide a

strong molecular bonding to the exposed metallic surfaces [1], and this will generate a protective low shear strength film to minimize friction and prevent metal-to-metal contact.

The chlorinated paraffin oils are being largely consumed in production to avoid galling, but surveys find insufficient awareness of risks and side effects to personnel health and working environment. Application of such hazardous lubricants requires additional costs for post-cleaning after stamping. Furthermore, insufficient post-cleaning promotes hazardous chemical residues on the sheet surface, which may be unacceptable in cases like biomedical and food container products. Here, efforts are made of reducing or preventing the hazardous lubricants in production, employing mechanical instead of chemical means.

1.2 Motivation

1.2.1 Textured Tool Surface Topographies to Improve Resistivity towards Galling

Liquid lubrication is commonly applied in sheet metal forming in progressive dies for deep drawing, punching and ironing operations. The liquid lubricant serves to separate the tool and workpiece surfaces by producing a thin, hydrodynamic film, here the mechanism is named *macro-hydrodynamic lubrication*, which can carry the load. Engineering of the workpiece surface topography by creating pockets for entrapment of lubricant may further improve lubrication. The trapped lubricant is pressurized and may subsequently escape from the pockets during forming by the so-called mechanism of *micro-hydrodynamic lubrication* identified and studied by Azushima and Kudo [2] and Bay et al. [3][4][5].

Industrial application of engineered surfaces has since the 1990-ies become state of the art in automotive stamping industry [6][7]. Normally, tailored sheet surfaces are made by skin-pass rolling in the final rolling step after annealing using large rolls roughened by Shot Blast Texturing (SBT) or Electro Discharge Texturing (EDT), Kijima and Bay [8]. A drawback is here the problem of reproducing the surfaces in large scale sheet production due to wear of the textured roll surfaces. Besides this drawback comes economic considerations and the fact that the technique is less feasible in multistage operations, since the pockets are flattened out after the first forming operation, Groche et al. [9]. Texturing of tool surfaces would be more economically feasible since a textured tool surface can be utilized for thousands of workpiece components. A few tests of surface engineered deep drawing tools by industries [10] and researchers [11][12] have shown very promising results indicating that the textured tool surfaces may lead to replacement of environmentally hazardous lubricants with benign lubricants. This has led to a detailed investigation on parameters involved in the application of textured tool surfaces for sheet metal forming to improve lubrication by the *micro-hydrodynamic lubrication* mechanism.

1.2.2 Anti-Seizure Tool Coatings for Improved Resistivity towards Galling

A promising way to eliminate the hazardous lubricants is to perform the sheet stamping under dry lubrication condition or using a minimum quantity of hazard free lubricant by depositing an overlay hard coating layer to the tools, which impedes pick-up. A few promising tool coatings, i.e, Diamond-Like Carbon (DLC) coating [13][14] and pure diamond coating [15], have been reported to produce thousands of sheet components with no galling in deep drawing of aluminium, stainless steel and titanium under dry condition. Drawbacks of the pure diamond coating are cost and the fact that it can only be deposited on specific tool materials, e.g. tungsten carbide. Furthermore, it leaves a rough surface of crystalline diamond, which needs to be polished by a special ultrasonic vibration technique [16][17] to obtain a smooth surface. Adopting DLC may solve the galling problem, however literature reports the necessity of a good boundary lubrication in sheet stamping at high normal pressures such as ironing or blanking [18] due to the generation of a high shear stress in the DLC coating resulting in peeling off of the coating from the tool surface. Due to this, it is of importance to understand the DLC coating characteristics that can function in severe tribological stamping environments.

1.3   Project Work Plan

The present PhD project includes three work packages; WP1, WP2 and WP3.

WP1: Development of measurement technique for lubricant compressibility

In order to understand the *micro-hydrostatic lubrication* mechanism of lubricant entrapped in situations where the pressurized lubricant can carry the load, an important lubricant property designated as the bulk modulus is needed for characterizing the compressibility of the trapped lubricant at the tool/workpiece interface. The following tasks are described for laboratory tests to determine the bulk modulus:

WP1.1   Development and testing of a simple laboratory test with an inverse Finite Element Method (FEM) analysis to determine the bulk modulus.

WP1.2   Development and testing of a high-pressure equipment for directly measuring the bulk modulus.

WP2: Development and testing of structured tool surfaces

Surface textures are being utilized to improve lubrication and to reduce friction. The present work is centered on manufacturing structured textures on the tool surface. The following tasks are planned to promote lubricant entrapment and subsequent escape by the *micro-plasto-hydrodynamic lubrication* mechanism:

WP2.1   A detailed investigation and fundamental analysis of different textured tool arrangements in Strip-Reduction-Test (SRT), replicating an ironing operation.

WP2.2   A theoretical friction model for friction and lubrication based on the feasible textured tool patterns found in WP2.1.

WP3: Testing of anti-seizure DLC tool coatings

Sheet stamping operations without lubrication or using a minimum quantity of hazard free lubrication can diminish the application of hazardous oils in production. The following tasks are planned:

WP3.1   Screening test of DLC coatings in SRT under severe tribological test conditions.

WP3.2   Repetitive, laboratory simulation of industrial production using the promising coating candidate found in WP3.2.

1.4   Outline of the Thesis

In this thesis, literature and background for the project are reviewed in Chapter 2. The review covers the tribological systems analysis, lubrication mechanisms and factors that affect the mechanism of lubrication in sheet metal forming as well as measures taken to improve lubrication for sheet metal forming. Chapter 3 describes characterization methods of the metal materials involved in the project.

Techniques to impede galling in sheet metal forming are investigated and discussed in three major parts. Part I covers Chapter 4 and Chapter 5 regarding compressibility of liquid lubricants. Part II includes Chapter 6 and Chapter 7 on the subject of structured tool surfaces. Part III presents Chapter 8 and Chapter 9 concerning anti-seizure tool coatings.

Chapter 4 describes a first rough estimate in determining lubricant bulk modulus by means of a simple laboratory test and inverse FEM analysis. Chapter 5 elucidates a more advanced laboratory test based on a newly designed equipment for a direct determination of the bulk modulus at various pressure levels.

Chapter 6 presents a detailed background analysis of textured tool surfaces in SRT. Chapter 7 proposes a theoretical friction model of textured tool surfaces based on results found in Chapter 6.

Chapter 8 presents screening testing of DLC coatings from mild to severe tribological conditions. Chapter 9 deals with a more severe tribological test condition in a laboratory simulation of an industrial production process with the aim of determining the durability, as regards persistence of the promising coating found in Chapter 8, to pick-up and galling.

Finally, conclusions from the study and suggestions for future research are drawn in Chapter 10.

Chapter 2: Literature Review

2.1   Sheet Metal Forming and Lubrication

Lubrication is essential in most sheet metal forming processes. The lubricant film has two basic functions: i) to separate the workpiece and tool surfaces and ii) to cool the workpiece and the tool. Separation of the tool-workpiece surfaces by the lubricant film implies lower friction facilitating deformation, lowering the tool loads, reducing wear and avoiding pick-up of workpiece material on the tool surface.

2.1.1   Mechanisms of Lubrication

Four basic mechanisms of lubrication are identified in sheet metal forming [19]: i) hydrodynamic lubrication, ii) mixed lubrication, iii) boundary lubrication and iv) dry lubrication. The four mechanisms are shown schematically in Figure 2.1.

2.1.1.1 Hydrodynamic Lubrication

In hydrodynamic lubrication, the liquid lubricant film is thick enough to ensure complete separation between tool and workpiece asperities and the load is completerly carried by the pressurized, viscous film, see Figure 2.1a. The hydrodynamic lubrication is defined by metal surfaces separated by a continuous lubricant film having a thickness considerably greater than the height of the surface asperities of the metal. The hydrodynamic lubrication is seldom observed in sheet metal forming, however it is commonly observed in slide bearings where the lubricant is present in the bearing.

2.1.1.2 Mixed Lubrication

In sheet metal forming with liquid lubrication, the tribological conditions are insufficient for complete separation of the tool and workpiece. In the mixed lubrication regime, where the average film thickness is smaller, some asperity contacts are established and the load is supported partly by the asperities aand partly by the pressurized film trapped in the pockets of the rough workpiece surface, Figure 2.1b. At the asperity contacts, pick-up of workpiece material on the tool surface is typically prevented by a thin boundary lubricant film, Figure 2.1b. The assperity contacts may also be lubricated by escape of pressurized lubricant in pockets in the workpiece surface by so-called microhydrodynamic lubrication.

2.1.1.3 Boundary Lubrication

In case of pure boundary lubrication, as shown in Figure 2.1c, the interface load is completely carried by the asperities in contact and pure metal-to-metal contact is avoided by a lubricant film only one or a few molecular layers thick. The film may be physically adsorbed or chemisorbed on the metal surface. The classical phenomena of boundary lubrication are exhibited by organic films that contain molecules with permanent dipole moments, primarily derivatives of fatty oils, such as fatty acids, alcohols, and amines. They are characterized by a long hydrocarbon chain and a polar end that reacts with metal surface oxides. The long hydrocarbon chains are oriented perpendicular to the metal surface and further layers subsequent to the layer chemisorbed to the surface are held by weaker forces with increasing disorientation on moving from the surface monolayer into the bulk of the fluid.

Extreme Pressure Additives

Extreme Pressure (EP) additive is one of the special additive types. Mineral oils containing EP additives are commonly used in high volume sheet stamping production [20]. When subjected to a sufficiently high contact pressure, the lubricant can be squeezed out from between some of the asperities, permitting metallic contact at those points. Chemical interaction plays an important role in which the EP additive reacts as the interface temperature increases and generates a film by a chemical reaction with the oxide of the metal surface. This will generally provide a low shear strength film to reduce friction and physically help separating the workpiece from the tool. Since the EP additives may contain either chlorine, phosphorus or sulphur, the mineral oils with EP additives may have different levels of effectiveness, for instance, phosphorus is effective up to 250 °C, chlorine is effective between 205 and 700 °C, and sulphur is effective between 700 and 960 °C [21,22]. In most deep drawing operations, a thick lubricant film with extreme pressure additives is of major advantage in controlling friction and separating the workpiece against the drawing die and the blank holder.

2.1.1.4 Dry Lubrication

In case of dry lubrication, the interface load is completely carried by the asperities in contact when no lubricant film is present, see Figure 2.1d. Larger friction is present than in the boundary lubrication regime and this leads to an extreme, dry frictional contact in the absence of lubricant. The adhesion of the sliding metal surfaces can easily occur. This implies direct cold welding of the softer and weaker workpiece material to the tool surface and subsequently tearing of fragments out of the surface. The adhering particles plough through the surface and this leads to a quick progressing pickup development and galling.
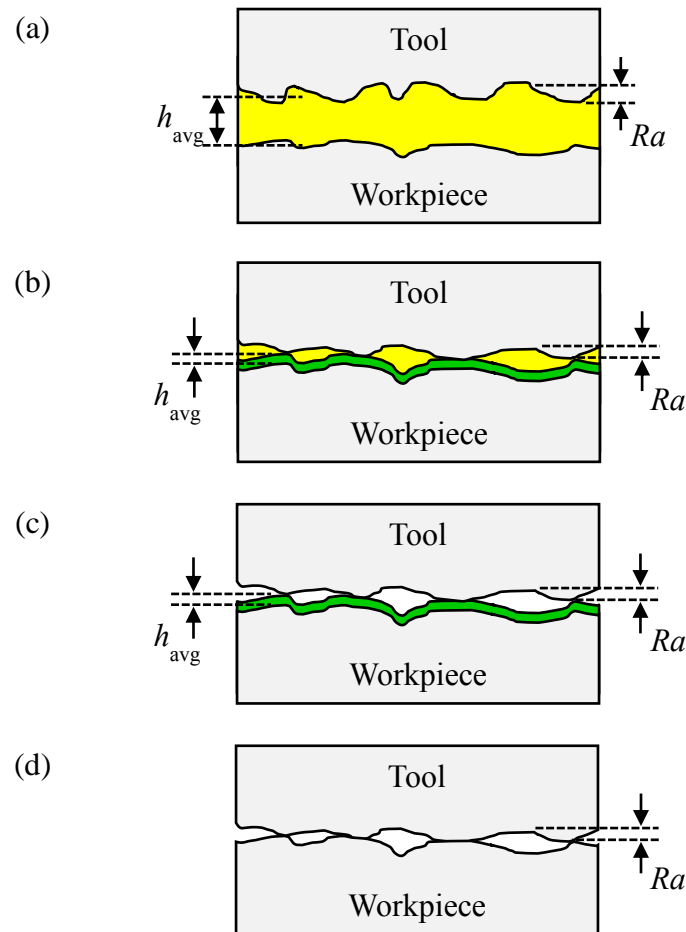
Figure 2.1: Schematic of lubrication mechanisms; a) hydrodynamic lubrication, b) mixed lubrication, c) boundary lubrication and d) dry lubrication. h_{avg} and Ra denotes average lubricant film thickness and average surface roughness. Yellow and green colours representing lubricant and boundary lubricant films respectively.

2.1.2   Mechanical Lubrication Mechanism of Entrapment and Escape

The micro-hydrodynamic lubrication mechanism was first introduced as an additional mechanism in the mixed lubrication regime by Mizuno and Okamoto [23] and later verified by Kudo et al. [24] and Azushima et al. [2,25]. Bay et al. have further investigated this mechanism and set up a mathematical model predicting the onset of this mechanism [3][26]. Similar modelling has later been done by Lo and Wilson [27], Azushima [28] and Stephany et al. [29].

Parameters controlling the micro-hydrodynamic lubrication mechanism are surface topography (pocket geometry), lubricant properties (viscosity and compressibility), sliding velocity, contact pressure (appearing pressure gradient across the individual lubricant pockets) and workpiece material [30]. The lubricant entrapment and escape within the pockets implies that the surrounding contact pressure can be

exceeded by the lubricant pressure acting on the edges of the lubricant pockets, thus the lubricant moves from a high- to a low-pressure regime occurring on the asperity plateaus.
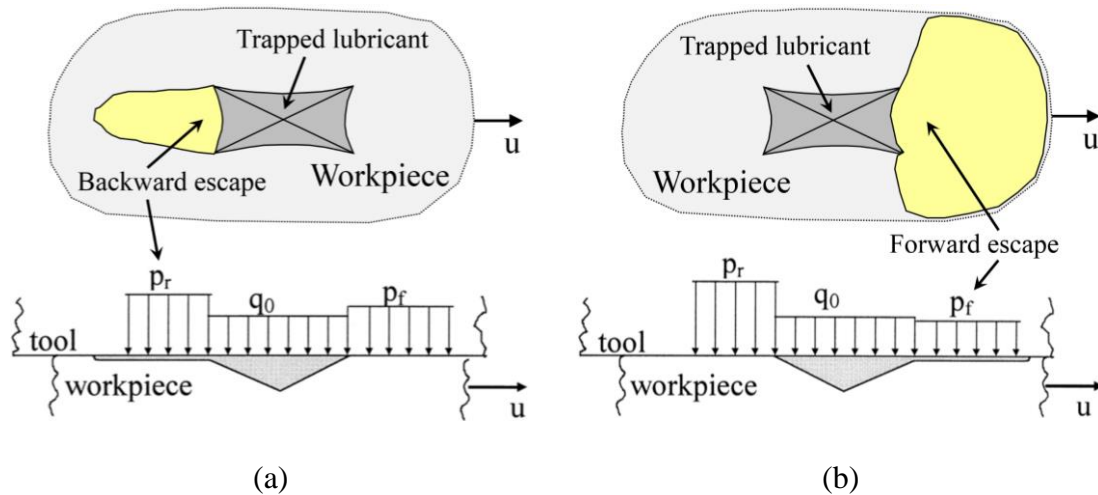

Figure 2.2: a) Backward and b) forward escape of lubricant [30]. Top view (top) and side view (bottom). Yellow, dark grey and light grey colours representing lubricant escape, trapped lubricant and tool/workpiece interface respectively.

The trapped lubricant may escape either backward, i.e. opposite to the sliding direction (Figure 2.2a) or forward (Figure 2.2b) or both [30]. The backward escape is identified as *Micro Plasto HydroDynamic Lubrication* (*MPHDL*) caused by viscous forces due to the relative sliding speed between the strip and tool surfaces. Distinguished from this, the forward escape is here interpreted as *Micro Plasto HydroStatic Lubrication* (*MPHSL*) occurring when the hydrostatic pressure in the trapped lubricant exceeds the tool/workpiece interface pressure on the surrounding plateau.

2.2 Galling

Galling occurs in situations where a sufficient load during the relative sliding between a smooth tool surface and a workpiece surface breaks a thin protective layer of lubricant film and oxides covering the metal surface asperities, and this permit metal-to-metal contact, see Figure 2.3a. It is, however, a disadvantageous situation since pick-up may take place under a sufficiently high load to permit welding of the workpiece to the tool surface, Figure 2.3b. A protective, thin layer may prevent this galling problem. It is often the case with stamping of sheet materials utilizing efficient but hazardous lubricants such as chlorinated mineral oils. In this way, the relative sliding between the metal surfaces activates the reaction of additives in the oils at elevated temperature by oxidation that can provide a strong molecular bonding to the exposed metal surfaces.
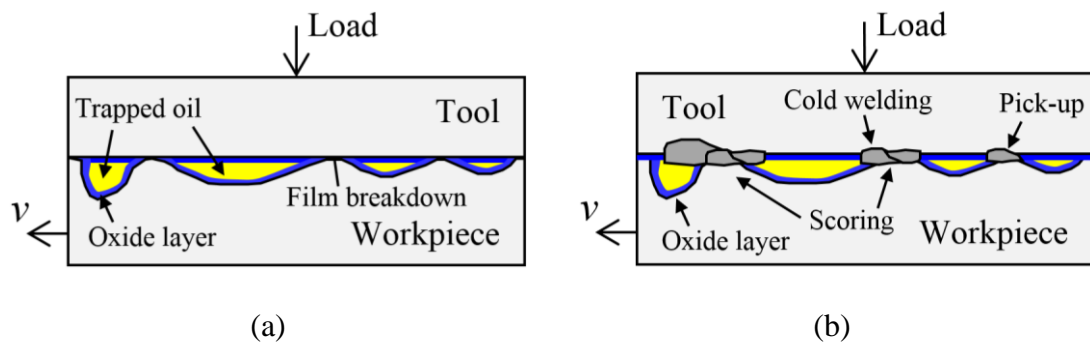
Figure 2.3: Schematic of a) lubricant film breakdown and lubricant entrapment by pressurization, and b) pick-up of workpiece material on the tool surface.

2.3 Laboratory Simulation Tests for Sheet Metal Forming

Reducing the environmentally hazardous lubricant consumption is a top priority within development and research in sheet metal forming tribology. The aim of the PhD project is to find alternatives, by means of mechanical approaches, to impede galling by less harmful lubricants or using no lubricant at all. In order to investigate potential measures and possibility of changing the most important process parameters influencing tribology systems, i.e. normal pressure, sliding length and tool temperature, under close control, full scale testing of tribological improvements is time-consuming and costly. It is however imperative to simplify the testing of tribology systems utilized for sheet metal forming by pilot simulative testing, enabling cost-effective screening of candidate tribological concepts.

Figure 2.4 shows laboratory simulation tests, where a blank slides against a deep drawing die. It functions to identify some unknown process parameters promoting a poor tribological system, and propose suggestions to prevent the identified problem afterwards. The parameters include lubricant types, coatings, surface topography, process speed, tool material, sheet thickness, tool geometry, etc. Typical simulative tests emulating various sheet metal forming processes are Bending-Under-Tension (BUT), Draw-Bead-Test (DBT), Strip-Reduction-Test (SRT), and PUnching-Test (PUT) [31][32]. The above mentioned simulative tests can be classified into ranks according to the severity of the tribological conditions, i.e. normal pressure, surface expansion and tool temperature, see Table 2.1. The BUT test possess the lowest risk of galling, followed by DBT, SRT and lastly, PUT considered as a high risk of galling. Two tribological simulation tests, BUT and SRT tests, are used in the present PhD project in order to investigate varying tribo-systems.
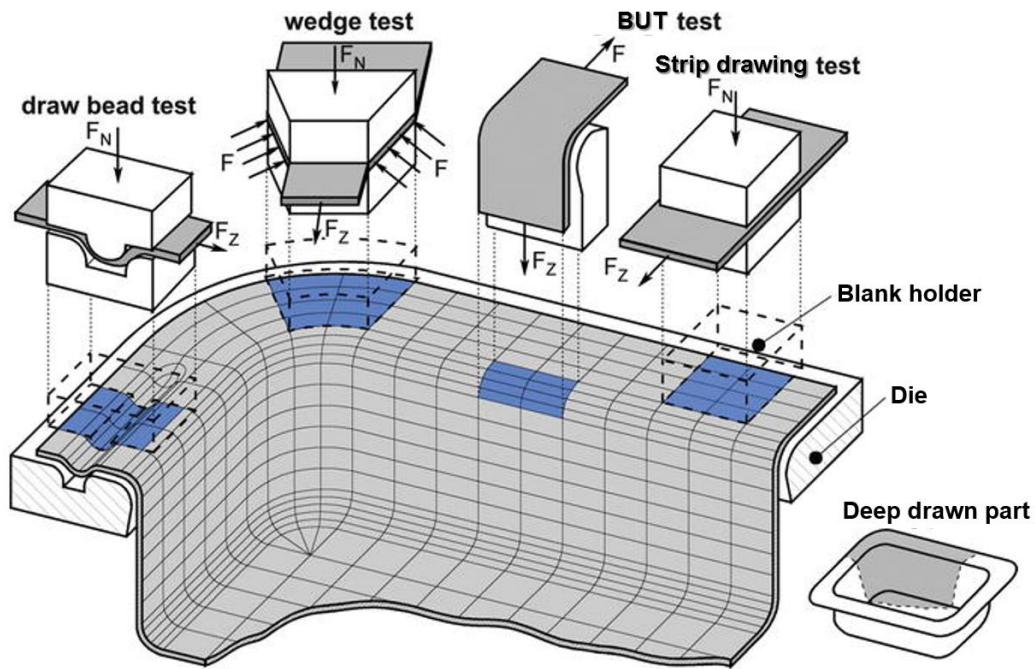
Figure 2.4: Tribological simulation tests emulating deep drawing [33].

Table 2.1: Sheet tribo-tests characteristics [34].

Test	Normal pressure	Surface expansion	Tool temperature	Tribological severity
BUT	Low	0	Low	Low
DBT	Medium	0	Medium	Medium
SRT	High	Medium	High	High
PUT	Medium-high	Infinite	Very high	Very high

2.3.1   *Bending-Under-Tension (BUT)*

The Bending-Under-Tension test, also called the BUT test, equipment shown in Figure 2.5a developed earlier at DTU-MEK specifically for studying a large number of parameters on friction and limits of lubrications, for instance, lubricants, speeds, workpiece materials and tool-pin radii. The influence of varying tool temperature can also be taken into consideration in the study in which electric heaters can be inserted into the tool-pin holder heating up the tool-pin to maximum 100 °C.
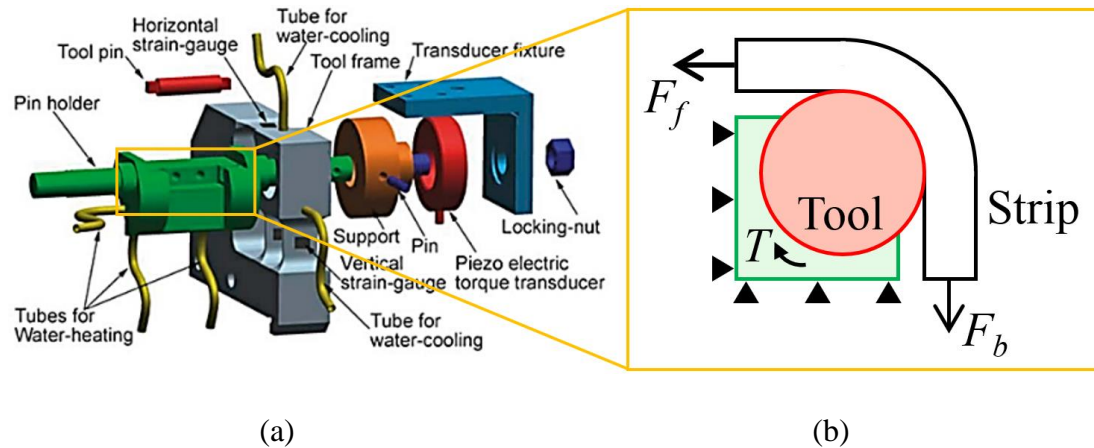
(a)   (b)

Figure 2.5: a) Exploded view of BUT equipment [35] and b) Schematic of the BUT test.

The BUT test is performed by drawing a strip around a fixed, circular cylindrical tool-pin, Figure 2.5b. The strip is pulled by a front claw while the back claw with a controlled force ensures sliding of the strip around the tool-pin under controlled back tension force. Front and back tension forces are delivered by hydraulic cylinders. The experiments can be performed while measuring front tension force F_f and back tension force F_b of the strip by load cells as well as measuring torque T on the tool pin by a piezoelectric transducer. As such, friction on the tool-pin can then be measured directly by the piezoelectric torque transducer.

2.3.2   *Strip-Reduction-Test (SRT)*

The Strip-Reduction-Test, also called the SRT, has been developed specifically for the same purpose as mentioned in the BUT test to evaluate a large number of parameters on friction and limits of lubrications, for instance, lubricants, speeds, materials, radii and tool temperature. Two different tool-pin geometries were developed for the SRT set-up at DTU-MEK. One is a round tool surface and the other is a flat tool surface. The advantage of circular tool surface is that the set-up allows four tests with the same tool-pin by turning the tool 90° after each test. It is possible to run the SRT test up to a maximum of eight tests, when the end surface of the tool pin is designed as an octagon.
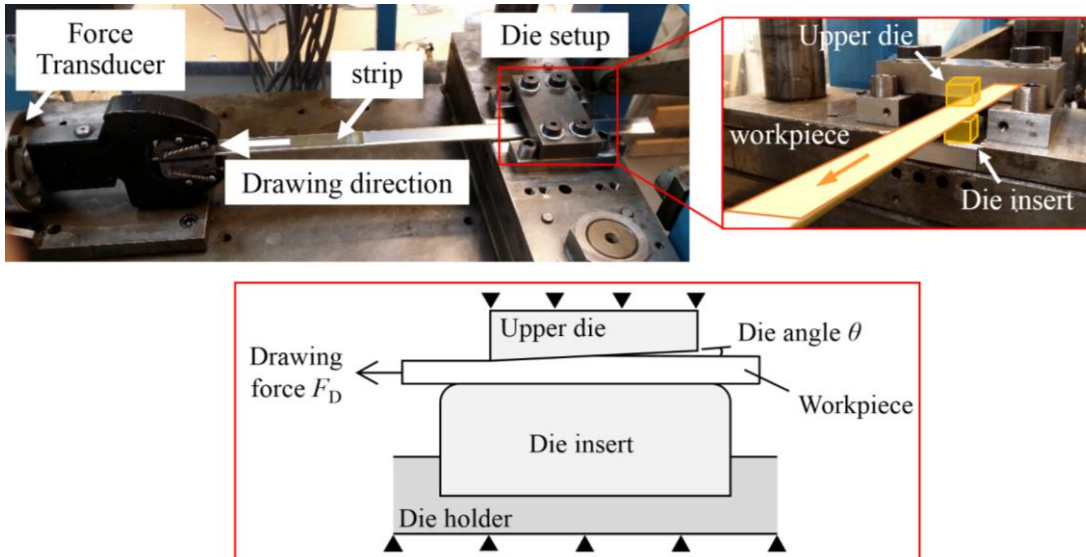
Figure 2.6: Outline of the SRT set-up (top) with interchangeable squared, flat die surface (bottom). The black triangles stand for a fixed support.
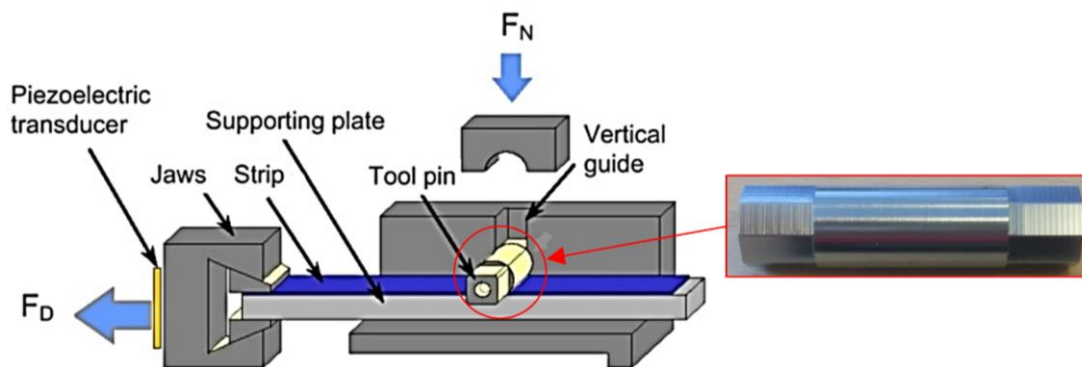

Figure 2.7: SRT set-up [36] (left), and the circular tool-pin fabricated with octagonal end shape (right).

The schematic of the SRT set-up by utilizing a flat die insert is shown in Figure 2.6 and by using a round tool-pin in Figure 2.7. The SRT experiment can be performed by drawing a strip over a fixed, circular tool-pin or a fixed, flat die insert in horizontal direction up to varying sliding length under constant thickness reduction. The reduction r in sheet thickness may be varied. Drawing force is measured by a piezoelectric transducer. Threshold sliding for the onset of galling is determined by visual inspection of the drawn strip and by roughness profile measurements of the strip perpendicular to the drawing direction. In this PhD project, the SRT set-up with the flat die surface was used for studying structured tool surfaces, as described in Part II in Chapter 6 and Chapter 7. Meanwhile, the SRT set-up for the round tool-pin was used for investigation of anti-seizure DLC tool coating, as explained in Part III in Chapter 8 and Chapter 9.

2.4   Severity of Tribological Conditions

Sheet stamping includes single- and multi-stage operations. In single-stage operations, a single tool set will shape a strip or a sheet metal into a desired form. In a multi-stage operation, the workpiece undergoes a series of deformation steps in multiple dies in order to attain a designated form. Figure 2.8 shows multi-stage sheet stamping of stainless steel in a progressive tool [37]. The process starts with blanking (1 and 2), followed by a deep drawing operation (3) and two redrawing operations (4 and 5), sharp pressing of the flange (6) and punching the bottom hole (7).
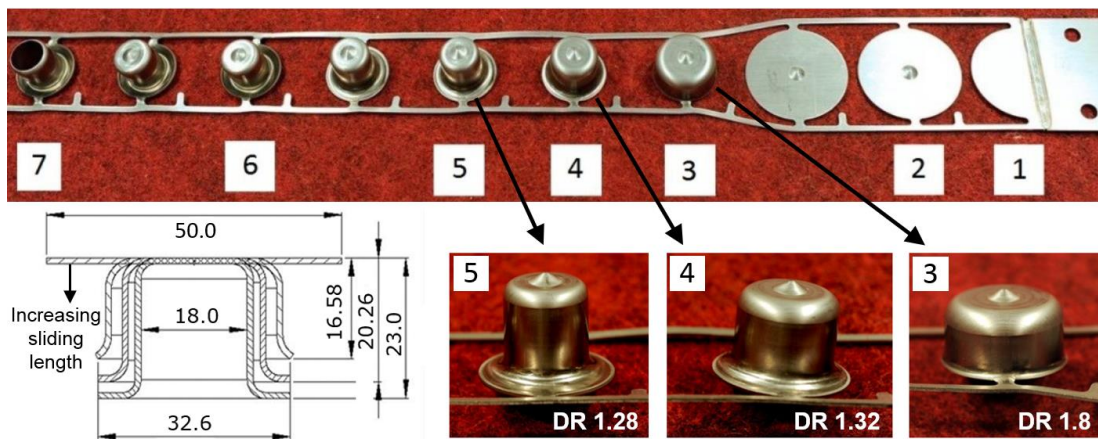
Figure 2.8: Sheet stamping production layout in progressive dies [37].
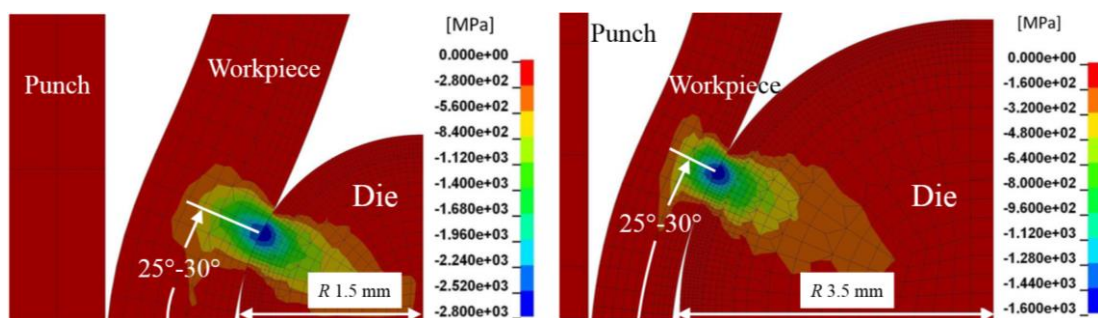
Figure 2.9: In operation 3, a localized normal pressure on the die surface appears at 25°-30° die angle. Die radius R1.5mm (left) and R3.5mm (right) [38].

The tribological severity of the multi-stage operation increases from stage to stage due to increased sliding length, temperature and strain hardening of the workpiece. From Figure 2.8, the occurrence of galling was identified in stage 5. This is due to a very small die radius that reduces the contact area, and as a result, a very high localized normal pressure of 2,800 MPa exists at a 25°-30° die angle. To avoid galling,

the die radius was then increased since a larger die radius implies a decrease of the localized normal pressure to 1,600 MPa, see Figure 2.9. Here, the numerical analysis revealed that the normal pressure is a dominant process parameter that can cause lubricant film breakdown and pick-up of workpiece material on the tool surface.
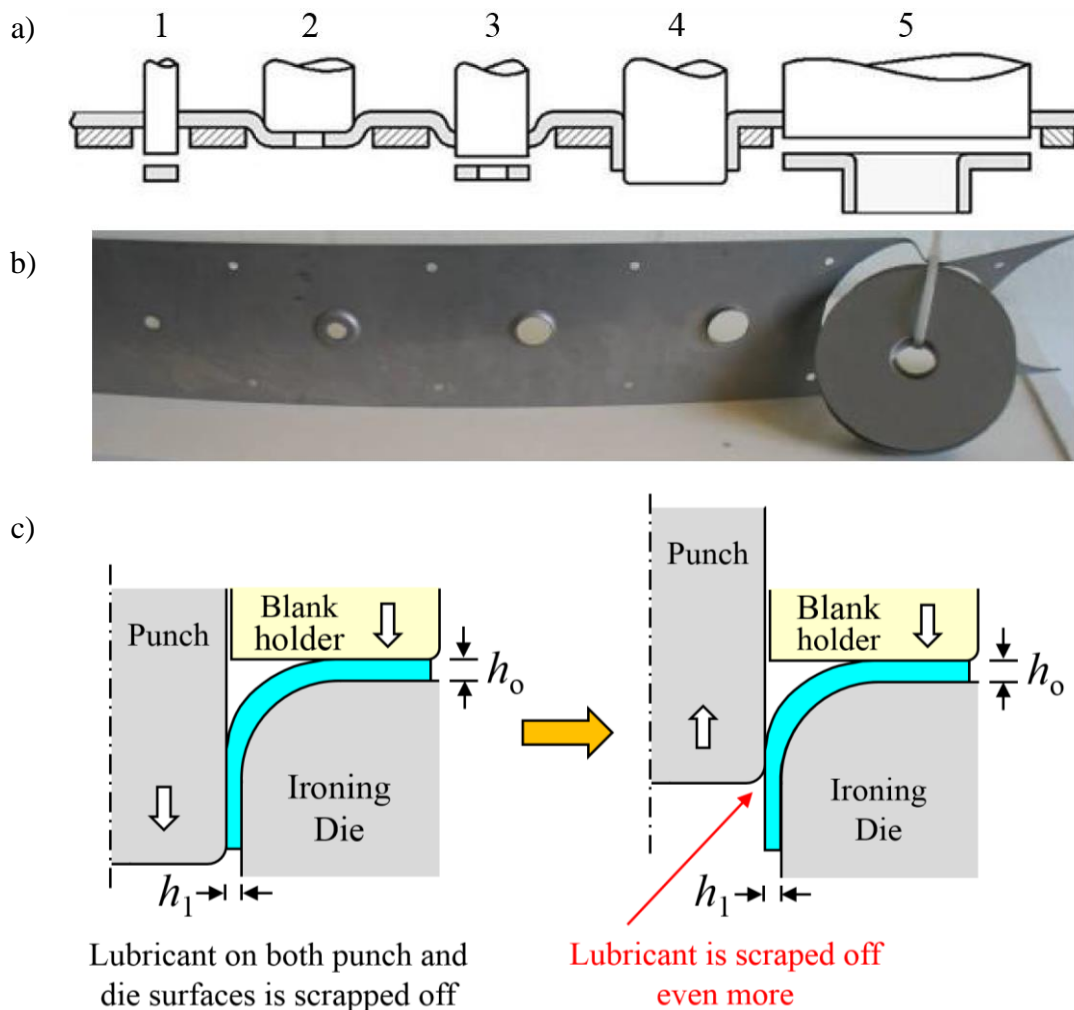
Figure 2.10: Production test in a progressive tool. a) Schematic outline of a five-step operation, b) deformed strip, and c) outline of collar drawing and ironing operation [39].

Stamping of sheet metals in progressive tools offers high volume metal stamping capabilities. Figure 2.10a and Figure 2.10b illustrates a schematic outline of a five-step progressive tool producing a stainless steel component [39]. The five steps are as follows: 1) Punching, 2) deep drawing, 3) punching, 4) collar drawing and ironing, and 5) blanking of the finished components. Operation 4 shown in Figure 2.10c is found to be the tribologically most critical operation leading to lubricant film breakdown and galling. Due to this, very efficient boundary lubricants are applied. Other factors than the high normal pressure in operation 4, such as repetitive strokes

and a fast production rate, can also be a main issue to this galling problem when it comes to large volume of sheet metal produced. More produced units per minute increases productivity, however the drawback here is that the temperature increase at the tool/workpiece interface will decrease lubricant viscosity, which promotes pick-up and galling.

While the punch return to its original position, the lubricant is scraped off further when the punch moved upwards, see Figure 2.10c. At this stage, galling occurs between the punch and the workpiece surfaces. Two possible reasons contribute to this galling problem. First, direct metal-to-metal contact in which almost no lubricant is present, and this can cause temperature increase and larger friction on the punch and the workpiece surfaces. Second, elastic deformation of the punch and springback of the deformed workpiece [40,41] may also contribute to extra reduction in thickness during the back stroke.

2.5   Mechanical Modification Techniques of the Tool Surface

A large amount of lubricant is necessary for a high volume sheet stamping production. This will further increase the risks to health hazards if the efficient but hazardous lubricant is being employed in production as the only reliable solution to impede galling. Aside from the good boundary lubricants, other techniques by means of mechanical approaches exist to impede galling, for instance, anti-seizure tool materials, structured surface topographies, and anti-seizure tool surface treatments (either by coatings or by thermochemical diffusion). To date, some of them are being used in production, i.e., application of structured workpiece surfaces by using large rolls roughened by Shot Blast Texturing (SBT) or Electro Discharge Texturing (EDT) [8].

In this PhD project, the target is set towards development and testing of tailored tool surfaces by means of mechanical surface modification. In the following sub-sections, trends and applications of two potential measures taken to decrease the environmentally hazardous lubricant consumption as regards modifications to the tool surface were reviewed and discussed; 1) structured tool surfaces and 2) anti-seizure tool coatings.

2.5.1   Structured Tool Surfaces

Surface textures are progressing rapidly with the aim to achieve an efficient lubrication system. Significant knowledge gains regarding surface textures have meant that the technique is feasible to improve the lubrication system in engineering applications, i.e. bearings, internal combustion engines, metal cutting, and metal forming.

Engineered workpiece surface topography by creating pockets for the entrapment of lubricant has become state-of-the-art in the past years but it is less feasible in multi-stage operations since pockets are flattened out after the first forming operation [9]. Texturing of the tool surfaces would be much more economically feasible, since a textured tool surface can be utilized for thousands of workpiece components before it is worn out. A few tests of surface engineered deep drawing tools have shown very promising results [42–46] indicating that tailored tool surfaces may lead to replacement of environmentally hazardous lubricants with benign lubricants. A great number of surface texturing techniques are available for texturing of hard tool materials such as combined milling, grinding and manual polishing [47], chemical etching [48], rolling ball indentation [49] and laser radiation [50,51]. It is however important to understand the influence of the surface texture parameters and the mechanism of lubricant entrapment and escape.
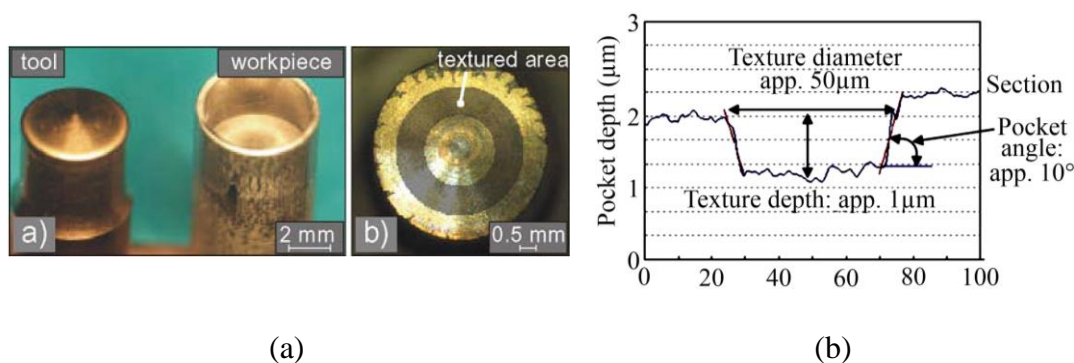

(a)   (b)

Figure 2.11: a) Textured punch nose used for backward can extrusion and b) the lubricant was manufactured with a small pocket angle [52].

Some potentially determining surface texture parameters needs to be identified in order to promote micro-hydrodynamic lubrication mechanism. One of the feasible surface texture parameters is lubricant pocket geometry. A small pocket angle can improve lubrication and it works by pressurization of trapped lubricant inside the pocket and subsequent escape by micro-plasto-hydrodynamic lubrication [53]. The smaller the pocket angle, the easier it is to drag out the trapped lubricant. Application of such small pocket angles, less than 10°, on a punch nose in backward can extrusion has shown significant improvements in the tool life [16], Figure 2.11. The friction reduction is more pronounced with a smaller pocket angle since the elimination of the sharp curve bend at the pocket edges prevents mechanical interlocking of the penetrating workpiece material into the pocket edges [42]. Robot Assisted Polishing (RAP) technique is advantageous to produce the small pocket angle oriented to the sliding direction. BUT tools manufactured with a contact ratio between the pocket area and total area at approximately 5 percent to 25 percent by using the RAP technique improves the tool life in comparison to the smooth tool surface [54]. In strip drawing

tests, a low friction can be achieved when the contact ratio between pocket area and total area is approximately 20 percent [55] and it is shown that increasing drawing speed enhances these effects [49].

Closed lubricant pockets are much more advantageous than open pockets [56]. The developed hydrostatic pressure of the lubricant trapped in the closed pockets share the external load with the asperities, thus reducing the normal pressure on the asperities, which results in lower friction. A study of open and closed pockets manufactured on the deep drawing die surface has shown that the open pockets increased the friction. The open pockets are meant to function effectively in controlling material flow of the workpiece material sliding against the textured die surface, Figure 2.12b. Reduction of friction by pressurization of the trapped lubricant inside the closed pockets further enhanced lubrication [57], Figure 2.12c.
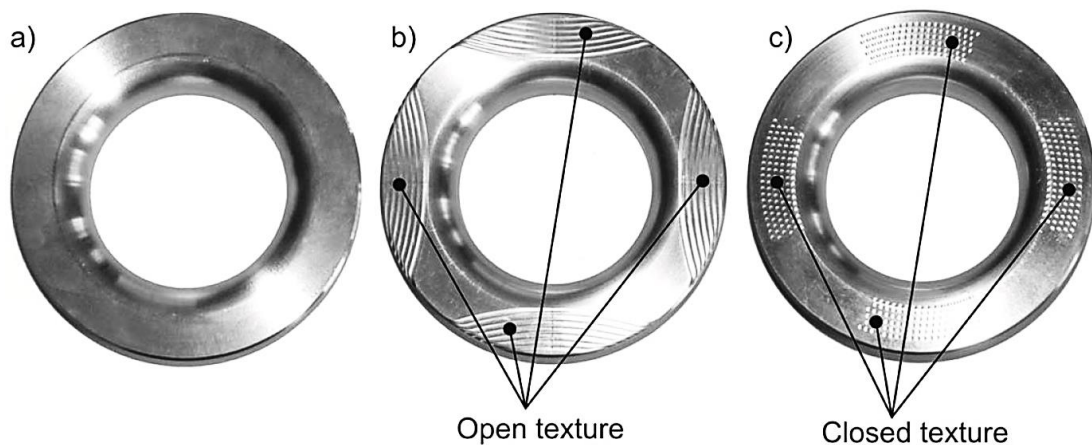

Figure 2.12: Deep drawing die manufactured with a) non-textured, b) open lubricant pockets and c) closed pockets [57].

A proper selection of orientation of the lubricant pockets enhances the retention mechanism. A transverse, long groove perpendicular to the sliding direction enhanced lubrication in comparison to a smooth surface and other surface features such as dimple pockets, chevron pockets and a parallel groove oriented to the sliding direction [18]. A similar effect has been found in transverse grinding and polishing techniques on the tool surface in the Bending-Under-Tension (BUT) test [17], [12]. The transverse textured surface profiles restrained lubricant flow and probably entrapped more lubricant in order to carry some of the external load. Strip reduction tools manufactured with a transverse arrangement of the closed pockets perpendicular to sliding direction minimizes friction when a small amount of a hazardous lubricant is applied [58]. Similar findings of manufacturing the transverse, long groove perpendicular to sliding direction on a strip drawing tool can also be found in [59]. Application of a hard coating to the structured tool surfaces further reduced galling occurrence.

In this study, the application of structured surfaces to the tools is carried out without coating with the aim directed towards surface texture parameters that are beneficial to promote micro-hydrodynamic lubrication mechanism.

2.5.2 Anti-Seizure Tool Coatings

The deposition of a hard coating to the tool surface is known to prevent galling [39]. A study of tools with titanium-based coating and without coating under different tribo-systems such as initial temperatures of 20 °C and 50 °C in SRT has demonstrated that the coated tool is generally superior in all tribo-systems at room temperature, see Figure 2.13a. A more pronounced result is found at higher tool temperatures, where the lubricant film is stressed more, see Figure 2.13b.

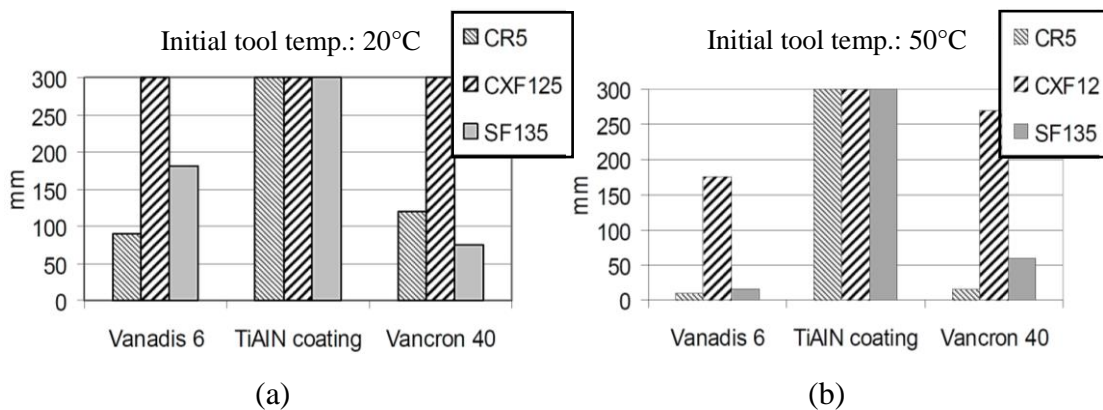(a)   (b)

Figure 2.13: Threshold sliding length before galling in SRT of different tribo-systems, with initial tool temperature of a) 20 °C and b) 50 °C [39].
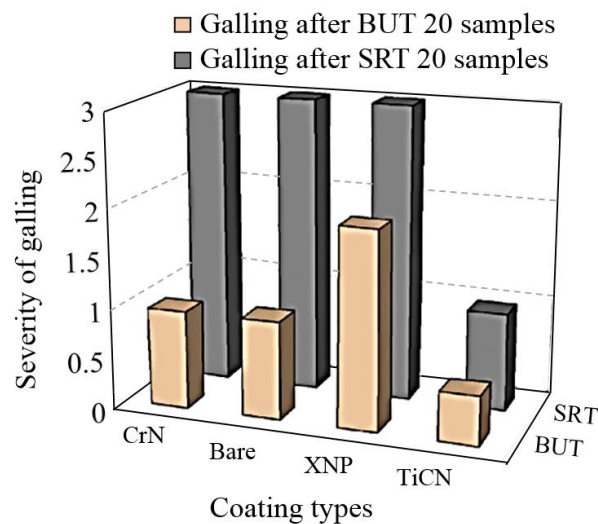

Figure 2.14: Ranks of galling relating to comparisons based on die surface qualities for various tool coatings performed in BUT and SRT [60].

(a) Configuration of specimen (yellow) and the die insert (grey)

(b)
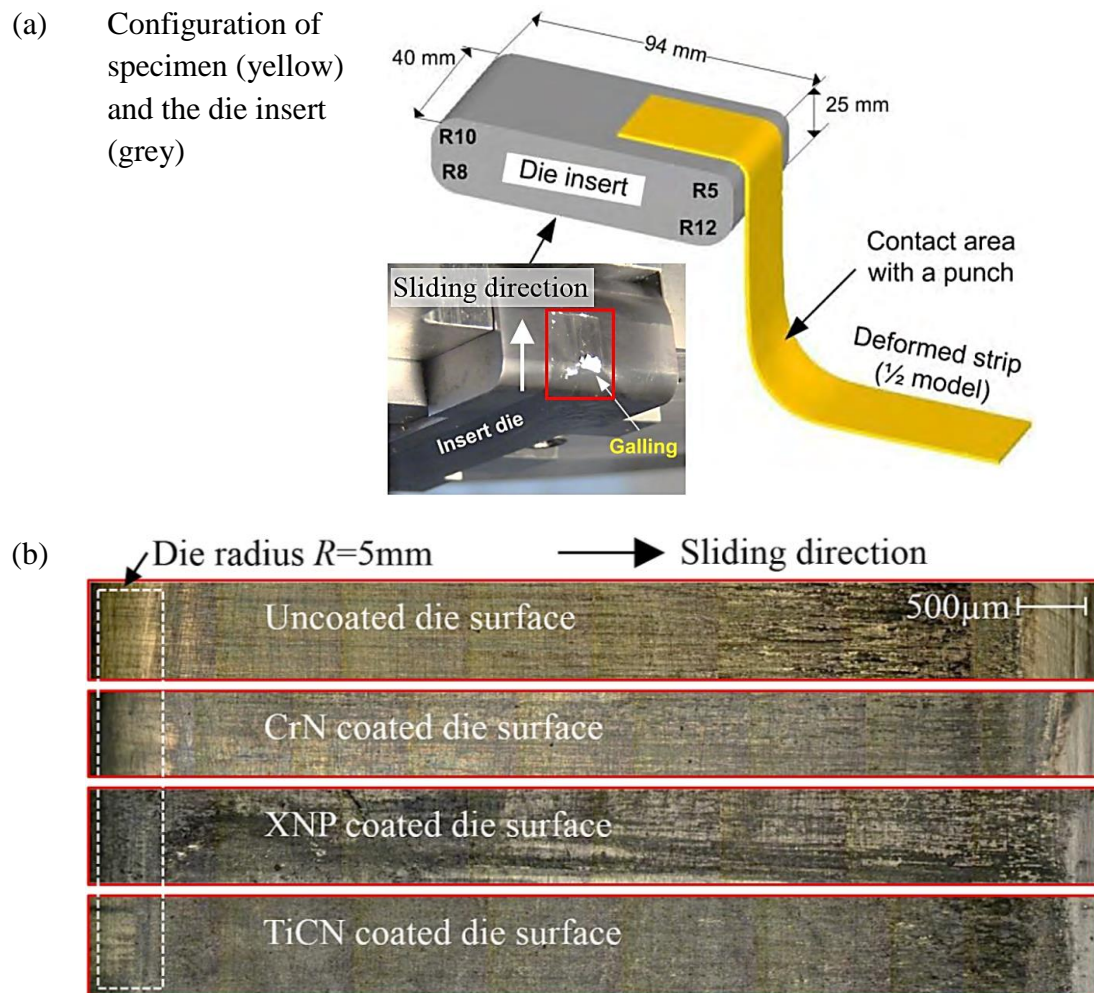
Figure 2.15: a) Schematic of BUT and SRT tests, and b) surface topographies of uncoated and coated die inserts after conducting repetitive experiments in the SRT (bottom) [61]. The red square in (a) marked the approximate location of the micrographs in (b).

A similar result, adopting the titanium-based coating such as TiCN, can be seen in Figure 2.14. The titanium-based, chromium-based and nitride-based coatings were deposited on the tool surface and they were tested in BUT and SRT of Advanced High Strength Steel (AHSS), i.e, DP590, TRIP780 and DP980, at room temperature. The severity of galling was qualitatively ranked with a visual inspection after conducting 20 specimens in BUT and SRT tests by using various tool coatings [60]. The results have shown that the titanium-based coating is found to be the best tool coating in reducing galling in BUT and SRT. A more severe tribological condition is observed when testing the coated tools in SRT, where the titanium-based coating is the only coating that can work effectively at a larger normal pressure occurring at the tool/workpiece interface, see Figure 2.15 [61]. The experimental results concluded that a polymer based lubricant

with pressure additives is found necessary in both operations involved in sheet metal forming [60].

A promising way to eliminate hazardous lubrication issues is to perform the sheet stamping under dry lubrication condition or using a small amount of hazard free lubricant to the hard coated tools, which impedes pick-up. A few promising tool coatings have been reported to work in deep drawing of aluminium, stainless steel and titanium under dry friction conditions or with minimum lubrication. They include Diamond-Like Carbon (DLC) coating [13,14] and pure diamond coating [15]. Both coating types are able to produce thousands of sheet components without galling. In addition, a diamond coated die resulted in a 20% reduction of the drawing force in dry deep drawing with a subsequent 10% ironing of magnesium alloy at elevated temperature as compared to lubrication with MoS_2 [62]. Drawbacks of the pure diamond coating are cost and the fact that it can only be deposited on specific tool materials, e.g. tungsten carbide. Furthermore, it leaves a rough surface of crystalline diamond, which needs to be polished by a special ultrasonic technique to obtain a smooth surface. Adopting DLC, literature reports the necessity of lubrication in sheet stamping at high normal pressures such as ironing or blanking [18] due to the generation of a high shear stress in the DLC coating resulting in peeling off of the coating from the tool surface.

Although a thin layer coating deposited on the tool surface can improve frictional and wear properties of the coated tool surface, stresses induced in the coated tool become a major problem since it always influences the adhesion strength of the coating. Tailoring the interaction between the coating and the tool surface is a method to prevent the adhesion problem. For instance, depositing multilayer coating structures on the tool surface offers films with improved internal stresses of each coating layer, while retaining high hardness, good adhesion and wear properties [63], [64]. The multilayer coatings with optimized layer thickness condition serves to improve hardness and modulus of elasticity of the coating structure, which increases the load-carrying capacity due to improved mechanical properties of the coated tool surface [65]. Adopting an increased surface roughness of the tool substrate prior to coating [66] is a useful technique for improved coating adhesion but it generates a larger surface roughness after coating, which is difficult to polish to a sufficiently low final surface roughness.

A proper selection of interlayer coating types, number of interlayer coatings and interlayer coating thickness promotes an improved Young's modulus and hardness of the coating. This will enhance persistence of the coated tool towards pick-up [63], where a graded multilayer structure is a better alternative compared to a conventional one [64]. A good combination of high hardness and low friction coating further promotes low wear rate [67]. This is attributed by the Physical Vapor Deposition (PVD) depositing technique, which yields coatings with high levels of adhesion, dense and packed structures, and provides a smooth macro particle free surface [68].

Chapter 3: Material Characterization

3.1   Introduction

The flow stress curve of a material is important when analyzing material deformation in sheet metal forming processes. The flow stress curve characterizes the strain hardening of the sheet metal. The flow stress curve of a material can be determined in different ways, e.g. by uniaxial tensile testing or by uniaxial compression testing. The main challenge is, however, to determine strength of a material at large strain without extrapolation. Therefore, investigations of different experimental methods were studied to evaluate strength of workpiece materials.

Each different material test has its limitation to determine strength of the material as a function of strain. Some common material strain hardening expressions being used in this study are shown below.

$$\text{Hollomon:} \quad \sigma_f = C\varepsilon_{eff}{}^n \qquad\qquad \text{[MPa]} \qquad (3.1)$$

$$\text{Swift:} \quad \sigma_f = C\big(\varepsilon_o + \varepsilon_{eff}\big)^n \qquad\qquad \text{[MPa]} \qquad (3.2)$$

$$\text{Voce:} \quad \sigma_f = B + (B - C)\big[1 - exp\big(-P\varepsilon_{eff}\big)\big] \qquad \text{[MPa]} \qquad (3.3)$$

$$\text{Ludwik:} \quad \sigma_f = \sigma_o + C\varepsilon_{eff}{}^n \qquad\qquad \text{[MPa]} \qquad (3.4)$$

where, σ_f is the flow stress, ε_{eff} is the effective strain, n is the strain hardening exponent, ε_o is the pre-straining, σ_o is the initial yield stress, B and C are the strength coefficients and P is a constant.

3.2   Characterization Methods of Metal Materials

The following section describes experimental techniques used for determining the flow stress curve of a raw material.

3.2.1   Tensile Test

Uniaxial tensile testing is commonly used to determine the material behaviour. However, the strain range is limited by necking which occurs at rather low strain. In the tensile test applied here, the test workpiece was commercial aluminium 99.5% with dimensions L 250 mm x W 20 mm x t 4 mm. The experimental stress-strain curve was computed using MATLAB. The MATLAB code is shown in Appendix A1. Figure 3.1 indicates the resulting stress-strain curve fittings according to Hollomon (Eqn. 3.1), Swift (Eqn. 3.2), Voce (Eqn. 3.3) and Ludwik (Eqn. 3.4) material models. The strain

hardening behaviour of the aluminium can only be determined by the tensile test to a strain 0.18 due to necking. In this tensile test of the aluminium workpiece, the experimental data fitted very well to the Hollomon, Swift and Ludwik materials' models in which both Ludwik and Swift material models have been reduced to Hollomon model. The Voce material model does not satisfy the fitting curve for the experimental data.
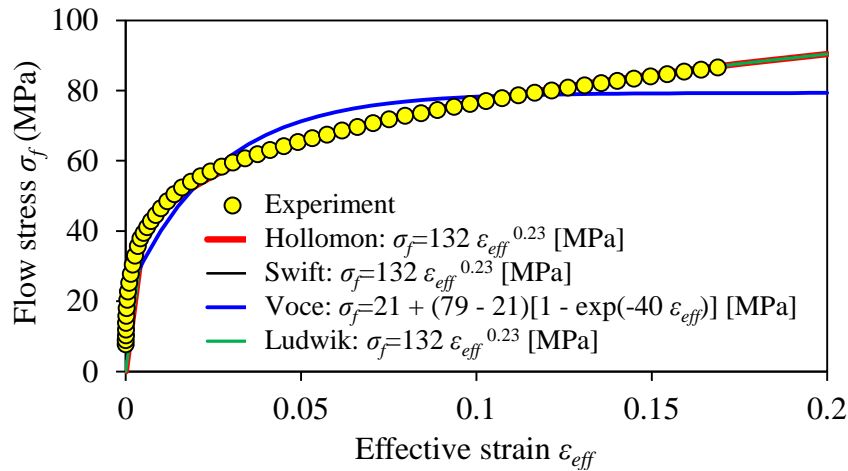

Figure 3.1: Stress-strain curve for Al 99.5 % with different material models determined by tensile testing.

3.2.2   *Cylindrical Compression Test*

A cylindrical compression test, also known as upsetting test, was performed for characterizing work hardening at larger strains. There are two billet types that were used; a cylindrical billet (Figure 3.2a) and a Rastegaev specimen having an oil recess on both end billet surfaces (Figure 3.2b). In this test, Teflon as well as grease were used to ensure low friction in the tool/billet interface and to ensure homogenous metal deformation during the test.

In this cylindrical compression test, the workpiece material was commercially pure aluminium Al 99.5 % in form of a hot extruded cylindrical rod. Friction minimizers used in the tool-billet interface were Teflon and grease (Molycote DX paste). The experimental stress-strain curve was computed using MATLAB. The MATLAB code is shown in Appendix A2. Figure 3.3 presents experimental stress-strain data on all billet types and they were approximated by Hollomon's material model, Eqn. 3.1. The determined material constants up to an effective strain of approximately 0.7 was obtained for this aluminium material. In this test, the cylindrical specimen lubricated with Teflon gave excellent lubrication condition and remain almost cylindrical during testing.
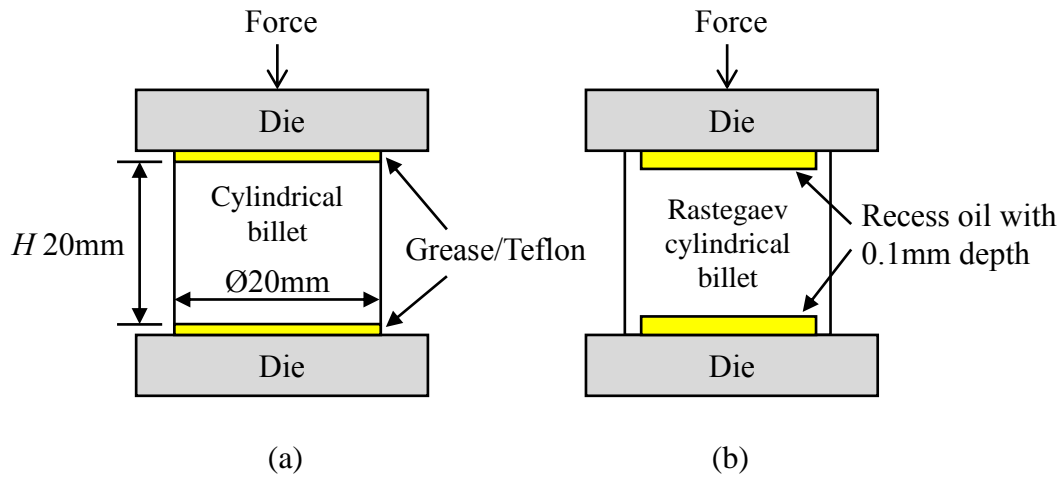
Figure 3.2: Upsetting tests with a) cylindrical specimen and b) Rastegaev specimen having an oil recess of 0.1 mm (figure not drawn to scale).
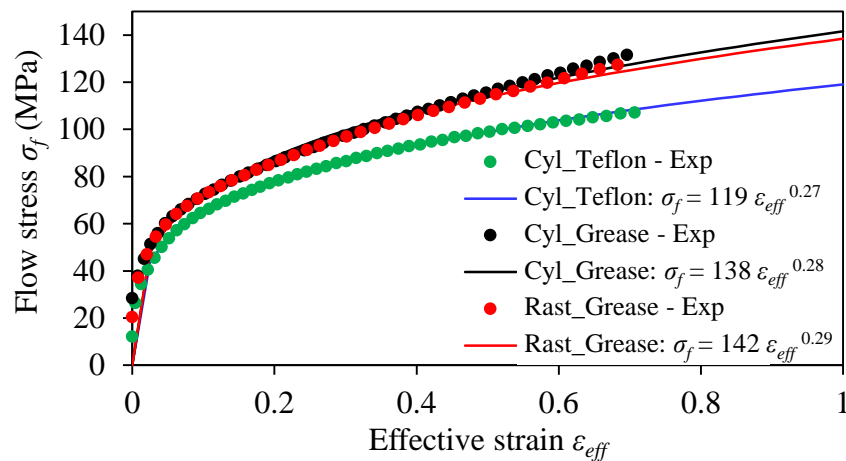
Figure 3.3: Stress-strain curves for Al 99.5 % based on Hollomon's material model for the tests with cylindrical specimen lubricated with grease and Teflon, and Rastegaev specimen lubricated with grease. The unit for the Hollomon flow stress curve is MPa.

3.2.3 Plain Strain Compression Test

Figure 3.4 shows a schematic of the setup for the plane strain compression test. The test is also known as Watts & Ford test. The plain strain compression tests with two specimen types were performed. One was a solid specimen, Figure 3.5a, and the other one was a stack of sheet specimens, Figure 3.5b. The accuracy and reliability of the results has been confirmed by ref. [69], where the stress-strain curve of the compression tests with a stacked cylindrical specimen was found to be similar to that of a conventional solid cylindrical specimen.
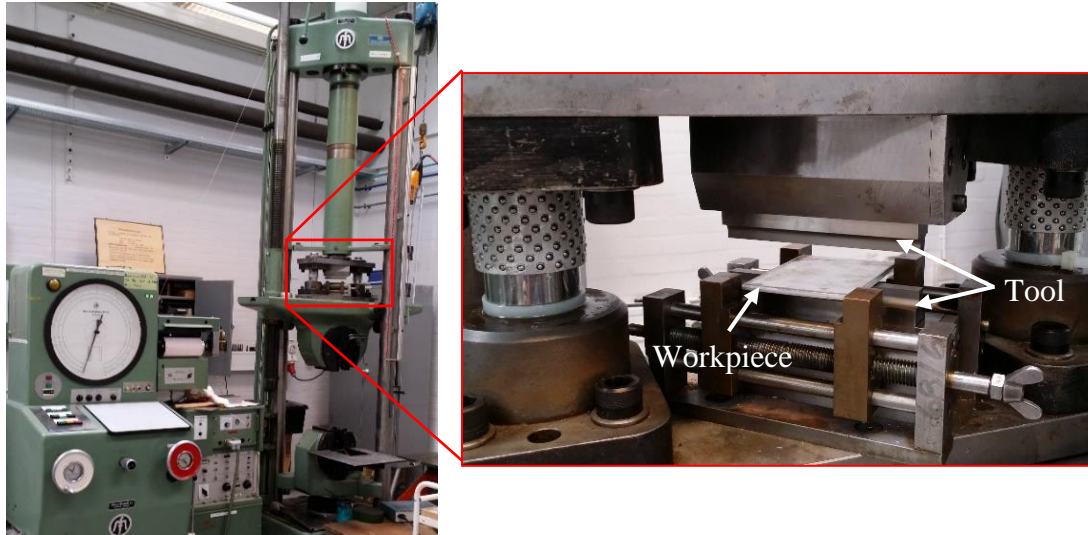
Figure 3.4: Plain strain compression test setup mounted in a 60 tons hydraulic press.

In this test, the material dimensions where: l x b x t = 100 mm x 70 mm x 4 mm. The lubricant was grease, Molycote DX paste. During testing, the specimen was indented by three different tool widths w of 2.5, 5 and 10 mm that accounts for the ratio of thickness to width $t/w = 0.25 - 0.5$. The ratio t/w is essential to ensure homogenous plastic deformation during compression and minimum influence of friction. Figure 3.6 shows the experimental results of 4 mm thick aluminium Al 99.5% − H111 material with determined materials constants according to the Hollomon (Eqn. 3.1) and Voce (Eqn. 3.3) material model expressions up to larger effective strain values. The experimental stress-strain curve was computed using MATLAB. The MATLAB code is shown in Appendix A3.
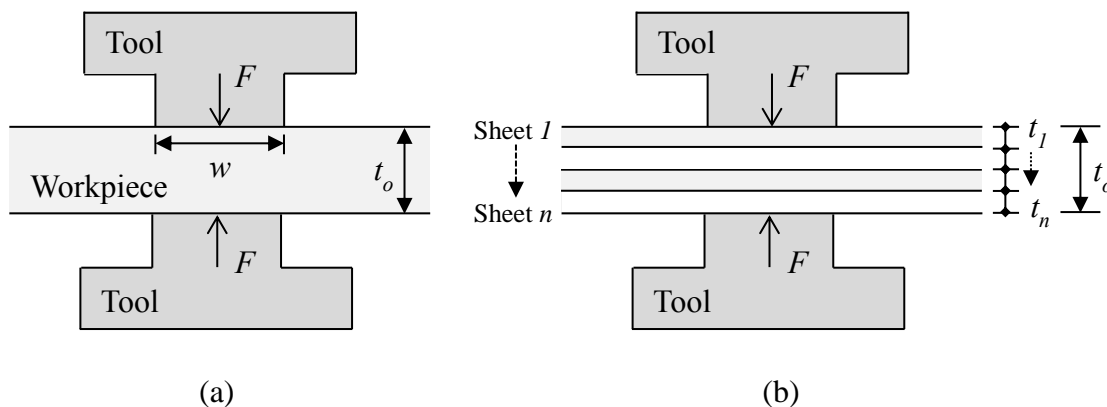
Figure 3.5: The plane strain compression test of a) solid and b) stacked specimens.
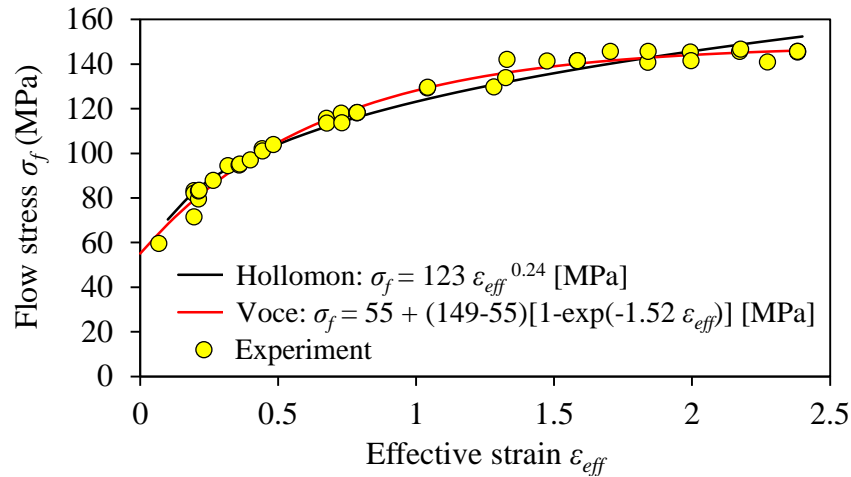
Figure 3.6: Stress-strain curve for 4 mm aluminium Al 99.5 % plate.

Compression of a stacked specimen was performed on a 1 mm thick stainless steel EN1.4307, with a total of 5 pieces of plates that is equivalent to 5 mm thickness. This has led to a stress-strain curve with a strain value up to 0.5, see Figure 3.7. Although the plain strain compression test, which is utilized here, can predict the flow stress curve of soft materials, such as aluminium, up to a higher strain values of approximately 1 to 2, it is noticed that the stainless steel sheet tends to fracture at a lower strain value of approximately 0.3 to 0.5 when applying the tool width w of 2.5. If the tool width w of 5 mm is to be used to determine the flow stress of the stainless steel at larger strain, a larger force is necessary, where the current press machine can only supplied forces up to a maximum value of 50 tons, which is equivalent to 500 kN.
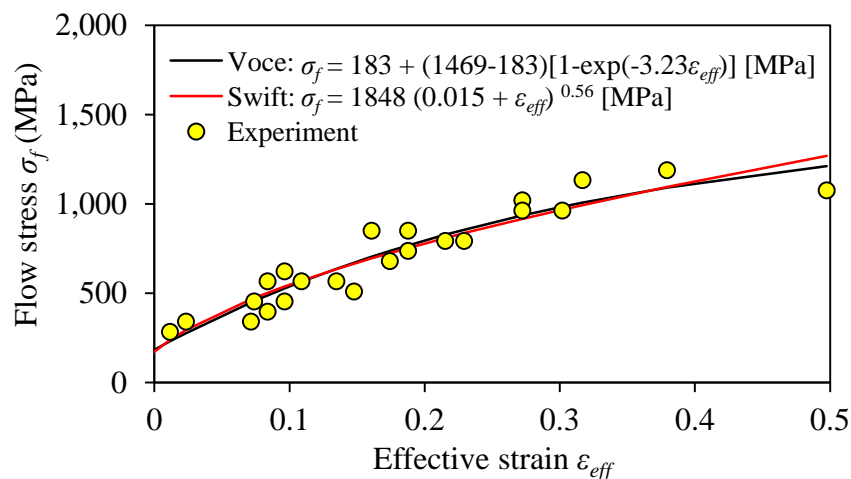
Figure 3.7: Stress-strain for 1 mm stacked stainless steel EN1.4307 plate.

25

The plain strain compression test has demonstrated that the strain hardening of the stainless steel sheet material ($n = 0.56$) is larger than the aluminium sheet material ($n = 0.24$). Both tests have shown that the Voce model fitted well to the experimental stress-strain data. Hence, the Voce model was chosen for the study of textured tool surface (Part II) where the aluminium material was used and for the study of anti-seizure tool coatings (Part III) where the stainless steel material was used.

3.3   Summary

In this study, the flow stress curve obtained by plain strain compression test is more appropriate use for sheet material than tensile testing, since higher strains can be reached. The plain strain compression test convey stress-strain data at higher strain values with Voce's material model fitting very well with the experimental results.

Part I
Compressibility of Lubricants

Overview

Metal forming in the mixed lubrication regime implies that the forming load in the tool/workpiece interface is shared between the metal-to-metal asperity contacts and the pressurized lubricant in the pockets between the asperity contacts. Kudo [70] and Wanheim [71] pointed out the large load carrying capacity of such enclosed pockets filled with lubricant, the resulting poor surface quality and considerable reduction of friction. Theoretical models determining the resulting contact area considering the elastic compression of the liquid in the closed pockets were established by Kudo [70] and Nellemann et al. [72]. The concepts of *Micro-Plasto-HydroStatic Lubrication* (*MPHSL*) and *Micro-Plasto-HydroDynamic Lubrication* (*MPHDL*) were introduced by Mizuno and Okamoto [23] and later verified by Kudo et al. [24] and Azushima et al. [25], [2]. Bay et al. have further investigated *MPHDL* and set up a mathematical model predicting the onset of this mechanism [3], [26]. Similar modelling has subsequently been carried out by Lo and Wilson [27], Azushima [28] and Stephany et al. [29].

The lubricant volume changes with the hydrostatic pressure [72]. This change is expressed by the bulk modulus *K* of the compressed lubricant as stated in Eqn. 4.1.

$$K = -V \frac{dp_{lub}}{dV} \tag{4.1}$$

where K is bulk modulus, V is volume, dp_{lub} is differential of hydrostatic pressure and dV is differential of volume.

From Eqn. 4.1, it appears that calculation of the pressure increase of lubricant trapped in closed pockets in the workpiece surface in metal forming requires knowledge on the lubricant bulk modulus. Data are difficult to find in the literature, and standard test methods requires advanced laboratory equipment [73], [74], [75]. Most of the advanced laboratory equipment is determining the lubricant pressure indirectly by measuring the punch load outside the pressure chamber. The drawback of this approach is that the measured force includes friction in the sealing and thereby overestimates the pressure in the lubricant, see Figure 4.1.
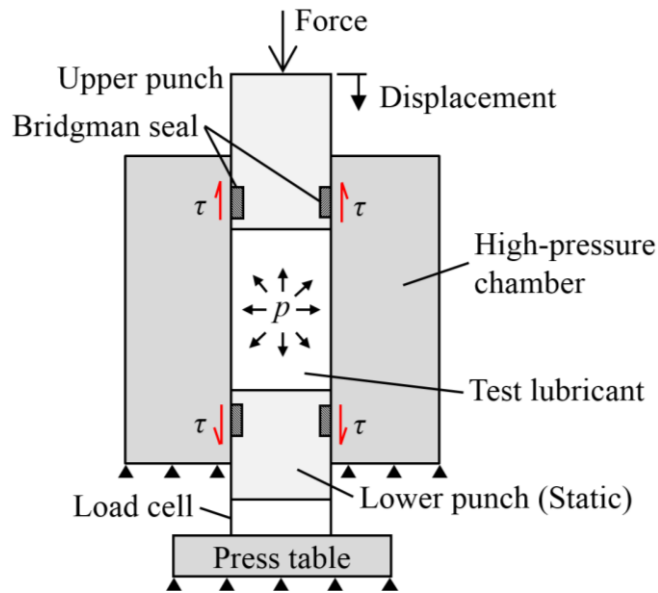
Figure 4.1: Illustration of the overestimated force due to extra contribution of friction stress τ in the sealing from both upper and lower punches.

A simple laboratory test combined with an inverse Finite Element (FE) analysis to determine the lubricant bulk modulus was designed and developed, but the methodology was only applied to the low pressure range. The experiment is described in Chapter 4.

An experimental compression test of liquid lubricants with direct measurement of the lubricant pressure build-up and the subsequent determination of the lubricant bulk modulus in a wide pressure range was also designed and developed. The work includes design and construction of a new high-pressure compressibility equipment and testing of the liquid lubricant compressibility up to 500 MPa, i.e. in a pressure range similar to the one appearing in the tool-workpiece interface in stamping of stainless steel sheet [46]. The experiment is described in Chapter 5.

Chapter 4: A Simple Laboratory Test with an Inverse FE Analysis

4.1   Introduction

The test principle outlined in Figure 4.2 is inspired by an early experiment studying the importance of lubricant entrapment by Butler [76]. A circular cylindrical workpiece is machined with a truncated cone cavity in the center of the upper end surface. The cavity is filled up with the lubricant to be tested, after which the workpiece is compressed between two flat parallel die plates. The outer part of the upper end surface has a slightly inclined angle to the upper die plate of $\gamma = 2°$ in order to ensure perfect sealing of the lubricant in the cavity. The inclined wall of the pocket facilitates scanning of the cavity geometry after deformation, and the steep angle prevents lubricant escape from the pocket. No lubrication is applied on the upper end surface of the workpiece, whereas the lower end surface is lubricated by a 0.1 mm Teflon film. The dimensions of the workpiece are given in Table 4.1.

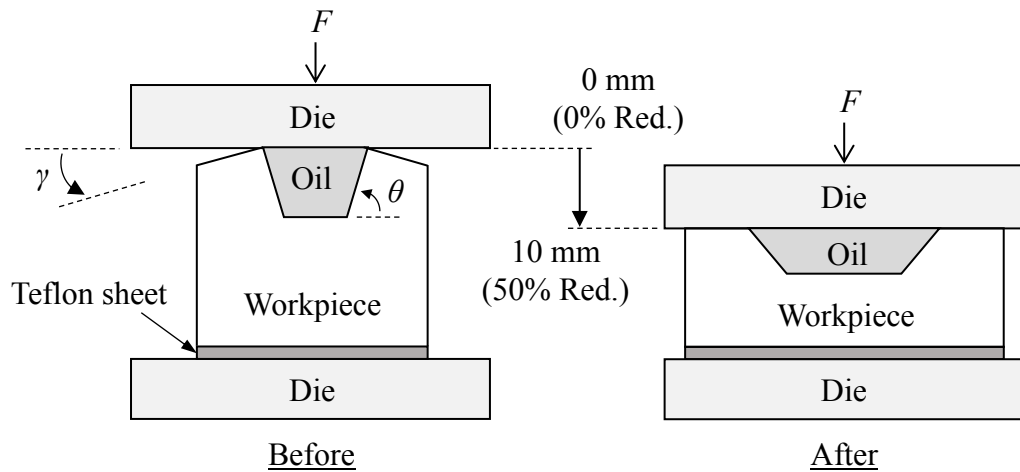**Figure 4.2:** Principle of lubricant compressibility experiment.

Table 4.1: Workpiece dimensions. Technical drawing is shown in Appendix B1.

Item	Dimensions	
Workpiece	Height H_o	: 20 [mm]
	Diameter D_o	: 20 [mm]
	Slope γ of inclined top surface	: 2°
Surface cavity	Height h_o	: 5 [mm]
	Top diameter d_o	: 6 [mm]
	Base diameter d_i	: 4 [mm]

4.2   Test Materials

The workpiece material was commercially pure aluminium Al2S in form of a hot extruded cylinder rod. The stress-strain curve of the as-received material was determined by upsetting tests. Table 4.2 gives the material composition and determined material work hardening constants according to Hollomon's power law $\sigma_f = C\varepsilon_{eff}^n$ to be used in FE simulations.

Table 4.2: Material properties of pure aluminium Al2S for numerical simulation.

Properties	Values
Composition	Al 99.7%, Fe 0.2%, Si 0.1%
Hollomon flow curve expression $\sigma_f = C\varepsilon_{eff}^n$	$\sigma_f = 119\varepsilon_{eff}^{0.27}$ [MPa]
Density ρ	2.7 g/cm^3
Poisson ratio v	0.33
Elastic modulus E	70 GPa

To demonstrate the lubricant compressibility experiment, two test conditions were investigated: a) pocket filled with pure, high viscosity mineral oil from Houghton designated CR5, and b) empty lubricant pocket designated NO for No Oil. Data on the lubricant is listed in Table 4.3.

Table 4.3: Lubricant properties.

Test lubricant	Type of lubricant	Dynamic Viscosity η_o (Pa.s)	Kinematic Viscosity η_v @ 40°C (cSt)	Density ρ @ 15°C (g/cm^3)
CR5 Houghton Plunger	Mineral oil	0.607	660	0.92

4.3   Experimental Procedure

A complete workflow for determination of the lubricant bulk modulus is shown in Figure 4.3. At first, the lubricant compressibility experiment is conducted. This includes cleaning of the pocket from any remnants of oil, grease and other contaminants. Before testing, the workpiece geometry including the pocket was scanned on a 3Shape QC Scanner Type D700. To facilitate good scanning, a thin layer of washable white paint was sprayed onto each workpiece prior to scanning to avoid reflections from the shiny metal surfaces. Although this procedure causes an error due

to a few micrometres film thickness of the paint, it is not considered to affect the actual measurement of pocket volume and otherwise it ensures good accuracy of the scanned pocket surface.
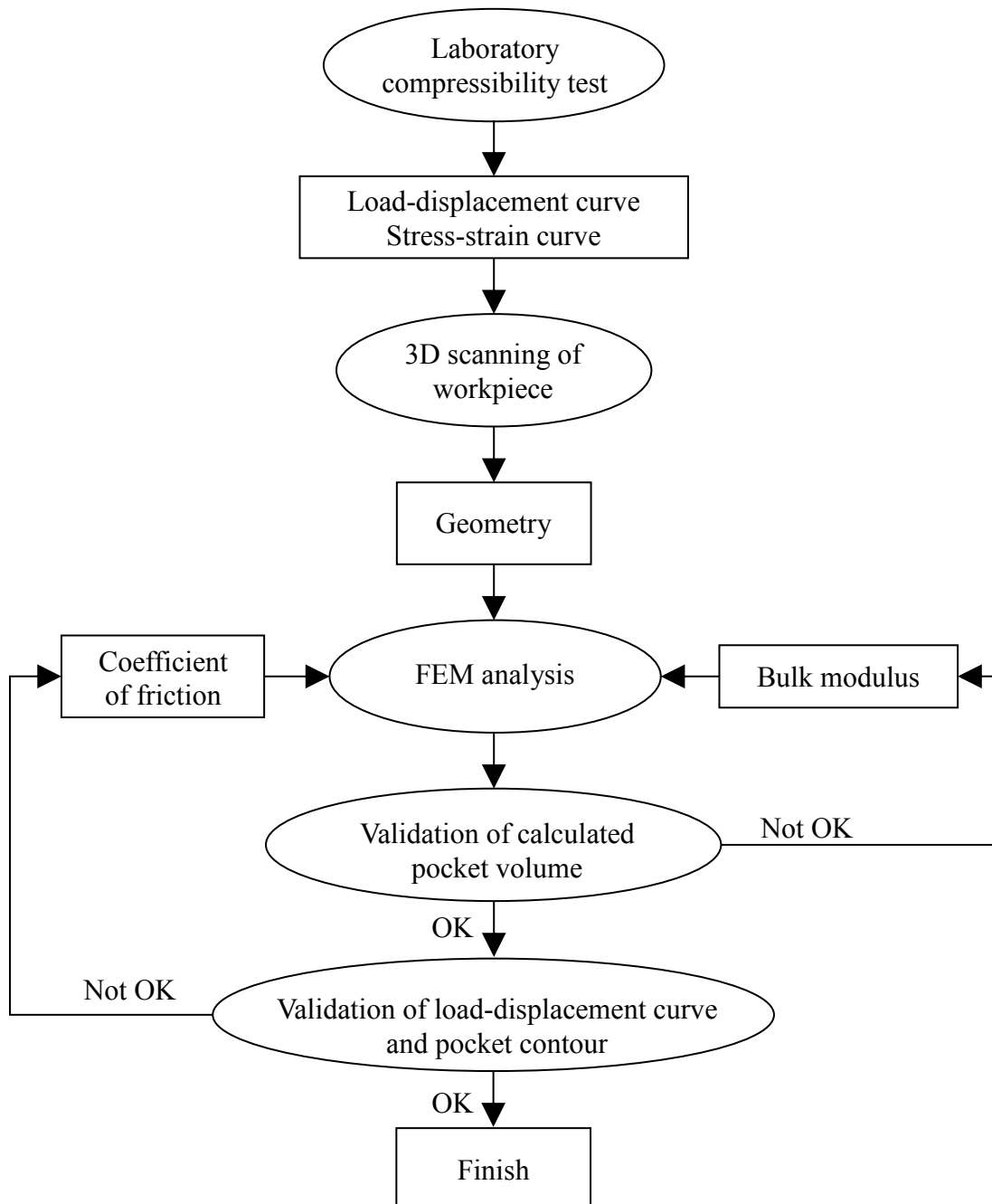

Figure 4.3: The complete workflow for determination of lubricant bulk modulus.

Subsequently the test lubricant was poured carefully into the surface cavity. A circular piece of Teflon film corresponding to the size of the lower end surface of the workpiece was cut out and placed on the lower die and the workpiece placed on top of

this. The upsetting was performed on a 600 kN hydraulic press at first loading the workpiece with 2 tons at low punch speed $v = 0.1$ mm/s, after which the deformed workpiece was removed for scanning. During the experiment, the load and the die displacement were recorded, and the load-displacement data were saved in a LabView program. The whole procedure was repeated for 3, 4, 5, 6, 7 and 8 tons load. The same procedure was followed for the workpiece with an empty pocket.

After that, each scan was analysed using a dimensional analysis software to determine overall geometry of the workpiece including the pocket surface, Figure 4.4, and the experimental pocket volume was computed using MATLAB. An error is visible due to scanning, however it is not affecting the actual scanning of the pocket. An FEM analysis of the workpiece deformation was carried out to calculate the pocket surface coordinates at specific height reductions and the resulting pocket volume was computed in MATLAB from the simulation.
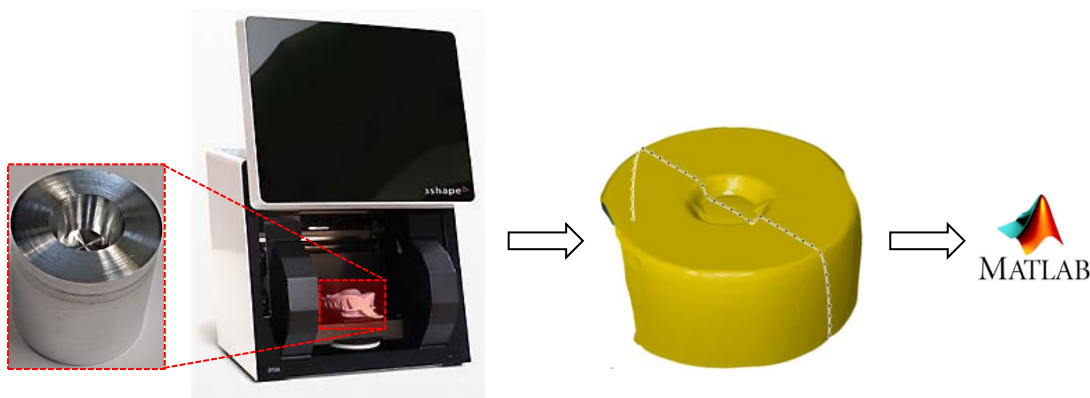
Figure 4.4: Dimensional analysis for determination of volume and scanned pocket contour.

Contour plots of the measured and numerically calculated pocket surfaces were made by extracting nodal coordinates located on the pocket surface from the FE software and scanned files. Comparison between the numerical and experimental pocket surface contour at each workpiece height reduction were plotted using MATLAB. The MATLAB code is shown in Appendix B2. In this way calibration of the bulk modulus of the test oil was conducted. Calibration of the coefficient of friction on the upper and lower die/workpiece surfaces was done by trial-and-error comparing the contour plots of the measured and predicted workpiece geometry in the same way as determining the bulk modulus and ensuring a good fit to the measured load-displacement curve.

4.4 Finite Element Analysis

The numerical analysis coupling deformation of the lubricant and the metal was performed with LS-DYNA v. R7.1.1, using implicit time integration. The FE simulation of the compressibility test made use of an axisymmetric model with 6940 linear quadrilateral elements. Figure 4.5 presents the axisymmetric FE model of the compressibility test with an empty pocket, whereas a pocket filled with lubricant is shown in Figure 4.6. A fine, uniform mesh was applied in the contact between the workpiece and the lubricant.
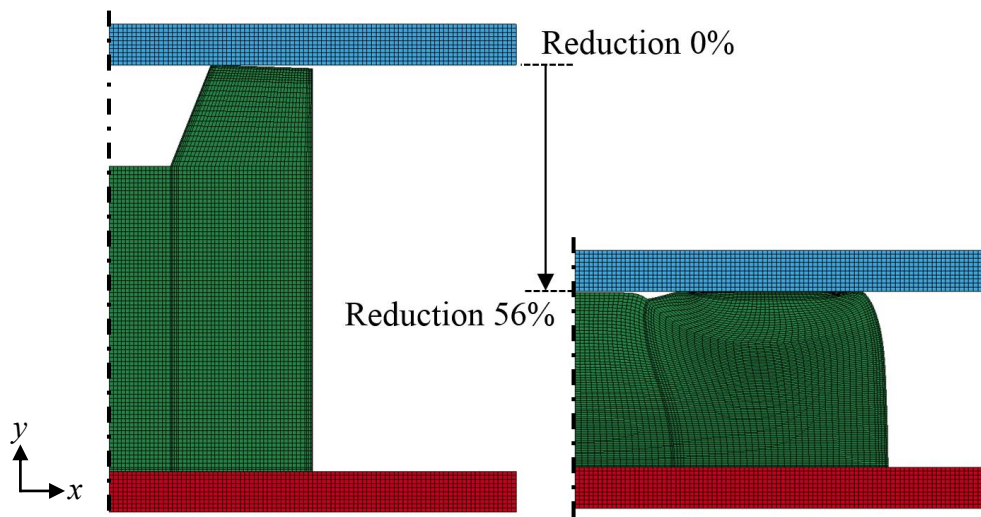

Figure 4.5: Axisymmetric FE model of a compressibility test of an empty pocket.
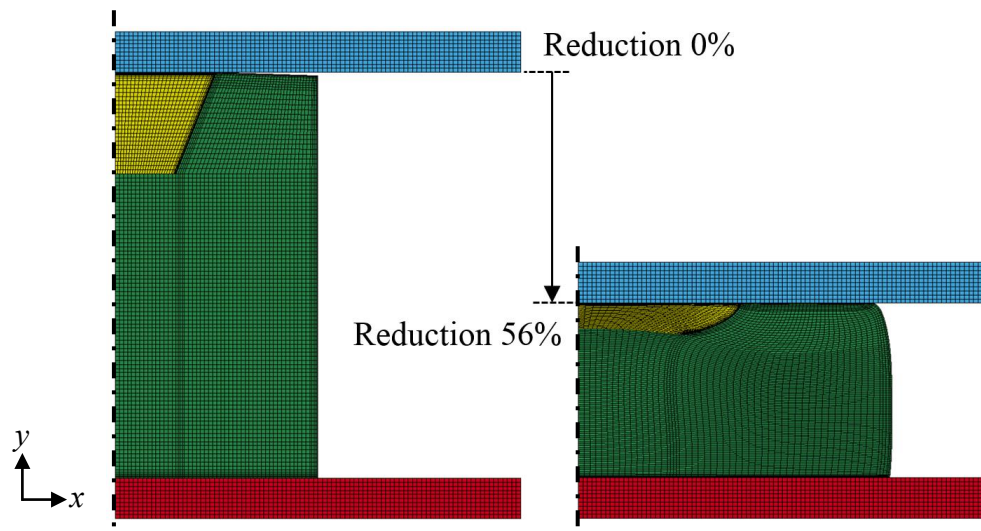

Figure 4.6: Axisymmetric FE model of a compressibility test of a pocket filled with lubricant.

The upper and lower die plates were modelled as rigid objects. The workpiece material was treated as an elastic-plastic object following a Hollomon hardening power law $\sigma_f = C\varepsilon_{eff}^n$, where strength coefficient C and strain-hardening n are listed in Table 4.2. The lubricant in the pocket was treated as a fluid with properties as listed in Table 4.3 and with a bulk modulus assumed constant throughout the simulation of the test. The bulk modulus was varied in the calculation until one giving the best fit between the calculated and the measured pocket volume was determined. The Coulomb friction model $\tau = \mu p$ was used in the numerical analysis of the surface contact between the dies and workpiece.

Before   *After*
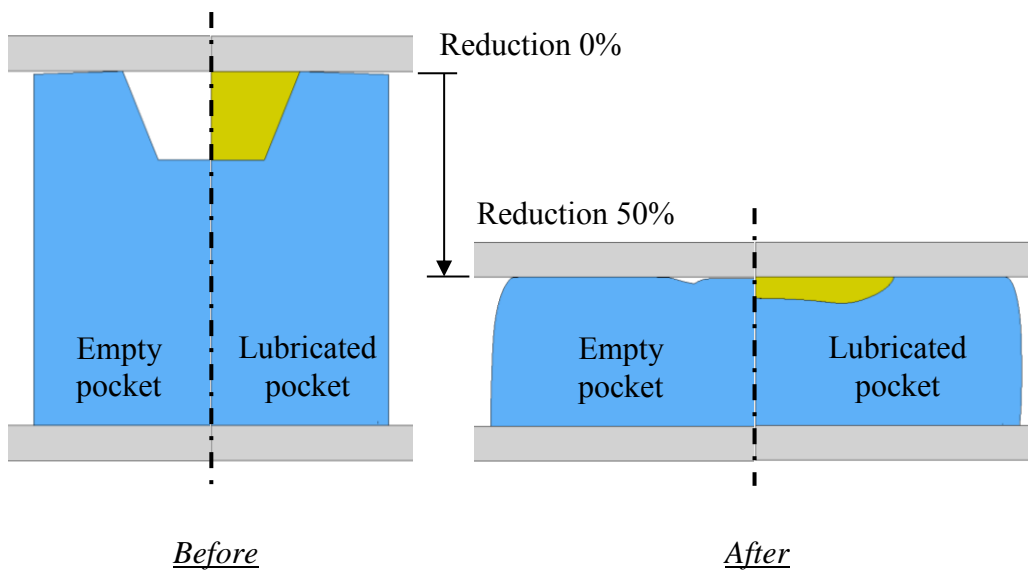
Figure 4.7: FE analysis of empty (left) and lubricated (right) pockets.

The lubricant is assumed to be a Newtonian fluid. The presence of trapped lubricant implies that the hydrostatic pressure in the lubricant changes with the pocket volume [72], Figure 4.7. The bulk modulus of the trapped lubricant is defined as stated in Eqn. 4.1. A larger normal pressure has been observed on the upper die/workpiece contact for the workpiece with the empty pocket (Figure 4.8) in comparison to that of the workpiece with the pocket filled with lubricant (Figure 4.9). This is due to the hydrostatic pressure of the lubricant sharing the load, see Figure 4.10, which causes less workpiece contact to the tool surface and thereby less friction.
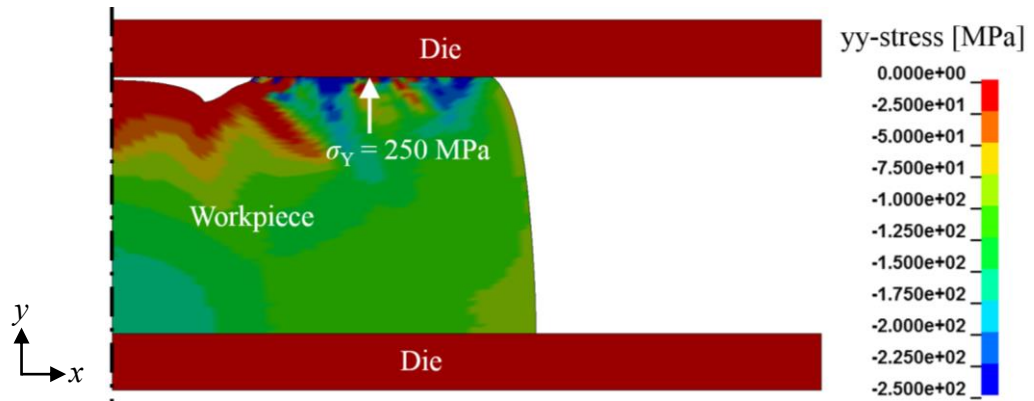
Figure 4.8: Normal stress along the die surface for the workpiece with the empty pocket.
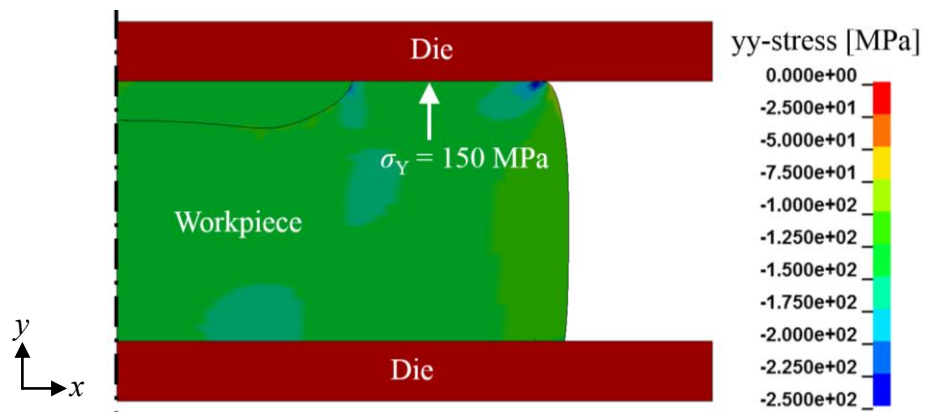
Figure 4.9: Normal stress along the die surface for the workpiece with the pocket filled with lubricant.
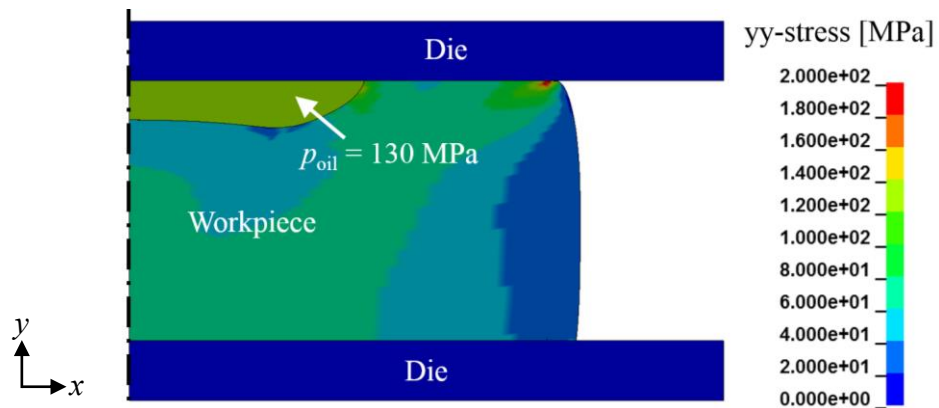
Figure 4.10: Hydrostatic pressure for the workpiece with the pocket filled with lubricant.

4.5   Results and Discussion

4.5.1   Pocket Volume

Figure 4.11 shows measured and calculated ratios V/V_o between deformed and undeformed pocket volumes for different bulk moduli. It is seen that the FEM analysis based on a bulk modulus $K = 1.7$ GPa gives the best fit within the experimental pocket volume. Jacobson [74] has experimentally determined the bulk modulus for six different oils at ambient pressure to be in the range $1.4 - 1.8$ GPa. The bulk modulus found in the present work is thus in the high end of this range, which fits well with the fact that the present bulk modulus is determined at an elevated pressure where the bulk modulus is known to be larger [72]. Figure 4.12 shows the pocket volume ratio for the two investigated cases 1) pocket with liquid (CR5) and 2) pocket without liquid (NO). The difference in pocket volume between the filled and empty pockets is significant due to the large bulk modulus of the oil, which creates a high hydrostatic pressure build-up in the lubricant, which prevents excessive deformation of the pocket. During deformation the trapped lubricant acts like an elastic spring, where a larger bulk modulus increases the spring constant.
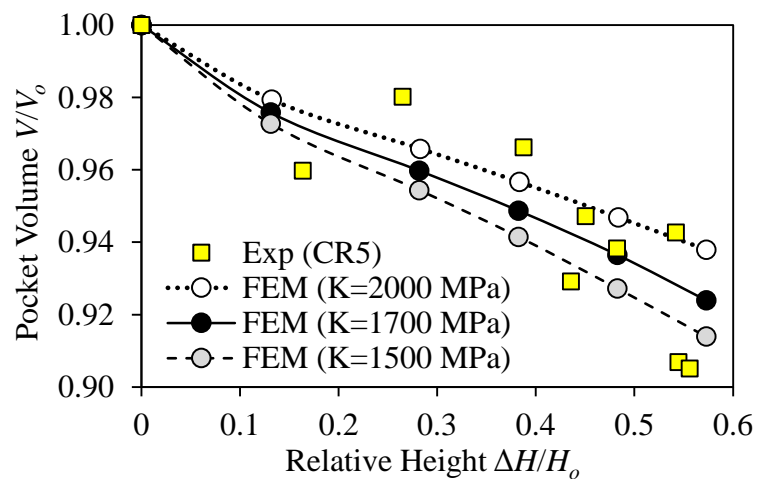
Figure 4.11: FEM predicted and experimentally determined relative pocket volume as a function of relative workpiece height reduction for different bulk moduli of CR5 oil.
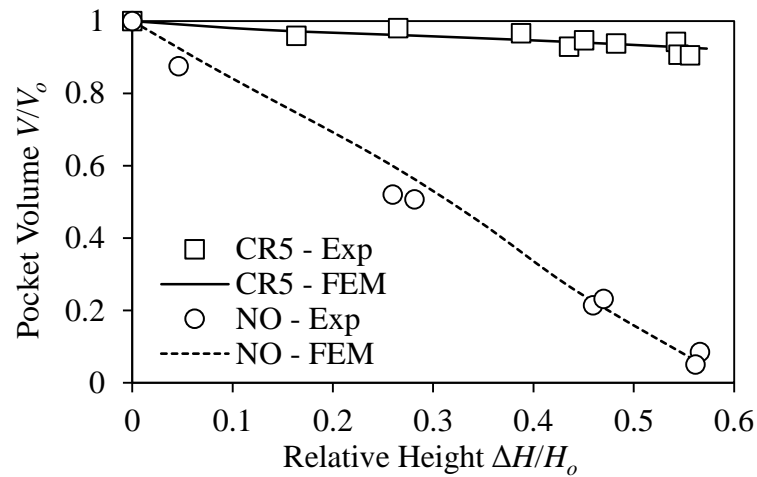
Figure 4.12: FEM predicted and experimentally determined relative pocket volume as a function of relative workpiece height reduction for CR5 oil and no lubricant (NO).

4.5.2 Calibration of Friction

As illustrated in Figure 4.3, calibration of friction was done after calibration of the bulk modulus in an iterative manner to obtain the best fit of both parameters. Calibration was based on obtaining a best fit of the calculated load-displacement curves with the measured ones. Figure 4.13 represents the best fit for a filled pocket, whereas Figure 4.14 shows the best fit for an empty pocket. The experimentally and numerically calculated load-displacement curves are in good agreement with less than 1 % difference, when a coefficient of friction $\mu = 0.16$ on the upper die/workpiece contact is chosen. The friction coefficient on the bottom die/workpiece contact $\mu = 0$ was chosen for both pockets filled with CR5 and empty pockets.
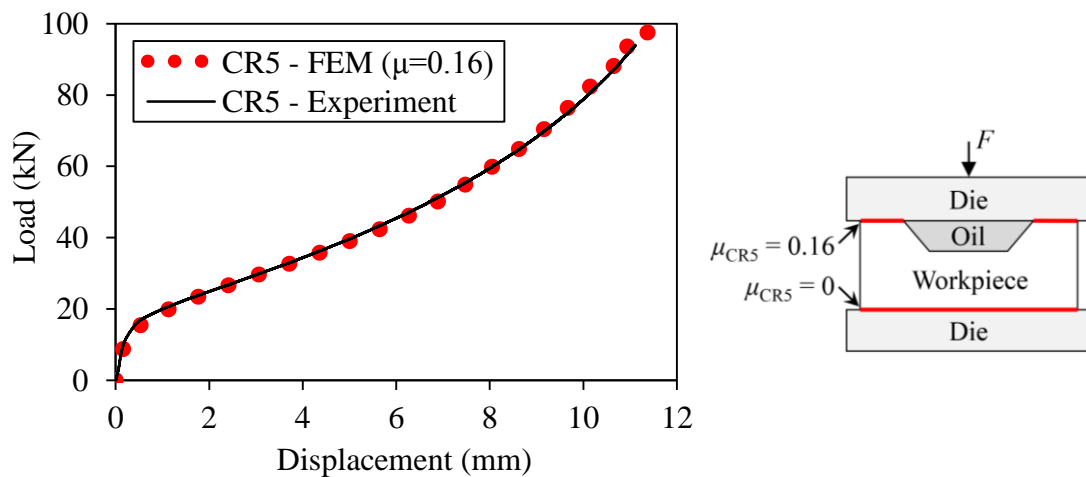
Figure 4.13: Load-displacement of FEM and experiment for a pocket filled with CR5 oil.
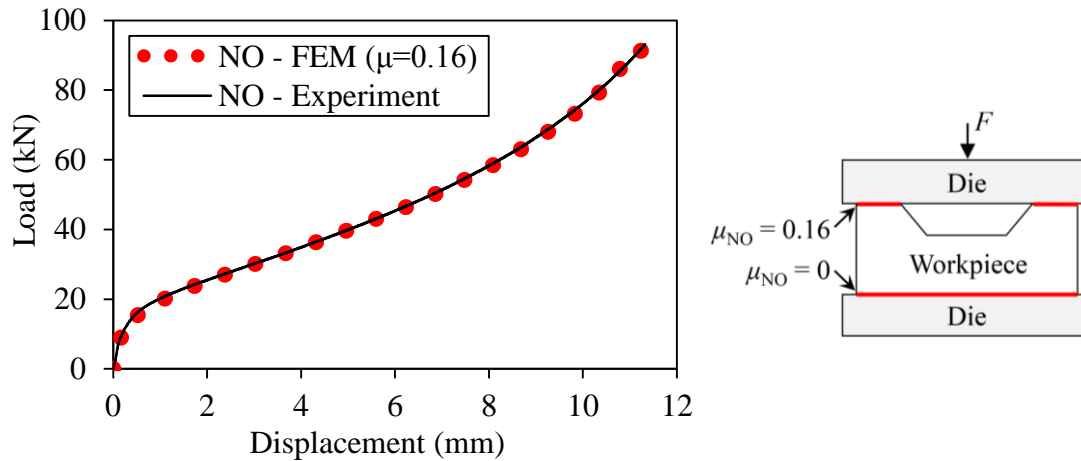
Figure 4.14: Load-displacement of FEM and experiment for an empty pocket.

4.5.3   Pocket Contour

Figure 4.15 shows a photo of the a) undeformed and deformed workpiece for the two cases: b) pocket with CR5 and c) empty pocket. As further documentation of the calibration of the FEM analysis, Figure 4.16 shows contour plots of the top end of workpieces with and without filled pockets and various reductions. Good agreement is seen between the experimentally determined contours and the ones predicted by FEM analysis at three different reduction levels.

(a)   (b)   (c)
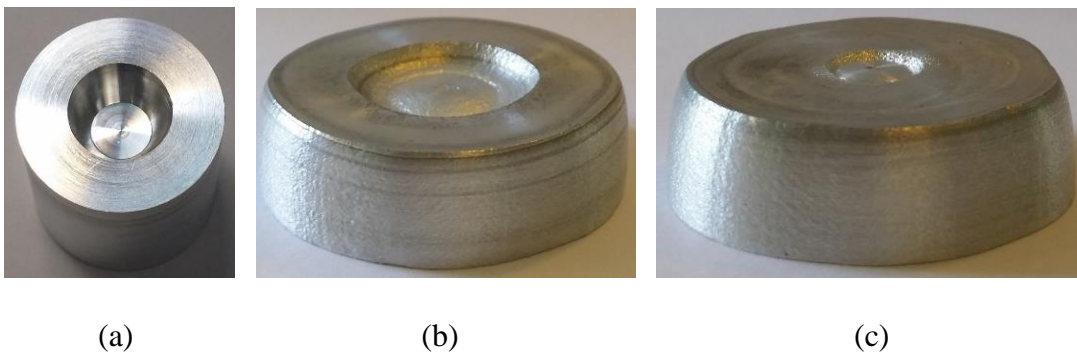
Figure 4.16: The workpiece geometry of (a) undeformed pocket, and deformed pocket at 56 % reduction for (b) CR5 and (c) empty pocket.
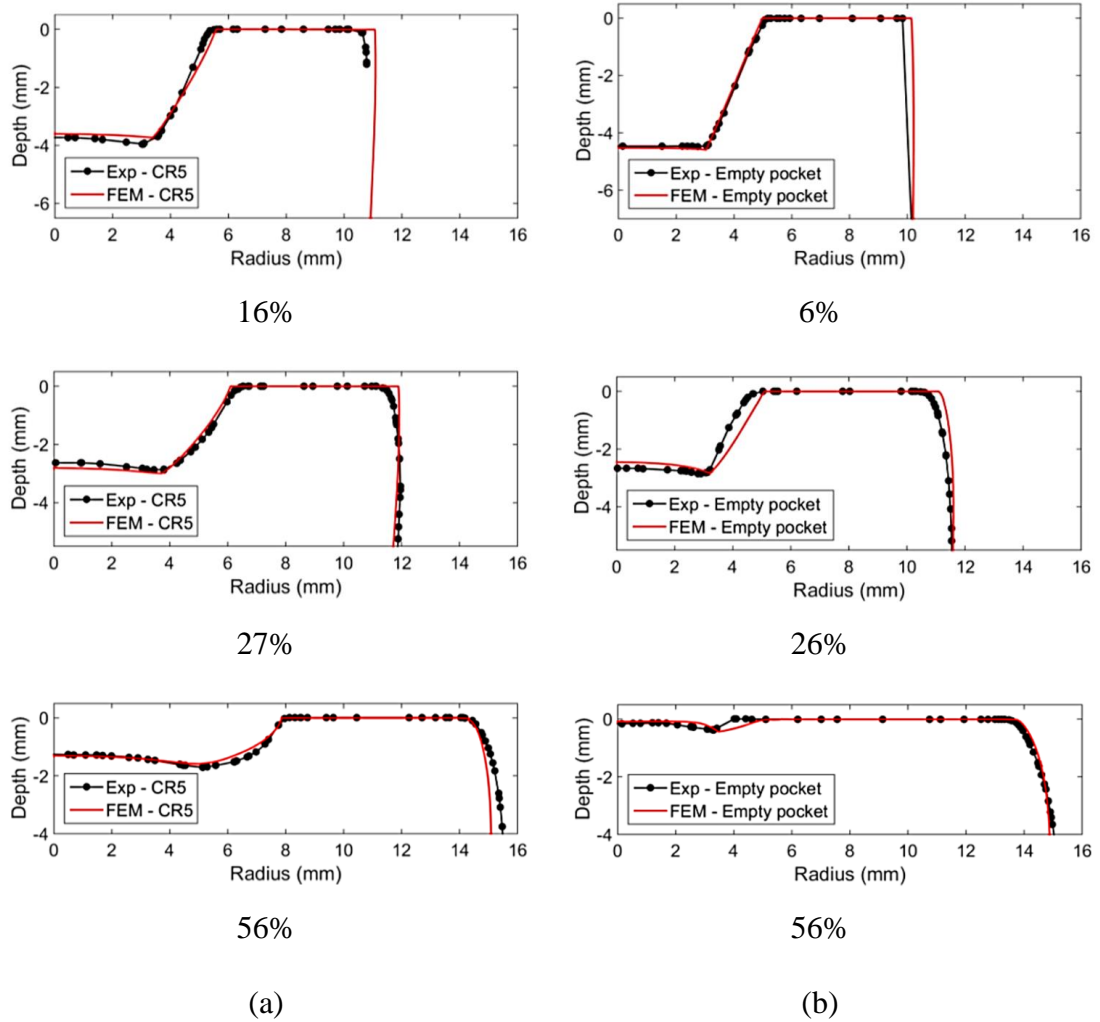
Figure 4.15: Contour plot of the workpiece with (a) lubricated and (b) unlubricated pockets.

4.6   Applications

This new, simple method has been applied to other lubricants. Testing of water has also been tried. The properties of the test lubricants and the water are shown in Table 4.4. All test conditions and procedures were kept the same including the material and the geometry of the test specimen as mentioned earlier.

Figure 4.17 shows experimentally determined relative pocket volumes as function of relative height reduction and corresponding FEM simulations utilizing different bulk moduli. The bulk modulus of the different lubricant types were fitted within the experimental pocket volume, and the bulk modulus values of each lubricant type were presented in the figure. The largest bulk modulus has been obtained by TDN81, followed by PN226, CR5 and lastly, the water. The bulk modulus of water is quite different from the measured value accessible from online information, where the

bulk modulus is 2.2 GPa. In this sense, it is realized that this new, simple laboratory methodology cannot be applied to test water due to scattered experimental results. It was observed experimentally that the water escaped easily during the deformation due to its low viscosity. In the case of the liquid lubricants, the bulk modulus seems independent of viscosity, Table 4.5.

Table 4.4: Properties of test lubricants and water.

Test lubricant	Type of lubricant	Dynamic viscosity η_o (Pa.s)	Kinematic viscosity η_v @ 40ºC (cSt)	Density ρ @ 15ºC (g/cm^3)
CR5	Naphthenic plain mineral oil	0.607	660	0.92
TDN81	Highly viscous chlorinated paraffin oil	0.168	150	1.117
PN226	Medium viscous chlorinated paraffin oil	0.067	67	1.004
Water	-	0.653 x 10^{-3}	0.658	1.000
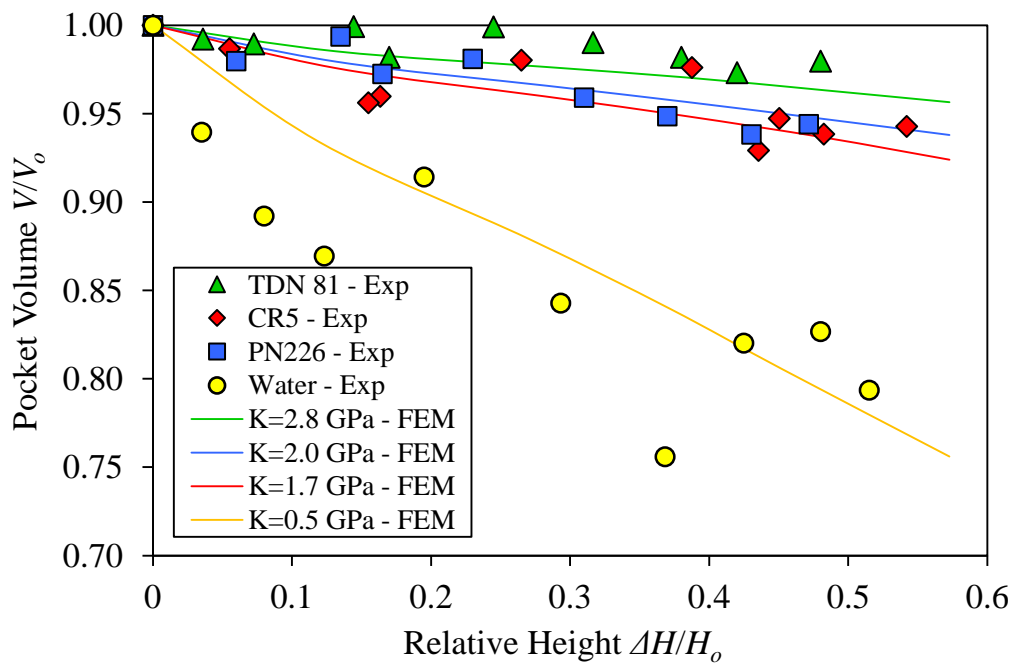
Figure 4.17: Measured bulk modulus for different lubricants and water.

Table 4.5: Comparison of lubricant properties (viscosity and bulk modulus).

Test lubricant	Type of lubricant	Kinematic viscosity η_v @ 40ºC (cSt)	Bulk modulus (GPa)
CR5	Naphthenic plain mineral oil	660	1.75
TDN81	Highly viscous chlorinated paraffin oil	150	2.8
PN226	Medium viscous chlorinated paraffin oil	67	2.0

4.7   Summary

The proposed methodology consists of a simple laboratory test and an inverse FEM analysis for determining the bulk modulus. It has proven to work satisfactory in the low pressure regime of approximately 100 MPa. Further verification of the simple laboratory experimental methodology can also be explored to the higher pressure range. Such an experiment requires higher strength test material such as steel. However, the next test campaign focuses on the development and testing of a high-pressure equipment based on a new design concept. The new design concept is planned for measuring the bulk modulus at varying pressure range.

Chapter 5: Advanced Compressibility Testing

5.1   Introduction

In metal forming modelling of mechanisms of lubricant entrapment and escape, two important lubricant properties, viscosity and bulk modulus, are needed. The viscosity is needed for characterizing shearing ability of lubricants. Meanwhile, the bulk modulus characterizes the compressibility of lubricants. The optimization of these lubricant properties plays a crucial role in preventing galling in sheet metal forming. This is especially the case when liquid lubricants are applied in situations where increased workpiece surface roughness facilitates the lubricant entrapment, pressurization and possible escape by *Micro-Plasto-HydroDynamic Lubrication* (*MPHDL*).

Components:

1) Hydraulic punch, 2 MN
2) Upper punch stem
3) Pre-stressed, high-pressure container
4) Lower punch plate
5) Displacement sensor (max. 50 mm stroke length)
6) Pressure sensor (max. 1.5 GPa)
7) Open/close pressure valve controller
8) Excess lubricant release valve

Figure 5.1: Schematics of components for measuring compressibility of liquid lubricants. Detailed drawings are shown in Appendix D1.

A new equipment has been designed and built to determine the lubricant properties in a wide pressure range. The new equipment has been designed by Lund and Hansen [77]. The construction of the new equipment has also included some components for measuring lubricant pr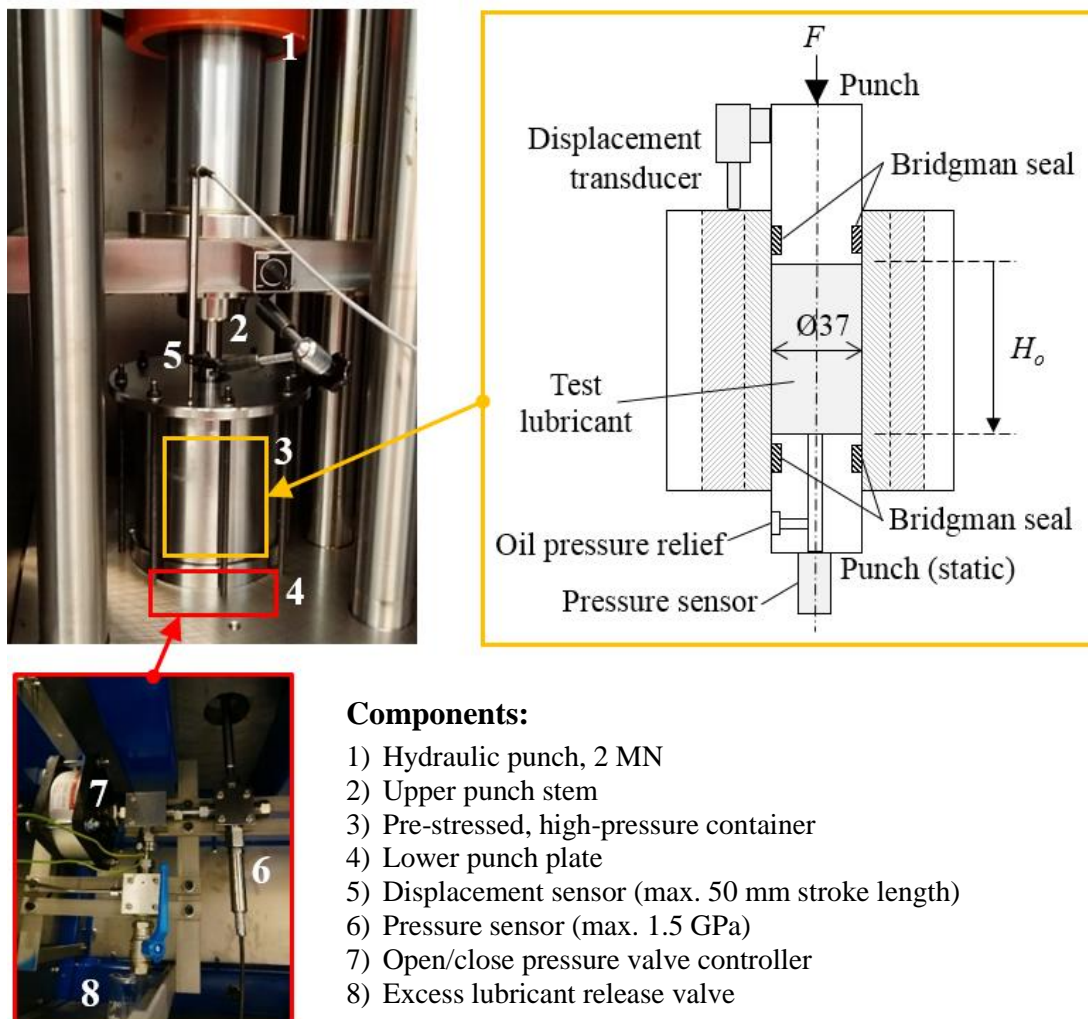essure build-up with decreasing lubricant volume in a pre-stressed Ø37 mm pressure container with two fitting punches, see Figure 5.1, and subsequent calculation of the lubricant bulk modulus.

The lower punch is stationary, whereas the upper punch is moving in order to compress the liquid between the punches. Load is delivered by a 2 MN hydraulic cylinder. Custom made Bridgman seals are mounted on the punches. Figure 5.2 shows the seal components comprising of three rings. For testing of lubricants to a pressure of 500 MPa, ring 1, which has a triangular cross section is made of copper, ring 2 with a square cross section is made of Teflon, whereas ring 3 is a commercial U-shaped rubber seal, Variseal M2S from Trelleborg, Sweden. A central bore in the bottom punch leads the oil to a pressure sensor (HBM, P3MBP BlueLine, measuring range 0 – 1.5 GPa). The volume change of the oil is determined by measuring the punch travel by a length transducer (HBM, WA/50mm, measuring length range 0 – 50 mm).

Components:
1) Ring 1 – Copper
2) Ring 2 – Teflon
3) Ring 3 – Commercial U-shaped seal
4) Punch cap
5) Punch

(a)   (b)
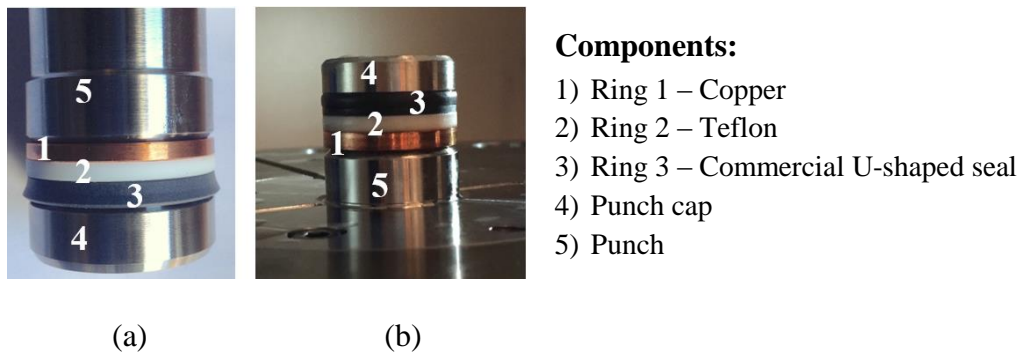
Figure 5.2: Bridgman seal on a) upper and b) lower punches. For pressures up to 500MPa. Technical drawings are shown in Appendix D2.

5.2   Numerical Analysis of High-Pressure Compressibility Equipment

5.2.1   Tool Deflection

A numerical analysis using LS-DYNA v. R7.1.1 was performed to estimate the deflection of the tools under load by coupling deformation of the lubricant and the metal, Figure 5.3a. The FE simulation made use of an axisymmetric model with fully integrated, linear quadrilateral elements and implicit time integration. A fine, uniform mesh was applied in the contact between the container, the punches and the lubricant. The upper and lower punches as well as the container were modelled as elastic bodies in order to calculate the tool deflections and compare the pressure build-up and punch stroke with the one obtained by assuming rigid dies and punches in order to determine the size of the elastic deflections. The material properties are listed in Table 5.1. The

test lubricant was treated as a Newtonian fluid with a constant bulk modulus $K = 2200$ MPa. Coulomb friction $\tau = \mu p$ with $\mu = 0.1$ was assumed in all surface contacts.

(a)   (b)
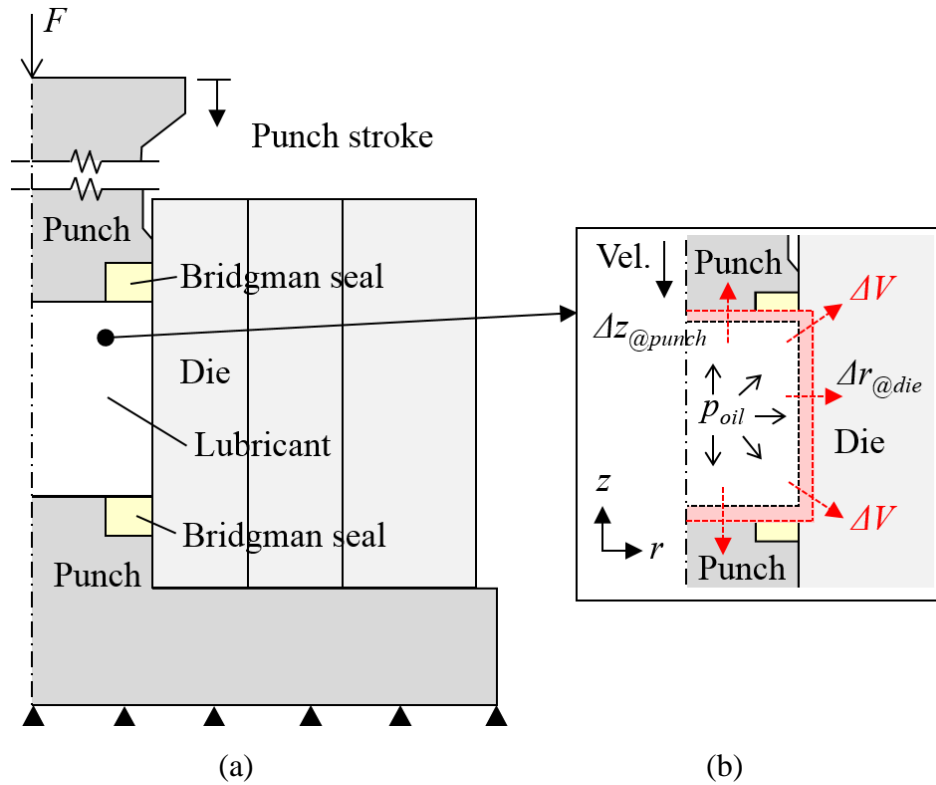
Figure 5.3: a) Schematic of the numerical model simulating the lubricant compressibility test, b) Elastic expansion of the die (r-axis) and compression of punches (z-axis) due to the pressurized lubricant.

Table 5.1: Tool materials and their properties.

Components	Material types	Density ρ (g/cm^3)	Poisson ratio v	Elastic modulus E (GPa)
		Properties		
Punches	Uddeholm Unimax	7.8	0.3	213
Punch cap	Uddeholm Unimax	7.8	0.3	213
Container	Uddeholm Vanadis 4E	7.7	0.3	206

The tool deflection is schematically displayed in Figure 5.3b. The elastic deflection, which reduces the volume decrease of the trapped liquid, occurs in the radial direction of the die and in the axial direction of the punches. A comparison of the

determined pressure versus punch stroke for elastic tools with that of rigid tools can be seen in Figure 5.4. It is noticed that the same punch stroke gives rise to almost the same pressure. The error in determining the bulk modulus disregarding elastic deflection of the tools will thus be insignificant in the pressure range 0 – 550 MPa, wherefore elastic deflection of the tools is neglected in the following.
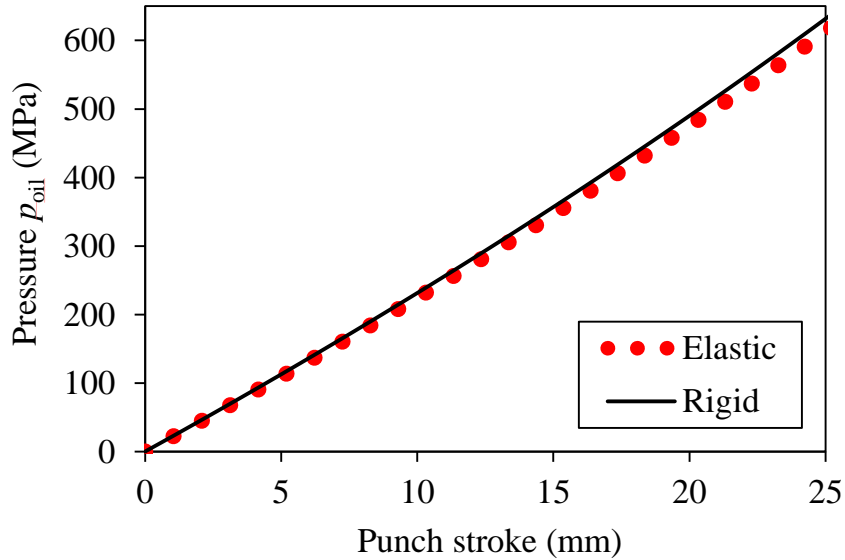
Figure 5.4: Comparison of pressure build-up as function of punch stroke assuming rigid or elastic tools.

5.2.2   *Leakage Control in Bridgman Seal*

A schematic of the Bridgman seal is seen in Figure 5.5a, and Figure 5.5b shows the deformation of the copper ring under load. The seal is not allowed to be extruded into the cylindrical part of the gap between the punch and the container. A FE simulation of the seal deformation was performed adopting an axisymmetric model with fully integrated, linear quadrilateral elements. In the simulation, ring 2 and ring 3 were assumed and simulated as rigid materials. This is because the main concern here is to evaluate the above mentioned extrusion of the ring 1 in order to prevent the ring 1 getting stuck in between the punch and the container during contraction. The simplifications will merely avoid additional constraints on the FE model, and thus reduce the simulation time. Based on the measured hardness of the copper ring (ring 1), $HV = 95$ kp/mm^2, the copper was assumed an elastic-plastic material with a linear stress-strain curve with flow stress $\sigma_f(\varepsilon_{eff}) = \sigma_f(0) = 310$ MPa at an effective strain of $\varepsilon_{eff} = 0$, while $\sigma_f(0.15) = 470$ MPa at $\varepsilon_{eff} = 0.15$ according to [78].

(a)   (b)
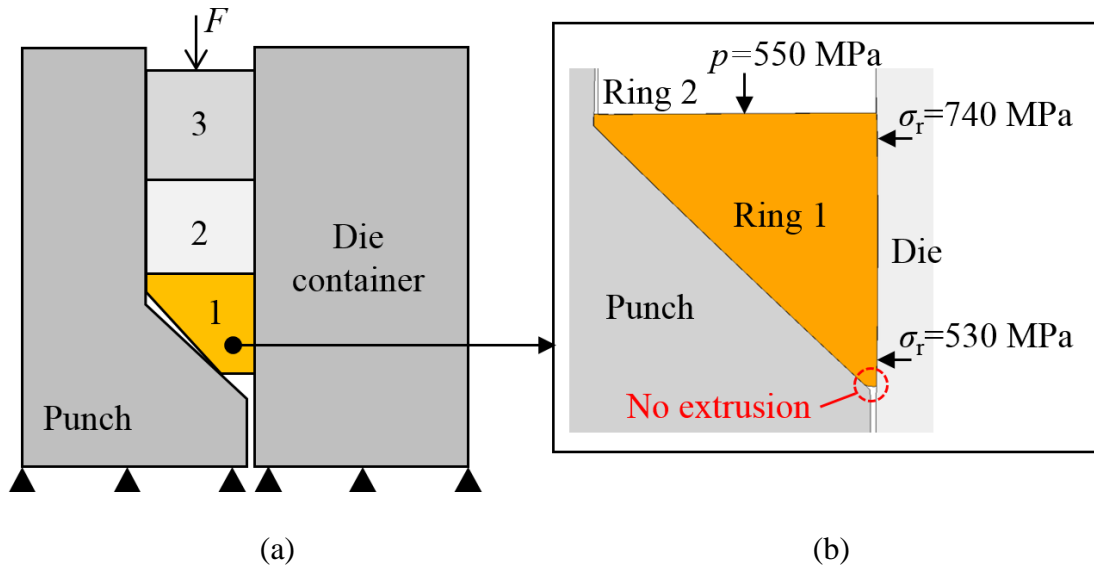
Figure 5.5: a) Numerical analysis of ring seal compression describing a deforming copper ring at high pressure, and b) the conical angle difference between copper ring and punch is enlarged for clarity in (a).

In order to ensure sufficient sealing pressure to prevent lubricant leakage, the conical part of the punches and ring 1 were designed with an angle of 46° and 45° towards vertical, respectively. A further modification to the Bridgman seal was to blunt the triangle tip of ring 1 to avoid extrusion of copper into the clearance between the punch and the die container at high pressures, see Figure 5.5a. The numerical analysis proved this to be an efficient solution until a fluid pressure of 550 MPa, see Figure 5.5b.

The copper ring shape obtained in experiments at the same pressure confirmed this, Figure 5.6. If an excessive pressure was applied, extrusion did occur as seen in Figure 5.7. To prevent the punch getting stuck in the container during extraction, a low-friction film of MoS_2 was sprayed on the copper ring prior to each test.

(a)   (b)

Figure 5.6: a) Copper ring before the test, b) ring after successful test, no extrusion at 550 MPa.
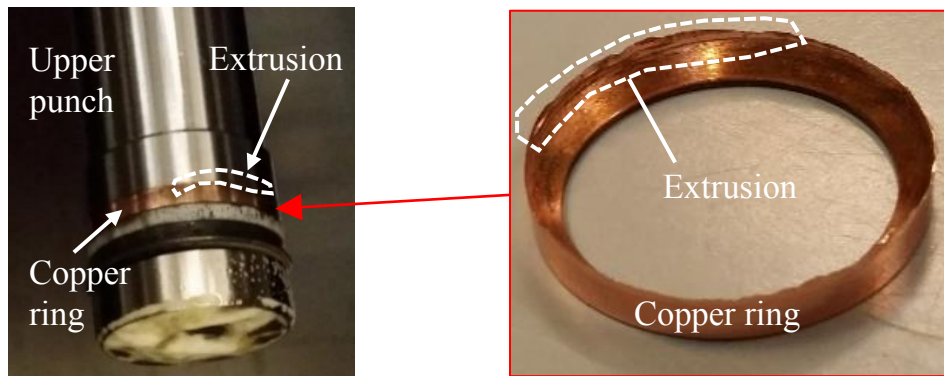
Figure 5.7: Extrusion of copper at excessive pressure.

5.3   Experimental Procedure

First, the punch and inner die wall are cleaned for any remnants of lubricant, grease and other contaminants. 100 mℓ fluid is poured into a beaker. The volume is measured by weighing before the test. The fluid is poured carefully into the container. The small remnants of fluid in the beaker are measured by subsequent weighing. The actual weight and volume of fluid is then determined, see Table 5.3. The compressibility test is started by moving the upper punch slowly downwards thereby pressurizing the lubricant. During testing the pressure and punch travel are recorded and saved by a LabView program. The test is stopped when the applied pressure reaches 500 MPa. The upper punch is slowly unloaded and the Bridgman seal on the punches are carefully checked for possible damage. If damage has occurred, then the seals are replaced.

5.4   Data Treatment

Figure 5.8a shows an example of the measured punch stroke – pressure curve for water. A Matlab code was used to process the recorded data of pressure p vs. punch stroke L. A line segment that connects two experimental points on the pressure–punch stroke (p–L) graph is used for computing the pressure gradient by the finite difference method. Due to scatter in the acquired data, the finite difference method gives rise to large oscillations in the value of the bulk modulus. Thus, the experimental p–L data points are approximated by a second order polynomial (Figure 5.8b), which can then be differentiated for determining the bulk modulus K. Figure 5.9 shows the curve fit for water.

(a)

(b)
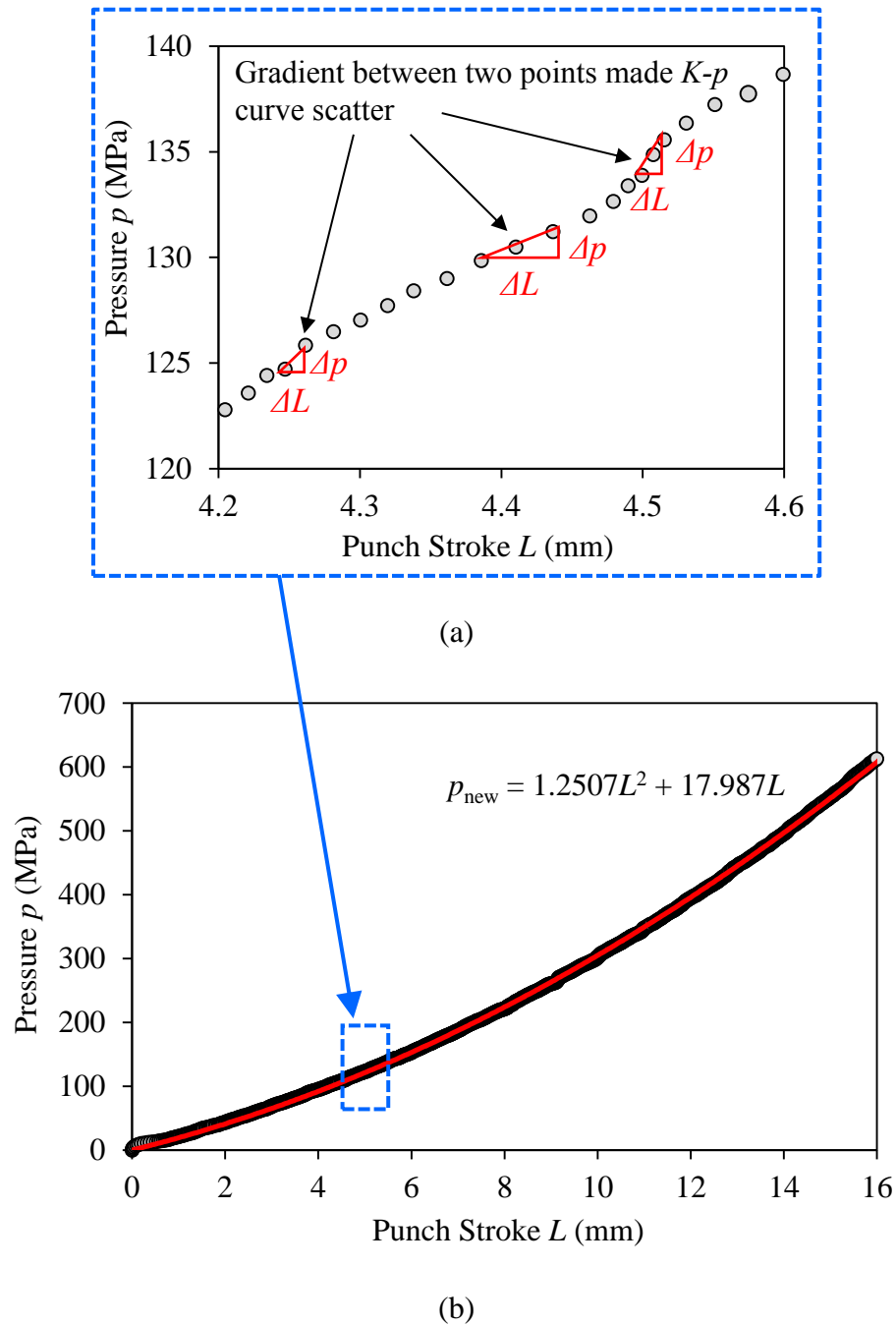
Figure 5.8: Punch stroke – pressure curve for water. a) Oscillations in the collected data giving rise to scattered values of the slope dp/dL computed by finite differences, and b) a second order (cubic) polynomial approximation to the experimental data measured in the laboratory.

A Matlab code shown in Appendix D3 was used to process the recorded data of pressure p vs. punch stroke L by calculating the instantaneous pressure p_i based on a second order polynomial approximation as described in Figure 5.8b. Next, calculating the volume change ΔV and volume V based on Eqn. 5.2 and Eqn. 5.3. Finally, to compute the bulk modulus K as a function of pressure p, use Eqn. 5.1, Eqn. 5.4 and Eqn. 5.5. Using the curve fit in Figure 5.8 the bulk modulus determined for water is shown in Figure 5.9.

$$dp_i = p_{\,i+1} - p_i \tag{5.1}$$

$$\Delta V_i = A_o L_i \tag{5.2}$$

$$V_i = V_o - \Delta V_i \tag{5.3}$$

$$dV_i = V_{i+1} - V_i \tag{5.4}$$

$$K_i = -V_i \frac{dp_i}{dV_i} \tag{5.5}$$
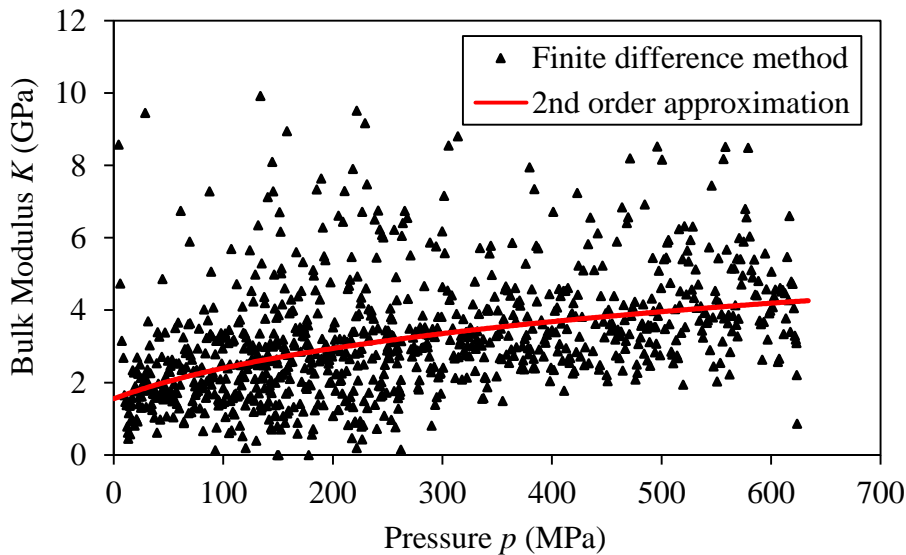
Figure 5.9: Bulk modulus versus pressure for water determined by a second order polynomial approximation and by finite difference method.

5.5   Verification of Test

In order to ensure that the high-pressure equipment is capable of measuring the compressibility of fluids accurately at high pressures, a verification was performed with water as a reference fluid. Properties of water at room temperature are listed in Table 5.2, where the bulk modulus at ambient pressure is 2.2 GPa. Figure 5.10 shows that the bulk modulus of water increases almost linearly with pressure. Besides measurement of pressure at 0 MPa, a reasonable agreement was achieved with T. Hayward [79] for the bulk modulus of water at elevated pressures, especially at pressures above 100 MPa.

Table 5.2: Properties of water at room temperature.

Properties	Value	Unit
Density	1.02	g/cm^3
Kinematic viscosity at 40°C	0.658	cSt
Bulk modulus at ambient pressure	2200	MPa
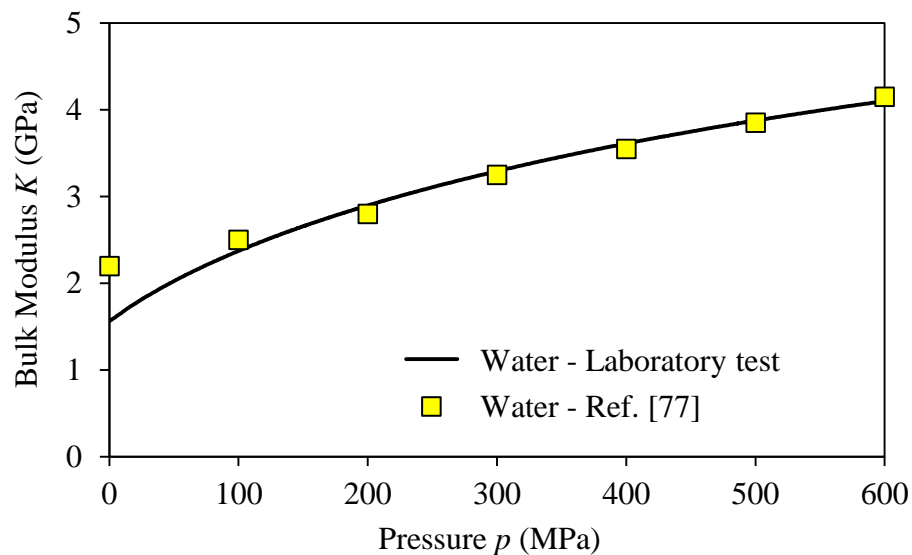
Figure 5.10: Bulk modulus K of water at increasing pressure.

5.6   Test Lubricants

Besides water, five different mineral oils were selected for the experiments, see Table 5.3. Most of the oils are common lubricants applied in sheet stamping operations of high strength steel and stainless steel. Two of them – with medium and high viscosity, respectively – contains additives with boundary lubrication properties. The

other two were mineral oils with no special additives. One of these was a high viscous oil, and the other one was a mixture of this and a low viscosity oil, giving a rather low, resulting viscosity. The last one was a chlorinated mineral oil, which is known to efficiently prevent galling but also considered to be hazardous to personnel and environment. Data for the test lubricants are listed in Table 5.3.

5.7   Results and Discussion

Figure 5.11 shows the measured volume change at various pressure levels. The TDN81 shows less compressibility in comparison to the other lubricants. Figure 5.12 shows the bulk modulus for the different types of liquid lubricants at various pressure levels. The other three lubricants, R300, R800 and CR5, have approximately the same bulk modulus.

Testing of the lubricant compressibility at elevated pressures has revealed that the lubricant bulk modulus is independent of lubricant viscosity, see Table 5.4 for the different lubricant viscosities. Larger viscosity lubricants do not provide larger bulk modulus. It is noticed that TDN81, which has medium viscosity, has the largest bulk modulus, whereas the oils R800, R300 and CR5 have approximately the same, lower bulk modulus. The mixed oil CR5-Sun has slightly lower bulk modulus than those.

Table 5.3: Properties and measured volume of the test fluids.

Lubricant type	Product name	Properties			Weight (g)	Volume (mℓ)
		Notation	Density (g/cm^3)	Kinematic viscosity at 40°C (cSt)		
Water	Water	Water	1.02	0.658	95.6	93.6
Plain mineral oil	CR5 Houghton Plunger	CR5	0.92	660	83.0	90.2
Plain mineral oil	CR5-Sun 60*	CR5-Sun	0.93	60	82.4	88.7
Mineral oil with additives	Rhenus LA722086	R800	1.11	800	96.4	87.1
Mineral oil with additives	Rhenus LA722083	R300	1.07	300	93.8	87.4
Chlorinated paraffin oil	TDN81	TDN81	1.20	150	107.6	99.3

50 wt. % mixture lubricant – Houghton Plunger CR5 (η=660 cSt) and Sunoco Sun 60 (η=10 cSt).
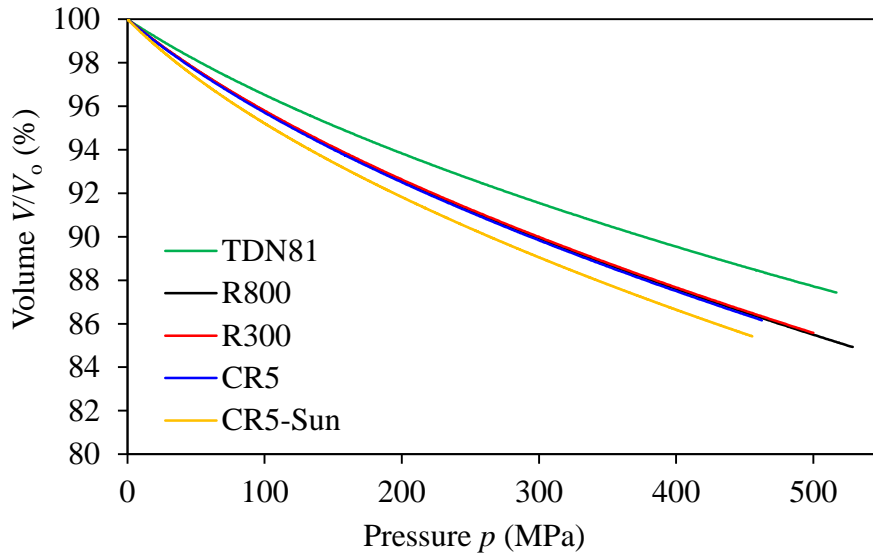
Figure 5.11: Relative volume V/V_o of the test lubricants at increasing pressure.
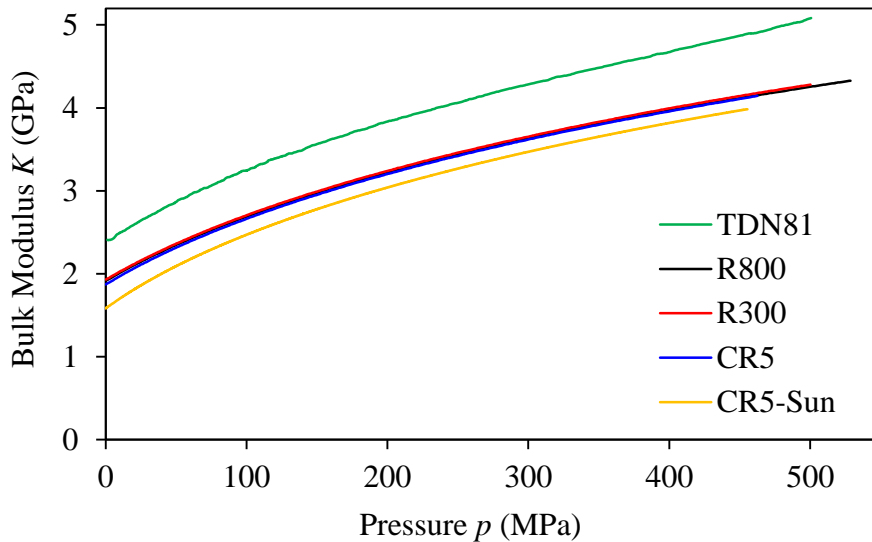
Figure 5.12: Bulk modulus K of the test lubricants at increasing pressure.

A nonlinear increase in bulk modulus with pressure is observed. At lower pressures, the bulk modulus increases more rapidly than at higher pressures. The bulk modulus at 500 MPa is about 2 to 2.5 times larger than at ambient pressure, and the compression of the lubricant is about 13 to 15 percent. In modelling of *MPHSL*, the compressibility of the lubricants versus pressure is an important input data if the pressure distribution and friction is to be calculated. Escape of the trapped lubricant can occur if the trapped lubricant generates a larger pressure than the sealing pressure

between the lubricated workpiece and the die [30] by the earlier mentioned *MPHDL* mechanism. Prediction of this also requires data on the lubricant bulk modulus.

5.8   Summary

A high-pressure equipment were developed for determining lubricant bulk modulus and has proven to work satisfactorily up to a pressure of 500 MPa. The pressure is measured directly inside the high-pressure container, which means that the test equipment allows a direct determination of the bulk modulus at varying pressure with no influence from friction in the sealing.

Part II
Structured Tool Surfaces

Overview

The PhD study is aimed at replacing the use of hazardous lubricants with hazard free lubricants. Part II presents investigations of creating lubricant pockets on tool surfaces with a focus on beneficial texture parameters to improve lubrication in sheet metal forming.

In this work, surface textures are shown to reduce friction in strip reduction of aluminium sheet. The textured tools were manufactured on a small pocket angle, shallow pocket depth, and oblong pockets oriented perpendicular to the sliding direction, with varying distances between the pockets. The use of tool texture leads to a positive result. The present work explains this by lubricant escape from the pockets due to micro-plasto-hydrodynamic lubrication, which influences a number of factors such as drawing load, resulting workpiece surface roughness and resistance to galling. The textured tool surface lowers friction and improves lubrication performance, provided that the distance between the pockets is 2–4 times larger than the pocket width. Larger drawing speed facilitates escape of the entrapped lubricant in the pockets. Experiments with low-to-medium viscosity lubricants lead to a low sheet roughness on the plateaus, but also local workpiece material pick-up on the tool plateaus. Large lubricant viscosity results in higher sheet plateau roughness and also prevents pick-up and galling.

A theoretical model for friction in strip reduction of a soft workpiece sliding on a table mountain-like topography of the tool surface is developed. The model elucidates the formation of an array of plastic waves in the soft workpiece surface when sliding on the hard, textured tool surface. The theoretical friction model supports the experimental findings of an optimum distance between the pockets, where the contribution to friction by mechanical interlocking of the strip in the tool pockets is limited and lubrication of the plateaus is enhanced by micro-plasto-hydrodynamic lubrication.

Chapter 6: Tool Texture for Improved Lubrication

6.1 Introduction

The application of structured tool surfaces in sheet metal forming is quite new. A simulative laboratory tribology test, i.e. Strip-Reduction-Test (SRT), was adopted to investigate the influence of tool texture. A number of flat mountain-like table topographies with flat plateaus and different pocket spacing were manufactured on the flat SRT. Low as well as high viscosity oils were tested at varying sliding speeds. Micro-textured surfaces on the tools were made using an in-house micro-milling machine. The present experiments on SRT are aimed at finding an optimal pocket spacing of the tool patterns described in the Chapter.

6.2 Tool Texture in Strip Reduction/Ironing

A detailed analysis of the flat mountain-like table topographies with flat plateaus and different pocket spacing was carried out. The investigation adopted a strip reduction/ironing of a soft sheet material sliding onto the flat table mountain-like topography of the tool surface in order to establish the possible influence between the textured tool surfaces and the micro-plasto-hydrodynamic lubrication mechanism.

6.2.1 Experimental Setup

A schematic outline of the SRT is shown in Figure 6.1, whereas Figure 6.2 shows a schematic of the experimental setup with the textured tool. A square die insert, supported by a thicker die holder, is pressed towards the strip. The reduction r in sheet thickness may be varied. The reduction r in each experiment was 15%, which emulates an ironing operation in aluminium can production. The strip and the die insert were subsequently drawn in horizontal direction up to a maximum sliding length of 300 mm under constant reduction. Drawing force was measured by a piezoelectric transducer. The front part of each aluminium workpiece strip was first flattened by rolling in an initial process, in order for the drawing jaw to be able to grip the end of the workpiece. Threshold sliding for the onset of galling was determined by visual inspection of the drawn strip and by roughness profile measurements of the strip perpendicular to the drawing direction. Two different drawing speeds (v = 240 and 65 mm/s) were applied with four different tool surfaces, as described in the following. The high and low drawing speeds were intended to identify the possible influence of the micro-plasto-hydrodynamic lubrication mechanism.
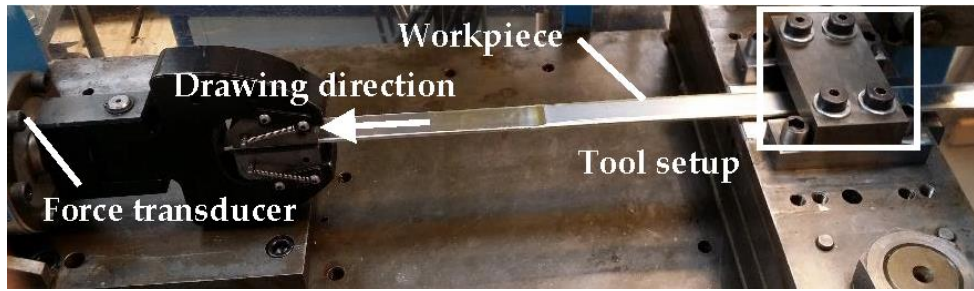
Figure 6.1: The strip reduction test. Detailed drawings are shown in Appendix E1.
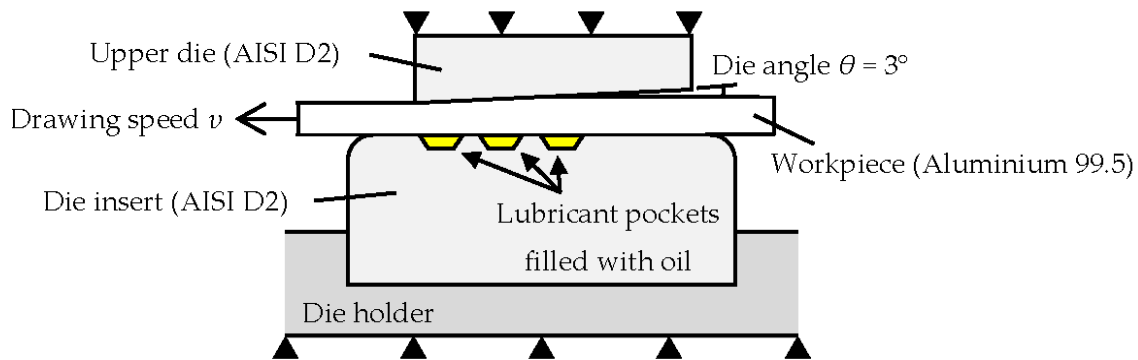
Figure 6.2: Schematic of the experiment with textured tool surface. The black triangles stand for a fixed support (a fixed press table, as shown in Figure 6.1).

6.2.2 Manufacturing of Surface Textures

A great number of surface texturing techniques are available for the texturing of hard tool materials, such as combined milling, grinding, and manual polishing [47], combined turning and Robot Assisted Polishing (RAP) [80], chemical etching [81], rolling ball indentation [49], and laser radiation [50][51]. In this study, high-speed hard machining combined with manual polishing was chosen as manufacturing method.

Figure 6.3 shows the process sequence for the manufacturing of a textured tool surface starting with the plane tool surface being lapped for ensuring the flatness of the die insert for alignment in the milling machine. Then, the tool surface was milled to Ra = 0.14 µm by the five-axis high speed milling machine, Mikron HSM 400U LP shown in Figure 6.4. After this, the transverse pocket geometry was machined with the previously mentioned milling tool running at 42,000 rpm and a feed of 600 mm/min.
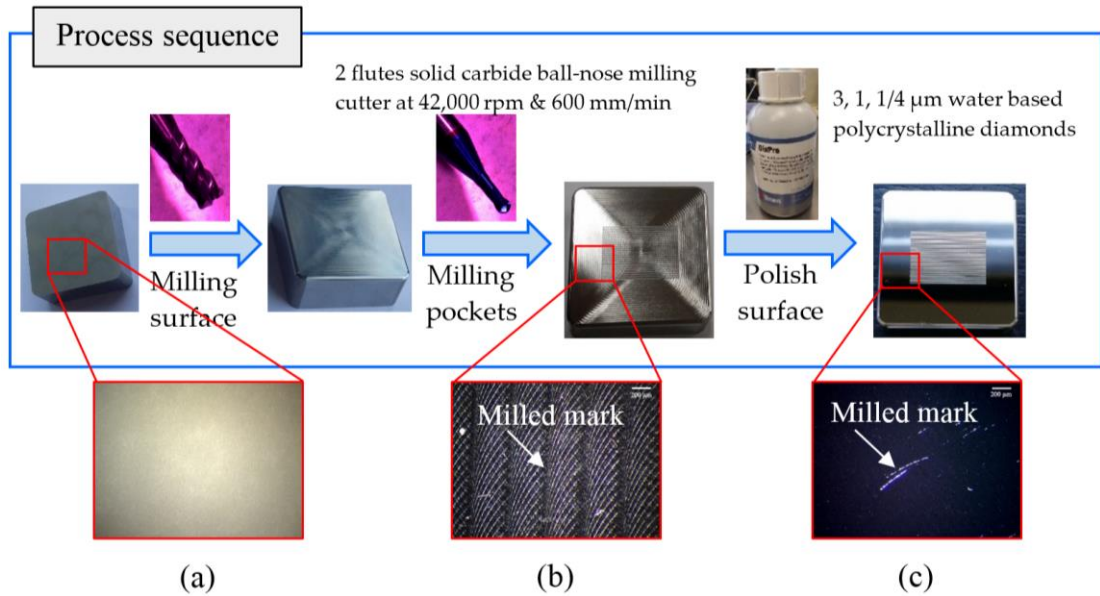
Figure 6.3: Pocket manufacturing process sequence starting with a) lapping, b) milling to create pockets and lastly, c) finish-polishing with various sizes of water-based diamonds producing an average roughness *Ra* 0.14 µm, 0.07 µm and 0.04 µm, respectively (left to right).

Figure 6.4: Five-axis high speed milling machine for machining the pockets.

6.2.2.1 Surface Texture Parameters

Two surface texture features are important parameters to promote the micro-hydrodynamic lubrication mechanism [20]; these are (1) small pocket angle γ and (2) shallow pocket depth d, see Figure 6.5. The pocket angle γ and the pocket depth d were chosen to be 5° and 0.01 mm, respectively. The small values of the pocket angle γ and the pocket depth d requires a large radius R of the milling tool for machining the pocket. The surface texture parameters can be calculated by Equations 6.1 and 6.2.

$$\tan \gamma = \frac{d}{a} \tag{6.1}$$

$$R^2 = a^2 + H^2 = a^2 + (R - d)^2 \tag{6.2}$$
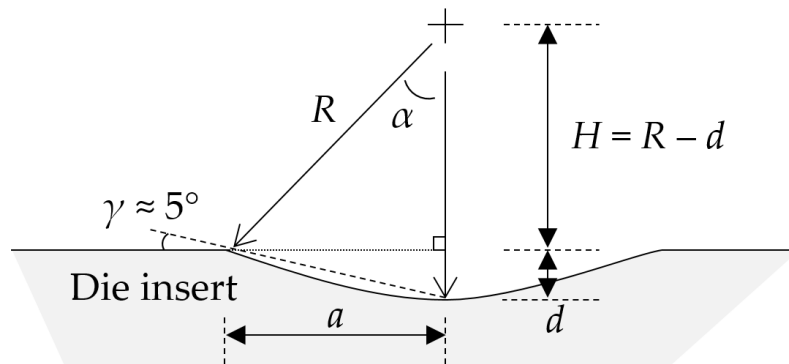
Figure 6.5: Selection of milling tool based on lubricant pocket geometry.

Figure 6.6 shows a schematic of the SRT die insert consisting of a deformation region (X x Y = 11.5 mm x 20 mm) and the transverse pocket length y = 16 mm. A TiAl70 coated milling tool having a two-flute solid carbide ball-nose and a radius R of 1.25 mm was used for machining the transverse flat-bottomed lubricant pockets in the surface of the hardened tool, see Figure 6.7. Three different inserts where manufactured, the only difference being the distance between the pockets x. Table 6.1 lists the surface texture parameters for the SRT tool in which varying distance between pockets x = 0.23, 0.46 and 0.92 mm gave contact area ratios A_{ro}/A_o = 60, 74 and 84 %, respectively.
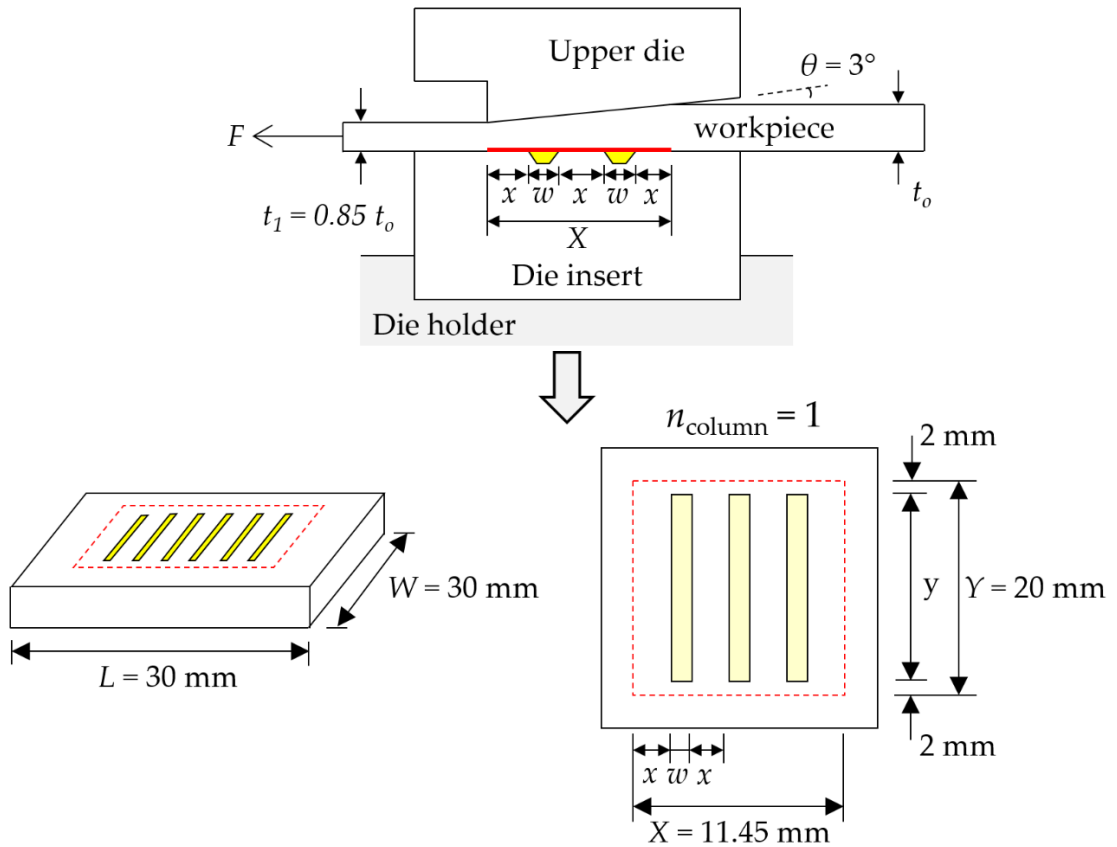
Figure 6.6: Texturing parameters: distance between pockets x, pocket depth d, pocket width w, and number of pockets n. The red dotted frame shows the contact region between the textured features and the workpiece surface. $n_{\text{column}} = 1$ is the number of grooves in a column position. Technical drawings are shown in Appendix E2.

(a)   (b)
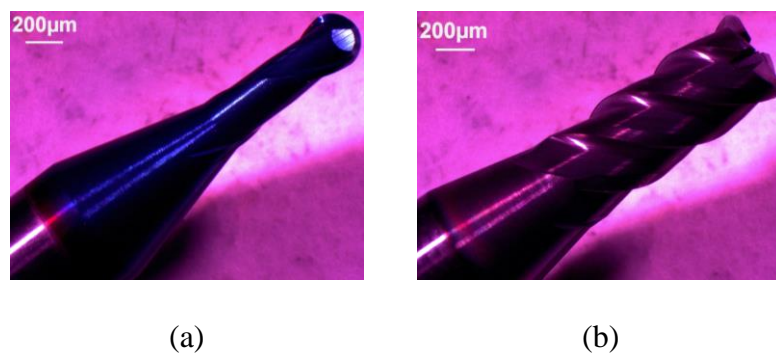
Figure 6.7: Tools used for a) milling the pocket and b) milling the whole flat surface.

Table 6.1: Target surface texture parameters.

Parameters	Value		
Pocket angle γ	5°		
Pocket width $w = 2a$	0.23 mm		
Pocket depth d	0.01 mm		
Pocket ratio d/w	0.05		
Distance between pockets x	$1 \times w$ (x=0.23 mm)	$2 \times w$ (x=0.46 mm)	$4 \times w$ (x=0.92 mm)
Number of pocket rows n_{row}	25	16	10
Number of pocket columns n_{column}	1	1	1
Contact area ratio (A_{ro} / A_o)	60 %	74 %	84 %

6.2.2.2 Characterization of Textured Features

After machining and polishing, the resulting textured patterns were examined. The textured die insert pocket geometries and the surface was measured by a tactile roughness profilometer, Taylor Hobson Form TalySurf Series 2 50i and the images and roughness were then analysed by an analytical software for microscopy, SPIP. Figure 6.8 and Figure 6.9 represent the resulting, measured pockets with dimensions: length y = 16 mm, angle $\gamma = 5° \pm 0.5°$, width $w = 0.23 \pm 0.01$ mm, depth $d = 7 \pm 1$ μm, and distance between pockets of x = 0.23, 0.46, and 0.92 mm, respectively. Subsequent polishing of the tool surfaces were done in three steps with water based polycrystalline diamonds of grain sizes 3, 1, and 0.25 μm, resulting in a final roughness Ra = 0.01−0.04 μm. The pocket depths were reached within the tolerance gap, whereas the pocket angles turned out to be somewhat smaller than the target value. However, this only promotes the micro-hydrodynamic lubrication mechanism and prevents mechanical interlocking.
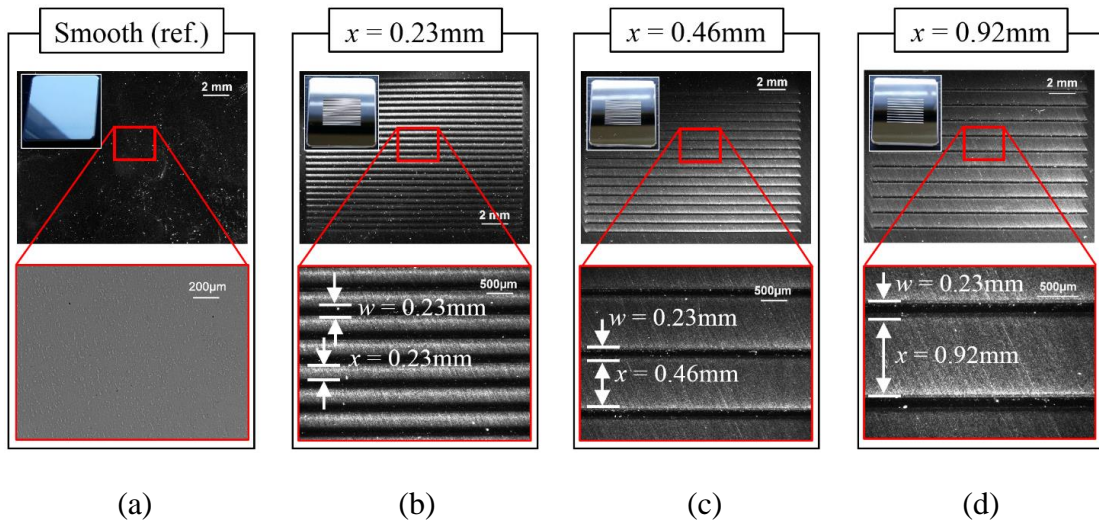
Figure 6.8: Die inserts with a) smooth surface as reference, and with varying pocket interspacing x of b) 0.23mm, c) 0.46mm and d) 0.92mm. The flat plateaus were polished down to a roughness Ra $0.01 - 0.04$ µm.
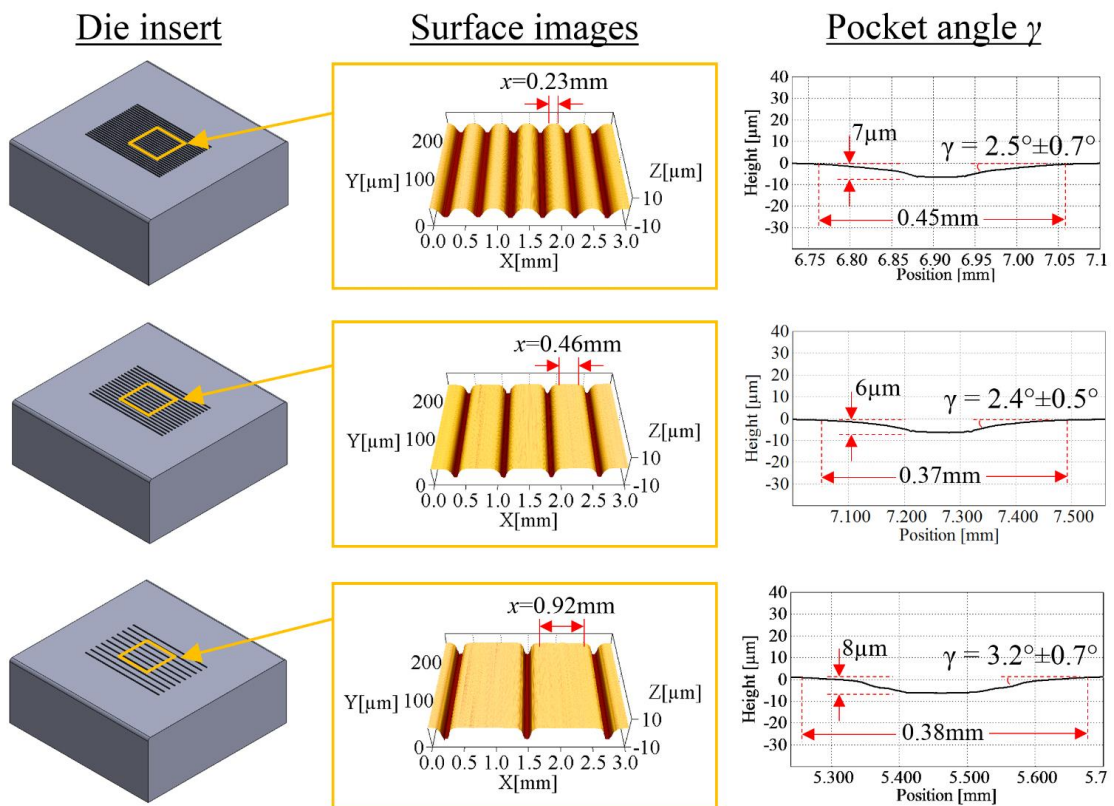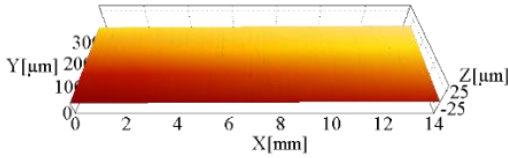
Figure 6.9: Textured die insert pocket geometries.

6.2.3   Test Materials

6.2.3.1 Tool Material

The tool material was made of Sverker 21 corresponding to AISI D2 cold work tool steel (Uddeholm AB, Hagfors, Sweden), a high carbon, high chromium tool steel alloyed with molybdenum and vanadium. The tools were through-hardened and tempered to 60 HRC before the surface texturing procedure described above. After this, the surface finish of the upper die and the die insert were polished to a low roughness *Ra* as shown in Table 6.2. The tool material is feasible for forming of aluminium sheet material, due to its high wear resistance, high compressive yield strength, and resistance towards pick-up of ductile materials like pure aluminium. It is furthermore easy to remove possible pick-up of aluminium by etching in a warm sodium hydroxide solution.
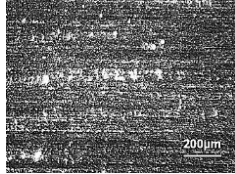
Table 6.2: Surface finish of the dies before the first experiment.

Components	Material type	Roughness *Ra* (µm)	Surface images
Upper die	Sverker 21	0.01	
Die insert (Smooth surface) – "Reference"	Sverker 21	0.02	

6.2.3.2 Workpiece Material

The workpiece material was a commercially pure Al 99.5 %, H111 (from Metal service, Horsens, Denmark) with dimensions 480 mm × 20 mm × 4 mm. The 4 mm sheet thickness ensures a sufficient deformation region (tool/workpiece contact length) for a fairly large number of pockets to be within the deformation zone. This will reduce the experimental scatter due to the results being less sensitive to the exact number of pockets within the deformation zone. The sheet width was chosen to be large enough to ensure approximately plane strain deformation conditions resembling ironing. The as-received workpiece surface roughness was *R*a = 0.21 µm, Table 6.3. The stress–strain curve of the material shown in Figure 6.11 was determined by plane strain compression test. Figure 6.11 also shows a curve fit and the determined material constants according to the Voce flow curve expression.

Table 6.3: Surface finish of the workpiece before the first experiment.

Components	Material type	Roughness Ra (µm)	Surface images
Workpiece	Aluminium Al 99.5 %	0.21	
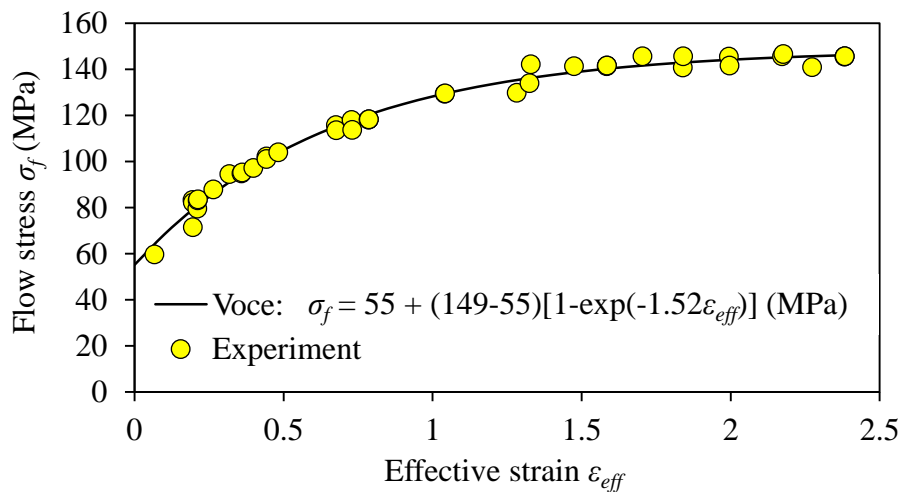
Figure 6.11: Voce flow stress curve expression for the aluminium Al 99.5 % sheet.

6.2.3.3 Lubricants

Four different mineral oils were chosen for the experiments. Two of them – with medium and high viscosity, respectively – contained additives with boundary lubrication properties. The other two were mineral oils with no special additives. One of these was a high viscous lubricant, and the other one was a mixture of this lubricant and a low viscous lubricant, giving a rather low resulting viscosity. Data on the test lubricants are listed in Table 6.4.

Table 6.4. Properties of the test lubricants.

Lubricant Type	Product Name	Kinematic Viscosity η (cSt @ 40°C)
Mineral oil with additives	Rhenus LA 722086	800
Mineral oil with additives	Rhenus LA 722083	300
Pure mineral oil	CR5 Houghton Plunger	660
Pure mineral oil	CR5–Sun 60	60

6.2.4 Experimental Procedure

The test started by cleaning the tool and workpiece surfaces from any remnants of pick-up, lubricant, grease, and other contaminants. Subsequently, the lubricant was applied to the different tool surfaces, after which the sheet drawing experiment was carried out. During the experiment, the drawing load was recorded, and the load versus time data was saved by a custom made LabView program. The same procedure was repeated for the different lubricants. The plotted results were based on three to five repetitions of each parameter investigated (i.e., lubricant, drawing speed, and tool texture). Before and after the experiment, the tool and workpiece surfaces were scanned in a light optical microscope (LOM, Leica Microsystems, Heerbrugg, Switzerland) and measured by a tactile roughness profilometer, Taylor Hobson Form TalySurf Series 2 50i. The listed roughness Ra was based on an average of six measurements.

6.2.5 Analysis of Varying Plateau Distance

The drawing load reaches steady-state condition after a short time, as seen in Figure 6.12, which shows the results for the two different lubricants at lower drawing speed $v = 65$mm/s. No load difference is observed at lower speed except that the transverse pocket with $x = 0.23$ mm leads to a larger forming load.
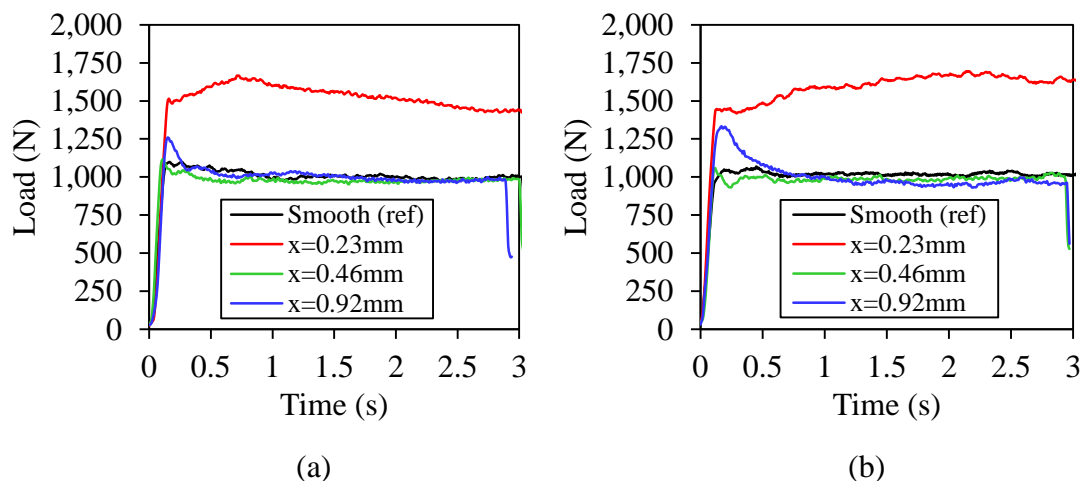
Figure 6.12: Forming load at speed $v = 65$ mm/s for (a) Rhenus oil $\eta = 800$ cSt; and (b) Rhenus oil $\eta = 300$ cSt.

Figure 6.13 shows similar forming load patterns for the four different lubricants at larger drawing speed $v = 240$ mm/s in which the drawing load reaches steady-state after a short time. The influence of tool texture is significant at higher speed regardless of the lubricant applied. The small distance between the pockets ($x = 0.23$ mm) leaves

only a small, flat plateau between the pockets (see Figure 6.9 top). This promotes metal flow into and out of the pockets, which will provide a mechanical gripping effect of the workpiece. The indent depth of the workpiece onto the surface pocket are smaller than the pocket width, hence the pockets are not completely emptied when the workpiece goes in and out of the pockets. Marks of the die insert texture on the strip can be seen at the end of the reduction zone, Figure 6.15 (left).
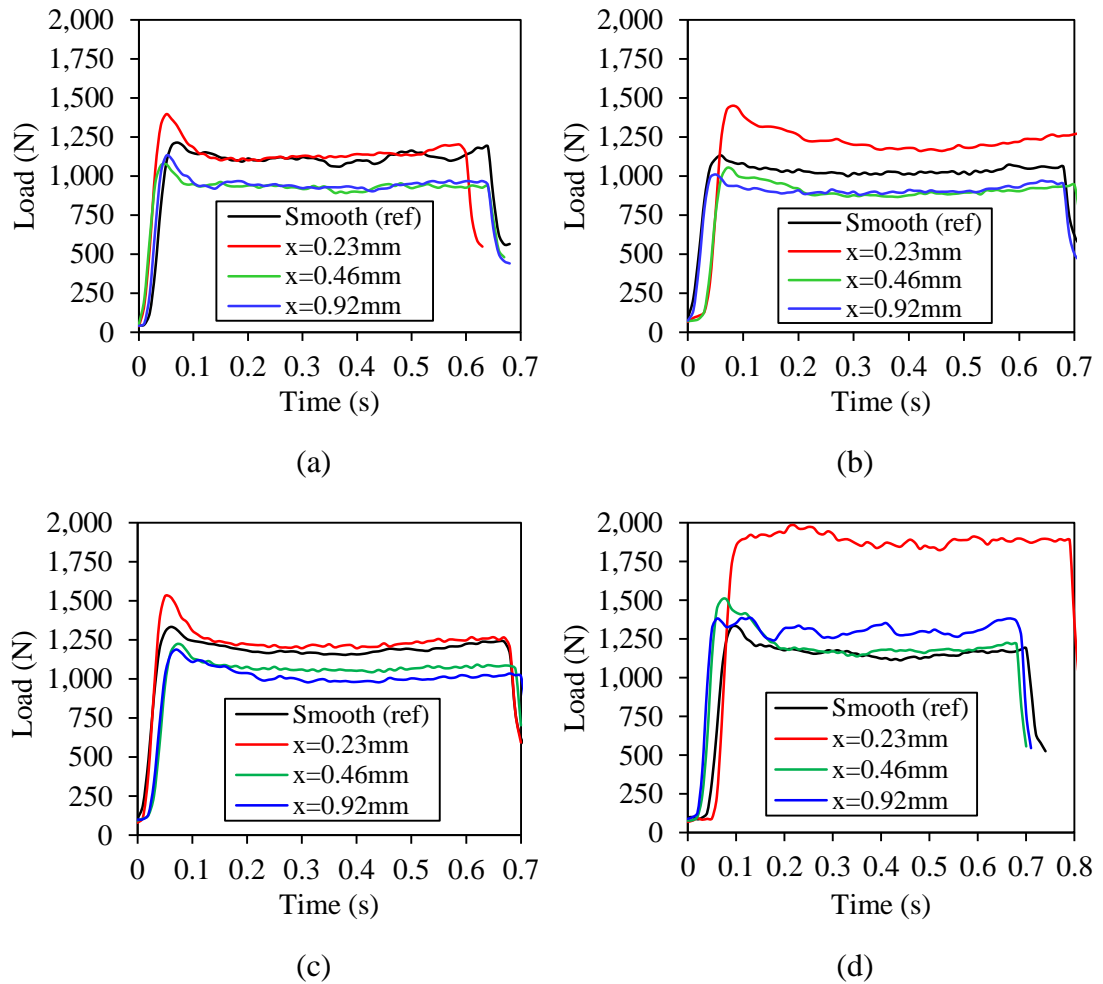
Figure 6.13: Drawing load at speed v = 240 mm/s for (a) Rhenus oil η = 800 cSt; (b) Rhenus oil η = 300 cSt; (c) mineral oil CR5 η = 660 cSt; and (d) mineral oil mixtures CR5-Sun 60 η = 60 cSt.

The positive influence of high drawing speed is explained by micro-plasto-hydrodynamic lubrication, which is promoted by high sliding speed and high lubricant viscosity [21]. Since no improvements were noted on the drawing load when testing tool textures at the lower speed (65 mm/s, Figure 6.12), the rest of the discussion is focused on the tool texture at larger speed (240 mm/s, Figure 6.13). It is noticed here that the tool texture with x = 0.46 mm and x = 0.92 mm (two to four times the pocket

71

width *w*) has reduced the drawing load as compared to the smooth tool surface when testing with the larger viscosity lubricants, while testing with the low-viscosity pure mineral oil CR5-Sun 60 had the opposite effect. This is believed to be due to the previously mentioned relationship between viscosity and micro-plasto-hydrodynamic lubrication.
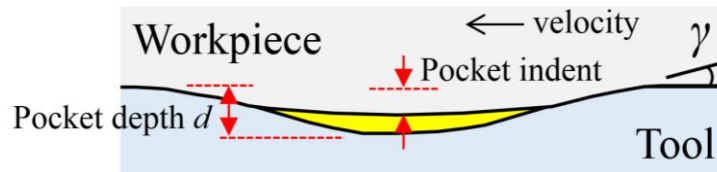
Figure 6.14: Illustration of pocket indent and the pressurization of the trapped lubricant in a pocket.

Figure 6.15 shows that the tool texture increases the sheet roughness as compared to the smooth die surface, regardless of the test lubricants investigated. The tool texture with pocket distance $x = 0.23$ mm gave smallest sheet roughness among the textured inserts. It is furthermore noticed that increasing viscosity leads to increasing roughness of the strip plateau. This may be explained by improved micro-plasto-hydrodynamic lubrication at higher viscosities, leading to an effective separation between the tool and the workpiece on the plateaus of the tool table mountain [22]. The sheet roughness profiles shown in Figure 6.16 confirm this. The *R*a values on the plateaus are measured by a tactile roughness profilometer, Taylor Hobson Form TalySurf Series 2 50i. They are based on an average of six measurements.

The Rhenus oil contains additives providing a protective boundary film, which can carry the load and prevent metal-to-metal contact. This contributes to lower friction and prevents lubricant film breakdown. The additives in the Rhenus oils furthermore prevent these oils from decomposition and vaporization [23].
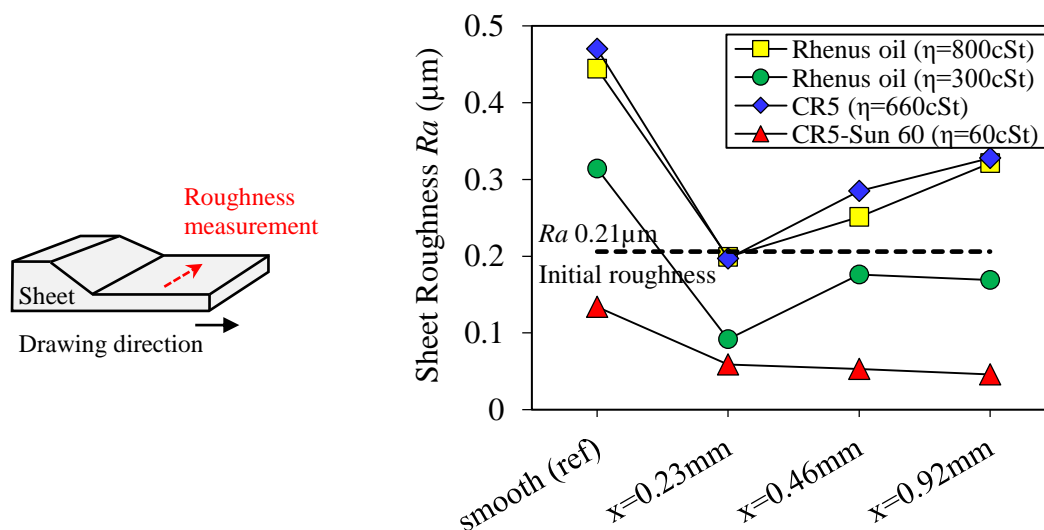
Figure 6.15: Sheet roughness on the plateaus at $v = 240$ mm/s drawing speed.
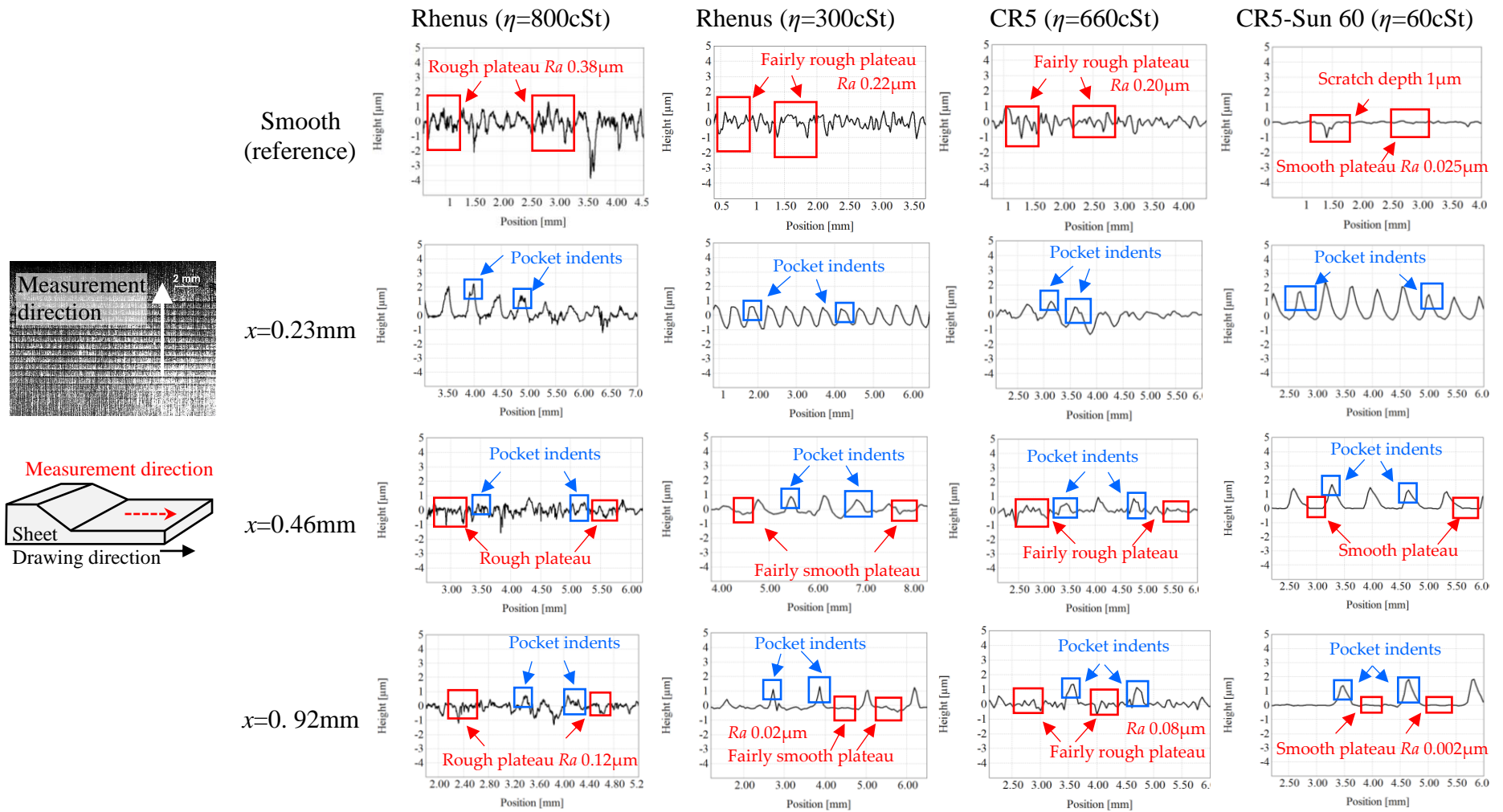
Figure 6.16: Roughness profiles of the sheets flowing into the pockets when testing with different tool textures and lubricants at v = 240 mm/s drawing speed.

Shiny, mirror-like surfaces of all the die inserts before and after experiments can be seen in Figure 6.17. It is difficult to observe pick up of aluminium material just by a visual inspection. Figure 6.18 shows images of the tool surface using a light optical microscope and scanning electron microscopy with energy dispersive X-ray spectroscopy (SEM/EDX), utilized to observe possible pick-up of workpiece material on the tool surface in the contact region. Testing of the Rhenus oil with a viscosity of 800 cSt showed no sign of pick-up, which is explained by the complete separation between the tool and the workpiece surface, as evidenced in Figure 6.15.
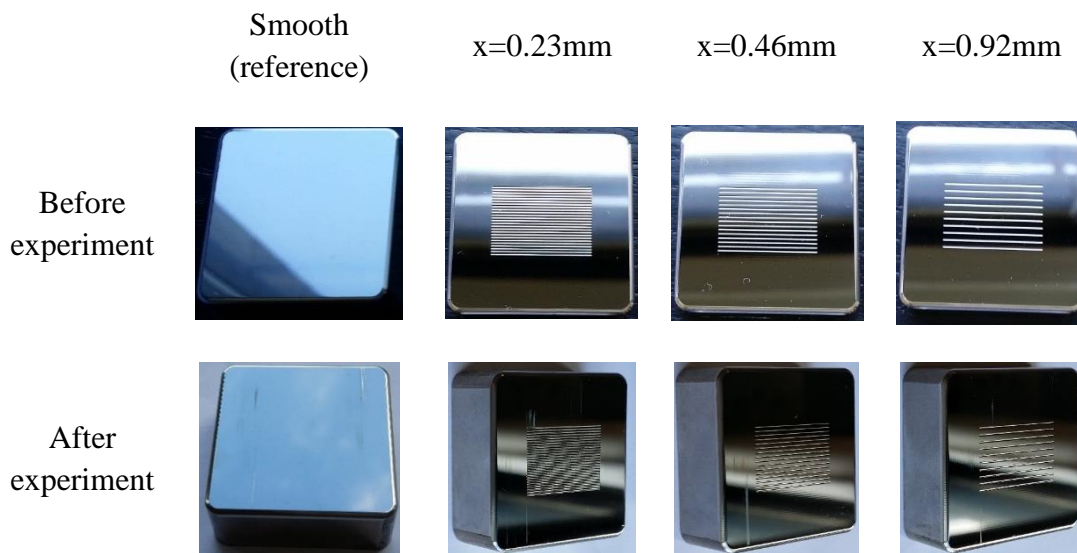
Figure 6.17: Shiny and mirror-like insert surface condition before and after experiments.

Pick-up of aluminium was observed on the plateaus of the table mountain structure, especially in the last part of the tool/workpiece contact region corresponding to a thickness reduction r close to 15%. The rectangular frames in the LOM images marked A, B, C, and D in Figure 6.18 indicates the approximate locations of the SEM images, although the frames are larger than the SEM images. Testing of the Rhenus oil with a viscosity of 300 cSt and the pure mineral oil with a viscosity of 660 cSt resulted in 0.2–1.0 wt % and 0.1–0.2 wt % pick-up, respectively, while the low viscosity CR5-Sun 60 oil resulted in an increased amount of aluminium pick-up to 0.3–17.9 wt %. No pick-up was observed when testing the Rhenus oil with a viscosity of 800 cSt. This is as expected, since the low-viscosity mineral oil with no special additives does not promote micro-plasto-hydrodynamic lubrication and has no boundary lubrication properties, whereas the higher viscosity Rhenus oil and the high viscosity pure mineral oil may support micro-hydrodynamic lubrication and the Rhenus oil furthermore has boundary lubricating properties. The slightly better performance of CR5 compared to

the lower viscosity Rhenus oil further supports the hypothesis of micro-hydrodynamic effects.
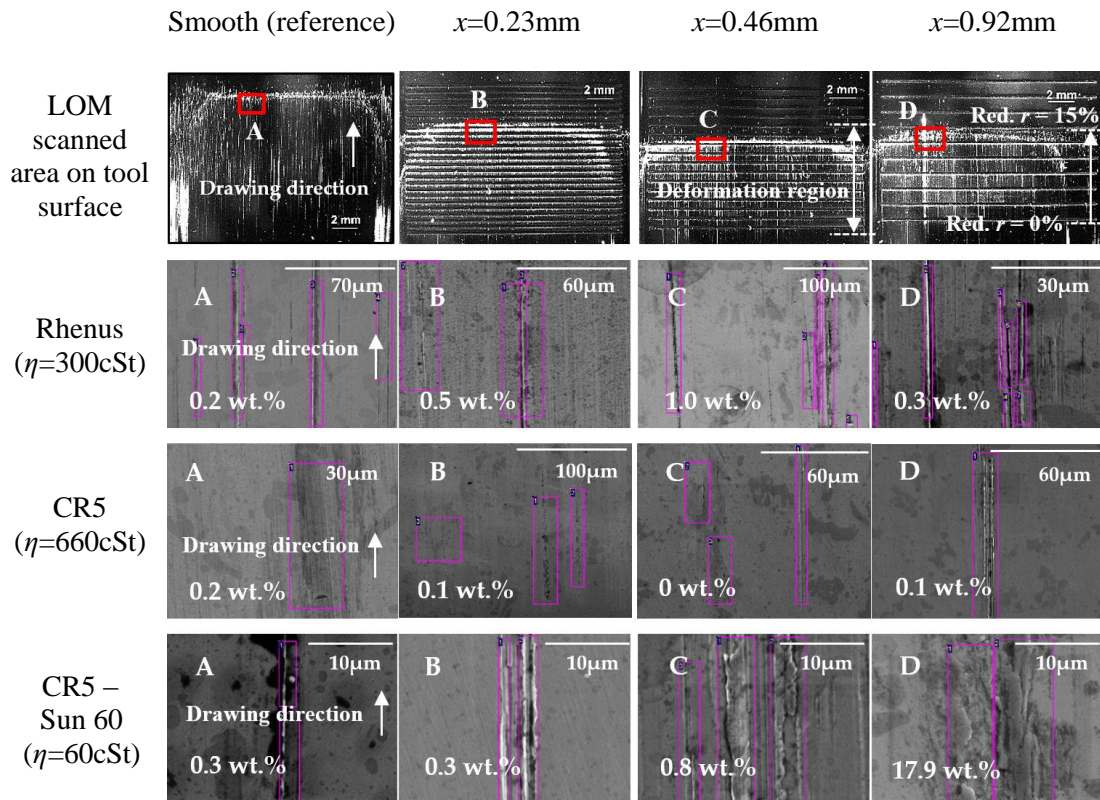
Figure 6.18: Pick-up at the larger reduction region r of 15%. The red marked locations named A, B, C and D in the LOM micrographs are shown in larger magnification in the SEM micrographs below the first row. The purple squares indicate where the amount of pick-up was determined.

6.3 Analysis of Varying Contact Area Ratio α

Further investigation on a larger contact area α has been performed by creating a small gap y in between the oblong pockets. Figure 6.19 shows the die insert consisting of a deformation region, X x Y = 11.5 mm x 20 mm, and a transverse pocket length y = 16 mm. Varying textured features between the pockets were manufactured both transversal (*Tool A*), Figure 6.4, and longitudinal (*Tool B* and *Tool C*), Figure 6.19, to the sliding direction. Table 6.5 lists the surface texture parameters in form of contact area ratio α along the tool/workpiece interface. The smooth tool surface with no textures on the tool surface has a contact area ratio $\alpha = 1$. The target surface texture parameters listed in Table 6.1 were also applied in this investigation of the varying contact ratio except the number of pocket columns n_{column}. The number of pocket columns n_{column} =

1 for *Tool A* is identical to details for n_{column} value as described in Table 6.1. Meanwhile, $n_{column} = 4$ was manufactured onto *Tool B* and *Tool C* surfaces. The pocket length *y* for *Tool B* is 4 mm and *Tool C* is 2.5 mm. This gives the plateau distance in longitudinal direction for *Tool B* is 0.8 mm and *Tool C* is 2 mm. The *α*–value for *Tool B* and *Tool C* are described in Table 6.5. The *α*–value for *Tool A* remains identical to the one listed in Table 6.1.

(a)   (b)
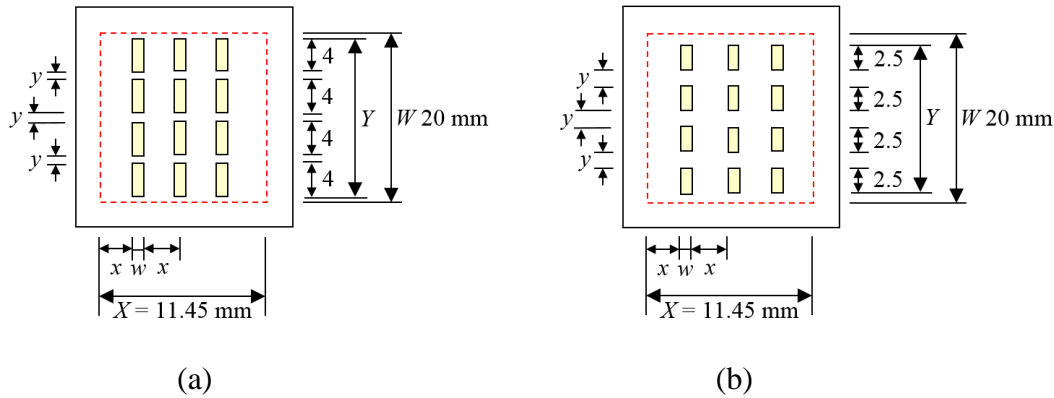
Figure 6.19: Different textured insert surfaces with varying distance between pockets in longitudinal to the sliding direction for a) longitudinal pocket length of 4 mm (*Tool B*) and b) longitudinal pocket length of 2.5 mm (*Tool C*). Sliding occurs in vertical direction. Technical drawings are shown in Appendix E2.

The strip reduction test was adopted to evaluate the influence of varying contact area ratio. The target surface pocket geometries shown in Table 6.5 is identical to the oblong pockets manufactured on the die inserts with varying plateau distance *x* in the previous section. The target surface texture parameters are listed in Table 6.6. Notation of tool types for *Tool A*, *Tool B* and *Tool C* with varying contact area ratio *α* are described in Table 6.7.

Table 6.5: Target pocket geometries.

Parameters	Value
Pocket angle γ	5°
Pocket width $w = 2a$	0.23 mm
Pocket depth d	0.01 mm
Pocket ratio d/w	0.05

Table 6.6: Target surface texture parameters. Technical drawings for the die inserts with varying pocket geometries are shown in Appendix E1.

Tool types	Tool A	Tool B	Tool C
Distance between pockets x (mm)	$1 \times w$ ($x = 0.23$mm)	$2 \times w$ ($x = 0.46$mm)	$4 \times w$ ($x = 0.92$mm)
Number of pocket rows n_{row}	25	16	10
Number of pocket columns n_{column}	1	4	4
Distance between pocket columns y	-	0.8 mm	2 mm

Table 6.7: Notation of tool types with varying contact area ratio α.

Tool types / Plateau distance x	Notation / Contact area ratio α (%)		
Tool A ($x = 0.23$mm)	A1 ($\alpha = 60\%$)	A2 ($\alpha = 74\%$)	A3 ($\alpha = 84\%$)
Tool B ($x = 0.46$mm)	B1 ($\alpha = 60\%$)	B2 ($\alpha = 74\%$)	B3 ($\alpha = 84\%$)
Tool C ($x = 0.92$mm)	C1 ($\alpha = 75\%$)	C2 ($\alpha = 84\%$)	C3 ($\alpha = 90\%$)

The similar test materials used in the previous experiment was also applied in this experiment. Reduction $r = 15\%$, a maximum sliding length of 300 mm under constant reduction, a drawing speed of $v = 240$ mm/s and the Rhenus oil with a viscosity of 800 cSt were also applied in this experiment. This experiment adopted the positive influence of high drawing speed and high lubricant viscosity in order to promote micro-plasto-hydrodynamic lubrication.

This section discusses all oblong pockets with different longitudinal gap y (*Tool B* and *Tool C*) in regards to contact area ratio α in more detail (see Figure 6.19 and Table 6.7). Figure 6.20 shows measurements of average drawing loads in the steady-state condition as a function of contact area ratio at a drawing speed of 240 mm/s. Tool textures with too large amount of pocket area, i.e, with low α-value, was found to increase the drawing load. Too small amount of pocket area, on the other hand, may also lead to increased drawing load since the lubricant escape by micro-plasto-hydrodynamic lubrication may not be sufficient to cover the entire flat plateau. This implies an increase in drawing load due to increased metal-to metal contact. Otherwise, the drawing load decreases with larger α-value. It is noticed that an optimum α-value exists in which the contribution to mechanical interlocking of the workpiece into the pockets is limited and lubrication is enhanced by the micro-plasto-hydrodynamic lubrication.
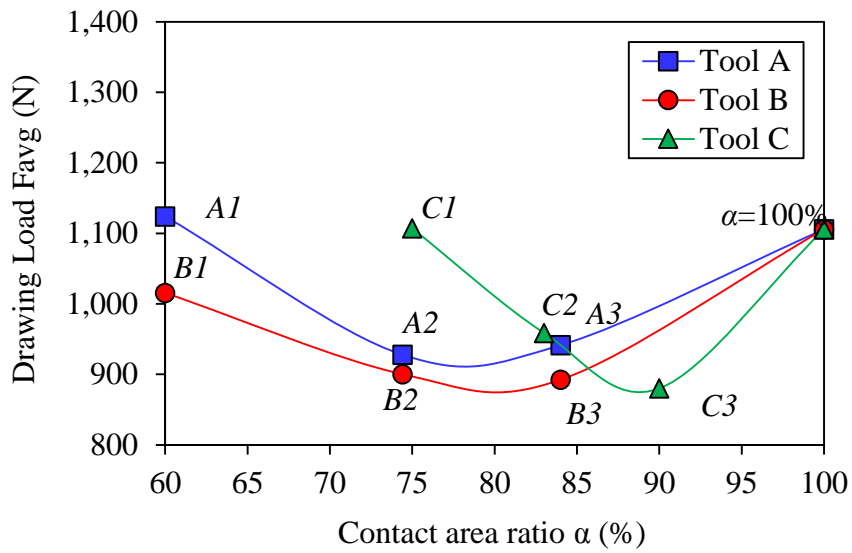
Figure 6.20: Influence of contact area ratio α on the drawing load.
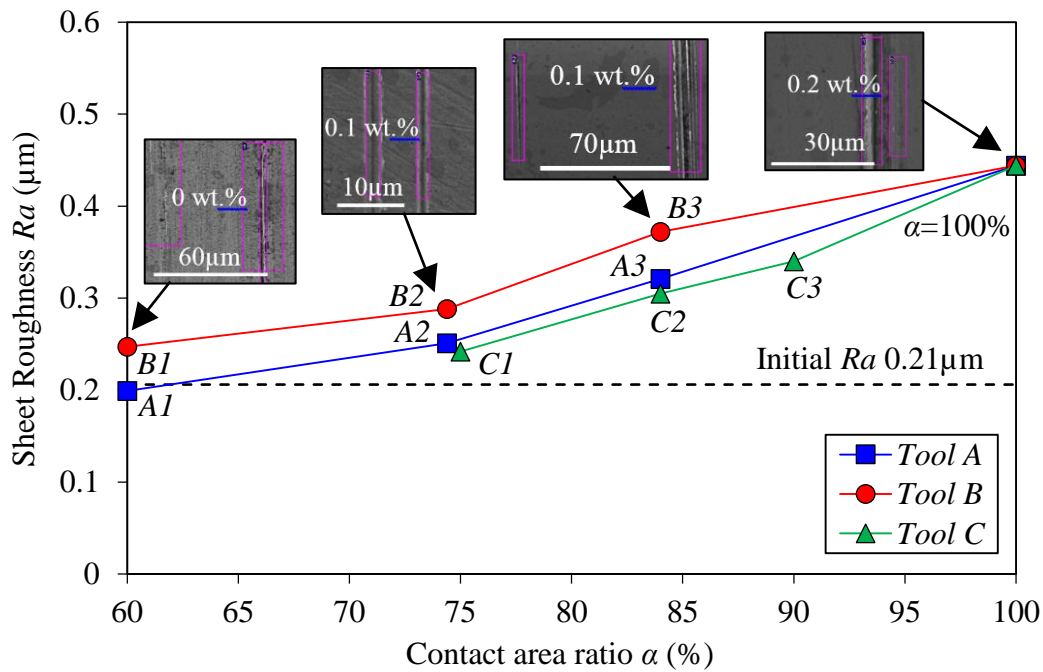
Figure 6.21: Influence of contact area ratio α on the sheet roughness in SRT. SEM pictures with the amount of aluminium pick-up is also seen.

The tool texture with a large amount of pocket area, i.e, low α-value, gave smallest sheet roughness in comparison to the smooth tool surface. This may be explained by improved micro-plasto-hydrodynamic lubrication at larger viscosities

leading to an effective separation between the tool and the workpiece on the plateaus of the tool table mountain [30]. In addition, application of the Rhenus oil generates a thin, protective film to separate the tool/workpiece interface. LOM images presented in Figure 6.21 confirmed this, where almost no pick-up of aluminium is observed on the plateaus of the table mountain structure.

6.4   Summary

A technique to improve resistivity towards galling by applying textured tool surface topographies was investigated. Oblong shallow pockets with small pocket angles, oriented perpendicular to the sliding direction with a distance of 2–4 times the pocket width were tested. A strip reduction test, which emulates the tribological conditions in an ironing process, was used for experimental measurements of friction and determination of possible pick-up and galling. The study included testing of four different lubricants—two plain mineral oils with a low and a high viscosity, and two mineral-based oils with boundary lubrication additives having medium and high viscosity. The results confirmed that the tool texture can lower friction and improve lubrication performance in comparison to that of a fine polished tool surface when the pocket distance is larger than the pocket width, which ensures a table mountain structure of the tool topography. The tool textures were advantageous at greater sliding speeds, when using higher viscosity oils, which facilitates the escape of trapped lubricant by micro-plasto-hydrodynamic lubrication.

Chapter 7: A Theoretical Friction Model for Textured Tool Surfaces

7.1   Introduction

The experimental studies in Chapter 6 have shown tool textures to be advantageous at increased sliding speeds, when using higher viscosity oils, in which lubricant escape from the pockets is promoted by micro-plasto-hydrodynamic lubrication. This contributes to a number of factors such as drawing load, resulting workpiece surface roughness, and resistance to galling. Since frictional conditions between the textured tool and the workpiece are important, the present chapter is presenting a friction model of a soft workpiece sliding on a tool with a table mountain-like topography surface. The model elucidates a mechanism of an array of plastic waves in the soft workpiece surface interacting with flat plateaus and narrow pockets in between the plateaus.

Figure 7.1a shows a schematic of the strip reduction test, whereas Figure 7.1b shows the table-mountain-like tool surface topography obtained by a tactile roughness profilometer, Taylor Hobson Form TalySurf Series 2 50i. The images were then analysed by a surface analysis software for microscopy, SPIP. Three surface texture features are important parameters to promote the micro-hydrodynamic lubrication mechanism and to avoid mechanical interlocking of the strip in the pocket valleys [82][83], which are 1) oblong pockets oriented perpendicular to the drawing direction, 2) small pocket angle γ and 3) shallow pocket depth d.

Three different texture designs were chosen with a width of flat plateaus between the lubricant pockets of $x = 0.23$, 0.46 and 0.92 mm, respectively. The oblong pockets were made with a small pocket angle $\gamma \cong 3°$, width $w \cong 0.3$ mm and shallow depth $d = 7 \pm 1$μm by hard machining and subsequent manual polishing of the tools. The milling tool running at 42,000 rpm and a feed of 600 mm/min on the a five-axis high speed milling machine, Mikron HSM 400U LP, whereas the subsequent polishing of the tool surfaces were done in three steps with water based polycrystalline diamonds of grain sizes 3, 1, and 0.25 μm, resulting in a final roughness Ra = 0.01−0.04 μm.

The pocket angle was chosen according to recommendations by Popp and Engel [84], the depth was determined by the width, which was chosen small enough to ensure a sufficient number of pockets along the tool/workpiece interface. The length of the pockets $l = 16$ mm, were smaller than the workpiece width in order to ensure pressure build-up of the trapped lubricant. The workpiece material was Al 99.5 % − H111 strips, 4 mm thick and 20 mm wide and used in the "as-received" condition. The reduction was kept constant as $r = 15\%$. The drawing speed v was 240 mm/s.
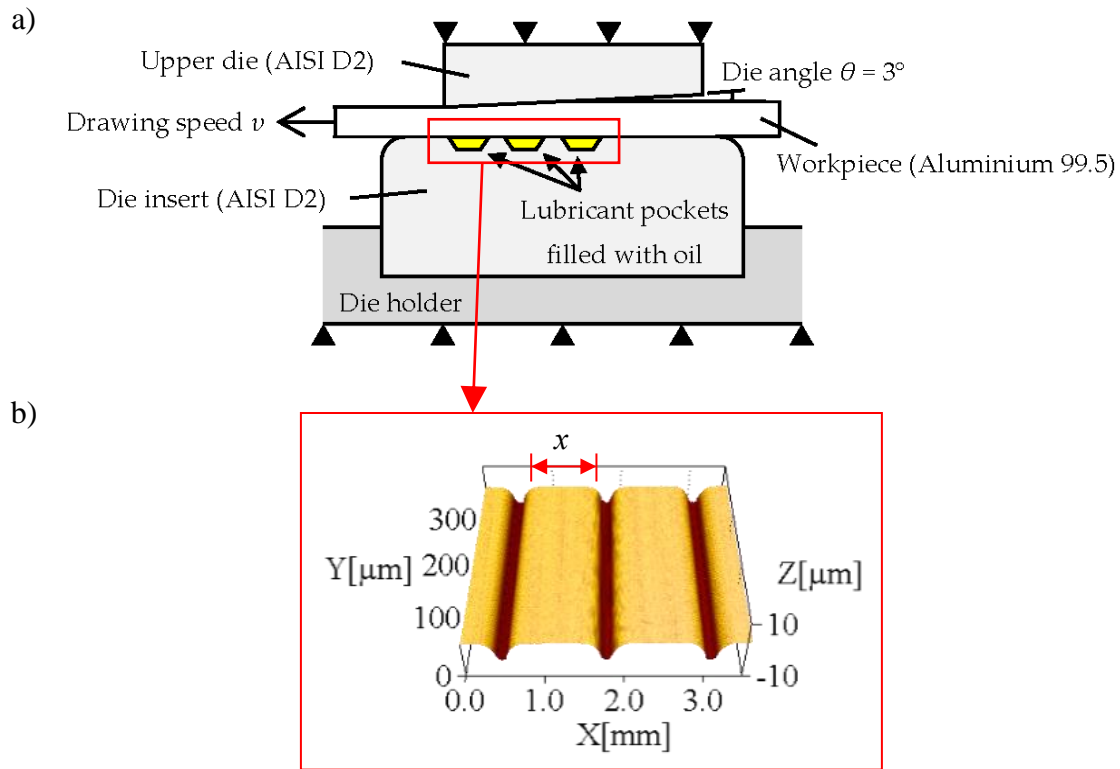
Figure 7.1: a) Strip reduction test with interchangeable die inserts and b) table mountain-like topography die surface obtained by SEM.

7.2 Theoretical Friction Model for Micro-Hydrodynamic Lubrication Mechanism on Textured Tool Surfaces

Figure 7.2a shows the contributions to friction in the lower, textured tool/workpiece interface. They include a contribution from the metal-to-metal contact area with relative area α and a contribution from the contact between the workpiece and the lubricant filled pocket. Partly penetration of the workpiece material into the pocket and pressurization of the lubricant appears as shown in Figure 7.2b, when loading is applied. When sliding is superimposed, the workpiece material forms a wave motion moving in and out of the pocket, when passing it. At the same time the lubricant is dragged out of the pocket by viscous forces and thereby providing lubrication to the flat tool part by the micro-hydrodynamic mechanism as illustrated in Figure 7.2c.
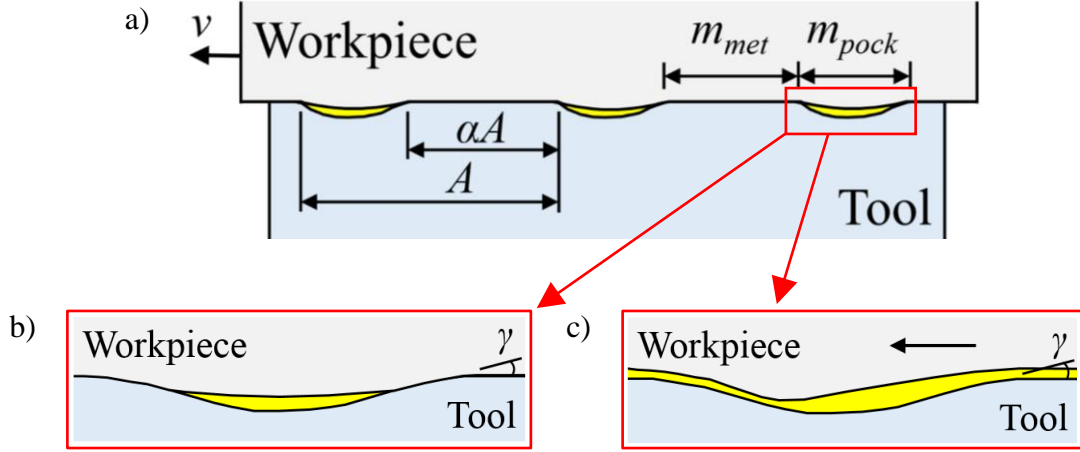
Figure 7.2: (a) Notation, (b) compression of lubricant trapped in pocket, (c) lubrication of plateaus by lubricant escaped from the pocket.

The overall friction factor m_{tex} representing the combined friction factor of the lower, textured tool surface is determined by:

$$m_{tex} = \alpha m_{met} + (1 - \alpha) m_{pock} \tag{7.1}$$

where $\alpha = A_{met}/A$ is the metal-to-metal contact area ratio between the flat plateau A_{met} and the total contact area A in the deformation zone. The relative area of contact between the pocket and the strip is then $(1 - \alpha)$. m_{met} is the local friction factor between the strip and the flat plateau. The local pocket friction factor m_{pock} is given by:

$$m_{pock} = m_{lub} + m_{wave} \tag{7.2}$$

where m_{lub} is the friction factor due to viscous drag forces between the strip and the trapped lubricant in the pockets and m_{wave} is the apparent friction factor caused by the material wave movement into and out of the pockets. The viscous drag effect of the lubricant in the pocket is assumed minimal, i.e. $m_{lub} = 0$. Thus, the local friction factor m_{pock} becomes:

$$m_{pock} = m_{wave} \tag{7.3}$$

The value of m_{wave} can be interpreted from the work by Wanheim and Abildgaard [85]. Their model for a metallic friction mechanism is based on a plastic wave formed by the workpiece surface moving into and out of a long groove with triangular cross section in the tool. Figure 7.3 illustrates the mechanism by impression of many small undulations from a hard surface on to a larger asperity of a softer surface. Subsequent sliding results in a multitude of plastic waves. Figure 7.4 shows in more detail the slip-line field for a single plastic wave.
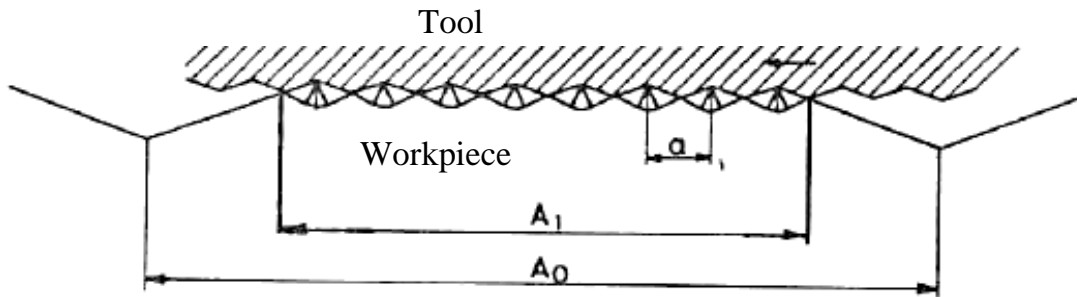
Figure 7.3: Array of plastic waves on top of a deforming workpiece asperity, Abildgaard and Wanheim [85].
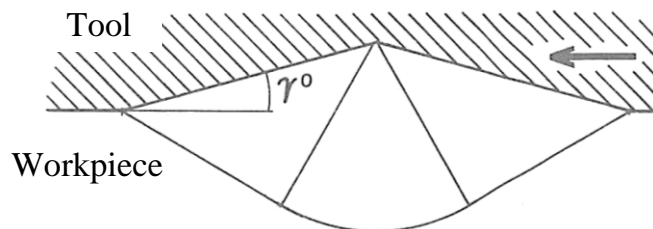
Figure 7.4: Slip-line field of plastic wave in a single cavity filled with workpiece material, Abildgaard and Wanheim [85].

Implementing this model to the present, textured tool illustrated in Figure 7.2, the plastic wave moves into and out of the pockets experiencing an apparent friction stress $\tau = m_{wave}k$, which is plotted as a function of the tool asperity slope γ in Figure 7.5. m^* is the local friction factor between the pocket surface and the workpiece. For $\gamma = 0°$ thus $m^* = m_{wave}$. Due to the wave motion in and out of the pocket, an extra contribution to the apparent friction factor m_{wave} appears, whereby it becomes larger than m^*. In the present case $\gamma = 3°$ and assuming $m_{lub} = m^* = 0$ due to the entrapped lubricant, Figure 7.5 shows $m_{wave} \cong 0.1$. Accordingly the overall friction factor m_{tex} of the textured tool in Eqn. 7.1 becomes;

$$m_{tex} = \alpha m_{met} + (1 - \alpha)m_{pock}$$

$$m_{tex} = \alpha m_{met} + (1 - \alpha)m_{wave}$$

$$m_{tex} = \alpha m_{met} + (1 - \alpha) \times 0.1 \tag{7.4}$$
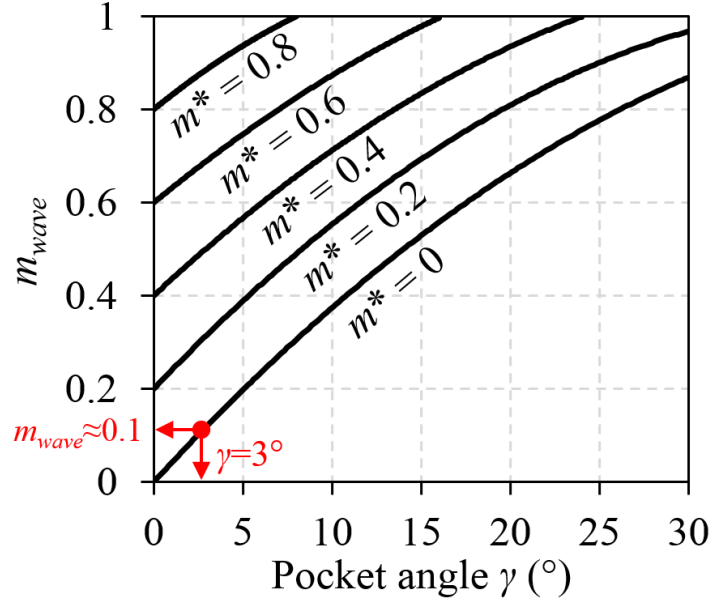
Figure 7.5: Apparent friction factor m_{wave} as a result of pocket angle γ and m^*, Abildgaard and Wanheim [85].

7.3   Theoretical Analysis of Strip Reduction

Based on a plane strain slab analysis, the normalized drawing stress σ_d in strip reduction through an inclined upper die and a flat lower die is [86];

$$\frac{\sigma_d}{2k} = \left[1 + (m_{low} + m_{up})\frac{1}{2\tan\theta}\right]\ln\frac{h_1}{h_0} \tag{7.5}$$

where k is the mean shear flow stress in the deformation zone ($k = \sigma_f/\sqrt{3}$), m_{low} and m_{up} are the friction factors on the lower and upper tool surfaces respectively, θ is the die angle, h_o is the initial sheet thickness and h_1 is the final sheet thickness.

7.4 Test Materials

7.4.1 Workpiece Material

The stress–strain curve of the workpiece material Al 99.5 % - H111 was determined by plane strain compression testing. The material work hardening turned out to follow Voce's model quite well, Figure 7.6, and this gives the determined material constants according to the Voce flow curve expression, Eqn. 7.6, where σ_o, σ_∞ and n were 55 MPa, 149 MPa and 1.52 respectively.

$$\sigma_f = \sigma_o + (\sigma_\infty - \sigma_o)\left[1 - exp(-n\varepsilon_{eff})\right] \tag{7.6}$$
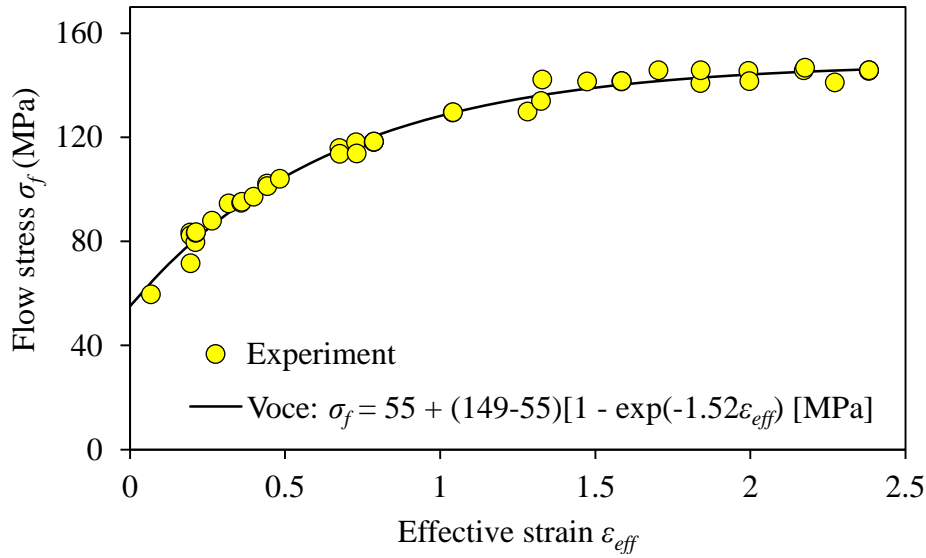
Figure 7.6: Voce flow curve expression for the workpiece material Al 99.5 % – H111 sheet.

Assuming zero prestrain and setting ε_1 = the effective strain of the material after drawing, the following average flow stress in the deformation zone is determined:

$$\bar{\sigma}_f = \frac{1}{\varepsilon_1} \int_0^{\varepsilon_1} \sigma_f(\varepsilon_{eff}) \, d\varepsilon_{eff} = \frac{1}{\varepsilon_1}\left\{\sigma_\infty \varepsilon_1 + \frac{\sigma_\infty - \sigma_0}{n}\left[exp(-n\varepsilon_1) - 1\right]\right\} \tag{7.7}$$

7.4.2 Lubricants

The test lubricants and their properties are listed in Table 7.1. The Rhenus oil is a medium viscosity, mineral oil containing additives with boundary lubrication properties. The CR5 Houghton Plunger oil is a high viscosity, pure mineral oil with no special additives.

Table 7.1: Properties of the test lubricants.

Oil type	Product name	Kinematic viscosity η (cSt @ 40°C)
Mineral oil with additives	Rhenus LA 722083	300
Pure mineral oil	CR5 Houghton Plunger	660

7.5 Analysis of Textured Tool Surface

7.5.1 The Overall Friction Factor m_{tex} and the Drawing Load

The smooth tool surface with no textures on the tool surface has an apparent contact area ratio $\alpha = 1$. For the textured tools, the plateau distances $x = 0.23$, 0.46 and 0.92 mm results in $\alpha = 0.60$, 0.74 and 0.84, respectively. From the experimentally measured drawing force, it is possible to determine the overall friction factor on the lower tool by applying Eqn. 7.4 and Eqn. 7.5 in the following way. The friction factors m_{low} and m_{up} are considered equal for the smooth, non-textured tool. The obtained friction factor $m_{low} = m_{up}$ is then applied to the untextured upper tool (m_{up}) for the experiments with the textured, lower tool surfaces. This leaves only the value of $m_{low} = m_{tex}$ as unknown, which is then determined, so that experimental and theoretical drawing loads are matching, Figure 7.7. The theoretical drawing load was computed using MATLAB. The MATLAB code is shown in Appendix F1. Figure 7.8 shows the corresponding values of the overall friction factor m_{tex} on the textured tool surface. It is noticed that minimum drawing force and m_{tex} appears when $\alpha \cong 0.8$ in good accordance with experimental findings in literature for plane strip drawing test [55].
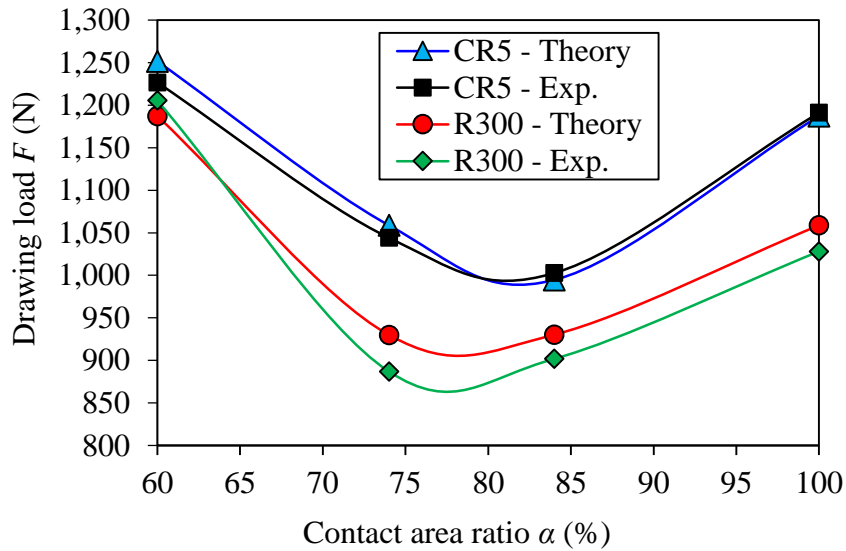
Figure 7.7: Theoretical and experimental drawing load as a function of contact area ratio.
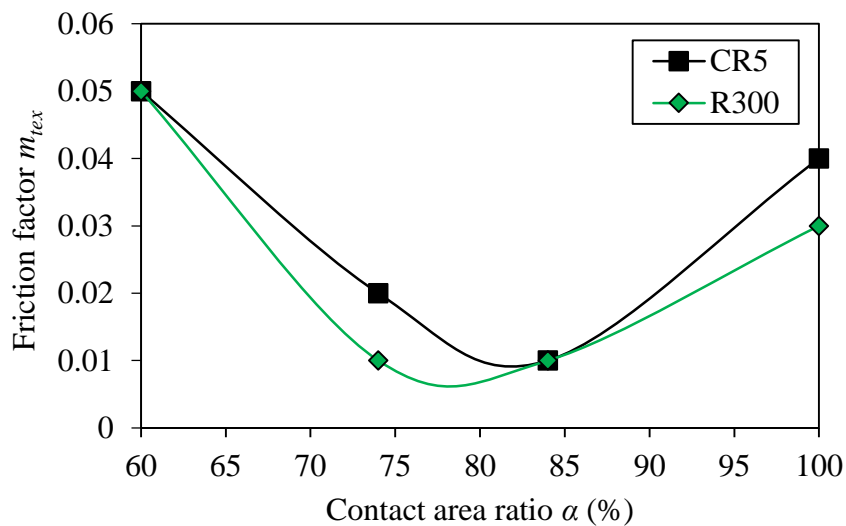
Figure 7.8: Friction factor m_{tex} as a function of contact area ratio for two different lubricants.

7.5.2 *Comparison with Wanheim-Abildgaards Theoretical Model*

Assuming micro-hydrodynamic lubrication to occur on the flat plateaus of the textured tool surface due to the escape of the trapped oil from one pocket to its neighbour, the value of m_{met} is assumed zero. In this case, the Eqn. 7.4 is reduced to:

$$m_{tex} = (1 - \alpha)m_{wave} \qquad\qquad (7.8)$$

where m_{wave} can be determined by Abildgaard and Wanheims theoretical model in Figure 7.5. A comparison between the overall friction factor m_{tex} of the textured tools determined in this way with the one determined in Section 6.1 by force measurement and slab method analysis is shown in Figure 7.9. It is noticed that reasonable agreement appears between the two methods. The value of $m^* = 0$ was assumed for each individual case.

Tool texture with too large amount of pocket area, i.e. with low α-value, was found to increase the overall friction factor. Eqn. 7.8 explains this effect, since α becomes smaller. Too small amount of pocket area, on the other hand, may also lead to increased m_{tex}, since the lubricant escape by micro-plasto-hydrodynamic lubrication may not be sufficient to cover the entire flat plateau. This implies an increase in m_{met} in Eqn. 7.4. These two counteracting factors influence on m_{tex} are the reason for an optimum value of α, which gives minimum m_{tex}.
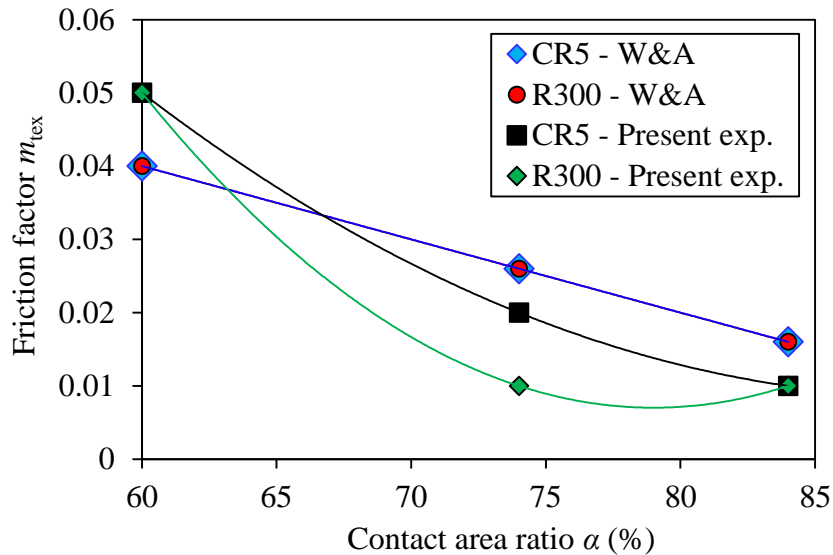
Figure 7.9: Comparison of the overall friction factor m_{tex} determined by adopting Wanheim and Abildgaards model (W&A) with the present calculations.

7.6   Summary

A friction model for a soft workpiece deforming against a textured tool surface was proposed. The model takes into account the plastic wave motion appearing when the workpiece material flows into and out of local pockets between the flat plateaus of a table mountain like tool surface topography. The model was evaluated by strip

reduction tests, which emulates the tribological conditions in an ironing process. The study included testing of two different lubricants, a plain mineral oil with a high viscosity, and a mineral-based oil with boundary lubrication additives having a medium viscosity. It was found that an optimum amount of tool texture exists which reduces friction and thus drawing load for the table-mountain-like tool surface topography. The overall friction factor in the interface between workpiece and textured tool surface can be satisfactory predicted by the theoretical model. However it is still necessary to obtain a friction factor for the metal-to-metal contact.

Part III
Anti-Seizure Tool Coatings

Overview

In tribologically severe stamping operations such as ironing of stainless steel, the phenomenon of galling, i.e. breakdown of the lubricant film followed by pick-up of workpiece material on the tool surface and scoring of subsequent workpiece surfaces may appear if the tribological system is inadequate. Mineral oils containing EP additives are therefore commonly applied to avoid galling in sheet stamping production. Application of these lubricants requires additional costs for pre-cleaning, lubrication as well as post-cleaning after stamping. Applying lubricants such as chlorinated paraffin oils to avoid galling furthermore poses risks to personnel health and working environment. Insufficient post-cleaning promotes hazardous chemical residues on the sheet surface, which may be unacceptable in cases like biomedical and food container products.

Application of hard coating to the tool surface is rather familiar in sheet metal forming, especially in progressive tools where the tribological conditions are severe and possible galling may occur. However, depositing Diamond-Like Carbon (DLC) coating is rather unusual in sheet metal forming. Although depositing the DLC coating to the tool surface is beneficial to reduce friction and to improve resistivity towards galling, stamping of sheet materials by utilizing these DLC coatings at larger normal pressures such as in ironing operations requires an efficient but hazardous lubricant in order to avoid peeling off of the coating from the tool surface. This may be due to the generation of a high shear stress in the DLC coating. Thus, further investigations into the effect of DLC coatings in such cases of larger normal pressure and higher temperature under severe tribological conditions would be of interest to investigate.

The present study focuses on depositing the DLC coatings as the top layer coating on tools to minimize galling. Two approaches were used; a screening experiment on a manually operated sheet tribo-tester was performed on all coating candidates and after that, the most promising coating candidate found from the screening experiment in the manually operated tribo-tester was then tested in an automatic sheet tribo-tester, where a laboratory simulation of an ironing operation replicating a continuous can production is performed. The tribologically severe strip reduction test, which emulates industrial ironing of stainless steel sheets, is suitable to examine promising coating candidates for severe forming conditions and is therefore used in this study. A numerical simulation, coupling mechanical and thermal analysis, was added to evaluate the interaction at the tool/workpiece interface.

The tool surfaces were deposited with single-, double- and multi-layer DLC coatings. The double-layer DLC coating is a new DLC coating that is specifically developed for the PhD study, aiming at finding a promising way to eliminate hazardous lubrication issues. The new, double-layer DLC coating has not been tested in industrial production at varying tribological conditions.

Chapter 8: Screening Analysis of DLC Tool Coatings

8.1   Introduction

The screening analysis of the DLC coated tool surface is concentrating on intermediate coating layer structures, while retaining the DLC as the top coating layer. The tribologically severe strip reduction test, which emulates industrial ironing of stainless steel sheets, is suitable to examine promising coating candidates for severe forming conditions and is therefore used in this study.

8.2   Strip Reduction Test

A schematic outline of the SRT is shown in Figure 8.1 (left). A round, non-rotating Ø15 mm tool pin with non-coated or DLC coated surface, see Figure 8.1 (right), is pressed towards the test strip supported by a thicker tool plate. Reduction in thickness can be varied, and it was held at 15–25% in the present screening experiments. The strip and the supporting tool plate are subsequently drawn in horizontal direction up to a maximum sliding length of 300 mm under constant reduction and constant drawing speed $v = 65$ mm/s. Drawing force is measured by a piezoelectric transducer. The tool pin can be preheated to a maximum of 200 °C by electric heaters embedded in the shoe thermally loading the tool pin. Threshold sliding before the onset of galling is determined by visual inspection of the drawn strip and more accurately by roughness profile measurements of the strip surface perpendicular to the drawing direction with 30 mm intervals. The experimental setup allows eight experiments with the same tool pin by turning the tool 45° after each experiment. The present experiment also included a non-coated tool surface to provide a reference for comparison purpose.
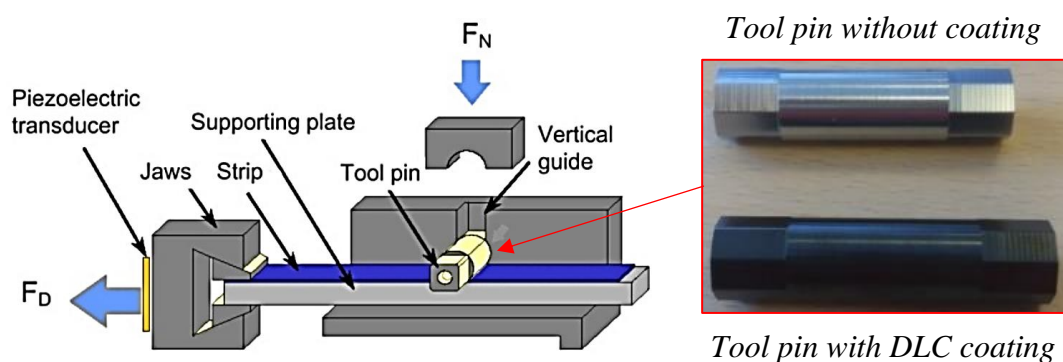
Figure 8.1: Strip reduction emulating ironing (left) [36], and the tool pins with and without the DLC coating (right). Technical drawing for tool pin holder and tool pin are shown in Appendix G.

8.3   Test Materials and Coating Types

8.2.1   Tool Material

The tool material was a Powder Metallurgical (PM) cold work tool steel, Uddeholm UHB Vanadis 4, with high carbon and chromium content and alloyed with manganese, molybdenum, silicon and vanadium. The tools were through-hardened and tempered to 62 HRC and subsequently polished to $Ra = 0.02$ µm before coating.

8.2.2   Workpiece Material

The workpiece material was austenitic stainless steel EN1.4307 (AISI 304L), 1.2 mm thick, 15 mm wide and 500 mm long. It was used in the "as-received" condition with a surface roughness $Ra = 1.4$ µm. The stress-strain curve of the workpiece material was determined by uniaxial tension test, which gave the following Swift flow curve expression: $\sigma_f = C (B + \varepsilon_{eff})^n = 1830 (0.091 + \varepsilon_{eff})^{0.76}$ MPa, see Figure 8.2.
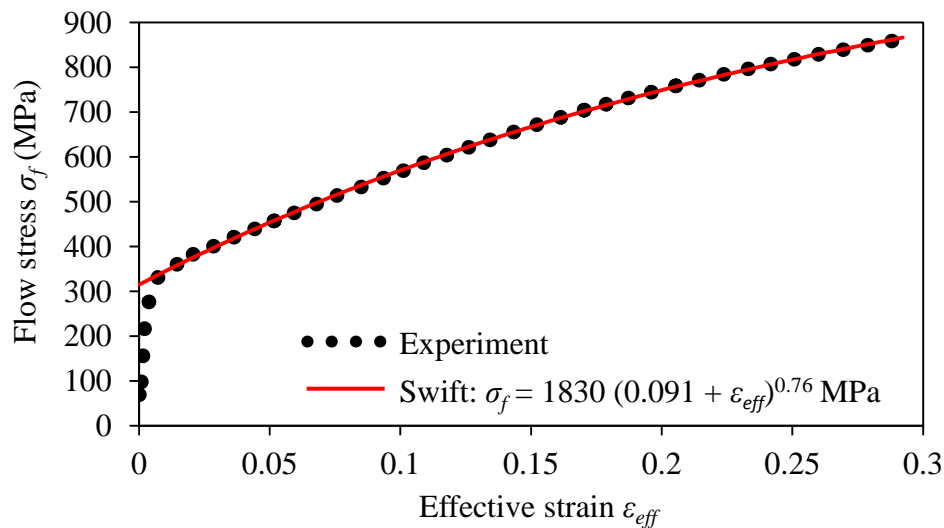
Figure 8.2: Swift flow curve expression for the workpiece material stainless steel EN1.4307 sheet.

8.2.3   Lubricants

Two severe lubrication conditions were chosen. One was lubrication with a low viscous, plain mineral oil without special additives as listed in Table 8.1, and the other one was reduction with no lubrication.

Table 8.1: Properties of the test lubricant.

Oil type	Product name	Kinematic viscosity η (cSt @ 40 °C)
Pure mineral oil	CR5-Sun 60[a]	60

[a] *50 wt % mixture of Houghton Plunger CR5 (η = 660 cSt) and Sunoco Sun 60 (η = 10 cSt)*

8.2.4 Coating Types and Structure

In this study, DLC coating was chosen to impede galling. In order to evaluate the interaction between the DLC coating and the tool surface, three DLC coating structures were evaluated; single layer, double layer and multi-layer coatings as described in Figure 8.3. The tool roughness after coating was the same as before, $Ra = 0.02$ µm. Coating binders, CrN and Cr interlayer coatings, were added to the DLC coating in form of a gradient coating structure.
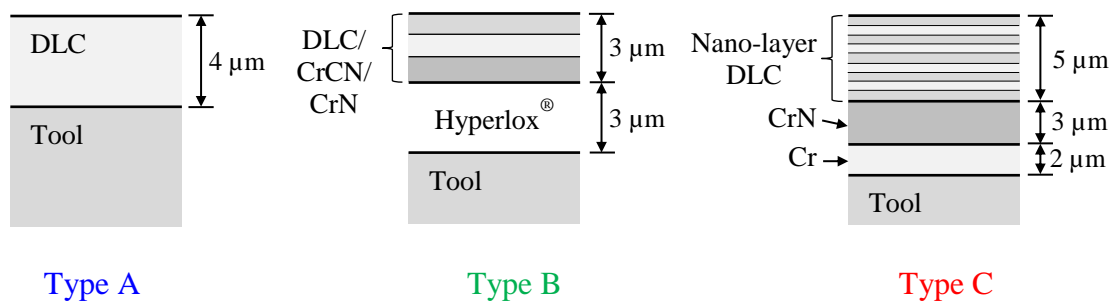
Figure 8.3: The three coating structures: Type A (single layer), Type B (double layer) and Type C (multi-layer).

8.4 Experimental Procedure

The experiment started by cleaning the tool and workpiece surfaces from any remnants of pick-up, oil and other contaminants. In case of lubricated experiments, lubricant was applied to the workpiece surfaces, after which reduction was carried out with 300 mm drawing length. In some of the experiments, the tool was pre-heated to either 80°C or 110°C, using a thermal cartridge heater inserted in the upper tool loading the tool pin, see Figure 8.1. During the experiments, the load and temperature were recorded and saved by a custom made LabView program. After the experiment, the tool surfaces were scanned in a light optical microscope (LOM) and the workpiece surface roughness was measured across the strip for every 30 mm drawing length by a tactile roughness profilometer, Taylor Hobson Form TalySurf.

8.5 Screening Analysis of DLC Coatings

8.4.1 Preliminary Experiment of DLC Coatings

A preliminary screening experiment was performed at 15% reduction in order to examine the performance of the DLC coatings. During the experiments, the tools were either kept at room temperature of 20°C or heated up to 80°C. Figure 8.4 shows the average drawing loads in steady-state condition using a tool with or without DLC coating at different lubrication conditions. Low load was observed with the DLC type B coating in all test conditions. Testing of all other tools without lubrication led to larger drawing loads. Low drawing loads were obtained when testing the tools with the CR5-Sun60 oil except for the non-coated tool at elevated tool temperature.
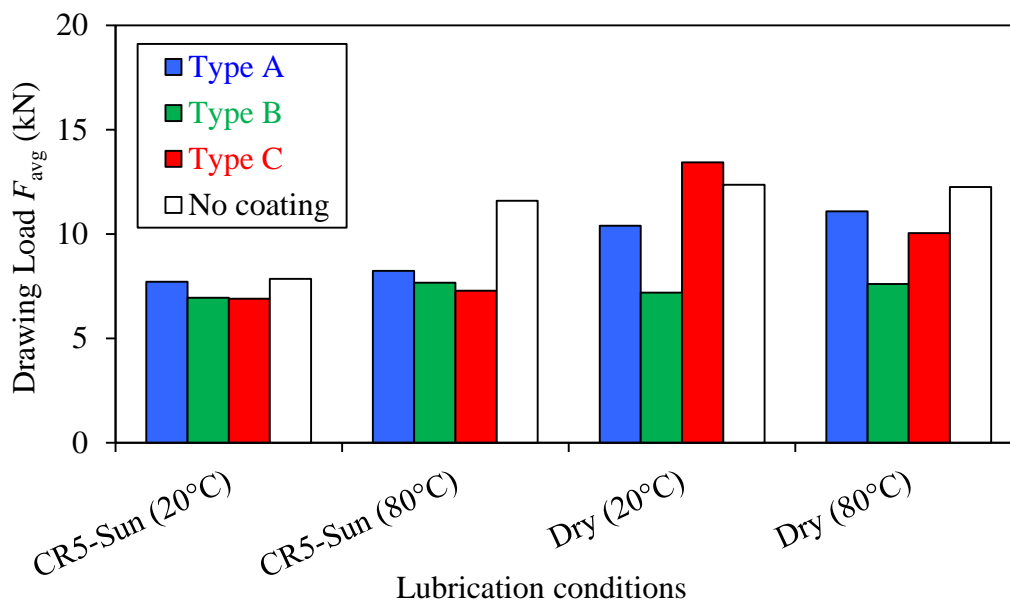
Figure 8.4: Average drawing load in steady-state condition at different tool and lubrication conditions.

Figure 8.5 shows measurements of the workpiece roughness for all test conditions. The DLC coatings A and B work satisfactorily when applying a thin layer of lubricant, both for tools at room temperature as well as elevated temperature, see Figure 8.5a and Figure 8.5b. Increased roughness was found when applying the DLC type C and the uncoated tool. Large surface roughness indicates that the tool surface experienced severe pick-up. For the case of dry lubrication, the DLC coating type B was the only one that could withstand the severe test conditions at room temperature as well as elevated temperature, as indicated by the low surface roughness, see Figure 8.5c and Figure 8.5d. The other two DLC coatings and the uncoated tool resulted in heavy scoring as seen by the large sheet roughness, and in some cases the strip broke after a short drawing length.

98
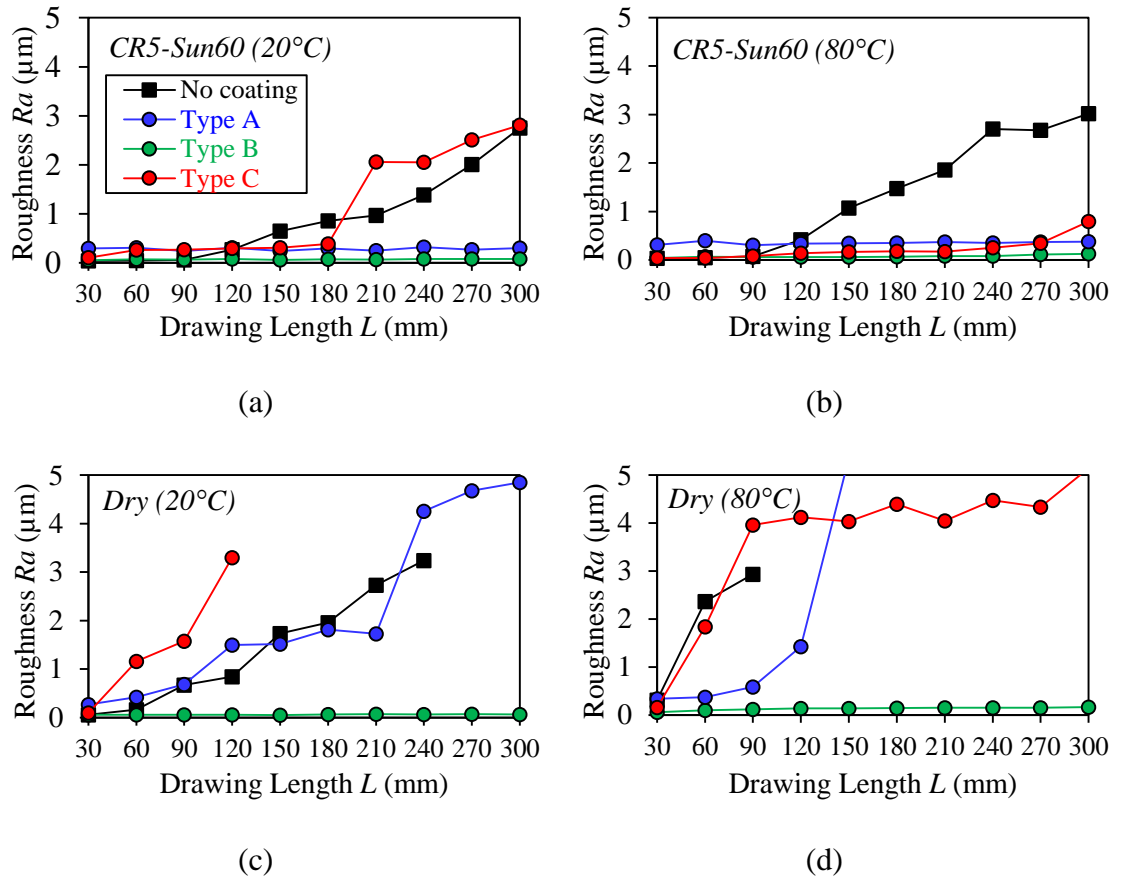
Figure 8.5: Sheet roughness versus drawing length with tool surface as parameter: a) CR5-Sun60 at 20°C, b) CR5-Sun60 at 80°C, c) Dry at 20°C, and d) Dry at 80°C.
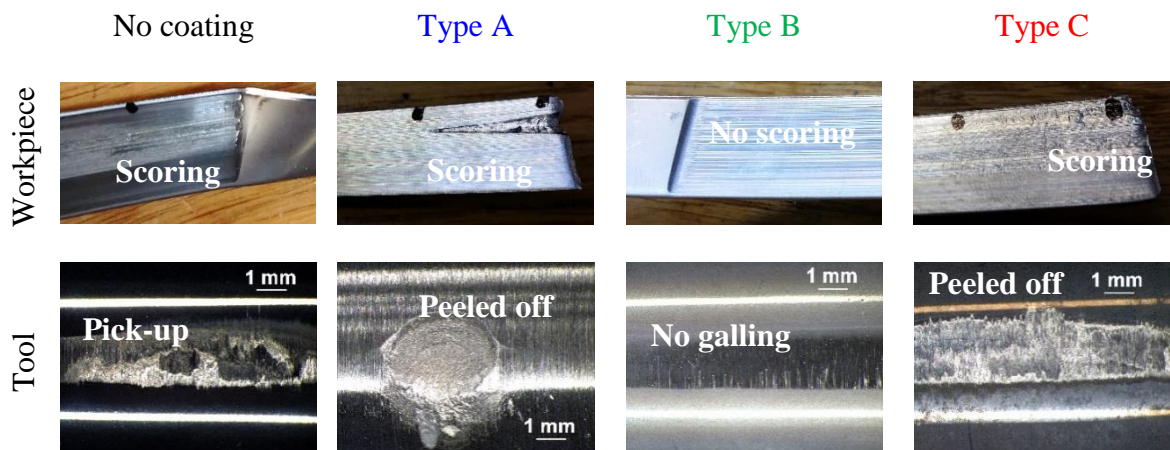
Figure 8.6: Images of workpiece and tool surface conditions after screening experiments under dry lubrication condition at a tool temperature of 80°C.

Table 8.2. Overall performance of the tools with and without DLC coatings (Rating: 1-Excellent, 2-Good, 3-Satisfactory, 4-Poor).

Lubrication condition	Tool temperature	No coating	Coating types		
			Type A	Type B	Type C
CR5-Sun 60	20 °C	4	2	1	3
CR5-Sun 60	80 °C	4	2	1	3
Dry	20 °C	4	4	1	4
Dry	80 °C	4	4	1	4

It was furthermore clear that the DLC type B showed the best adhesion to the tool substrate as seen on the LOM images in Figure 8.6. The other tools suffered peeling off of the DLC coating and pick-up of workpiece material on the tool surface. Table 8.2 summarizes that the DLC type B is superior in all test and lubrication conditions, and that the other DLC coatings can only function with the presence of a thin oil film.

8.4.2   A More Severe Testing of DLC Coating Type B

Two more severe experimental test series at 15% and 25% reduction with a tool temperature of 110°C were carried out using coating type B. Figure 8.7 shows an expected increase of the drawing load with increased reduction, whereas the surface roughness in both cases was lower than the initial surface roughness, see Figure 8.8. Adopting the double layer coating film by depositing a metallic coating layer like Hyperlox® in between the DLC film and the tool substrate can therefore improve adhesion strength in the DLC film and even perform well under the extreme test conditions in sheet stamping of stainless steel at elevated tool temperature. The present results are in good agreement with findings in literature [87] using a scratch test.
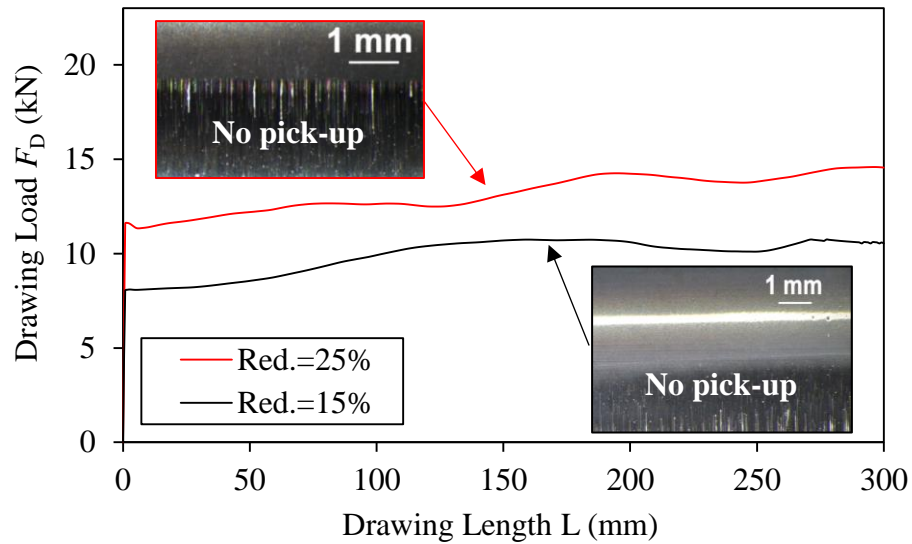
Figure 8.7: Measurements of drawing load and the tool surface appearance after drawing the stainless steel against the DLC coating type B under dry lubrication condition at different reductions and a tool temperature of 110°C.
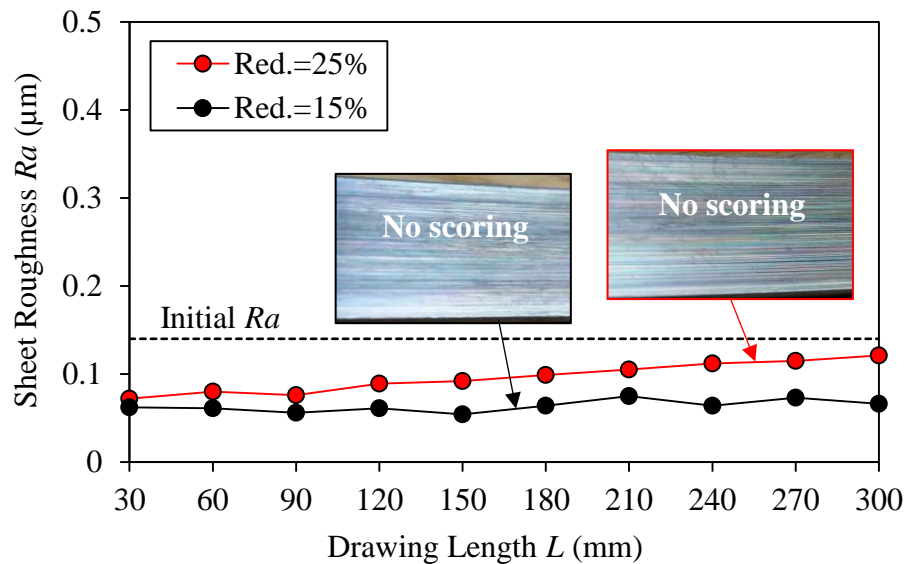
Figure 8.8: Measurements of sheet roughness *Ra* and the tool surface condition after drawing the stainless steel against the DLC coating type B under dry lubrication condition at different reductions and a tool temperature of 110°C.

8.4.3 Repetitive Experiments with DLC Coating Type B

A repetitive experimental test series was performed on the DLC coating type B under dry friction conditions with 15% reduction and a tool temperature of 110°C. The

investigation aimed at examining the durability of the coating as regards persistence towards pick-up. Figure 8.9 shows the drawing loads and the workpiece roughness Ra reaching a stable value after several strokes with no pick-up. This is verified by the workpiece roughness at the last stroke, where the workpiece surface roughness $Ra =$ 0.11 µm was lower than the initial roughness $Ra = 0.14$ µm, see Figure 8.10. The results indicate a good adhesion at the interface between the DLC, Hyperlox® and the tool substrate and a coating that can sustain a high, repetitive normal pressure and shear stress.
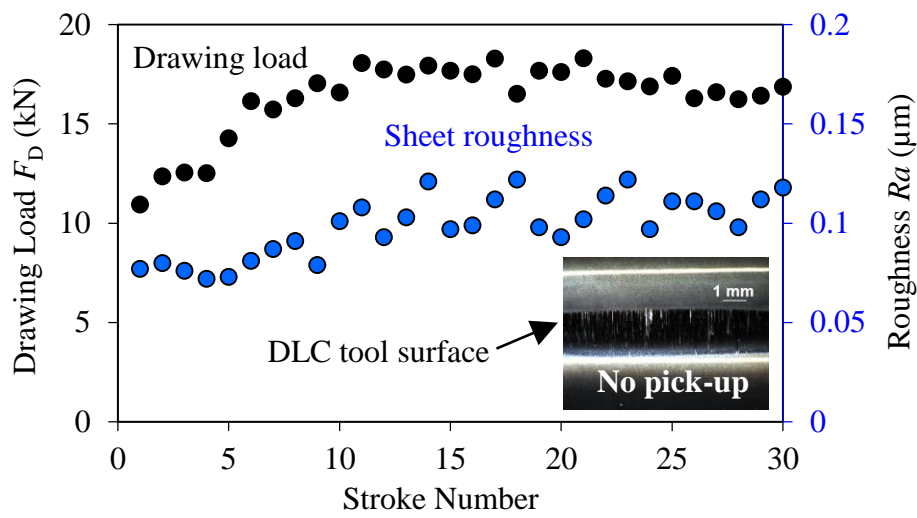
Figure 8.9: Measurement of drawing load and the tool surface condition after drawing the stainless steel against the DLC type B coating under dry condition with a reduction of 15% and a tool temperature of 110°C.
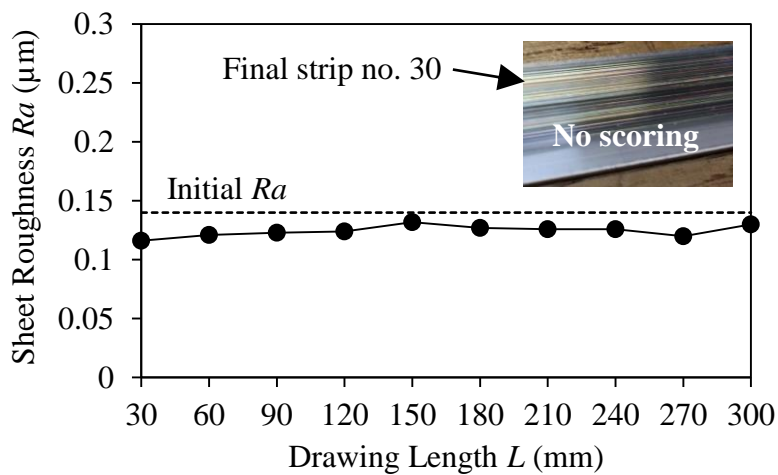
Figure 8.10: Measurement of sheet roughness Ra and the tool surface condition after drawing the final stainless steel strip no. 30 against the DLC type B coating under dry condition with a reduction of 15% and a tool temperature of 110°C.

8.6   Laboratory Simulation of an Industrial Production Case

A number of stamping operations before the actual ironing operation in progressive tools increases the flow stress of the stamped sheet material. Due to this, a high degree of deformation causes substantial temperature increase in the tool/workpiece interface. Higher temperatures leads to a thinner lubricant film and the risk of galling, i.e. breakdown of the lubricant film causing pick-up of workpiece material on the tool surface and scoring of subsequent workpiece surfaces, increases. In such cases, chlorinated paraffin oils have proved to be the only efficient lubricant [39]. This subsection presents a laboratory simulative experiment of an industrial production case and the promising DLC type B coating found in the screening evaluation above. The new experiment is carried out with similar test parameters as in industrial production except work hardening due to prior deformations in the industrial production.
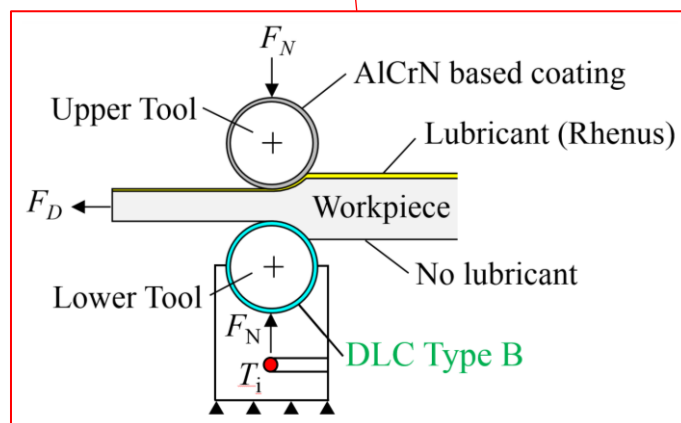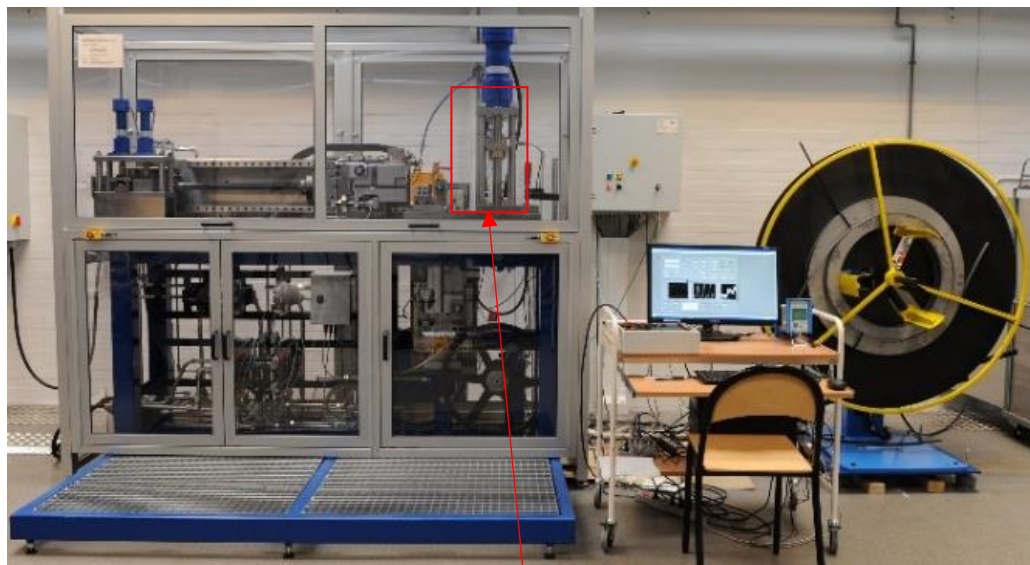
Figure 8.11: Automatic sheet tribo-tester at DTU-MEK (top) [38] and strip reduction test setup (bottom).

The laboratory simulation of an industrial production involving ironing of stainless steel cups of steel EN1.4307 was carried out using the Universal Sheet Tribo-Tester (UST2) shown in Figure 8.11, which can run multiple tests continuously from a coil [38]. The strip reduction test schematically shown in Figure 8.11 was selected to perform an off-production-line evaluation of coating type B. The test parameters were chosen in accordance with the industrial production process: 24% reduction, 50 mm/s drawing speed, idle time between each stroke of 1.8 s and a sliding length of 10 mm. The test materials are described in Table 8.3. The lower tool is the DLC type B coated test tool, which is tested under both lubricated and dry conditions, respectively, whereas the upper tool is a dummy tool provided with an AlCrN based coating and lubricated with an environmentally benign mineral oil with additives, see Table 8.4. No lubrication was applied to the lower tool in this experiment.

Table 8.3: Test materials.

Components	Dimension	Roughness Ra	Surface coating	Surface condition
Upper tool (Vanadis 4)	Ø15×82 mm	0.02 µm	AlCrN	Hardened and tempered to 62 HRC
Lower tool (Vanadis 4)	Ø15×34 mm	0.02 µm	DLC type B	Hardened and tempered to 62 HRC
Workpiece (EN1.4307)	$W×t =$ 30×1.0 mm	0.14 µm	-	"as-received" condition

Table 4. Properties of the test lubricant.

Oil type	Product name	Kinematic viscosity η (cSt @ 40 °C)
Mineral oil with additives	Rhenus LA 722086	800
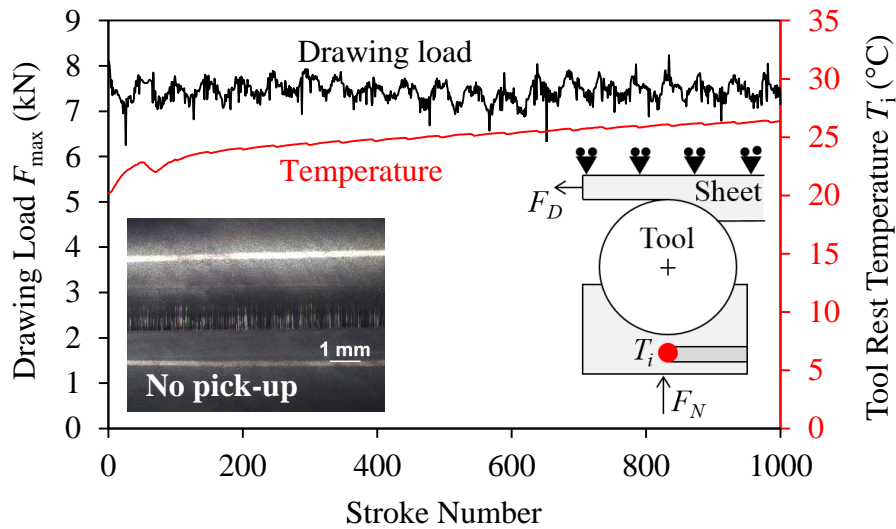
Figure 8.12: Measurement of drawing load and tool rest temperature when testing with the coating type B under dry lubrication condition with test parameters similar to the industrial case excluding work hardening due to prior deformations in the industrial production.

Figure 8.12 shows a constant drawing load and stable tool rest temperature even after 1,000 strokes, and no sign of pick-up on the tool surface was observed. This is verified by measurement of the sheet roughness Ra shown in Figure 8.13, where the surface roughness on both sides of the sheet is lower than the initial roughness. The results have thus shown that the DLC type B is capable of performing ironing without lubrication of stainless steel, which is otherwise very prone to galling.
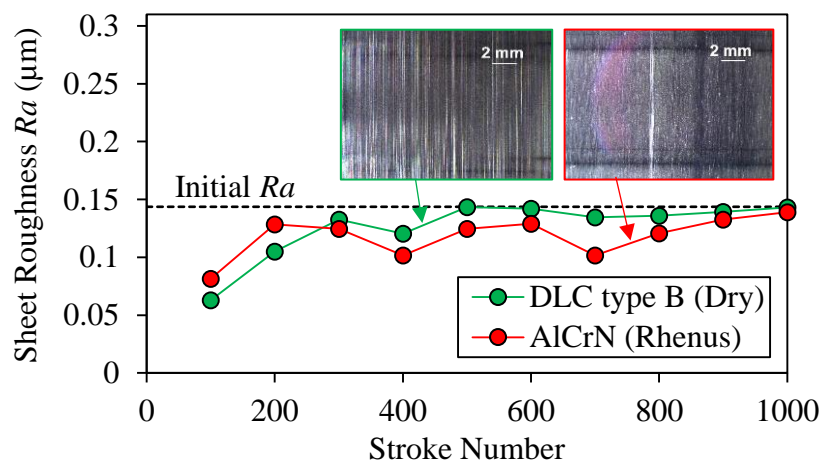
Figure 8.13: Measurement of sheet roughness Ra after testing with the coating type B under dry lubrication condition with test parameters identical to the industrial case excluding work hardening due to prior deformations in the industrial production.

8.7   Summary

The present study adopted a strip reduction test for emulating industrial ironing of stainless steel cups to test promising DLC coatings at room temperature as well as elevated tool temperature. Three DLC coating types were evaluated; single layer DLC, double layer (DLC/Hyperlox®) and multi-layer (DLC/CrN/Cr). The experiments revealed that the new coating recipe, double layer (DLC/Hyperlox®) coating, is a promising coating candidate for production without lubrication. It gave a smooth surface finish of the tested strips with no pick-up on the coated tool surface. Intermediate metallic layers like Hyperlox® between the DLC film and the tool substrate ensured good adhesion of the DLC coating and are expected to work effectively under severe conditions in sheet stamping of stainless steel.

Chapter 9: Long-Term Analysis of a New DLC Tool Coating

9.1   Introduction

The earlier described screening experiment of the three different DLC tool coating structures have shown that the new DLC coating, the double-layer DLC/Hyperlox® coating, is advantageous to be applied in sheet stamping operations without lubrication. However, a major issue when testing, has been to determine the onset of galling as a function of most important process parameters, i.e. normal pressure, sliding length and tool temperature. These process parameters need to be identical to the production conditions since the new, double-layer DLC coating has not been tested in industrial production at varying tribological conditions. Hence, a long-term experiment of the new DLC coating under conditions similar to industrial production is therefore important to determine the risk of galling.

The present investigation is focused on such a long-term experiment of the new DLC coating, which is a double-layer DLC/Hyperlox® coating. For the long-term experiment, the double-layer DLC coating is compared with a good wear and temperature resistant coating, double-layer Hyperlox® coating, as recommended by the SHETRIB industrial partner, CemeCON A/S. The Hyperlox® is an AlTiN-based coating. The high content of aluminium in the Hyperlox® coating results in high hardness. Previous experience by the company has shown that the very good adhesion of the Hyperlox® coating reduces the wear and thereby increases tool life and productivity. A numerical simulation, coupling mechanical and thermal analysis, was also performed to evaluate the material deformation and heat generation at the tool/workpiece interface.

9.2   Coating Types

A preliminary series of experiments of a variety of tool coatings demonstrated that the double-layer coating structure, DLC/Hyperlox®, showed promising results under severe test conditions, i.e. at high thickness reduction and tool temperature, with no sign of galling in ironing of stainless steel, as reported in Chapter 8.

In the present study, further investigations are carried out with two double-layer coating structures, namely DLC/Hyperlox® and Hyperlox®/Hyperlox®. Figure 9.1 and Figure 9.2 depicts schematically the cross section surface morphologies of the two single-layer coating films, DLC and Hyperlox®, deposited directly to the tool substrates. The DLC comprises of a gradient DLC coating structure supported by two other coating films, CrN and CrCN, which acts as bonding layers. Meanwhile, the Hyperlox® is a stand-alone, modified TiAlN coating film. The thickness of the two coating layers, DLC and Hyperlox®, was 3 µm each.
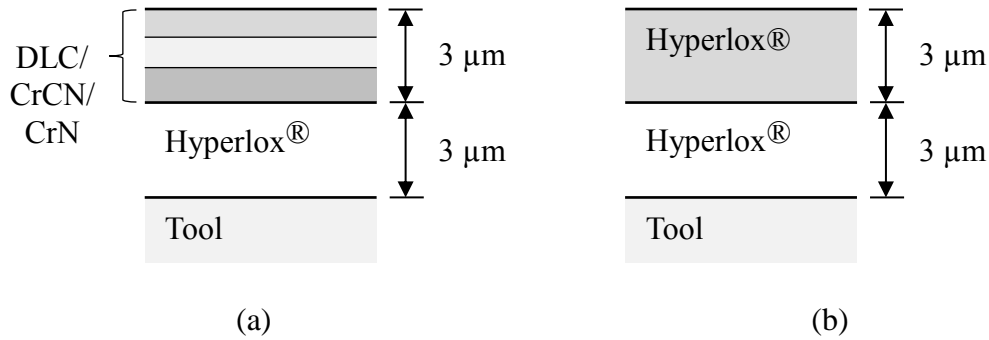
Figure 9.1: Double-layer coating structures: a) DLC/Hyperlox® coating and b) Hyperlox®/ Hyperlox® coating.
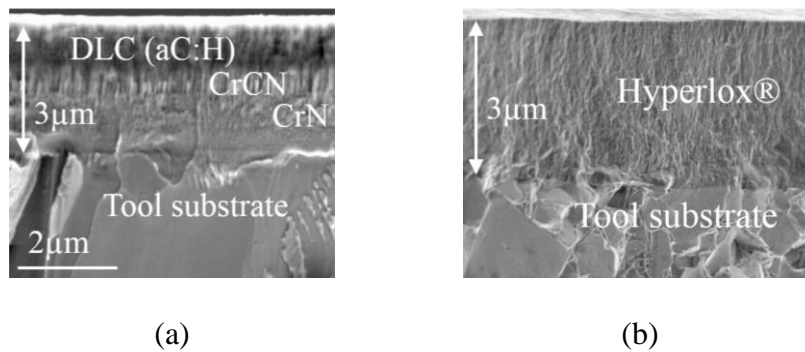
Figure 9.2: Cross sectional surface morphologies of a) DLC and b) Hyperlox® coatings. aC:H denotes amorphous Carbon Hydrogen. Images courtesy of CemeCON Scandinavia A/S [88].

9.3   Screening Analysis of Tool Coatings in a Manual Tribo-Tester

9.2.1   Experimental Setup

At first, the screening experiment, adopting the strip reduction test on a manual tribo-tester shown in Figure 8.1, was carried out. The purpose of the screening experiment utilizing the similar test conditions as described in Chapter 8 is to identify the capability of the test coatings prior to the next test campaign on the automatic tribo-tester under close control of the tribologically severe test conditions. This is to avoid the need to use money, time or other resources on too many long-term tests. The strip reduction test schematically shown in Figure 8.1 was used for the screening test. It has been conducted on a manually operated sheet tribo-tester [36]. Testing has been performed by drawing the stainless steel strip over a fixed Ø15 mm tool pin while the upper, shoe-formed tool loads the tool pin. The tool pin has been coated with the above

mentioned coatings shown in Figure 9.1. Before coating the tool pins are polished to a surface roughness $Ra = 0.02$ µm and the roughness is the same after coating. The workpiece material is austenitic stainless steel EN1.4307 (AISI 304L), 1.2 mm thick, 15 mm wide and 500 mm long. It is used in the "as-received" condition with a sheet surface roughness $Ra = 1.4$ µm. A drawing speed $v = 65$ mm/s and a thickness reduction $r = 15\%$ are applied.

9.2.2 Results and Discussion

Figure 9.3 shows drawing load as function of drawing distance. A lower drawing load was observed with the DLC/Hyperlox® coating than with the double-layer Hyperlox® coating and no pick-up on the coated tool surface was observed with the former coating. As regards the double-layer Hyperlox® coating, severe pick-up was detected on the tool surface and in some areas, the coating was peeled off. The results were further verified by measurement of the final workpiece roughness seen in Figure 9.4.

A very low surface roughness was achieved by the DLC/Hyperlox® coating, while the Hyperlox®/Hyperlox® coating resulted in heavy scoring on the strip surface, and the strip broke after a short drawing length. The results indicate that the Hyperlox® coating offers a good adhesion between the DLC and the tool surface but is unable to act as the anti-seizure coating film that can sustain high shear stresses, see Figure 9.5. The screening test suggests that the DLC/Hyperlox® coating shall be the only one tested in the following, continuous test campaign.
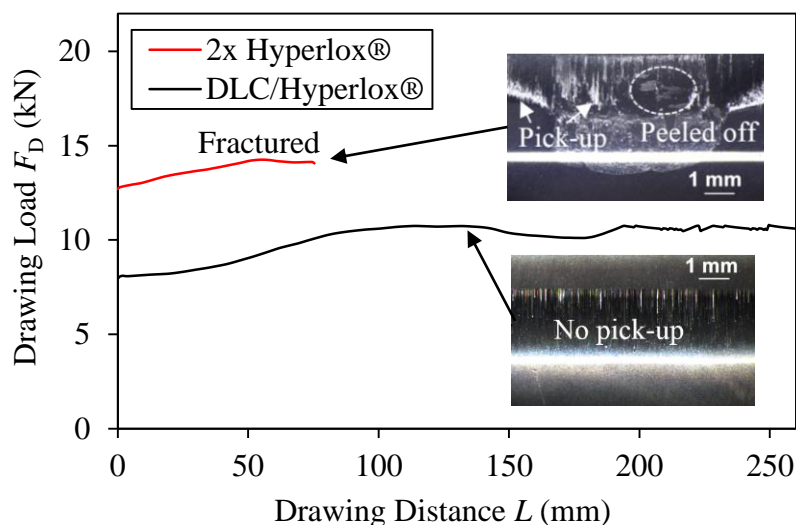
Figure 9.3: Measurement of drawing load and tool surface condition after drawing the stainless steel in the DLC/Hyperlox® and the Hyperlox®/Hyperlox® coated tools under dry lubrication condition.
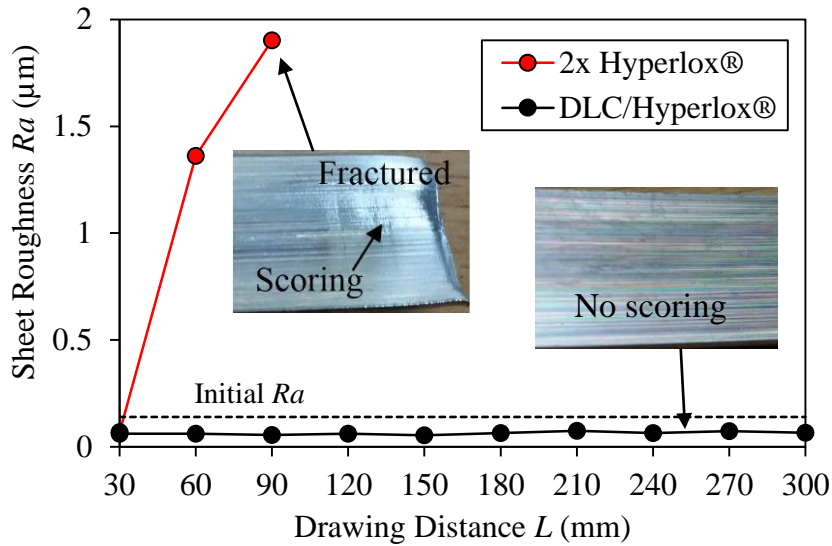
Figure 9.4: Measurement of sheet roughness *Ra* and formed sheet surface condition after drawing the stainless steel against the DLC/Hyperlox® and the Hyperlox®/Hyperlox® coated tools under dry lubrication condition.
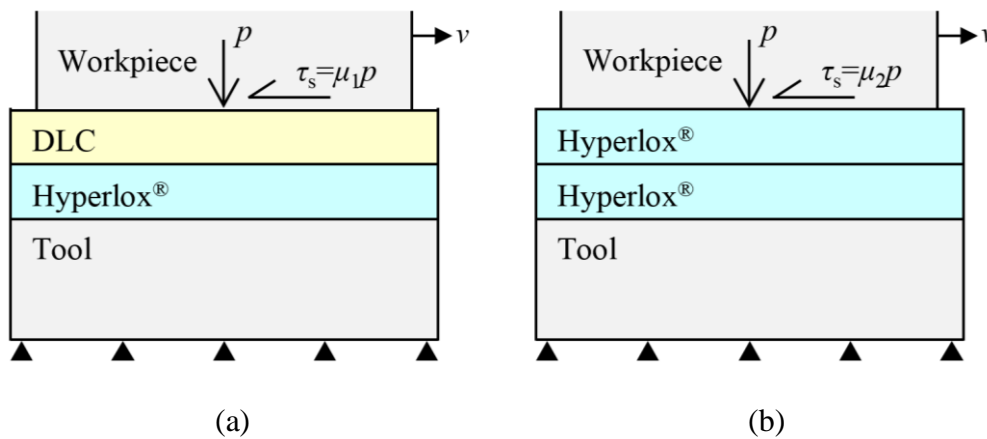
Figure 9.5: Illustration of a good adhesion by a) the DLC/Hyperlox® coating in comparison to b) the Hyperlox®/Hyperlox® coating due to the difference in friction at the tool/workpiece interface.

9.4   Long-Term Analysis of Tool Coatings in Automatic Tribo-Tester

9.3.1   Introduction

A full-scale simulation replicating the ironing stage in a continuous production was carried out to evaluate the DLC/Hyperlox® coating performance after 1,500 strokes, since the collaborating stamping industry partner [12] has experienced that if a

tribo-system can function with a threshold of 1500 strokes without galling, it is a promising candidate for full-scale production tests.

9.3.2 Experimental Setup

Laboratory simulation of an industrial production with ironing of stainless steel EN1.4307 cups is carried out using the Universal Sheet Tribo-Tester (UST2) shown in Figure 9.6 (top), which can run multiple tests continuously from a coil at pre-set sliding length and sliding speed. The strip reduction test, schematically shown in Figure 9.6 (bottom), was selected to perform an off-line evaluation of the DLC/Hyperlox® coating. The test parameters were chosen in accordance with a specific industrial production process as listed in Table 9.1.
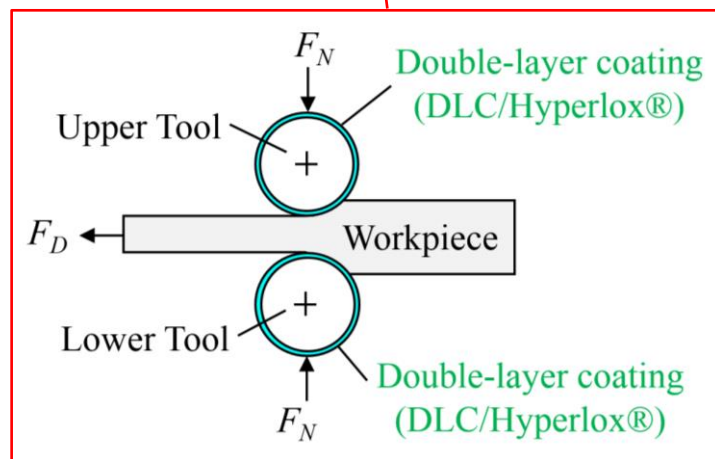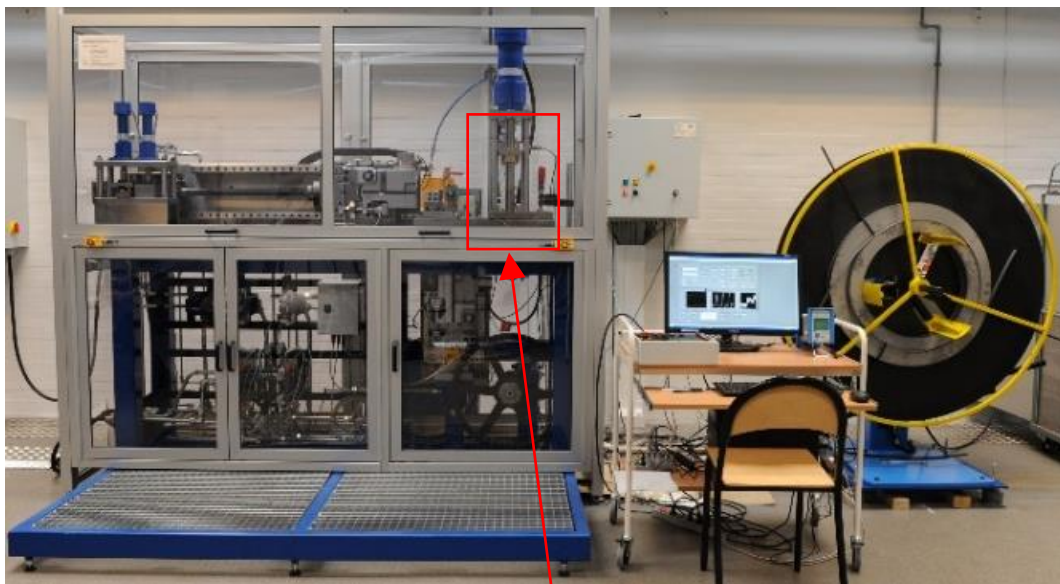
Figure 9.6: Tribo-tester, UST2, (top) and strip reduction emulating ironing (bottom).

Table 9.1: Industrial production process parameters.

Test parameters	Values
Reduction	24 %
Drawing speed	50 mm/s
Idle time between each stroke	1.8 s
Sliding length	10 mm

A round, non-rotating Ø15 mm tool pin, see Figure 9.6 (bottom), is pressed towards the test strip supported by a thicker tool plate. Reduction in thickness can be varied, and it was held at 24% in the present long-term experiments. The strip is subsequently drawn in horizontal direction up to a maximum sliding length 10 mm under constant reduction and constant drawing speed $v = 50$ mm/s. Drawing force is measured by a piezoelectric transducer. Threshold sliding before the onset of galling is determined by visual inspection of the drawn strip and by roughness profile measurements of the strip surface perpendicular to the drawing direction with 100 stroke intervals. The experimental setup allows eight experiments with the lower tool pin before changing to another tool pin, by turning the tool 45° after each experiment, whereas, four experiments is possible with the upper tool pin by turning the tool 90° after each experiment.

9.3.3 Test Materials

9.3.2.1 Workpiece Material

The test campaign was performed with a stainless steel EN1.4307 (AISI304L) coil, 1.0 mm thick and 30 mm wide. It was used in the "as-received" condition with a sheet surface roughness $Ra = 1.4$ µm. The stress–strain curve of the workpiece material was determined by plane strain compression test. The material work hardening shown in Figure 9.7 follows Voce's model quite well, $\sigma_f = \sigma_o + (\sigma_\infty - \sigma_o)[1\text{-exp}(-n\ \varepsilon_{eff})]$ MPa = $107 + (1368 - 107)[1\text{-exp}(-5.243\ \varepsilon_{eff})]$.
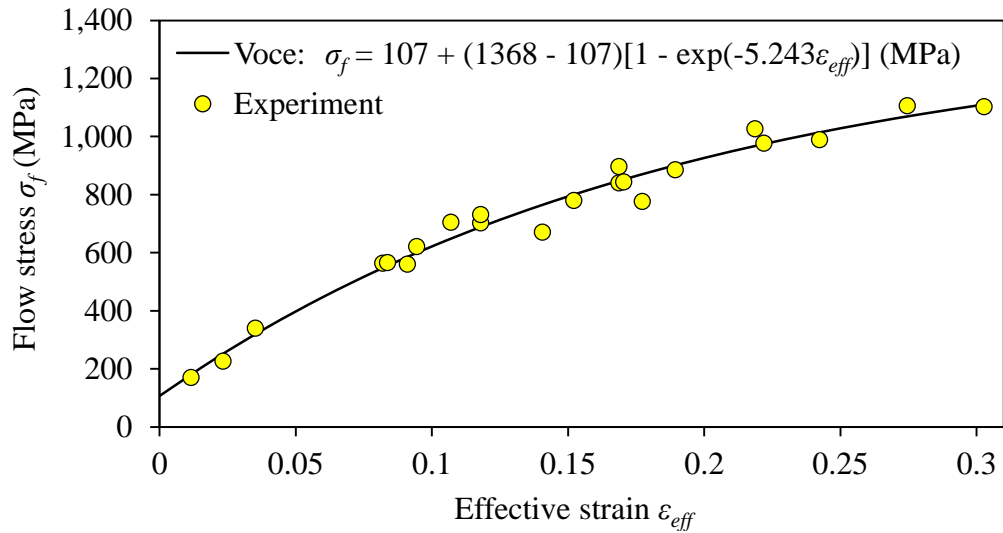
Figure 9.7: Experimental result and Voce flow curve expression for the stainless steel EN1.4307 sheet.

9.3.2.2 Tool Material

The tool material was a PM cold work tool steel, UHB Vanadis 4, with a high carbon and chromium content and alloyed with manganese, molybdenum, silicon and vanadium. The tools were through-hardened and tempered to 62 HRC and subsequently polished to $Ra = 0.02$ µm before coating. The roughness after coating was the same as before $Ra = 0.02$ µm. The tool material properties are listed in Table 9.2. The upper and lower tool geometries are shown in Figure 9.8.

Table 9.2: Tool materials and specifications.

Components	Dimension	Roughness *Ra*	Tool condition
Upper tool (Vanadis 4)	Ø15×82 mm	0.02 µm	Hardened and tempered to 62 HRC
Lower tool (Vanadis 4)	Ø15×34 mm	0.02 µm	Hardened and tempered to 62 HRC

9.3.2.3 Test Lubricant

Two lubrication conditions were chosen for the experiments. One of them was a dry friction condition. The other one was lubrication with a hazard free lubricant, a high viscosity plain mineral oil without special additives. The lubricant properties are listed in Table 9.3.

(a)   (b)

Figure 9.8: The Ø15 mm non-rotating a) upper and b) lower tool pins deposited with the double-layer DLC/Hyperlox® coating. Technical drawings are shown in Appendix G2.

Table 9.3: Tool materials and specifications.

Oil type	Product name	Kinematic viscosity η (cSt @ 40 °C)
Pure mineral oil	CR5 Houghton Plunger	660

9.3.4 Experimental Procedure

Each experiment started by cleaning the tool surfaces from any remnants of pick-up, oil and other contaminants. The experiment was run up to 1,500 strokes. If galling was detected before reaching 1,500 strokes, it was stopped. During the experiment, the maximum drawing load F_{max} and tool rest temperature T_i were recorded and saved by a custom made LabView program. After the experiment, the tool surfaces were scanned in a light optical microscope (LOM) and the workpiece surface roughness was measured across the strip for every 100 strokes by a tactile roughness profilometer, Taylor Hobson Form TalySurf.

9.3.5 Results and Discussion

A continuous ironing test was performed with the DLC/Hyperlox® coating under tribologically severe test conditions. The experiment aimed at examining the durability of the coating as regards persistence towards pick-up. One of the experiments were performed under dry friction conditions whereas the other one were carried out with lubricated strip. 12.8 g of CR5 lubricant was applied for 1,500 strokes, which covered a nominal contact area of 900,000 mm^2. This gives a lubrication amount of 14.2 g/m^2.

Figure 9.9 shows the maximum drawing load F_{max} reaching a stable value from the beginning in both experiments. The tool rest temperature T_i kept increasing slowly in both cases as seen in Figure 9.10. The dry friction test resulted in higher tool rest temperature T_i than the lubricated one. Figure 9.11 and Figure 9.12 present the

measurement of the sheet roughness *Ra* after every 100 strokes. No scoring was observed on the workpiece.
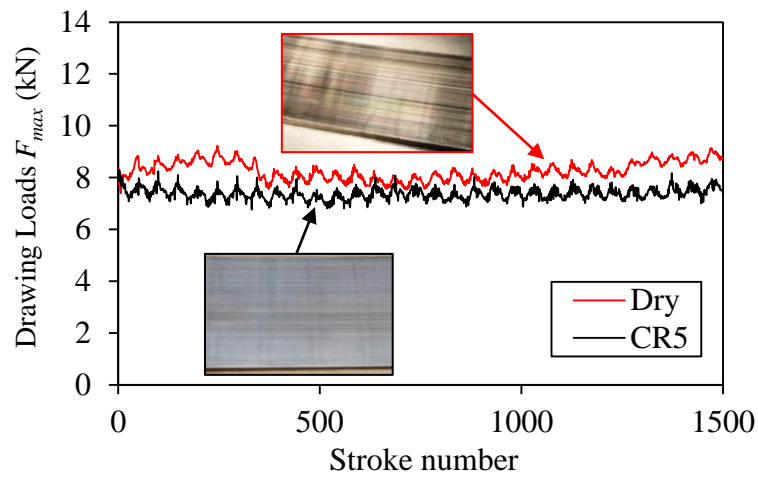
Figure 9.9: Measurement of maximum drawing load and final sheet surface appearance.
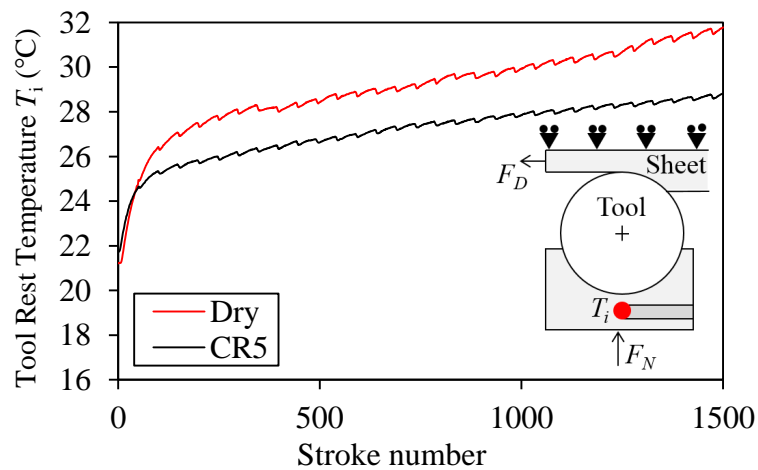
Figure 9.10: Tool rest temperature and schematic of thermocouple location.
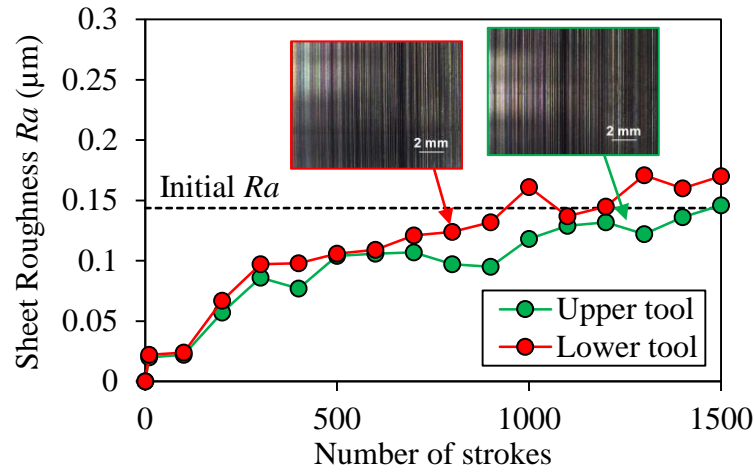
Figure 9.11: Measurement of sheet surface roughness *Ra* under dry condition and final sheet surface appearance.

In the dry friction test, no pick-up was observed after 1,000 strokes but slight peeling off of the DLC coating occurred after 1,500 strokes, see Figure 9.13. In the lubricated test, no pick-up was noticed after 1,500 strokes as seen in Figure 9.14. The results indicated good adhesion at the interface between the DLC, Hyperlox® and the tool substrate and a coating that can sustain a high, repetitive normal pressure and shear stress. In case of lubrication, monitoring the tool temperature is important since an increase of temperature at the tool/workpiece interface leads to lubricant film breakdown and galling [37]. These thermal effects are evaluated in the next section.
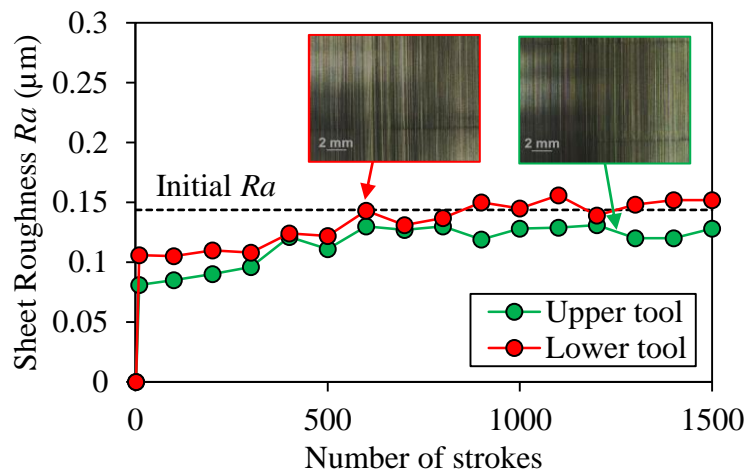
Figure 9.12: Measurement of sheet surface roughness *Ra* under well lubricated condition and final sheet surface condition.
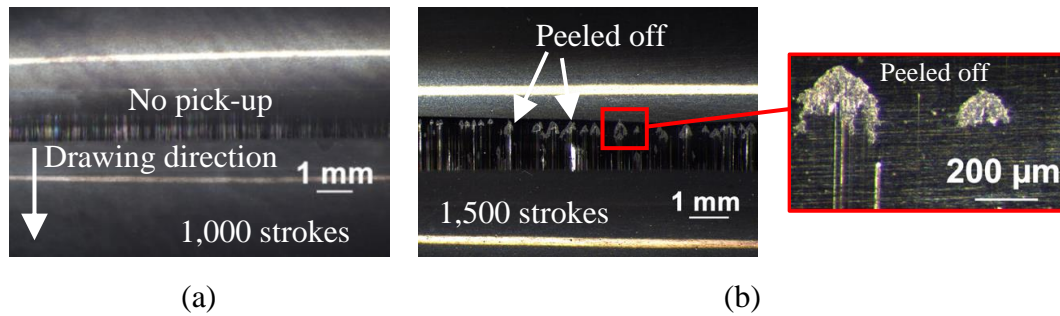
Figure 9.13: Tool surface appearance as a result of dry lubrication condition after a) 1,000 strokes and b) 1,500 strokes.
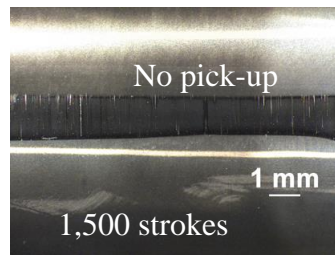
Figure 9.14: Tool surface appearance under lubricated condition after 1,500 strokes.

9.3.6 Numerical Simulation of Strip Reduction Test

A numerical analysis of the strip reduction test was performed with LS-DYNA v. R7.1.1 using implicit time integration. Figure 9.14 shows the FE model of the strip reduction assuming plane strain with 1,969 linear quadrilateral elements. Due to symmetry, only half of the process is modelled. A fine, uniform mesh was applied in the contact between the workpiece and the tool surface. The tool was modelled as an elastic object, while the workpiece was treated as an elastic-plastic object of stainless steel sheet material EN1.4307 according to Voce's stress-strain curve described in Figure 9.6.
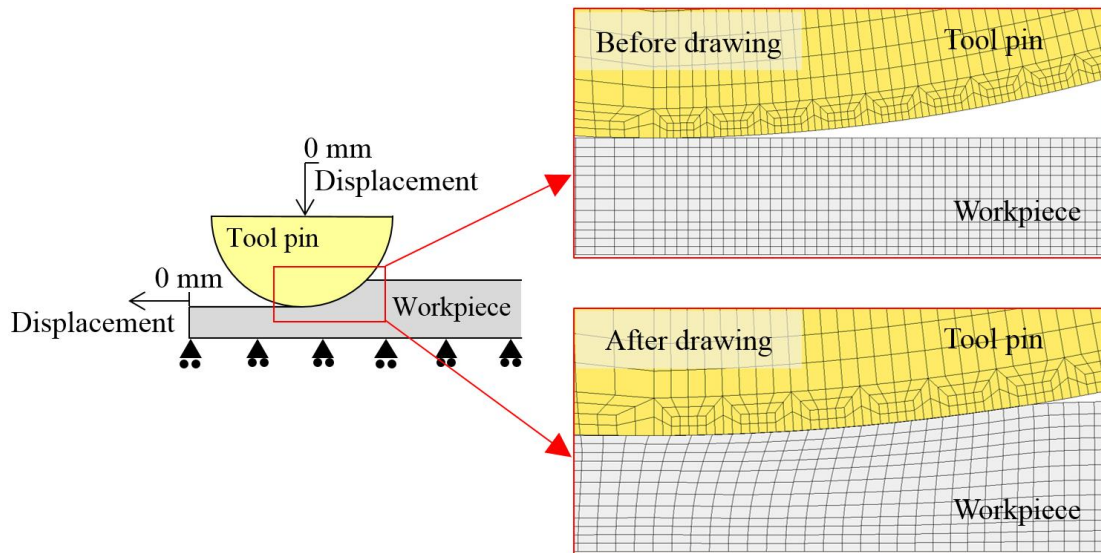
Figure 9.14: Numerical model of the strip reduction (left) and mesh elements of the numerical model in the tool/workpiece contact (right).

The test parameters adopted were similar to the ones listed in Table 9.1. The numerical simulation coupled a mechanical and a thermal analysis, simulating one stroke only. The mechanical and thermal properties applied are listed in Table 9.3 and Table 9.4, respectively. The Heat Transfer Coefficient *HTC* between the tool and the workpiece surface was assumed to be 40 kW/m^2K, replicating a thermo-mechanical simulation of strip reduction testing studied by Olsson et. al [32]. The initial temperature of the tool and workpiece were both assumed to be 20 °C. The Coulomb friction model was used for the surface contact between the tool and the workpiece. The coefficient of friction μ was determined by matching experimental and theoretical drawing load. Figure 9.15 shows the outcome of this, which resulted in $\mu = 0.4$ and $\mu = 0.2$ for dry and lubricated conditions, respectively.

Table 9.3. Material properties of the test materials.

Properties	Tool (Vanadis 4)	Workpiece (EN1.4307)
Density ρ (g/cm3)	7.56	7.90
Poisson ratio v	0.3	0.3
Elastic modulus E (GPa)	200	200

Table 9.4. Thermal properties of the test materials.

Properties	Tool (Vanadis 4)	Workpiece (EN1.4307)
Initial temperature T_i (°C)	20	20
Heat capacity (J/(kg.K))	460	500
Thermal conductivity K (W/(m.K))	26	15
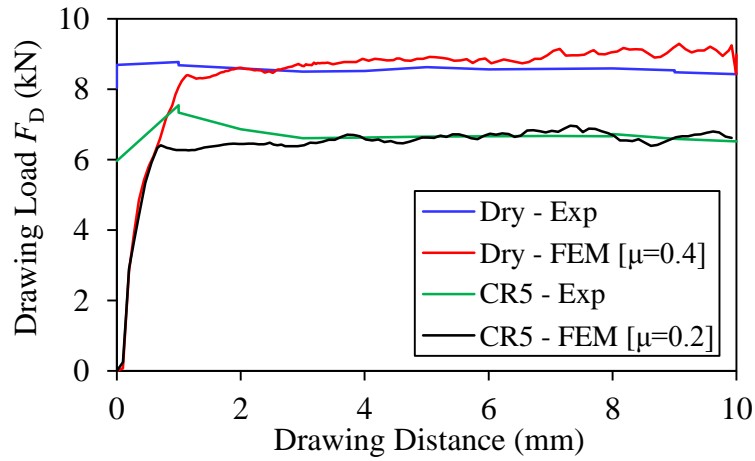
Figure 9.15: Drawing load at 1,500 strokes.
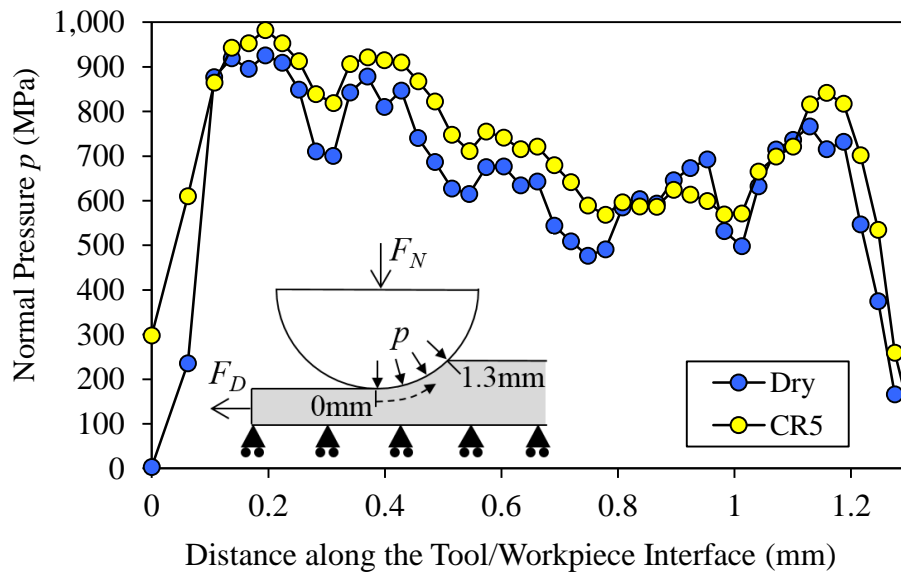
Figure 9.16: Distributions of normal pressure along the tool-workpiece interface in strip reduction.

Figure 9.16 shows the normal pressure distribution along the contact region, reaching a maximum of 900-1000 MPa with no significant difference between dry and lubricated conditions. Fluctuations in the normal pressure values could be caused by irregular meshes in the tool/workpiece contact, Figure 9.14. However, as seen in Figure 9.17, higher temperature at the tool/workpiece interface is predicted in the dry condition than the lubricated one, which is due to higher friction, see Figure 9.15. The temperature increase ΔT along the tool/workpiece interface is thus reduced by lubricating, and even the plain mineral oil without special additives applied results in prevention of galling.
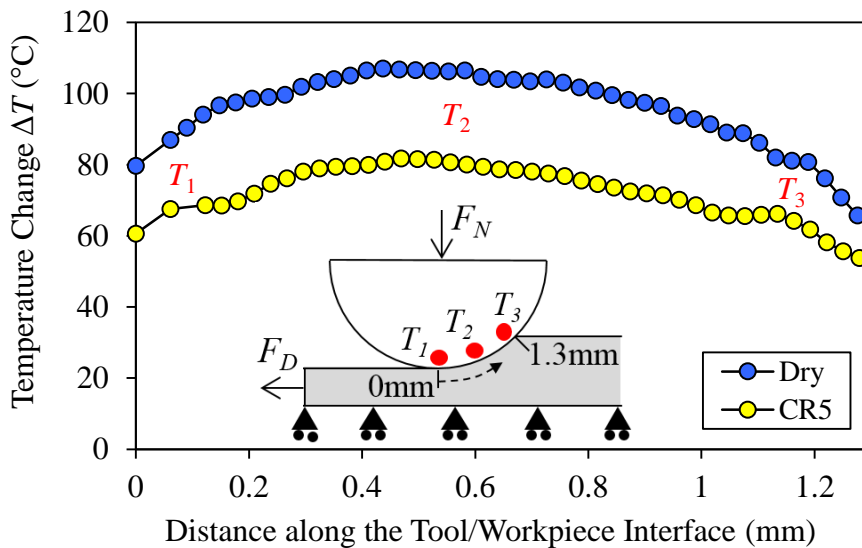
Figure 9.17: Temperature distributions along the tool-workpiece interface in strip reduction.

9.5   Summary

The present study adopted a strip reduction test to evaluate two double-layer coating structures deposited on the tool surface for industrial ironing of stainless steel cups. The two coatings comprised of DLC/Hyperlox® and Hyperlox®/Hyperlox®. The experiments revealed that DLC/Hyperlox® worked satisfactorily in all test conditions provided that a minimum amount of lubrication was utilized to avoid peeling off of the coating. A numerical analysis supported the experimental findings, where lubrication reduced friction and thereby the temperature increase at the tool/workpiece interface.

Chapter 10: Conclusion and Future Research

In this chapter, the concluding remarks are summarized on achievements against thesis aims and objectives set in Chapter 1. The key findings are highlighted and recommendations towards future research are suggested for each objective.

10.1 Objective 1: Compressibility of Liquid Lubricants

10.1.1 Conclusions

With the aim to determine the bulk modulus of fluids at elevated pressures, two methodologies were designed and developed. The relationship between the bulk modulus and the pressure has been established for characterizing the lubricant entrapment and deformation in micro-plasto-hydrodynamic lubrication.

The proposed methodology consisting of a simple laboratory test and an inverse FEM analysis, in order to determine the liquid bulk modulus, has proven to work reasonably in the low pressure regime. It is of importance to determine the lubricant bulk modulus at larger pressures above 100 MPa, which most of trapped lubricants experiences in sheet forming of tribologically difficult materials, e.g, stainless steel, aluminium alloys, and titanium alloys. Thus, this suggests an improved version of the simple laboratory test, where a stronger specimen material could be used to determine the bulk modulus at a larger pressure.

The high-pressure equipment for determining lubricant bulk modulus has proven to work satisfactorily until a pressure of 500 MPa. The pressure is measured directly in the pressurized lubricant inside the high-pressure container, hence the test equipment allows for the direct determination of the bulk modulus at various pressure levels with no influence from friction in the sealing on the moving punch building up the pressure.

10.1.2 Suggestions for Future Research

Numerical software progresses rapidly to fulfill the demands and applications in the field of tribology in sheet metal forming. The author believes that lubricant properties at high pressures will be highly needed in modelling liquid lubricants in the near future, i.e., micro-hydrodynamic lubrication mechanism for textured tool/workpiece surfaces. At present, the bulk modulus can be obtained from the high-pressure equipment designed and developed in this PhD study. The next aim would be the lubricant viscosity at high pressures in order to obtain a complete lubricant data set for metal forming.

10.2 Objective 2: Structured Tool Surfaces

10.2.1 Conclusions

The second objective of this study addresses textured tool surfaces with a focus to impede galling. The present experiments on the structured tool surfaces have shown a positive result regarding improvement of lubrication by facilitating the escape of trapped lubricant by micro-plasto-hydrodynamic lubrication and thereby reducing the friction. The theoretical and experimental results show strong agreement that back up the research claiming that an optimal pocket spacing exists to reduce friction and thus drawing load, at least for the tool patterns described in this experimental work.

A technique to improve resistivity towards galling by applying textured tool surface topographies was investigated. Oblong shallow pockets with small pocket angles, oriented perpendicular to the sliding direction with a distance of 2–4 times the pocket width were tested. A strip reduction test, which emulates the tribological conditions in an ironing process, was used for experimental measurements of friction and determination of possible pick-up and galling. The study included testing of four different lubricants—two plain mineral oils with a low and a high viscosity, and two mineral-based oils with boundary lubrication additives having medium and high viscosity. The results confirmed that tool texture can lower friction and improve lubrication performance in comparison to that of a fine polished tool surface when the pocket distance is 2–4 times larger than the pocket width, which ensures a table mountain structure of the tool topography. The tool textures were advantageous at greater sliding speeds, when using higher viscosity oils, which facilitates the escape of trapped lubricant by micro-plasto-hydrodynamic lubrication.

A friction model for a soft workpiece deforming against a textured tool surface was proposed. The model takes into account the plastic wave motion appearing, when the workpiece material flows into and out of local pockets between the flat plateaus of a table mountain like tool surface topography. The model was evaluated by strip reduction tests, which emulates the tribological conditions in an ironing process. The study included testing of two different lubricants, a plain mineral oil with a high viscosity, and a mineral-based oil with boundary lubrication additives having a medium viscosity. It was found that an optimum amount of tool texture exists which reduces friction and thus drawing load for the table-mountain-like tool surface topography. The overall friction factor in the interface between workpiece and textured tool surface can be satisfactory predicted by the model.

10.2.2 Suggestions for Future Research

Further investigation is needed for long-term analysis of the feasible textured tool surface with a pocket distance 2-4 times larger than the pocket width to the tool surface, since the present experiments involved a maximum of up to six repetitions.

Alternatively, application of hard coating to the structured tool surface may further improve resistivity towards galling. Such studies would provide engineers and researchers with more knowledge about fundamental aspects in the improvement of textured tool surface behaviour for a continuous production of sheet metal in the industry.

10.3   Objective 3: Anti-Seizure Tool Coatings

10.3.1 Conclusions

A new DLC coating for ironing of stainless steel under tribologically severe test conditions, i.e. dry lubrication, large normal pressure and elevated temperature, without pick-up and galling, was developed in collaboration with CemeCON A/S. The screening experiments were conducted under varied normal pressure at room temperature. The experiments were also carried out at elevated temperatures of 80 °C and 110 °C to investigate the effects of elevated tool temperature on the performance of a promising double-layer DLC/Hyperlox® tool coating. The new DLC coating deposited onto the tool surface seems to be able to reduce galling and extend the tool life.

The screening experiment adopted a strip reduction test on a manually operated tribo-tester for emulating industrial ironing of stainless steel cups to test DLC coatings at room temperature as well as elevated tool temperature. Three DLC coating types were evaluated; single layer DLC, double layer (DLC/Hyperlox®) and multi-layer (DLC/CrN/Cr). The experiments revealed that the double layer (DLC/Hyperlox®) coating is the only coating that can function without lubrication at least to 1,000 strokes. It gave a smooth surface finish of the tested strips with no pick-up on the coated tool surface. Intermediate metallic layers like Hyperlox® between the DLC film and the tool substrate ensured good adhesion of the DLC coating and are expected to work effectively under severe conditions in sheet stamping of stainless steel.

A long-term analysis of the promising DLC tool coating structure was performed. The analysis involved a strip reduction experiment on an automatic tribo-tester to evaluate two double-layer coating structures deposited on the tool surface for replicating industrial ironing of stainless steel cups. The double-layer coating types comprised of DLC/Hyperlox® and Hyperlox®/Hyperlox® coatings. The experiments revealed that the new DLC coating, DLC/Hyperlox® coating, specifically developed for this PhD study was the only tool coating working satisfactorily in all test conditions provided that a minimum amount of hazard free lubrication is utilized to avoid peeling off of the coating. A numerical analysis supports the experimental findings, where lubrication is necessary to reduce the temperature increase at the tool/workpiece interface by reducing the friction.

10.3.2 Suggestions for Future Research

Further investigations into the effect of the newly developed coating to industrial progressive tools could provide interesting findings. One major direction of future research is to better understand the effect of different, intermediate metallic coating films in order to find the most suitable one and to keep the DLC coating as the top layer and a better adhesion between the tool and the DLC coating surfaces.

Another direction of future research is to perform an industrial production testing of the new DLC coating, the double-layer DLC/Hyperlox® coating. The current thesis focused on the off-line tribological simulation testing of the new coating in which the process parameters are similar to the production. However, additional evidence is necessary to clearly demonstrate that the new DLC coating will function effectively without lubrication or using minimum amount of environmentally benign lubrication.

References

[1]   J.A. Schey, G.M. Dalton, Lubrication mechanism in the forming of galvanized steel sheet, J. Mater. Process. Technol. 24 (1990) 365–374. doi:10.1016/j.jmatprotec.2010.05.019.

[2]   A. Azushima, H. Kudo, Direct observation of contact behaviour to interpret the pressure dependence of the coefficient of friction in sheet metal forming, CIRP Ann. - Manuf. Technol. 44 (1995) 209–212. doi:10.1016/S0007-8506(07)62309-9.

[3]   J. Bech, N. Bay, M. Eriksen, A study of mechanisms of liquid lubrication in metal forming, CIRP Ann. Manuf. Technol. 47 (1998) 221–226. doi:10.1016/S0007-8506(07)62822-4.

[4]   N. Bay, J.I. Bech, J.L. Andreasen, I. Shimizu, Studies on micro plasto hydrodynamic lubrication in metal forming, in: Met. Form. Sci. Pract. A State-of-the-Art Vol. Honor. Prof. J.A. Schey., Woodhead Publishing Limited, 2002: pp. 115–134. doi:10.1016/B978-008044024-8/50007-2.

[5]   L. Dubar, C. Hubert, P. Christiansen, N. Bay, A. Dubois, Analysis of fluid lubrication mechanisms in metal forming at mesoscopic scale, CIRP Ann. - Manuf. Technol. 61 (2012) 271–274. doi:10.1016/j.cirp.2012.03.126.

[6]   M. Geiger, U. Engel, M. Pfestorp, New developments for the quantification of technical surfaces in forming processes, Ann. CIRP. 46 (1997) 171–174.

[7]   D. Schmoeckel, M. Prier, J. Staeves, Topography deformation of sheet metal during the forming process and its influence on friction, Measurement. 46 (1997) 175–178. doi:10.1016/S0007-8506(07)60802-6.

[8]   H. Kijima, N. Bay, Contact conditions in skin-pass rolling, CIRP Ann. - Manuf. Technol. 56 (2007) 301–306. doi:10.1016/j.cirp.2007.05.070.

[9]   P. Groche, J. Stahlmann, J. Hartel, M. Köhler, Hydrodynamic effects of macroscopic deterministic surface structures in cold forging processes, Tribol. Int. 42 (2009) 1173–1179. doi:10.1016/j.triboint.2009.03.019.

[10]   E. Madsen, Personal communication with Niels Bay, Grundfos A/S. (2012).

[11]   F. Lindvall, J. Bergstrom, P. Krakhmalev, N. Bay, The effect of grinding and polishing procedure of tool steels in sheet metal forming, in: Proc. 4th Int. Conf. Tribol. Manuf. Process., 2010: pp. 603–612. doi:10.1081/E-EEE2-120046011.

[12]   D. Wiklund, M. Liljebgren, J. Berglund, N. Bay, K. Kjellsson, B.-G. Rosén, Friction in sheet metal forming – A comparison between machined and manually polished die surfaces, in: Tribol. Manuf. Process. Proc. Int. Conf. Tribol. Manuf. Process. ICTMP4, 2010: pp. 613–622.

[13]   M. Murakawa, N. Koga, S. Takeuchi, Diamondlike carbon-coated dies for deep drawing of aluminum sheets, J. Manuf. Sci. Eng. Trans. ASME. 121 (1999) 674–678. doi:10.1115/1.2833101.

[14]   B. Podgornik, S. Hogmark, O. Sandberg, Proper coating selection for improved galling performance of forming tool steel, Wear. 261 (2006) 15–21. doi:10.1016/j.wear.2005.09.005.

[15]   S. Tsuda, S. Yoshihara, S. Kataoka, Dry deep drawing ironing of AZ31 magnesium alloy sheet using diamond coated dies, J. JSTP. 52 (2011) 480–484.

[16]   T. Yokosawa, J. Takagi, S. Kataoka, An attempt to polish CVD diamond film by

ultrasonic vibration polishing without abrasive grain, in: 20th Annu. Meet. Am. Soc. Precis. Eng. ASPE 2005, 2005.

[17]   M. Murakawa, S. Takeuchi, A. Alahelisten, M. Kasugai, An efficient mechanical polishing method for diamond-coated inserts and testing of their performance, Surf. Coat. Technol. 86/87 (1996) 686–691.

[18]   B. Podgornik, B. Zajec, N. Bay, J. Vizintin, Application of hard coatings for blanking and piercing tools, Wear. 270 (2011) 850–856. doi:10.1016/j.wear.2011.02.013.

[19]   N. Bay, Metal forming and lubrication. Invited paper. Chapter in Encyclopedia of Materials: Science and Technology, Elsevier Sci. Ltd. (2000) 5377–5380.

[20]   N. Bay, A. Azushima, P. Groche, I. Ishibashi, M. Merklein, M. Morishita, T. Nakamura, S. Schmid, M. Yoshida, Environmentally benign tribo-systems for metal forming, CIRP Ann. - Manuf. Technol. 59 (2010) 760–780. doi:10.1016/j.cirp.2010.05.007.

[21]   J.A. Schey, Tribology in Metalworking: Friction, Lubrication and Wear, Am. Soc. Met. 1 (1983) 1–736.

[22]   H. Kim, N. Kardes, Chapter 7: Friction and lubrication, Sheet Met. Form. - Fundam. 1 (2012) 89–103. doi:10.1016/0043-1648(68)90342-6.

[23]   T. Mizuno, M. Okamoto, Effects of lubricant viscosity at pressure and sliding velocity on lubricating conditions in the compression-friction test on sheet metals, J. Lubr. Technol. 104 (1982) 53–59. doi:10.1115/1.3253164.

[24]   H. Kudo, M. Tsubouchi, H. Takada, K. Okamura, An investigation into plasto-hydrodynamic lubrication with a cold sheet drawing test, CIRP Ann. - Manuf. Technol. 31 (1982) 175–180. doi:10.1016/S0007-8506(07)63292-2.

[25]   A. Azushima, T. Tsubouchi, H. Kudo, Direct observation of lubricant behaviors under the micro-PHL at the interface between workpiece and die, Proc. 3rd Int. Conf. Technol. Plast. 1 (1990) 551–556.

[26]   C.G. Sorensen, J.I. Bech, J.L. Andreasen, N. Bay, U. Engel, T. Neudecker, A basic study of the influence of surface topography on mechanisms of liquid lubrication in metal forming, CIRP Ann. Manuf. Technol. 48 (1999) 203–208. http://www.sciencedirect.com/science/article/pii/S0007850607631667.

[27]   S.-W. Lo, W.R.D. Wilson, A theoretical model of micro-pool lubrication in metal forming, J. Tribol. 121 (1999) 731–738. doi:10.1115/1.2834129.

[28]   A. Azushima, FEM analysis of hydrostatic pressure generated within lubricant entrapped into pocket on workpiece surface in upsetting process, J. Tribol. 122 (2000) 822–827. doi:10.1115/1.1286160.

[29]   A. Stephany, H.R. Le, M.P.F. Sutcliffe, An efficient finite element model of surface pit reduction on stainless steel in metal forming processes, J. Mater. Process. Technol. 170 (2005) 310–316. doi:10.1016/j.jmatprotec.2005.05.008.

[30]   J. Bech, N. Bay, M. Eriksen, Entrapment and escape of liquid lubricant in metal forming, Wear. 232 (1999) 134–139. doi:10.1016/S0043-1648(99)00136-2.

[31]   N. Bay, D.D. Olsson, J.L. Andreasen, Lubricant test methods for sheet metal forming, Tribol. Int. 41 (2008) 844–853. doi:10.1016/j.triboint.2007.11.017.

[32]   D.D. Olsson, N. Bay, J.L. Andreasen, Prediction of limits of lubrication in strip reduction testing, CIRP Ann. - Manuf. Technol. 53 (2004) 231–234. doi:10.1016/S0007-8506(07)60686-6.

[33] T. Mang, Encyclopedia of lubricants and lubrication: Sheet metal forming lubricants, (2014) 1747–1769. doi:10.1007/978-3-642-22647-2.

[34] N Bay, Trends and vision in metal forming tribology, Steel Res. Int. Planetary (2011) 15–26.

[35] J.L. Andreasen, D.D. Olsson, K. Chodnikiewicz, N. Bay, Bending under tension test with direct friction measurement, Proc. Inst. Mech. Eng. Part B J. Eng. Manuf. 220 (2006) 73–80. doi:10.1243/095440505X32913.

[36] J.L. Andreasen, N. Bay, M. Andersen, E. Christensen, N. Bjerrum, Screening the performance of lubricants for the ironing of stainless steel with a strip reduction test, Wear. 207 (1997) 1–5. doi:DOI: 10.1016/S0043-1648(96)07462-5.

[37] N. Bay, E. Ceron, Off-line testing of tribo-systems for sheet metal forming production, Adv. Mater. Res. 966–967 (2014) 3–20. doi:10.4028/www.scientific.net/AMR.966-967.3.

[38] E. Ceron, N. Bay, A methodology for off-line evaluation of new environmentally friendly tribo-systems for sheet metal forming, CIRP Ann. - Manuf. Technol. 62 (2013) 231–234. doi:10.1016/j.cirp.2013.03.062.

[39] P.S. Nielsen, K.S. Friis, N. Bay, Testing and modelling of new tribo-systems for industrial sheet forming of stainless steels, Proc. Inst. Mech. Eng. Part J J. Eng. Tribol. 225 (2011) 1036–1047. doi:10.1177/1350650111415331.

[40] K. Großmann, H. Wiemer, A. Hardtmann, L. Penter, S. Kriechenbauer, Adjusting the contact surface of forming tools in order to compensate for elastic deformations during the process, 7th Eur. LS-DYNA Conf. (2009).

[41] H. Kim, M. Kimchi, N. Kardes, T. Altan, Effects of variable elastic modulus on springback predictions in stamping Advanced High-Strength Steels (AHSS). Steel Research International, in: Spec. Ed. 10th Int. Conf. Technol. Plast. ICTP 2011, 2011: pp. 628–633.

[42] R. Krux, W. Homberg, M. Kalveram, M. Trompeter, M. Kleiner, K. Weinert, Die surface structures and hydrostatic pressure system for the material flow control in high-pressure sheet metal forming, Adv. Mater. Res. 6–8 (2005) 385–392. doi:10.4028/www.scientific.net/AMR.6-8.385.

[43] A. Godi, J. Grønbæk, L. De Chiffre, Off-line testing of multifunctional surfaces for metal forming applications, CIRP J. Manuf. Sci. Technol. 11 (2015) 28–35. doi:10.1016/j.cirpj.2015.06.001.

[44] D. Wiklund, M. Liljengren, N. Bay, K. Kjellsson, B. Rosén, Effects of tool die surface topography on friction and galling in sheet metal forming, Swedish Prod. Symp. (2009) 1–6.

[45] J. Berglund, C.A. Brown, B.G. Rosen, N. Bay, B.G. Rosén, N. Bay, Milled die steel surface roughness correlation with steel sheet friction, CIRP Ann. - Manuf. Technol. 59 (2010) 577–580. doi:10.1016/j.cirp.2010.03.140.

[46] E. Ceron, M. Olsson, N. Bay, Lubricant film breakdown and material pick-up in sheet forming of advanced high strength steels and stainless steels when using environmental friendly lubricants, Adv. Mater. Res. 967 (2014) 219–227. doi:10.4028/www.scientific.net/AMR.966-967.219.

[47] R.S. Eriksen, M. Arentoft, J. Grønbæk, N. Bay, Manufacture of functional surfaces through combined application of tool manufacturing processes and Robot Assisted Polishing, CIRP Ann. - Manuf. Technol. 61 (2012) 563–566. doi:10.1016/j.cirp.2012.03.020.

[48] H.L. Costa, I.M. Hutchings, Development of a maskless electrochemical texturing method, J. Mater. Process. Technol. 209 (2009) 3869–3878. doi:10.1016/j.jmatprotec.2008.09.004.

[49] V. Franzen, J. Witulski, A. Brosius, M. Trompeter, A.E. Tekkaya, Textured surfaces for deep drawing tools by rolling, Int. J. Mach. Tools Manuf. 50 (2010) 969–976. doi:10.1016/j.ijmachtools.2010.08.001.

[50] K. Wagner, R. Völkl, U. Engel, Tool life enhancement in cold forging by locally optimized surfaces, J. Mater. Process. Technol. 201 (2008) 2–8. doi:10.1016/j.jmatprotec.2007.11.152.

[51] B. Podgornik, J. Jerina, Surface topography effect on galling resistance of coated and uncoated tool steel, Surf. Coatings Technol. 206 (2012) 2792–2800. doi:10.1016/j.surfcoat.2011.11.041.

[52] M. Geiger, U. Popp, U. Engel, Excimer laser micro texturing of cold forging tool surfaces - Influence on tool life, CIRP Ann. - Manuf. Technol. 51 (2002) 231–234. doi:10.1016/S0007-8506(07)61506-6.

[53] I. Shimizu, J.L. Andreasen, J.I. Bech, N. Bay, Influence of workpiece surface topography on the mechanisms of liquid lubrication in strip drawing, J. Tribol. 123 (2001) 290. doi:10.1115/1.1308017.

[54] A. Godi, J. Grønbæk, L. De Chiffre, Characterisation and full-scale production testing of multifunctional surfaces for deep drawing applications, CIRP J. Manuf. Sci. Technol. 16 (2015) 64–71. doi:10.1016/j.cirpj.2016.07.001.

[55] M. Steitz, P. Stein, P. Groche, Influence of hammer-peened surface textures on friction behavior, Tribol. Lett. 58 (2015) 1–8. doi:10.1007/s11249-015-0502-9.

[56] U. Engel, Tribology in microforming, Wear. 260 (2006) 265–273. doi:10.1016/j.wear.2005.04.021.

[57] L. Hiegemann, C. Weddeling, N. Ben Khalifa, E. Tekkaya, Control of the material flow in deep drawing by the use of rolled surface textures, in: Offentl. Kolloquium - SFB 708, 2013: pp. 33–43.

[58] F. Klocke, D. Trauth, F. Schongen, a. Shirobokov, Analysis of friction between stainless steel sheets and machine hammer peened structured tool surfaces: experimental and numerical investigation of the lubricated interaction gap, Prod. Eng. 8 (2013) 263–272. doi:10.1007/s11740-013-0519-6.

[59] F. Klocke, D. Trauth, M. Terhorst, P. Mattfeld, Wear analysis of tool surfaces structured by machine hammer peening for foil-free forming of stainless steel, Adv. Mater. Res. 1018 (2014) 317–324. doi:10.4028/www.scientific.net/AMR.1018.317.

[60] H. Kim, S. Han, Q. Yan, T. Altan, Evaluation of tool materials, coatings and lubricants in forming galvanized advanced high strength steels (AHSS), CIRP Ann. - Manuf. Technol. 57 (2008) 299–304. doi:10.1016/j.cirp.2008.03.029.

[61] H. Kim, S.-S. Han, K. Kim, T. Altan, Investigation of galling in forming of galvanized advanced high strength steels - Sixth progress report: Evaluation of die coatings and stamping lubricants using the strip drawing test, CPF Rep. No CPF 2.3/08/02. (2008) 1–27.

[62] S. Tsuda, S. Yoshihara, S. Kataoka, Formability of AZ31 Mg alloy sheet in dry press forming using diamond coated dies, in: Proc. ASME 2009 Int. Mech. Congr. Expo. IMECE2009, 2009: pp. 1–6.

[63] T. Aizawa, E. Iwamura, K. Itoh, Nano-lamination in amorphous carbon for

tailored coating in micro-dry stamping of AISI-304 stainless steel sheets, Surf. Coatings Technol. 203 (2008) 794–798. doi:10.1016/j.surfcoat.2008.08.059.

[64] J. Vetter, 60 years of DLC coatings: Historical highlights and technical review of cathodic arc processes to synthesize various DLC types, and their evolution for industrial applications, Surf. Coat. Technol. 257 (2014) 213–240. doi:10.1016/j.surfcoat.2014.08.017.

[65] K. Holmberg, A. Matthews, H. Ronkainen, Coatings tribology—contact mechanisms and surface design, Tribol. Int. 31 (1998) 107–120. doi:10.1016/S0301-679X(98)00013-9.

[66] S. Kataoka, Improvements in adhesion of DLC thin film on the tool for dry deep drawing process, Mem. Shonan, Inst. Technol. 41 (2008) 11–18.

[67] B. Podgornik, S. Hogmark, O. Sandberg, Hard PVD coatings and their perspectives in forming tool applications, in: 6th Int. Tool. Conf., 2002: pp. 1053–1066.

[68] S. PalDey, S.C. Deevi, Single layer and multilayer wear resistant coatings of (Ti,Al)N: A review, Mater. Sci. Eng. A. 342 (2003) 58–79. doi:10.1016/S0921-5093(02)00259-9.

[69] L.M. Alves, C. V. Nielsen, P.A.F. Martins, Revisiting the fundamentals and capabilities of the stack compression test, Exp. Mech. 51 (2011) 1565–1572. doi:10.1007/s11340-011-9480-5.

[70] H. Kudo, A note on the role of microscopically trapped trapped lubricant at the tool-work interface, J. Mech. Sci. 7 (1965) 383–388. doi:10.1016/0020-7403(65)90066-4.

[71] T. Wanheim, Friction at high normal pressures, Wear. 25 (1973) 225–244. doi:10.1016/0043-1648(73)90074-4.

[72] T. Nellemann, N. Bay, T. Wanheim, Real area of contact and friction stress - the role of trapped lubricant, Wear. 43 (1977) 45–53. doi:10.1016/0043-1648(77)90042-4.

[73] ASTM International, Standard test method for determination of isothermal secant and tangent bulk modulus, in: ASTM Int. West Conshohocken, PA, 2012: pp. 1–5. doi:10.1520/D6793-02R12.

[74] B.O. Jacobson, Rheology and elastohydrodynamic lubrication, in: Elsevier New York USA, 1991: pp. 1–382.

[75] S. Bair, M. Baker, D.M. Pallister, Revisiting the compressibility of oil/refrigerant lubricants, J. Tribol. 139 (2016) 1–4. doi:10.1115/1.4033335.

[76] L.H. Butler, Surface conformation of metals under high nominal contact pressures, Metallurgia. 58 (1960) 167–174.

[77] M.T.O. Lund, N.S. Hansen, Design and construction of high pressure viscometer, Masters Thesis, Tech. Univ. Denmark. (2016) 1–271.

[78] B. Sundström, Handbok och formelsamling i Hållfasthetslära (in swedish), KTH, 1998.

[79] A.T.J. Hayward, Compressibility equations for liquids: a comparative study, Br. J. Appl. Phys. 18 (1967) 965–977. doi:10.1088/0508-3443/18/7/312.

[80] A. Godi, K. Mohaghegh, J. Grønbæk, P. Klit, L. De Chiffre, Testing of newly developed functional surfaces under pure sliding conditions, Tribol. Lett. 51 (2013) 171–180. doi:10.1007/s11249-013-0162-6.

[81]   H.L. Costa, I.M. Hutchings, Effects of die surface patterning on lubrication in strip drawing, J. Mater. Process. Technol. 209 (2009) 1175–1180. doi:10.1016/j.jmatprotec.2008.03.026.

[82]   M.H. Sulaiman, P. Christiansen, N. Bay, The influence of tool texture on friction and lubrication in strip reduction testing, Lubricants. 5 (2017) 1–11. doi:10.3390/lubricants5010003.

[83]   I. Shimizu, P.A.F. Martins, N. Bay, J.L. Andreasen, J.I. Bech, Influences of lubricant pocket geometry and working conditions upon micro lubrication mechanisms in upsetting and strip drawing, Int. J. Surf. Sci. Eng. 4 (2010) 42–54. doi:http://dx.doi.org/10.1504/IJSURFSE.2010.029628.

[84]   U. Popp, U. Engel, Microtexturing of cold-forging tools - Influence on tool life, Proc. Inst. Mech. Eng. Part B J. Eng. Manuf. 220 (2006) 27–33. doi:10.1243/095440505X32968.

[85]   T. Wanheim, T. Abildgaard, A mechanism for metallic friction, in: Proc. 4th Int. Conf. Prod. Eng. Tokyo, 1980: pp. 122–127.

[86]   E. Siebel, Untersuchungen über bildsame Formänderung unter besonderer Berück- sichtigung des Schmiedens, Maschinenbau/Betrieb. 9 (1923) 307–312.

[87]   S. Paskvale, M. Kahn, M. Cekada, P. Panjan, W. Waldhauser, B. Podgornik, Tribological properties of diamond-like carbon coatings prepared by anode layer source and magnetron sputtering, Surf. Coatings Technol. 205 (2011) 99–102. doi:10.1016/j.surfcoat.2010.06.006.

[88]   A. de Neergaard, Personal communication with M.H. Sulaiman, CemeCON Scand. A/S. March 22th, 2017. (2017).

Appendix A1: MATLAB code for tensile test

```matlab
clear all
clc

%% This program computes the stress-strain behaviour based on tensile
test

% Models that can be fitted
% 1: Hollomon
% 2: Swift
% 3: Voce
% 4: Ludwik

%% Import of data
Data = load('Data.txt'); % [Load [kp], length change [mm], width
[mm]]
Data_treatment = load('Data treatment.txt'); % [Material model,
Sample length [mm], sheet thickness [mm], sample length to start fit
[mm], sample length to end fit [mm]]

%% Data treatment

if length(Data(1,:)) > 3
    Data(:,1) = []; % Removing column with login time
end

% Converting numbers to positive
Data = abs(Data);

% Filtering of data
Filtersize = 1000;
Data_filtered = [zeros(Filtersize,3); Data]; % Inserting dummy data
in the beginning for the filtering process
Data_filtered(1:Filtersize,3) = Data(1,3); % Inserting initial width
of specimen
Data_filtered(:,1) =
filter(ones(1,Filtersize)/Filtersize,1,Data_filtered(:,1)); % Filter
force
Data_filtered(:,2) =
filter(ones(1,Filtersize)/Filtersize,1,Data_filtered(:,2)); % Filter
elongation
Data_filtered(:,3) =
filter(ones(1,Filtersize)/Filtersize,1,Data_filtered(:,3)); % Filter
width
Data_filtered(1:Filtersize,:) = []; % Removing dummy data
Data = Data_filtered;

% Offsetting data
Data(:,2) = Data(:,2) - min(Data(:,2)); % Setting initial elongation
to zero

[value,i] = max(Data(:,2)); % Removing data after maximum elongation
Data(i:end,:) = [];

Data = sortrows(Data,2); % Sorting data according to elongation

[value,i_start] = min(abs(Data(:,2)-Data_treatment(4))); % Starting
point of data treatment
[value,i_end] = min(abs(Data(:,2)-Data_treatment(5))); % End point of
data treatment
```

131

```matlab
% Initial dimensions
L0 = Data_treatment(2); % Measurement length [mm]
t0 = Data_treatment(3); % Initial thickness [mm]
W0 = max(Data(:,3)); % Initial width [mm]
A0 = W0*t0; % Initial cross sectional area [mm^2]

% Computation of deformation
L = L0+Data(:,2); % Length during deformation [mm]
W = Data(:,3); % Width during deformation
t = L0*W0*t0./(W.*L); % Thickness during deformation
A = W.*t; % Cross sectional area during deformation [mm^2]

% Force
F = Data(:,1)*9.80665; % Conversion from kp to N

% Stress and strains
Epsilon_L = log(L(i_start:i_end)/L(i_start)); % Length strain
Epsilon_W = log(W(i_start:i_end)/W(i_start)); % Width strain
Epsilon_t = -Epsilon_W - Epsilon_L; % Thickness strain
Epsilon = sqrt(2/3*(Epsilon_L.^2+Epsilon_W.^2+Epsilon_t.^2)); %
Effective strain
Sigma = F(i_start:i_end)./A(i_start:i_end); % Flow stress

Intermediate = [Epsilon Sigma]; % Intermediate matrix to sort
according to effective strain
Intermediate = sortrows(Intermediate,1); % Sorting according to
effective strain
Epsilon = Intermediate(:,1); % Overwritting effective strain
Sigma = Intermediate(:,2); % Overwritting effective stress

% Less points
EpsilonXX = Epsilon(1:100:7566);
SigmaXX = Sigma(1:100:7566);

% Computing Lankford coefficient
R = Epsilon_W./Epsilon_t; % Lankford coefficient
Epsilon_minimum_R = 0.05; % Minimum strain under which R is not
computed
[x,i_R] = min(abs(Epsilon-Epsilon_minimum_R)); % Only use strains
larger than a given minimum to compute average R
R_average = mean(R(i_R:end)); % Average Lankford coefficient

%% Data fitting

% Hollomon
if Data_treatment(1) == 1
    Hollomon = @(x) norm(x(1)*Epsilon.^x(2) - Sigma);
    Hollomon_constants = fminsearchbnd(Hollomon,[mean(Sigma) 0.1],[0
0]);
    C = Hollomon_constants(1);
    n = Hollomon_constants(2);
    Sigma_fit = C*Epsilon.^n;
    C_legend = num2str(C,'%10.0f');
    n_legend = num2str(n,'%10.3f');
    legend2 = ['Hollomon:
$\sigma_{o}=$',C_legend,'$\left(\bar{\varepsilon}^{pl}\right)^{',n_le
gend,'} [MPa]$'];
end

% Swift
if Data_treatment(1) == 2
```

```matlab
    Swift = @(x) norm(x(1)*(x(2)+Epsilon).^x(3) - Sigma);
    Swift_constants = fminsearchbnd(Swift,[mean(Sigma) 0.1 0.1],[0 0
0]);
    C = Swift_constants(1);
    B = Swift_constants(2);
    n = Swift_constants(3);
    Sigma_fit = C*(B+Epsilon).^n;
    C_legend = num2str(C,'%10.0f');
    B_legend = num2str(B,'%10.3f');
    n_legend = num2str(n,'%10.3f');
    legend2 = ['Swift:
$\sigma_{o}=$',C_legend,'$\left(',B_legend,'+\bar{\varepsilon}^{pl}\r
ight)^{',n_legend,'} [MPa]$'];
end

% Voce
if Data_treatment(1) == 3
    Voce = @(x) norm(x(1)+(x(2)-x(1))*(1-exp(-x(3)*Epsilon)) -
Sigma);
    Voce_constants = fminsearchbnd(Voce,[min(Sigma) max(Sigma) 10],[0
0 0]);
    a_Voce = Voce_constants(1);
    b_Voce = Voce_constants(2);
    c_Voce = Voce_constants(3);
    Sigma_fit = a_Voce + (b_Voce-a_Voce)*(1-exp(-c_Voce*Epsilon));
    a_legend = num2str(a_Voce,'%10.0f');
    b_legend = num2str(b_Voce,'%10.0f');
    c_legend = num2str(c_Voce,'%10.1f');
    legend2 = ['Voce: $\sigma_{o}=$',a_legend,'$+\left(',b_legend,'-
',a_legend,'\right)\left(1-exp\left(-
',c_legend,'\bar{\varepsilon}\right)\right) [MPa]$'];
end

% Ludwik
if Data_treatment(1) == 4
    Ludwik = @(x) norm(x(1)*Epsilon.^x(2)+x(3) - Sigma);
    Ludwik_constants = fminsearchbnd(Ludwik,[mean(Sigma) 0.1
min(Sigma)],[0 0 0]);
    C = Ludwik_constants(1);
    n = Ludwik_constants(2);
    Sigma_0 = Ludwik_constants(3);
    Sigma_fit = C*Epsilon.^n+Sigma_0;
    C_legend = num2str(C,'%10.0f');
    n_legend = num2str(n,'%10.3f');
    Sigma_0_legend = num2str(Sigma_0,'%10.0f');
    legend2 = ['Ludwik:
$\sigma_{o}=$',C_legend,'$\left(\bar{\varepsilon}^{pl}\right)^{',n_le
gend,'}+',Sigma_0_legend,' [MPa]$'];
end


%% Writting output stress-strain file
% Generating file and writting number of data points
Number_of_data_points_for_export = 20;

fid = fopen('Stress_strain.txt','w');
fprintf(fid,'%-5.0f\n',Number_of_data_points_for_export);
fclose(fid);
fid = fopen('Stress_strain.txt','a');

% % Linear distribution of strains
```

```matlab
% Epsilon_export =
linspace(0,max(Epsilon),Number_of_data_points_for_export)';
% Sigma_export = interp1(Epsilon,Sigma,Epsilon_export);
% Data_for_export = [Epsilon_export Sigma_export];
% fprintf(fid,'%-5.5f %-5.2f\n',Data_for_export');
% fclose(fid);

% Distributing strains according to a progressive series
Epsilon_min_export = 1E-4;
Epsilon_max_export = max(Epsilon);
a = Epsilon_min_export;
r =
(Epsilon_max_export/Epsilon_min_export)^(1/(Number_of_data_points_for
_export-2));
for i=1:Number_of_data_points_for_export-1
    Epsilon_export(i,1) = a*r^(i-1);
end
Epsilon_export = [0; Epsilon_export];
Sigma_export = interp1(Epsilon,Sigma,Epsilon_export);

% Distributing strains according to power law
Epsilon_min_export = 0;
Epsilon_max_export = max(Epsilon);
b = Epsilon_min_export;
n = log(Epsilon_max_export-
Epsilon_min_export)/log(Number_of_data_points_for_export);
[0:1:Number_of_data_points_for_export].^n;

% Writting data
Data_for_export = [Epsilon_export Sigma_export];
fprintf(fid,'%-5.5f %-5.2f\n',Data_for_export');
fclose(fid);

%% Plots

% Load-stroke
f1 = figure(1);
plot(Data(:,2),Data(:,1)*9.80665,'.k');
hold on
plot(L(i_start:i_end)-L0,F(i_start:i_end),'.r');
hold off
xlabel('Elongation [mm]')
ylabel('Force [N]')
legend('All data','Data used for stress-strain
fit','location','southeast')
orient landscape
%enhance_plot(0,20,0,0,0)
print(f1,'-dpdf','Load_stroke')
close all

% Stress-strain
f1 = figure(1);
plot(Epsilon,Sigma,'.k')
hold on
plot(Epsilon,Sigma_fit,'-r')
hold off
xlabel('True effective strain')
ylabel('True stress [MPa]')
orient landscape
%enhance_plot(0,20,0,0,0)
```

```matlab
legend1 = ['Experiment'];
legend({legend1,legend2},'Location','southeast','interpreter','latex'
);
print(f1,'-dpdf','Stress_strain')
close all

% Lankford coefficient
f1 = figure(1);
plot(Epsilon(i_R:end),R(i_R:end),'.r')
hold on
plot(Epsilon,R,'.k')
plot(Epsilon(i_R:end),R(i_R:end),'.r')
hold off
axis( [min(Epsilon) max(Epsilon) 0 2] )
R_label = num2str(R_average,'%10.2f');
legend_R1 = ['Experiment'];
legend_R2 = ['R= ',R_label];
legend({legend_R1},{legend_R2});
xlabel('True effective strain')
ylabel('Lankford coefficient R')
orient landscape
%enhance_plot(0,20,0,0,0)
print(f1,'-dpdf','Lankford_coefficient')
close all
```

Appendix A2: MATLAB code for compression test of cylindrical specimen

```matlab
clear all
clc

%% Program to compute stress-strain curves
 %% Loading of data
Test1 = load('Test 1.txt');
Test2 = load('Test 2.txt');

x_start = 300;
x_finish = 700;

D0 = 20.05;
H0 = 20.05;
A0 = D0*D0/4*pi;

Press_stroke = abs(Test1(x_start:x_finish,2) - Test1(x_start,2));
Press_force = Test1(x_start:x_finish,1)*1E3/10;

H = H0 - Press_stroke;
A = H0./H*A0;

Epsilon_eff = log(H0./H);
Sigma_eff = Press_force./A;

Epsilon_eff(1) = [];
Sigma_eff(1) = [];

%% Fitting of data
Hollomon = @(x) norm( x(1)*Epsilon_eff.^x(2) - Sigma_eff );
Constants_Hollomon = fminsearch(Hollomon,[150 0.2]);
Stress_Hollomon =
Constants_Hollomon(1)*Epsilon_eff.^Constants_Hollomon(2);

Ludwik = @(x) norm(x(1)*Epsilon_eff.^x(2) + x(3) - Sigma_eff);
Constants_Ludwik = fminsearch(Ludwik,[150 0.2 10]);
Stress_Ludwik =
Constants_Ludwik(1)*Epsilon_eff.^Constants_Ludwik(2)+Constants_Ludwik
(3);

Swift = @(x) norm(x(1)*(x(3)+Epsilon_eff).^x(2) - Sigma_eff);
Constants_Swift = fminsearch(Swift,[150 0.2 0.1]);
Stress_Swift =
Constants_Swift(1)*(Constants_Swift(3)+Epsilon_eff).^Constants_Swift(
2);

%% Plots
plot(Epsilon_eff,Sigma_eff,'.k')
hold on
plot(Epsilon_eff,Stress_Hollomon,'-r')
plot(Epsilon_eff,Stress_Ludwik,'-g')
plot(Epsilon_eff,Stress_Swift,'-b')
hold off
```

Appendix A3: MATLAB code for plain strain compression test

```matlab
clear all
clc

%% Computation of stress-strain behaviour based on Watts & Ford test

%% Loading of data
Data = xlsread('Watts & Ford EN1-4307.xlsx'); % [Effective strain,
Flow stress [MPa])

Data = sortrows(Data,1);

%% Curve fitting
Swift = @(x) norm(x(1)*(x(2)+Data(:,1)).^x(3) - Data(:,2));
Swift_constants = fminsearchbnd(Swift,[150 0.1 0.2],[0 0 0]);
%Stress = Swift_constants(1)*(Swift_constants(2)+Data(:,1)).^Swift_
constants(3);

Voce = @(x) norm(x(1) + (x(2)-x(1))*(1-exp(-(x(3)*Data(:,1)))) -
Data(:,2));
Voce_constants = fminsearch(Voce,[0 150 1]);
Stress = Voce_constants(1) + (Voce_constants(2)-
Voce_constants(1))*(1-exp(-(Voce_constants(3)*Data(:,1))));

%% Plots
f1 = figure(1);
hold on
plot(Data(:,1),Data(:,2),'.k')
plot(Data(:,1),Stress,'-k')
hold off
xlabel('Effective strain')
ylabel('Flow stress [MPa]')
%legend('Experiment','Voce','location','southeast')
%enhance_plot(0,30,4,20,0);
orient landscape
%print(f1,'-dpdf','Stress-strain_Swift')
print(f1,'-dpdf','Stress-strain_Voce')
close all
```

Appendix B1: Technical drawing for cylindrical special with truncated pocket
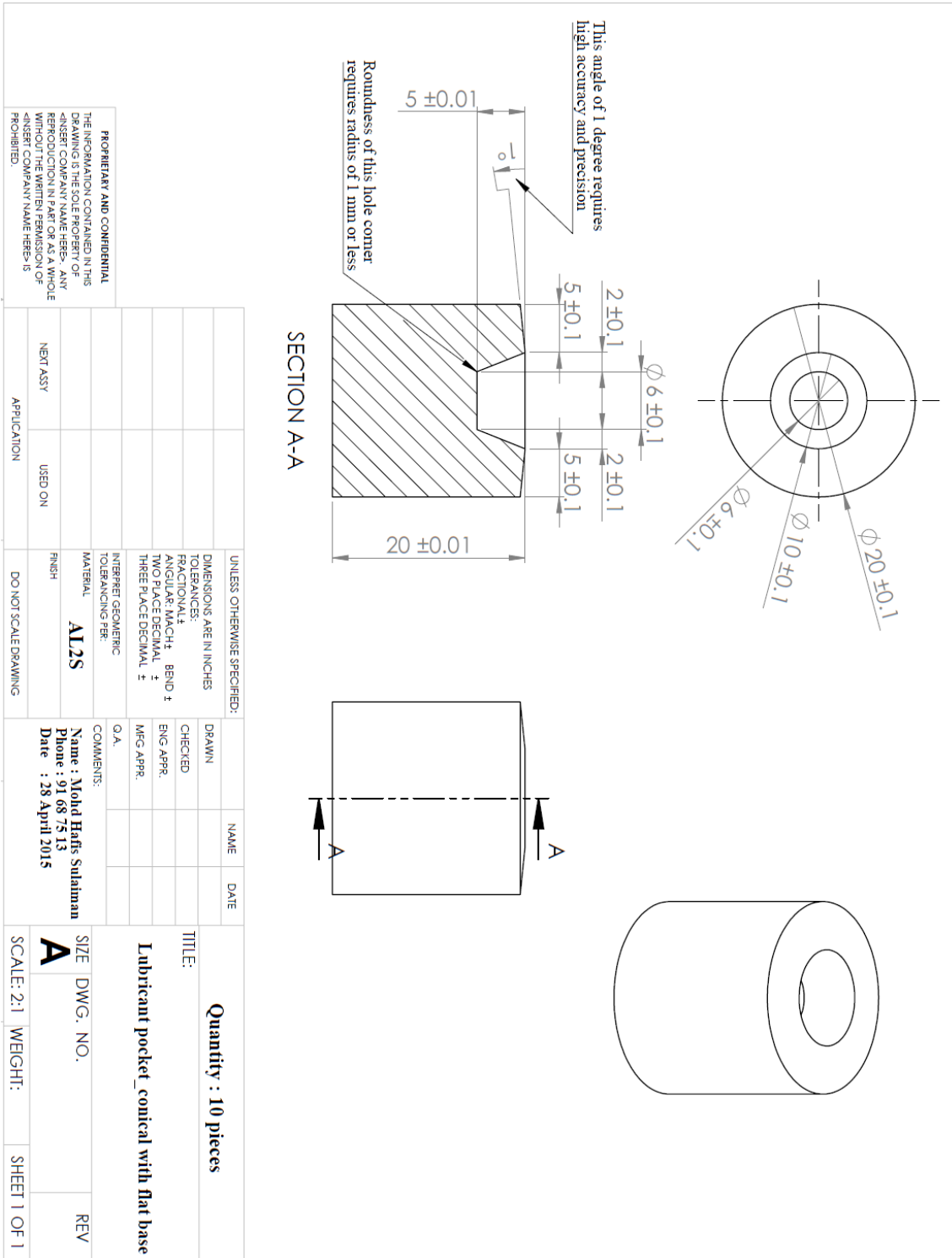
Appendix B2: MATLAB code for comparison of numerical and experimental surface pocket deformation

```matlab
clear all
clc

%% This program plots the difference of the pocket surface
deformation between the experimental and numerical analyses.

%% Experimental pocket surface

% Load Experimental data (at Reduction 0%)
Data = load('Sample no 7 - Before.txt'); % Loading data file [Node
number, x-coordinate, y-coordinate, z-coordinate]
Data_treatment = load('Sample no 7 - Before_data treatment.txt'); %
Loading data file [x_min, x_max, y_min]

N = 200; % Number of gridpoints for numerical integration

% Coordinate vectors
x = Data(:,1); % Loading data file [x-coordinate]
y = Data(:,3); % Loading data file [y-coordinate]

x_min = Data_treatment(1); % Loading data file [x_min]
x_max = Data_treatment(2); % Loading data file [x_max]
y_top = Data_treatment(3); % Loading data file [y_min]

x_integration = linspace(x_min,x_max,N)'; % Integrate x-coordinate
points and ditributed them evenly
y_integration = interp1(x,y,x_integration); % interpolate y-
coordinate points and distributed them evenly

i = find(y_integration < -0.01); % Find center points of x- and y-
coordinates

x_center = mean(x_integration(i)); % Determine center point of the
deformed pocket coordinates
x = x - x_center; % Centering of pocket
x_integration = x_integration - x_center; % Centering of pocket
x_center = 0;


%% FEM pocket surface

% Load FEM data (at Reduction 0%)
Node_numbers = load('NoLube_node_number2.txt'); % Vector with
relevant node numbers
Node_coordinates = load('NoLube_Coordinates_step0.txt'); % [Node
number, x-coordinate, y-coordinate, z-coordinate]
Node_coordinates(:,4) = []; % Removing z-coordinate

Number_of_nodes_relevant = length(Node_numbers);
Number_of_elements = Number_of_nodes_relevant - 1;

V_element = zeros(Number_of_elements,1); % Volume of each element
y_tool = max(Node_coordinates(:,3)); % Tool y-coordinate

for i=1:Number_of_nodes_relevant
```

139

```matlab
    Node_number = find(Node_numbers(i) == Node_coordinates(:,1)); %
Node number
    Coordinates_nodes_LS_DYNA(i,1) = Node_coordinates(Node_number,2);
    Coordinates_nodes_LS_DYNA(i,2) = Node_coordinates(Node_number,3);
end

% Moving the edge of the pocket
Coordinates_nodes_LS_DYNA(:,2) = Coordinates_nodes_LS_DYNA(:,2) -
max(Coordinates_nodes_LS_DYNA(:,2));


%break
% Plot
f1 = figure(1);
axes('fontsize',25)
hold on
plot(x,y,'.-k','markersize',25,'linewidth',1.5) % Plot x- & y-
coordinates
% plot([min(x) max(x)],[y_top y_top],'-r') % Plot planes for max y-
coordinates
% plot(x_integration,y_integration,'.r') % Plot Uniform Distributed
x- and y-coordinates
% plot([x_center x_center],[min(y) max(y)],'--r')
plot(Coordinates_nodes_LS_DYNA(:,1),Coordinates_nodes_LS_DYNA(:,2),'-
b','linewidth',1.8)
hold off
xlabel('Radius (mm)')
ylabel('Depth (mm)')
legend({'Exp - CR5','FEM -
CR5'},'FontSize',19,'location','Southwest')
axis equal
axis([0 11 -20 1]);
% orient landscape
print(f1,'-dtiff','Plot_of_contour_Red0%')
close all
```

Appendix D1: Schematic of compressibility test equipment to determine lubricant bulk modulus in a wide pressure range
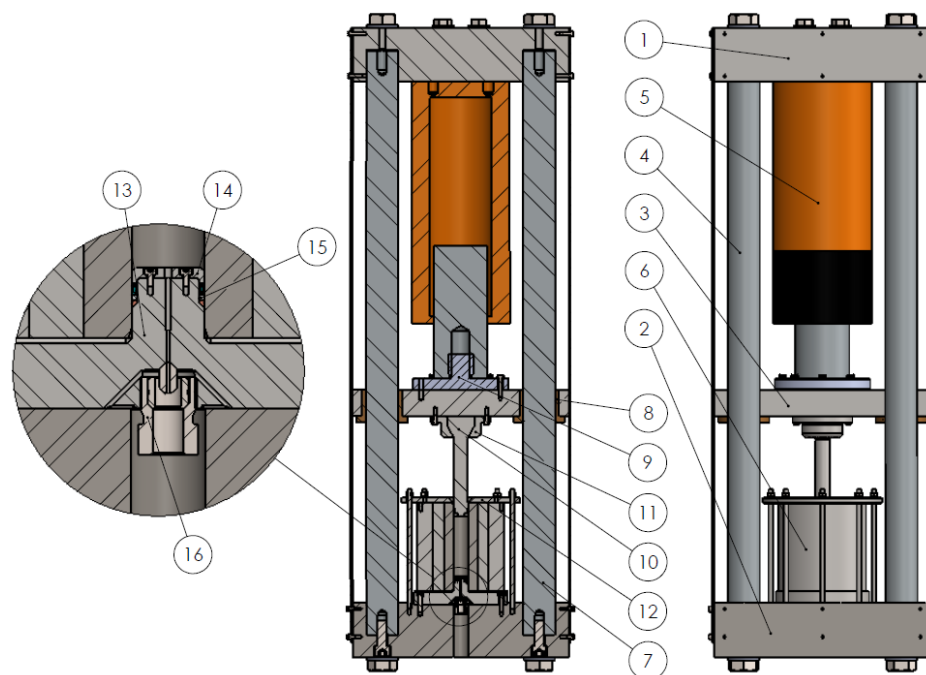
Components:

1) Top plate
2) Bottom plate
3) Press plate
4) Supporting column – 4 units
5) Hydraulic cylinder
6) Strip wound container
7) Guiding column – 2 units
8) Bushing
9) Upper punch holder
10) Upper punch
11) Upper punch holder
12) Bottom punch cover
13) Bottom punch plate
14) Lower punch cap
15) Bridgman sealing
16) Maximator fitting pipes, max. measuring pressure range 1.5 GPa

Upper punch

Threaded connection
Sealing face
Centering surface
Mounting surface for union

M16x1.5
Ø 30.80 h7
Ø 37 g6
Ø 35
45°
7
10
R20
R10
251
25
Ø 68 g6

Seal cap
Variseal, M2S
Soft ring
Conical ring
Punch
Union
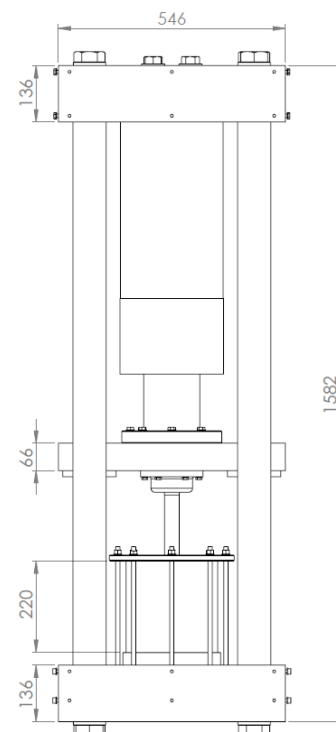
*Courtesy of Martin Thomas Overdahl Lund, Niels Schmidt Hansen, Niels Bay. Design and construction of high pressure viscometer, Master's Thesis, DTU Mechanical Engineering, 2016, pp. 1 – 271

Bottom punch

Appendix D2: Technical drawing for Bridgman sealing components

SECTION A-A

0.3 ±0.05

3.1 ±0.05

45° ±0.1°

Ø 28 -0.007/-0.020

Ø21.8 +0.033/0

Notes:
- All units in millimeters.
- For material selection:-
- The raw material for fabrication of this ring can be taken from any available copper materials in the DTU workshop.

MATERIAL	Copper		
DRAWN	09/05/2016		
CHECKED			
ENG APPR.			
MFG APPR.			
Q.A.			
Person in charge:			
Name : Mohd Hafis Sulaiman			
Phone : 52144			
Mobile : 91 68 75 13			

TITLE:

Quantity: 8 stk.

Ring 1 - Copper

SIZE	DWG. NO.		REV
A4	14		4
SCALE: 2:1		SHEET 14 OF 16	

2.9 ±0.05

SECTION A-A

Ø 21.8 +0.033 0

Ø28 -0.007 -0.020

A

A

Notes:
- All units in millimiters.
- It is suggested to use available Teflon or similar polymer materials in the DTU-MEK workshop.

MATERIAL	Teflon or polymer		Quantity: 8 stk.
DRAWN	09/05/2016		
CHECKED		TITLE:	
ENG. APPR.			Ring 2 - Teflon
MFG APPR.			
Q.A.			

Person in charge:

Name : Mohd Hafis Sulaiman
Phone : 52144
Mobile : 91 68 75 13

SIZE	DWG. NO.		REV
A4	15		3
SCALE: 2:1		SHEET 15 OF 16	

145

Appendix D3: MATLAB code for calculation of volume change and bulk modulus of test lubricants

```matlab
clear all
clc

%% Import of data
Data = load('Test_15_11_16_Water.txt');
Data(:,2) = [];  % Time [s] Oil Pressure (MPa)  Stroke length (mm)
Data_treatment = load('Test_15_11_16_Water_data_treatment.txt'); %
Time start of data treatment [mm]  Time end of data treatment
t = Data(:,1); % Time [s]
P_raw = Data(:,2); % Pressure [MPa]
L_raw = Data(:,3); % Stroke length [mm]

%% Finding start and stop of relevant data
t_start = Data_treatment(1);
t_end = Data_treatment(2);

[Value,index_start] = min(abs(t - t_start));
[Value,index_end] = min(abs(t - t_end));
P = P_raw(index_start:index_end);
P_plot = P;
P = P - min(P);
L = L_raw(index_start:index_end);
L = L - min(L);
Vo = 93.6*10*10*10;
V = Vo - L*37^2/4*pi;

%% Interpolation of pressure
pp = polyfit(V,P,2);

%% Computation of bulk modulus
ppder = polyder(pp);
K = -V.*polyval(ppder,V);

%% Fitting of bulk modulus
% Power law with offset
Power = @(x) norm(x(1)*(P+x(3)).^x(2) - K);
Power_constants = fminsearch(Power,[100 0.2 100]);
K_power =
Power_constants(1)*(P+Power_constants(3)).^Power_constants(2);

%% Figures
f1 = figure(1);
axes('fontsize',20)
hold on
plot(V,P,'.r','markersize',20);
plot(V,polyval(pp,V),'-k','linewidth',2)
hold off
xlabel('Volume [mm^3]')
ylabel('Pressure [MPa]')
legend('Water (Experiment)','Water (2nd. polyfit)','location',
'northeast')
axis([80000 100000 0 700])
print(f1,'-dtiff','Volume_pressure')
close all

f2 = figure(2);
```

```matlab
axes('fontsize',20)
hold on
plot(P,K,'.r','markersize',20)
plot(P,K_power,'-k','linewidth',2)
hold off
xlabel('Pressure [MPa]')
ylabel('Bulk modulus [MPa]')
legend({legend1;legend2},'location','southeast')
axis([0 700 0 6000])
print(f2,'-dtiff','Pressure_bulk_modulus')
close all

f3 = figure(3);
axes('fontsize',20)
hold on
plot(t,P_raw,'.k','linewidth',2)
plot(t(index_start:index_end),P_plot,'.b','linewidth',2)
hold off
xlabel('Time [s]')
ylabel('Pressure [MPa]')
print(f3,'-dtiff','Time_pressure')
close all

f4 = figure(4);
axes('fontsize',20)
hold on
plot(P,V/max(V),'.k','markersize',20)
hold off
xlabel('Pressure (MPa)')
ylabel('Relative volume (V/V_o)')
axis([0 700 0.8 1])
print(f4,'-dtiff','Relative_volume')
close all

f5 = figure(5);
axes('fontsize',20)
hold on
plot(t(index_start:index_end),V,'.k','linewidth',2)
hold off
xlabel('Time (s)')
ylabel('Volume (MPa)')
print(f5,'-dtiff','Time_volume')
close all
```

Appendix E1: Technical drawing for textured surfaces on SRT tool

**For display purposes only

Side bar**
Base**

(1) Upper die

(4) Workpiece
(2) Lower die

(1) Upper die (3° die angle)

γ=3°

t₀=4.0 mm

Δt=0.6 mm

x=11.45 mm

Textured surface
(L11.45 x W20mm)

(3) Die insert

(2) Lower die

DETAIL B
SCALE 2 : 1

(4) Workpiece

SECTION A-A
SCALE 1 : 2

B

A

A

Fabricated parts:
(1) Upper die
(2) Lower die
(3) Die insert (with varied texture surfaces)
(4) Sheet material (workpiece)

UNLESS OTHERWISE SPECIFIED:		NAME	DATE		SHETRIB project (No: 76640)		
DIMENSIONS ARE IN INCHES	DRAWN		18/01/2016				
TOLERANCES: FRACTIONAL±	CHECKED			TITLE:			
ANGULAR: MACH± BEND ±	ENG. APPR.				Experimental setup for		
TWO PLACE DECIMAL ± THREE PLACE DECIMAL ±	MFG. APPR.				tailored tool surfaces		
INTERPRET GEOMETRIC TOLERANCING PER:	Q.A.						
	Person in charge:			SIZE	DWG. NO.		REV
MATERIAL	Name : Mohd Hafis Sulaiman			**A4**	2		1
FINISH	Phone : 52144 Mobile : 91 68 75 13						
DO NOT SCALE DRAWING				SCALE: 1:5	WEIGHT:		SHEET 2 OF 16

149

Note:
- All units in millimeters.
- Tolerance is ±0.2 mm, unless otherwise stated.
- Hardened and tempered up to 60 HRC.

MATERIAL	Svetker 21		TITLE:	Quantity: 1 stk.	
DRAWN	18/01/2016				
CHECKED				Upper die	
ENG. APPR.				(3° die angle)	
MFG. APPR.					
Q.A.		SIZE **A4**	DWG. NO. 3		REV 1
Person in charge:		SCALE: 1:2	WEIGHT:		SHEET 3 OF 16
Name : Mohd Hafis Sulaiman					
Phone : 52144					
Mobile : 91 68 75 13					

58
14   30   14

12

29 +0.3 / 0

52 0 / -0.3

62

29 +0.3 / 0

12

18

74   110

18

φ12

8.6 0/-0.1

20 0/-0.1

R3

R2

R1

R3

23   35

8   18   8

3°

Ra 0.02

0.02

MATERIAL	IMPAX, HRC 38		Quantity: 1 stk.	
DRAWN	18/01/2016			
CHECKED		TITLE:		
ENG. APPR.			Lower die	
MFG. APPR.				
Q.A.				
Person in charge:		SIZE	DWG. NO.	REV
Name : Mohd Hafis Sulaiman		**A4**	4	1
Phone : 52144				
Mobile : 91 68 75 13		SCALE: 1:5	WEIGHT:	SHEET 4 OF 16

Note:
- All dimensions in millimeters.
- Tolerance is ±0.2 mm, unless otherwise stated.

Appendix E2: Technical drawing for textured patterns on SRT tools

Untextured tool surface

Note:
- All units in millimeters.
- Tolerance is ±0.1 mm, unless otherwise stated.
- Hardened and tempered up to 60 HRC.

12 -0.1 / 0

// 0.02 A

R1

A

R1

Ra 0.02

30 -0.1 / 0

30 -0.1 / 0

Remarks:
- After 10 stk. plain surfaces of die inserts were fabricated, 1 stk. will remain unchanged, while the other 9 stk. are going to be machined by LEGO machine (*as per suggested by Giuliano Bissacco) for making grooves.
- Detailed drawings of microscopic surface texturing for the other 9 stk. plain surfaces are described on the next pages, refer to Drawing no. 5A to 5I

DRAWN	18/01/2016	
CHECKED		
ENG APPR.		
MFG APPR.		
Q.A.		
MATERIAL	Sverker 21	

Person in charge:

Name : Mohd Hafis Sulaiman
Phone : 52144
Mobile : 91 68 75 13

Quantity: 10 stk.

TITLE:
Die insert (Plain surface - Ref.)
(Textured area - L11.45 x W20mm)

SIZE	DWG. NO.	REV
A4	5	1

SCALE: 2:1   WEIGHT: SHEET 5 OF 16

Textured tool surface (Tool A) with plateau distance between pockets x = 0.23 mm

Textured tool surface (Tool B) with plateau distance between pockets x = 0.23 mm

Note:
- All units in millimeters.
- Tolerance is ±0.1 mm, unless otherwise stated.
- Hardened and tempered up to 60 HRC.

SECTION A-A

// 0.02 A

Ra 0.02

DETAIL C
SCALE 10 : 1

Smooth surface

Grooves

Grooves

microscopic surface
texturing by LEGO
machine

DETAIL B
SCALE 140 : 1

Grooves:
- 25 columns
- 4 rows (Gap: 0.8 mm)
Gap: 0.8 mm

0.23 ±0.01

0.005

Ra 0.02

MATERIAL	Sverker 21		Quantity: 1 stk.	
DRAWN	04/04/2016	TITLE:		
CHECKED		Die insert (W1L1 - NC4 - G2)		
ENG APPR.		(Textured area - L1l.45 x W20mm)		
MFG APPR.				
Q.A.				
Person in charge:	SIZE	DWG. NO.		REV
Name : Mohd Hafis Sulaiman	A4	5C		2
Phone : 52144	SCALE: 2:1	WEIGHT:	SHEET 8 OF 16	
Mobile : 91 68 75 13				

Textured tool surface (Tool C) with plateau distance between pockets x = 0.23 mm

Grooves

Smooth surface

microscopic surface texturing by LEGO machine

DETAIL C
SCALE 10 : 1

0.005

Ra 0.02

0.23 ±0.01   0.23 ±0.01   0.23 ±0.01   0.23 ±0.01

Grooves:
- 25 columns
- 4 rows (Gap: 2 mm)

5°

DETAIL B
SCALE 140 : 1

MATERIAL	Sverker 21		Quantity: 1 stk.
DRAWN	04/04/2016		
CHECKED		TITLE:	
ENG. APPR.			Die insert (W1L1 - NC4)
MFG APPR.			(Textured area - L11.45 x W20mm)
Q.A.			Gap: 2 mm
Person in charge:		SIZE DWG. NO.	REV
Name : Mohd Hafis Sulaiman		A4 5B	2
Phone : 52144			
Mobile : 91 68 75 13		SCALE: 2:1 WEIGHT:	SHEET 7 OF 16

2.5   2.5   2.5   2.5

A

9.43

11.27

9.30

0
30 -0.1

C

A

7   2   2   2   7
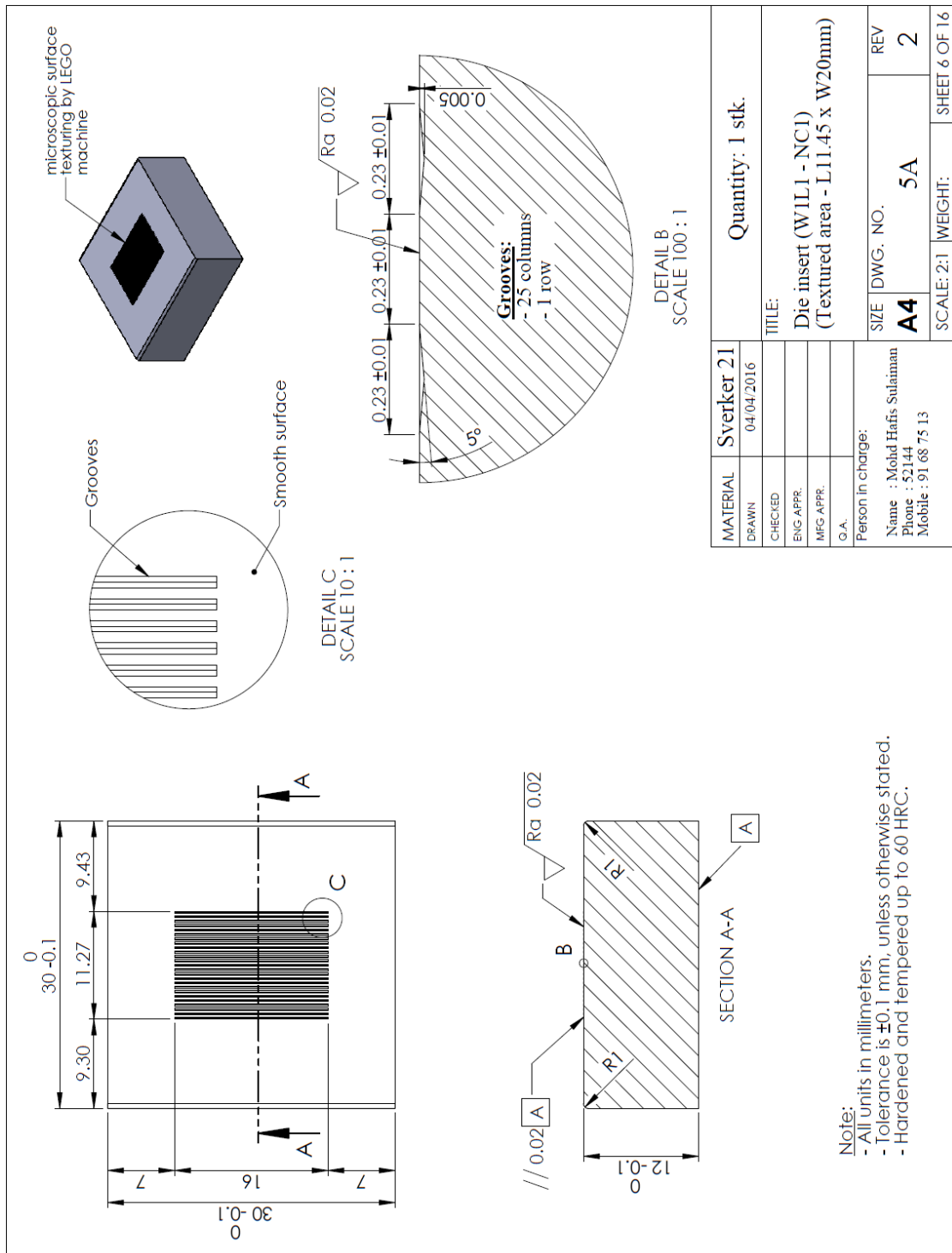
0
30 -0.1

A

B

R1

R1

Ra 0.02

// 0.02 A

A

SECTION A-A

0
12 -0.1

Note:
- All units in millimeters.
- Tolerance is ±0.1 mm, unless otherwise stated.
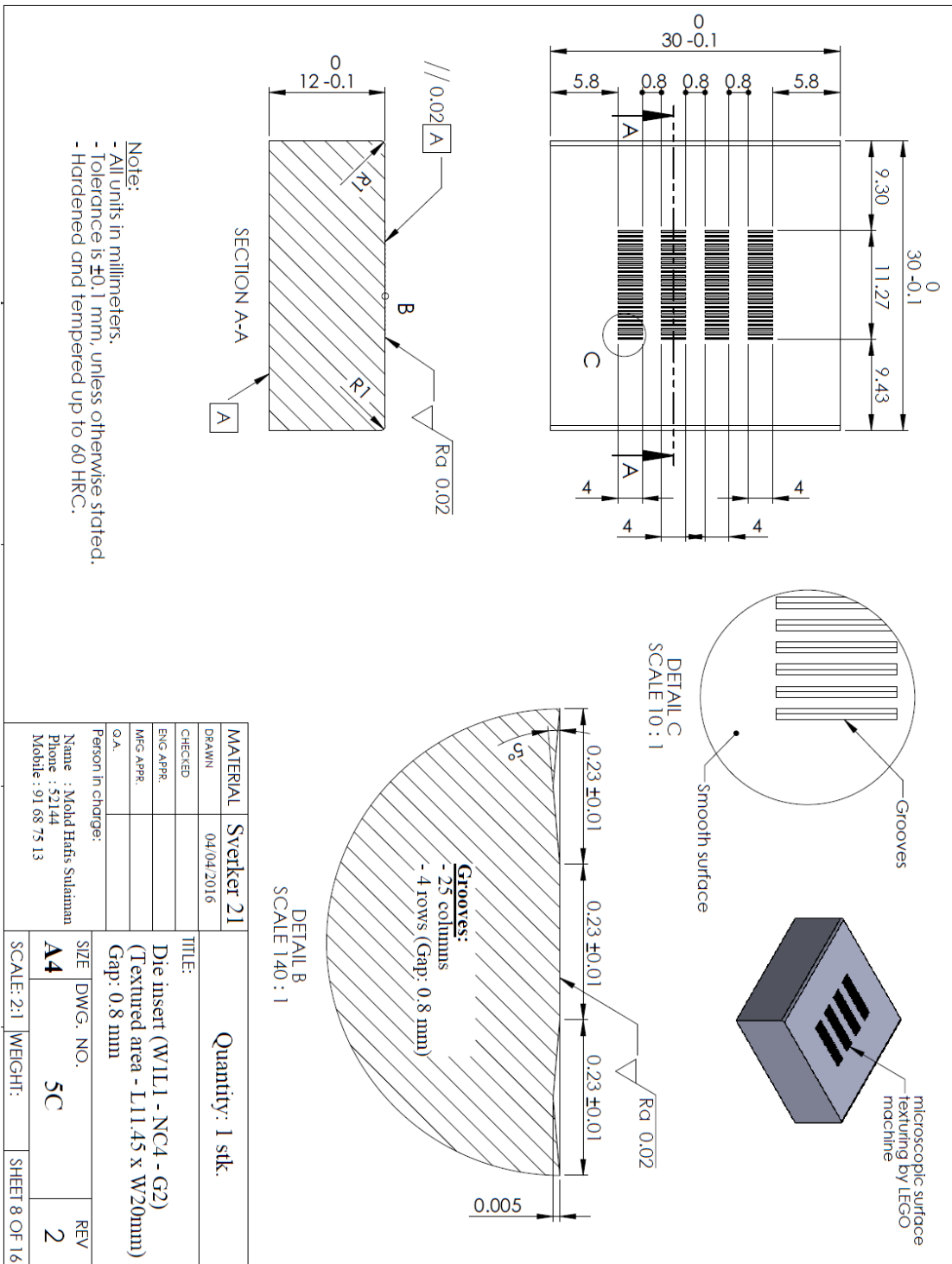- Hardened and tempered up to 60 HRC.

155

Textured tool surface (Tool A) with plateau distance between pockets x = 0.46 mm

Note:
- All units in millimeters.
- Tolerance is ±0.1 mm, unless otherwise stated.
- Hardened and tempered up to 60 HRC.

SECTION A-A

// 0.02 A

Ra 0.02

R1
R1
B
A

0
12 -0.1

0
30 -0.1

7 16 7

A
A
C
A

9.76
10.58
9.66

0
30 -0.1

DETAIL C
SCALE 10 : 1

Grooves
smooth surface

DETAIL B
SCALE 110 : 1

Grooves:
- 16 columns
- 1 row

5°
0.23 ±0.01
0.46 ±0.01
0.23 ±0.01
0.005
Ra 0.02

microscopic surface texturing by LEGO machine

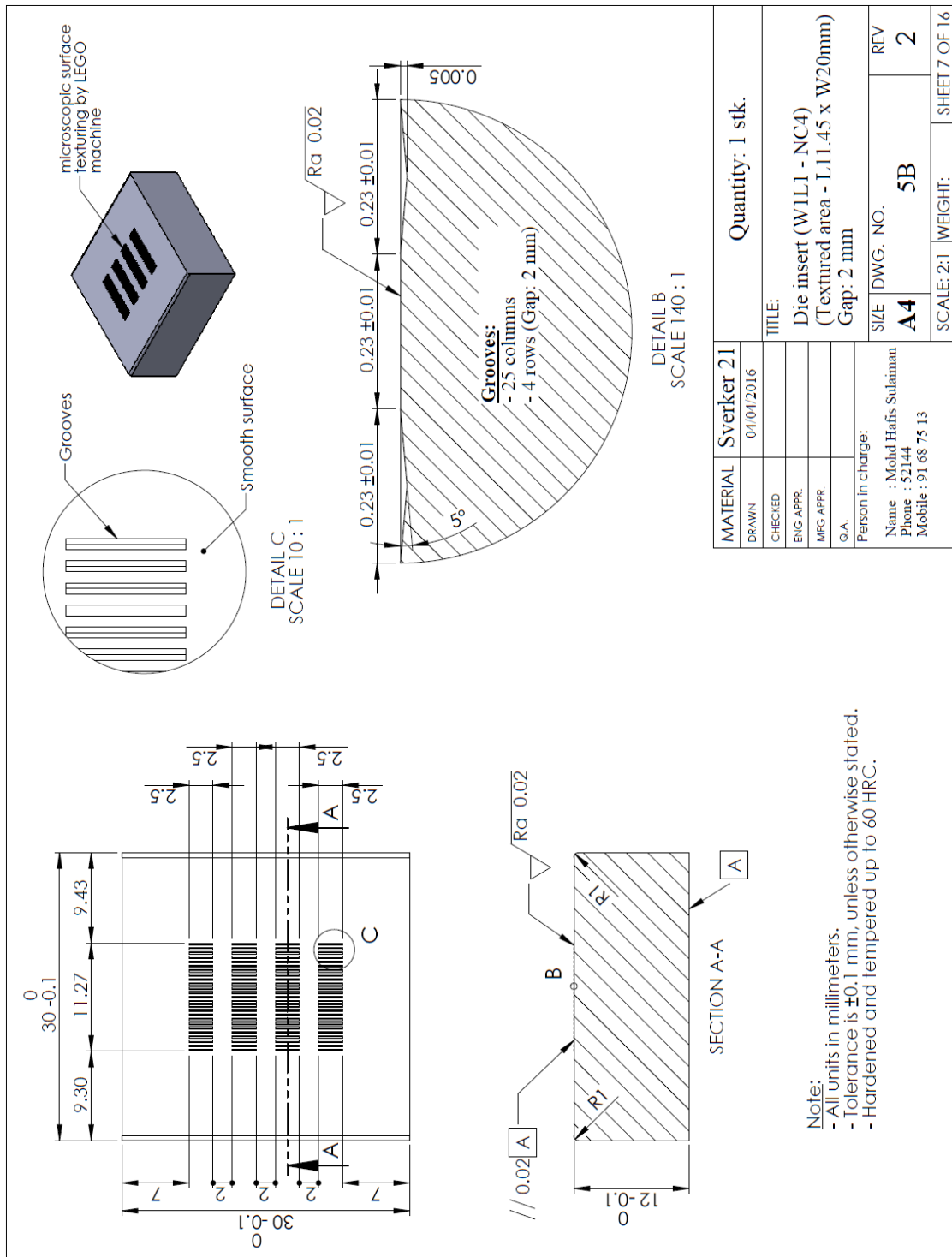| MATERIAL	Sverker 21		Quantity: 1 stk.	
DRAWN	04/04/2016			
CHECKED				
ENG APPR.		TITLE:		
MFG APPR.		Die insert (W1L2 - NC1)		
Q.A.		(Textured area - L11.45 x W20mm)		
Person in charge:				
Name : Mohd Hafis Sulaiman		SIZE	DWG. NO.	REV
Phone : 52144		A4	5D	2
Mobile : 91 68 75 13		SCALE: 2:1	WEIGHT:	SHEET 9 OF 16

156

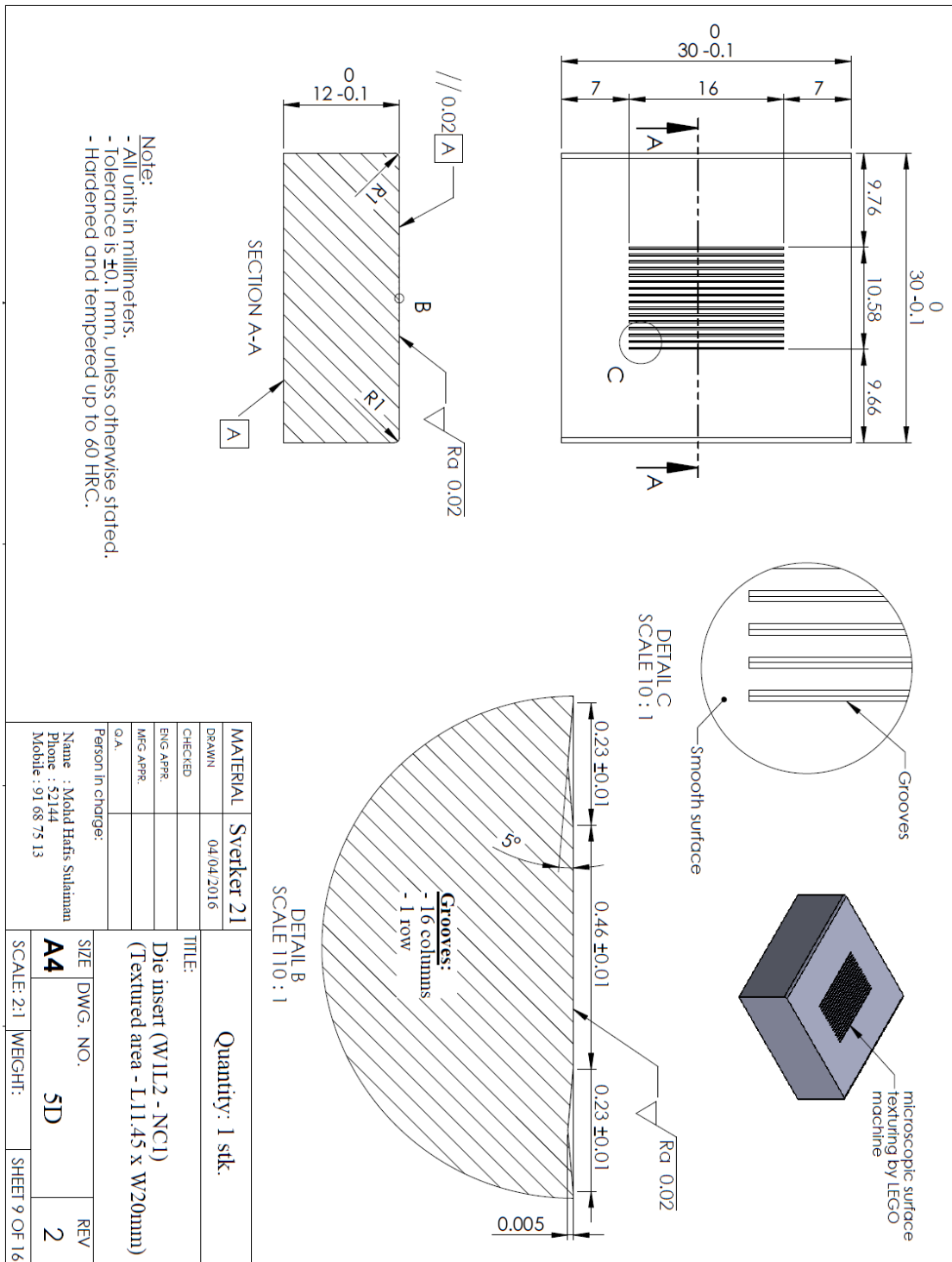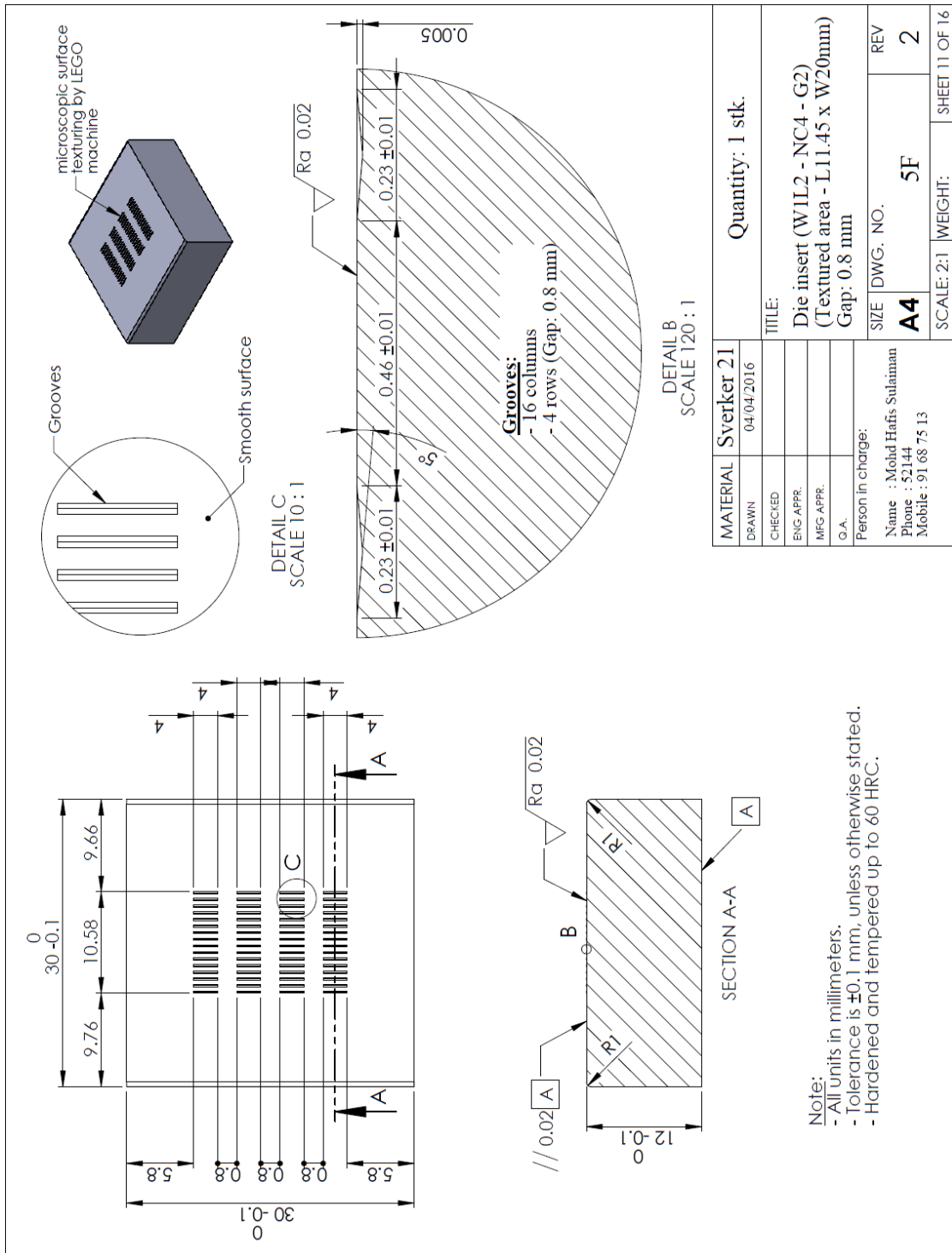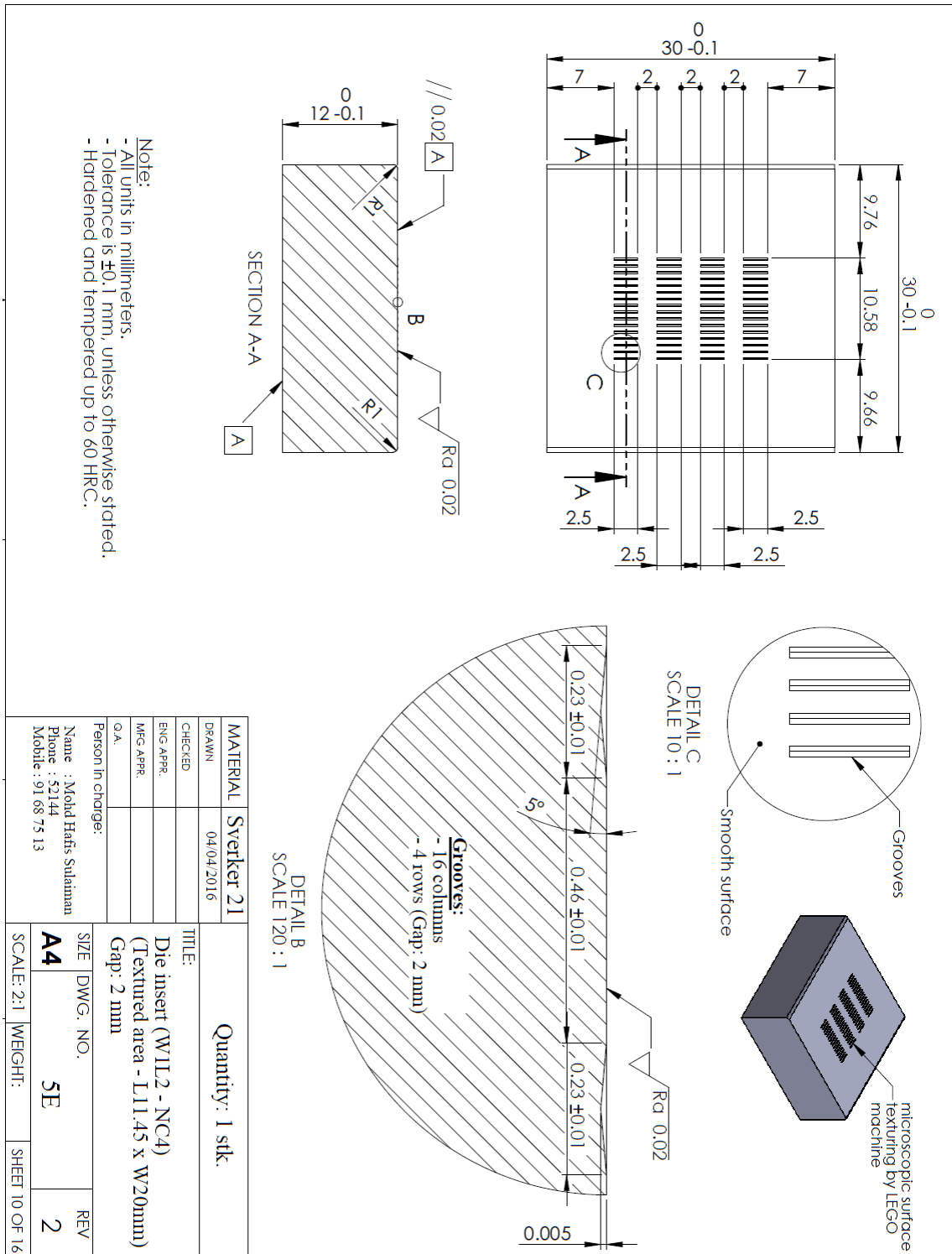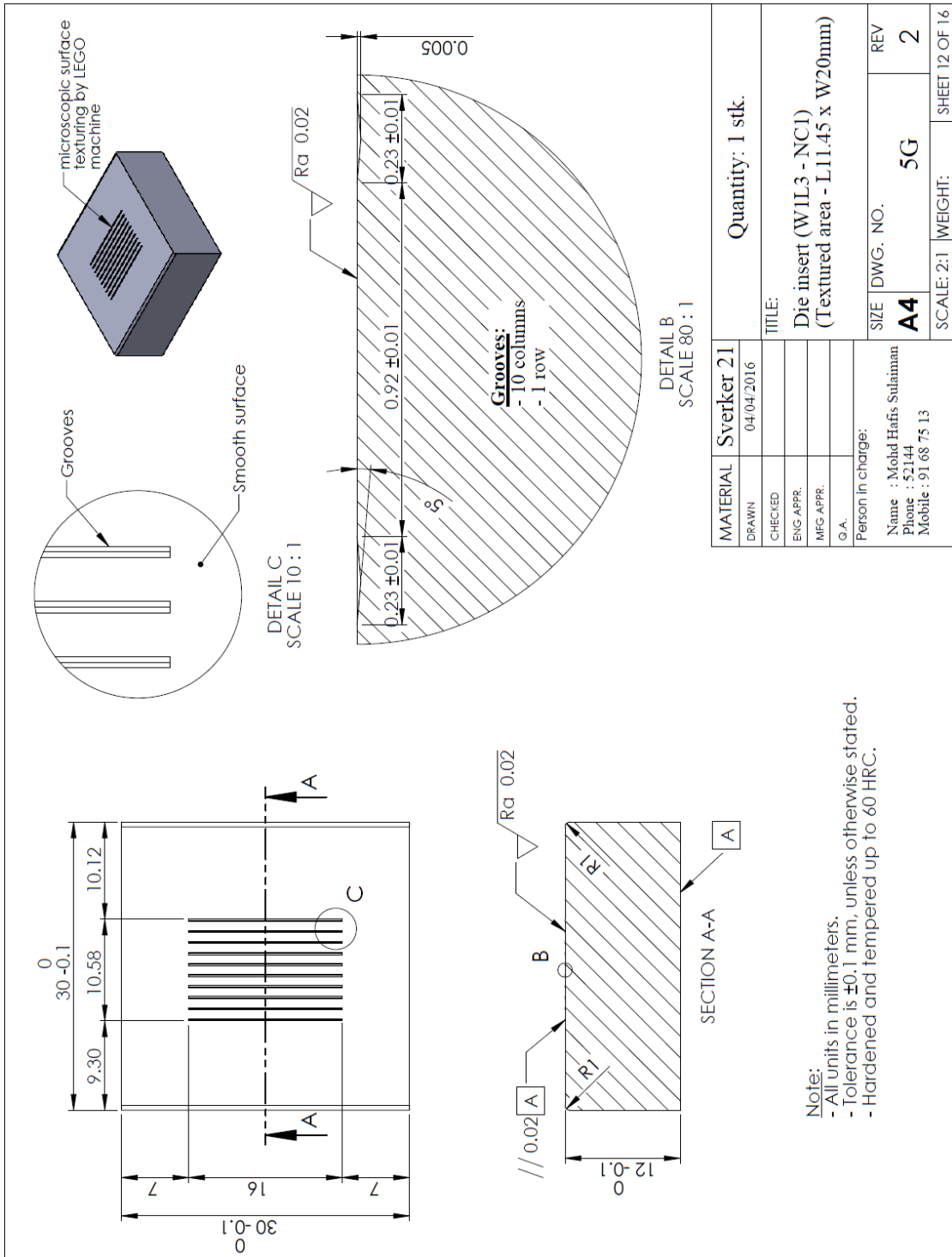*Textured tool surface (Tool B) with plateau distance between pockets x = 0.46 mm*

157

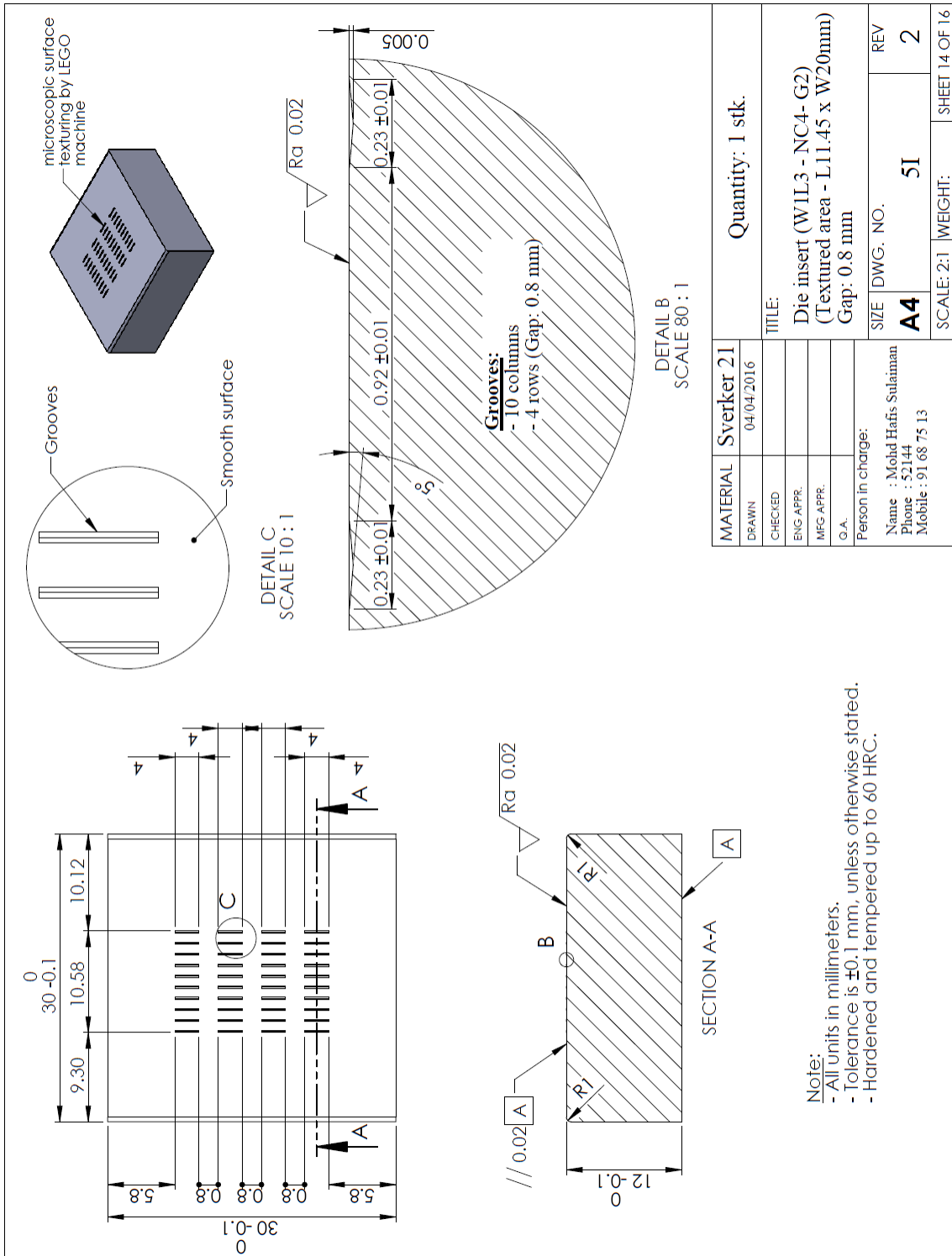*Textured tool surface (Tool C) with plateau distance between pockets x = 0.46 mm*
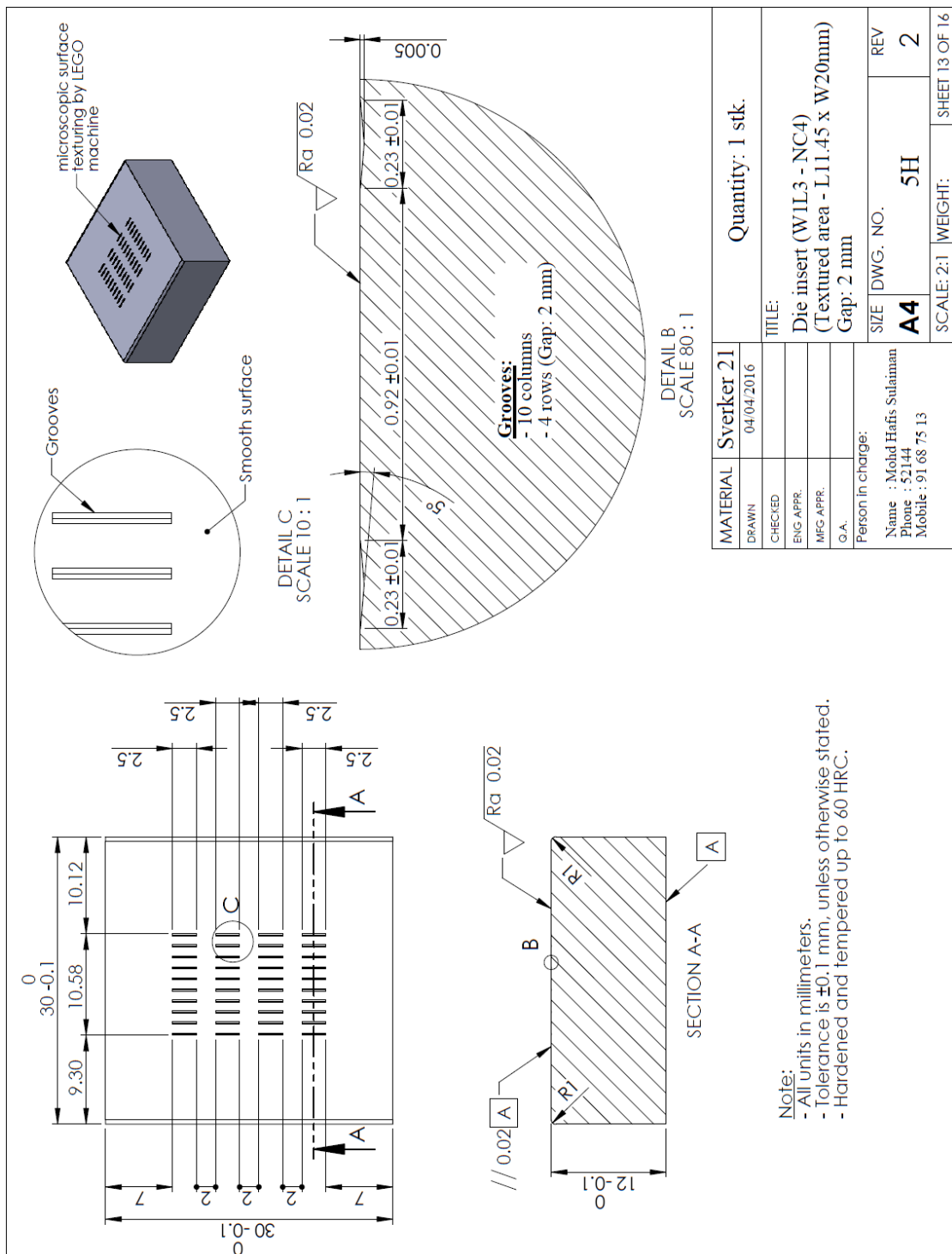

Note:
- All units in millimeters.
- Tolerance is ±0.1 mm, unless otherwise stated.
- Hardened and tempered up to 60 HRC.

SECTION A-A

// 0.02 A

0
12 -0.1

Ra 0.02

A

0
30 -0.1

0
30 -0.1

7   2   2   2   7

9.76   10.58   9.66

2.5   2.5   2.5   2.5

DETAIL C
SCALE 10 : 1

Grooves

Smooth surface

DETAIL B
SCALE 120 : 1

Grooves:
- 16 columns
- 4 rows (Gap: 2 mm)

0.23 ±0.01

5°

0.46 ±0.01

0.23 ±0.01

Ra 0.02

0.005

microscopic surface
texturing by LEGO
machine

MATERIAL	Sverker 21			
DRAWN	04/04/2016	TITLE:		
CHECKED				
ENG. APPR.		Die insert (W1L2 - NC4)		
MFG APPR.		(Textured area - L11.45 x W20mm)		
Q.A.		Gap: 2 mm		
Person in charge:				
Name.: Mohd Hafis Sulaiman		Quantity: 1 stk.		
Phone.: 52144				
Mobile : 91 68 75 13				

SIZE **A4** | DWG. NO. **5E** | REV **2**

SCALE: 2:1 | WEIGHT: | SHEET 10 OF 16

Textured tool surface (Tool A) with plateau distance between pockets x = 0.92 mm

microscopic surface texturing by LEGO machine

Grooves

Smooth surface

DETAIL C
SCALE 10 : 1

Ra 0.02

0.005

0.23 ±0.01

0.92 ±0.01

5°

0.23 ±0.01

Grooves:
- 10 columns
- 1 row

DETAIL B
SCALE 80 : 1

10.12

10.58

9.30

0
30 -0.1

C

A

A

7

16

7

0
30 -0.1

Ra 0.02

R1

B

R1

A

A

// 0.02 A

12 -0.1
0

SECTION A-A

Note:
- All units in millimeters.
- Tolerance is ±0.1 mm, unless otherwise stated.
- Hardened and tempered up to 60 HRC.

MATERIAL	Sverker 21		Quantity: 1 stk.
DRAWN	04/04/2016		
CHECKED		TITLE:	
ENG. APPR.		Die insert (W1L3 - NC1)	
MFG APPR.		(Textured area - L11.45 x W20mm)	
Q.A.			

Person in charge:
Name : Mohd Hafis Sulaiman
Phone : 52144
Mobile : 91 68 75 13

SIZE	DWG. NO.		REV
A4	5G		2
SCALE: 2:1	WEIGHT:	SHEET 12 OF 16	

159

Textured tool surface (Tool B) with plateau distance between pockets x = 0.92 mm

Textured tool surface (Tool C) with plateau distance between pockets x = 0.92 mm

## Appendix F1: MATLAB code for textured tool surfaces on SRT

```
clear all
clc
```

```matlab
%% This programme computes the drawing force of strip drawing with an
inclined tool and a flat tool

%% Input
h0 = 4;
h1 = 0.88*h0;
W = 20;
Die_angle = 3;
Sigma_0 = 55;
Sigma_inf = 149;
n_Voce = 1.52;
m1 = 0.03;
m2 = 0.02;

%% Computations
Epsilon_h = log(h1/h0);
Epsilon_eff = 2/sqrt(3)*(-Epsilon_h);
Sigma_mean = 1/Epsilon_eff*(Sigma_0*Epsilon_eff+(Sigma_inf-
Sigma_0)*Epsilon_eff+(Sigma_inf-Sigma_0)/n_Voce*(exp(-
n_Voce*Epsilon_eff)-1));
k_mean = Sigma_mean/sqrt(3);
Sigma_drawing = ((m1+m2)*k_mean/tand(Die_angle)+2*k_mean)*(-
Epsilon_h);
F_drawing = Sigma_drawing*h1*W
```
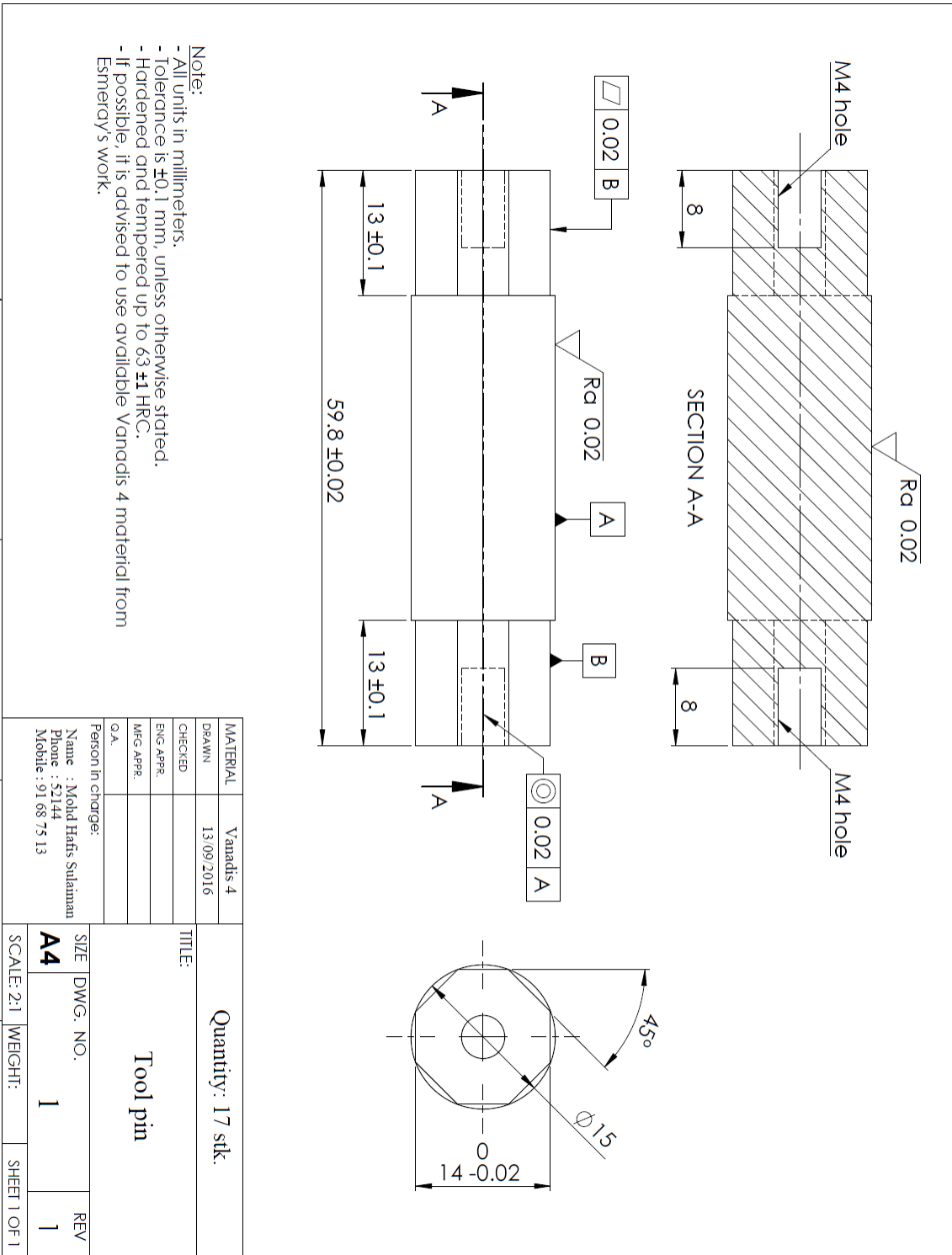
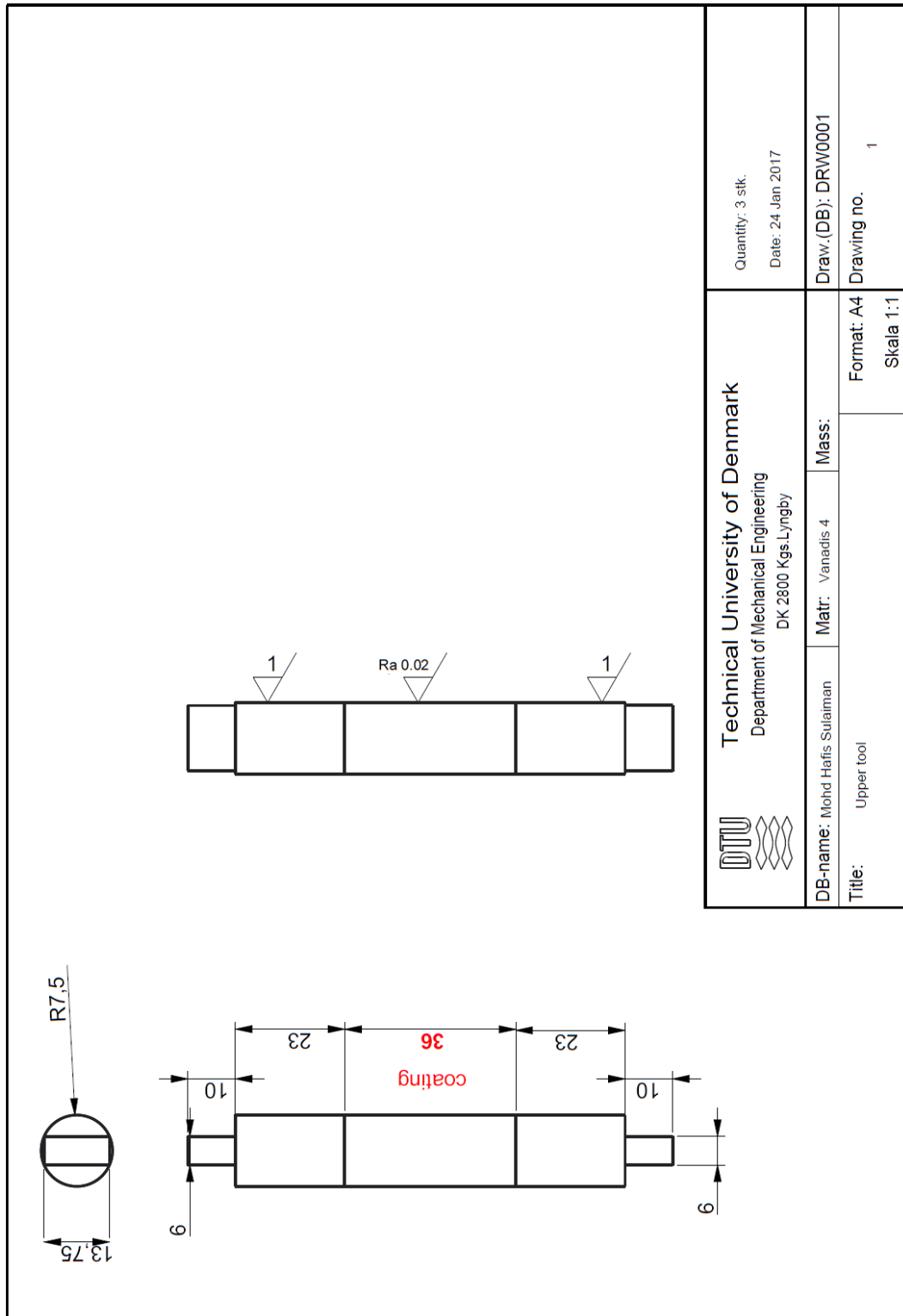## Appendix G1: Technical drawing for manually operated sheet tribo-test component
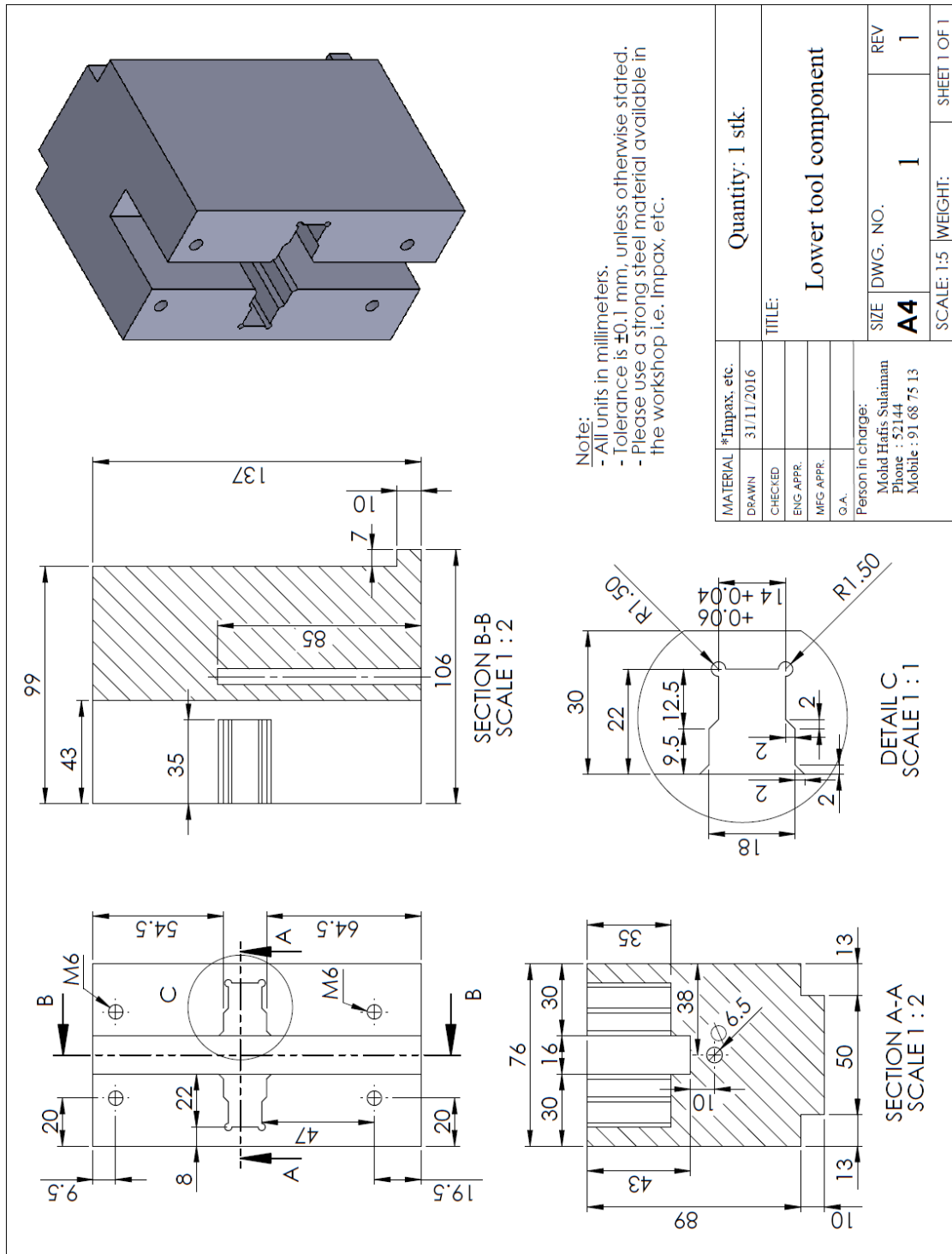
Appendix G2: Technical drawing for tool pin before coating procedure

Technical University of Denmark
Department of Mechanical Engineering
DK 2800 Kgs.Lyngby

DB-name: Mohd Hafis Sulaiman

Title: Upper tool

Matr: Vanadis 4

Mass:

Format: A4

Skala 1:1

Quantity: 3 stk.

Date: 24 Jan 2017

Draw.(DB): DRW0001

Drawing no.   1

Ra 0.02

1

1

R7,5

13,75

6

6

10

10

23

36
coating

23